THE UNIVERSITY OF TEXAS AT AUSTIN
CENTER FOR TRANSPORTATION RESEARCH

TECHNICAL REPORT 0-7093-1
TxDOT PROJECT NUMBER 0-7093

Refined Design Methods for Lean-on Bracing

Aiden Bjelland
Claire Gasser
David Fish
Todd Helwig
Matt Yarnold
Sunghyun Park
Shrey Patel
Stefan Hurlebaus
Matt Hebdon
Michael Engelhardt
Eric Williamson

January 2026
Published August 2026

https://library.ctr.utexas.edu/ctr-publications/0-7093-1.pdf

Technical Report Documentation Page

1. Report No. FHWA/TX-24/0-7093-1	2. Government Accession No.	3. Recipient's Catalog No.
4. Title and Subtitle Refined Design Methods for Lean-on Bracing		5. Report Date Submitted: January 12, 2026 6. Performing Organization Code
7. Author(s) Aidan Bjelland, Claire Gasser, David Fish, Todd Helwig, Matt Yarnold, Sunghyun Park, Shrey Patel, Stefan Hurlebaus, Matt Hebdon, Michael Engelhardt, and Eric Williamson		8. Performing Organization Report No. 0-7093-1
9. Performing Organization Name and Address Center for Transportation Research – Univ. of Texas at Austin 3925 W. Braker Lane, 4th Floor, Austin, TX 78759 Texas Transportation Institute - Texas A&M University 1111 Relis Parkway, Bryan, Texas 77807		10. Work Unit No. (TRAIS) 11. Contract or Grant No. 0-7093
12. Sponsoring Agency Name and Address Texas Department of Transportation Research and Technology Implementation Division 125 E. 11th Street Austin, TX 78701		13. Type of Report and Period Covered Technical Report September 1, 2020 - January 12, 2026 14. Sponsoring Agency Code
15. Supplementary Notes Project performed in cooperation with the Texas Department of Transportation and the Federal Highway Administration.		

16. Abstract

Cross frames are structural elements that are critical for the stability of steel bridges during erection and construction and also play an important role for completed bridges. Historically, the brace locations have been regions of fatigue concerns. In addition, the braces require significant handling and processing during fabrication and represent one of the most expensive components per unit weight on the bridge. Therefore, there are major benefits in terms of economics and structural performance to minimize the number of cross frames. Lean-on bracing concepts that replace full cross frames in certain bracing lines with top and bottom struts that allow a single cross frame to brace several girders is a method of minimizing the number of cross frames on a bridge. Lean-on concepts for bridge applications were developed in the early 2000's on TxDOT study 0-1772. While the previous study developed design guidelines, recent applications of lean-on bracing on TxDOT bridge designs demonstrated the need for improved efficiency and clarity.

The research conducted on this investigation include field monitoring, parametric finite element analyses, and the development of design equations based upon extensive parametric finite element analyses. Results of the research are presented and discussed and refined design methods were developed that provide guidance on effective use of lean-on bracing. The recommendations are demonstrated through design examples.

17. Key Words	18. Distribution Statement
Structural stability, stability bracing, lean-on bracing, cross-frame behavior	No restrictions. This document is available to the public through the National Technical Information Service, Alexandria, Virginia 22312; www.ntis.gov.

19. Security Classif. (of report)	20. Security Classif. (of this page)	21. No. of pages	22. Price
Unclassified	Unclassified	TBD [Total count excl. cover]	

Form DOT F 1700.7 (8-72) Reproduction of completed page authorized

Refined Design Methods for Lean-On Bracing

Aidan Bjelland, Ph.D.
Claire Gasser, Ph.D.
David Fish
Todd Helwig, Ph.D.
Matt Yarnold, Ph.D.
Sunghyun Park, Ph.D.
Shrey Patel
Stefan Hurlebaus, Ph.D.
Matthew Hebdon, Ph.D.
Michael Engelhardt, Ph.D.
Eric Williamson, Ph.D.

CTR and TTI Technical Report:	0-7093-1
Report Date:	Submitted: January 12, 2026
Project:	0-7093
Project Title:	Refined Design Methods for Lean-On Bracing
Sponsoring Agency:	Texas Department of Transportation
Performing Agencies:	Center for Transportation Research at The Univ. of Texas at Austin Texas Transportation Institute at Texas A&M University

Project performed in cooperation with the Texas Department of Transportation and the Federal Highway Administration.

Center for Transportation Research
The University of Texas at Austin
3925 W. Braker Lane, 4th floor
Austin, TX 78759

http://ctr.utexas.edu/

Texas Transportation Institute
Texas A&M University
1111 Relis Parkway
Bryan, Texas 77807

http://tti.tamu.edu

Disclaimers

Author's Disclaimer: The contents of this report reflect the views of the authors, who are responsible for the facts and the accuracy of the data presented herein. The contents do not necessarily reflect the official view or policies of the Federal Highway Administration or the Texas Department of Transportation (TxDOT). This report does not constitute a standard, specification, or regulation.

Patent Disclaimer: There was no invention or discovery conceived or first actually reduced to practice in the course of or under this contract, including any art, method, process, machine manufacture, design or composition of matter, or any new useful improvement thereof, or any variety of plant, which is or may be patentable under the patent laws of the United States of America or any foreign country.

Engineering Disclaimer

NOT INTENDED FOR CONSTRUCTION, BIDDING, OR PERMIT PURPOSES.

Project Engineer: Todd A. Helwig
Professional Engineer License State and Number: Texas No. 94280
P.E. Designation: Research Supervisor

Abstract

Cross frames are structural elements that are critical for the stability of steel bridges during erection and construction and play an important role for completed bridges. Historically, the brace locations have been regions of fatigue concerns. In addition, the braces require significant handling and processing during fabrication and represent one of the most expensive components per unit weight on the bridge. Therefore, there are major economic and structural performance benefits to minimizing the number of cross frames. Lean-on bracing concepts that replace full cross frames in certain bracing lines with top and bottom struts allow a single cross frame to brace several girders is a method of minimizing the number of cross frames on a bridge. Lean-on concepts for bridge applications were developed in the early 2000's on TxDOT study 0-1772. While the previous study developed design guidelines, recent applications of lean-on bracing on TxDOT bridge designs demonstrated the need for improved efficiency and clarity.

The research conducted on this investigation includes field monitoring, parametric finite element analyses, and the development of design equations based upon extensive parametric finite element analyses. Results of the research are presented and discussed and refined design methods were developed that provide guidance on effective use of lean-on bracing. The recommendations are demonstrated through design examples.

Note to Designers

This report includes a wide range of information, including the results of field monitoring, FEA validation, and extensive parametric finite element modelling. While much of this information provides valuable insight into the fundamental behavior of stability bracing and lean-on bracing behavior, readers mainly interested in application to design may find the length of the full report overwhelming. In these cases, readers may find it beneficial to initially focus on specific sections for guidance on design. Specific chapters of interest to design applications consist of 1) Chapter 1 – Introduction, 2) Chapter 2 – Background, 3) Chapter 9 - Refined Design Methodology, and 4) Chapter 10 - Design Examples. Beyond these chapters, which are of paramount importance, Chapters 6, 7, and 8 can provide important information on the development of the design recommendations.

Table of Contents

List of Tables

List of Figures

Chapter 1. Introduction

I-shaped girders are often utilized in steel bridge systems as an efficient and economical solution in a wide range of bridge applications. Steel girders provide significant flexibility for applications in highway bridges because the bridge girders can be fabricated in shorter lengths, shipped to the site, spliced together, and quickly erected. However, the high strength-to-weight ratio of steel often results in relatively slender components that are susceptible to stability-related limit states that must be considered in design. The primary stages for which stability is critical is generally during erection and other construction phases when the steel girders support the entire load and the bracing conditions can be highly variable. The controlling stability limit state is generally lateral-torsional buckling (LTB), which is a failure mode that involves lateral movement of the compression flange and twist of the section, as depicted in Figure 1-1. Stability in the finished bridge is rarely a concern. Once the composite concrete deck has cured, the deck and shear studs provide continuous lateral and torsional restraint to the girder. As a result, conventional LTB is not typically a concern in the completed bridge.

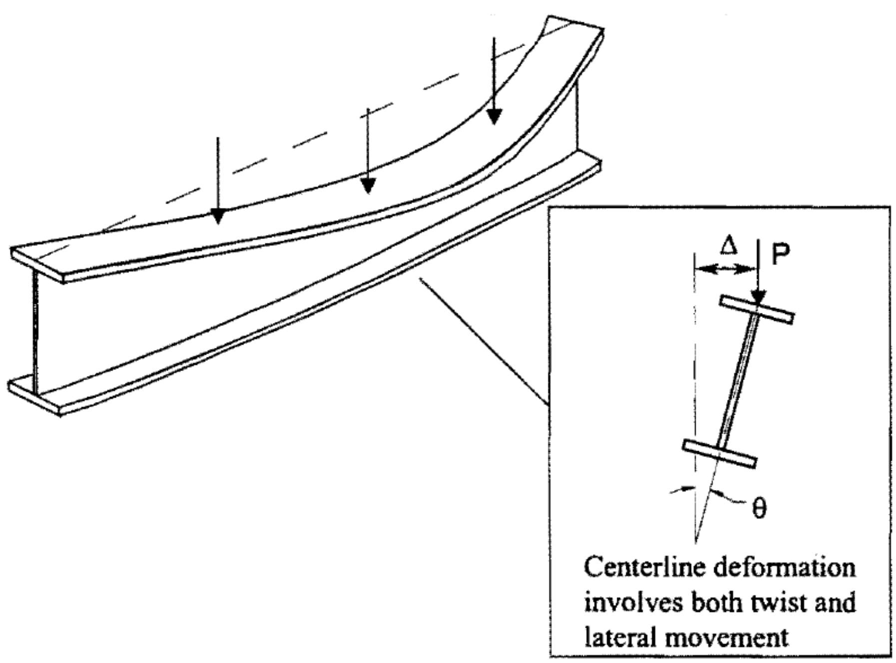

Figure 1-1. Lateral-Torsional Buckling. Adapted from Helwig and Wang (2003)

An increase in the LTB capacity is achieved by providing bracing that reduces the unsupported length of the girders. Effective beam bracing can be achieved by either restraining lateral displacement of the compression flange (lateral bracing), or by controlling the twist of the section (torsional bracing). The most common bracing used in steel bridges consists of cross-frames or diaphragms that control girder twist and therefore are categorized as torsional point braces. Though the braces are necessary for girder stability and other functions, such as restraining fascia girders from torsion applied by deck overhang brackets, they introduce some complexities into the design and require strategic placement along the length and width of the framing system. These complexities range from difficulties during fabrication and erection to concerns regarding the fatigue performance during the service life of the bridge. Due to the significant handling and fabrication requirements, the braces are often the most expensive component of steel bridges per unit weight. Therefore, it is advantageous to refine the design and detailing of cross-frame systems.

The AASHTO LRFD Bridge Design Specification (BDS) (2020) provides design, detailing, and analysis guidance for cross-frames and diaphragms, but this guidance is primarily limited to the fatigue limit state. The 9th edition of the AASHTO LRFD BDS (2020) has no formal guidance on stability bracing requirements of cross-frames and diaphragms, though a recent study that investigated the stability bracing characteristics of conventional cross-frames in steel I-girder systems resulted in recommendations that will be included in the 10th edition of the AASHTO LRFD BDS due out in 2024. However, due to the absence of formal design requirements in all current and previous editions of the AASHTO BDS, the typical practice has been to utilize standard brace details and layouts that are specified by state departments of transportation. Historically, the braces in straight bridges have not generally been sized for stability forces or demands. For example, a common member size in cross-frames specified by many bridge owners is an L4x4x3/8 angle.

For cross-frames in steel bridges, conventional detailing practice is to provide braces between adjacent girders across the full width of the bridge, as shown in Figure 1-2 (A). However, in some applications, such a layout can lead to large live-load induced forces as well as difficulty installing bracing, particularly in bridges with significant support skew. Instead of providing cross-frames across the full width of the bridge, selectively positioning cross-frames within the bridge cross-section and using top and bottom struts to "lean" other girders on the braced locations, as depicted in Figure 1-2 (B), can provide improved behavior and efficiency. This concept is referred to as lean-on bracing. Lean-on concepts are often employed in steel building frames where column bracing may be located in a bay and provide stability to columns in adjacent bays connected through the beams in the frame. In the early 2000s, lean-on concepts were adapted for implementation into steel I-girder bridges (Helwig and Wang, 2003). Lean-on braces offer a cost-effective solution by combining the versatility of a torsional bracing system with the simplicity of a lateral brace. In these systems, torsional braces (typically in the form of cross-frames) are strategically placed throughout the bridge and provide the primary source of stability to the girders. The position of the cross-frame in a given line is usually selected to minimize live-load induced forces or to facilitate installation.

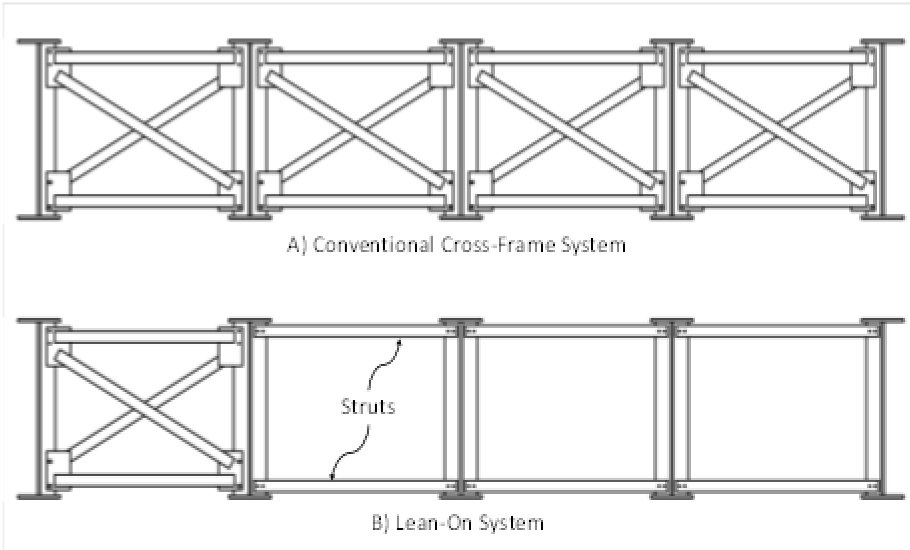

Figure 1-2. Conventional Cross-Frame System (A) versus a Lean-On System (B)

As noted previously, the current AASHTO LRFD provides no guidance on the design of cross-frames for stability bracing requirements. The recently approved AASHTO ballots focus on the stability bracing requirements for conventional bracing; however, lean-on bracing concepts will not be provided in the 10th edition of the AASHTO LRFD BDS. Methods have been developed and documented that aid designers, but some of the simplifications included in the original research may be overly conservative in some instances and unconservative in others. Furthermore, there has been an abundance of research conducted over the past few decades with respect to LTB and the bracing characteristics of cross-frames, but studies related to lean-on systems have been limited outside of the original investigation and implementation.

As noted previously, the current AASHTO LRFD provides no guidance on the design of cross-frames for stability bracing requirements. The provisions approved for inclusion in the 10th edition of AASHTO focus on the stability bracing requirements for conventional bracing. Provisions for lean-on bracing are not included in the 10th edition of the AASHTO LRFD BDS; however, there is interest in inclusion of guidance on lean-on concepts for future editions. Based upon the recommendations from TxDOT project 0-1772 (Helwig and Wang, 2003; Romage, 2008) there have been successful applications of lean-on bracing in bridges with both skewed and normal supports, primarily in the state of Texas. Some of the more recent applications have identified a number of aspects of lean-on bracing that would benefit from additional research. Furthermore, there has been an abundance of research conducted over the past few decades with respect to LTB and the bracing characteristics of cross-frames, but the application towards lean-on systems were not considered. Therefore, the present research investigation was conducted to refine the design process and develop improved guidance on design procedures for wider applications of lean-on bracing.

Some of the factors that are considered for inclusion in the present study include consideration of the effects of girder continuity, non-prismatic girder sections, and the number and location of cross-frames in a given bracing line. Though these do not comprise a complete list of the areas that may benefit from refinement, they do serve as an initial scope for the background studies reviewed in this research. The focus of this research is to study the behavior of lean-on bracing systems with the goal of refining and improving guidance that will allow designers to implement lean-on bracing more easily into steel bridge designs. If properly detailed and distributed along the bridge length and width, lean-on bracing systems can reduce the number of full cross-frames required while potentially improving the long-term bridge behavior. A well-designed and detailed lean-on bracing system potentially offers significant savings in fabrication costs, simplifies the erection process, and alleviates in-service cross-frame force demands in heavily skewed bridges. In short, the strategic use of lean-on braces can serve as an efficient alternative to traditional cross-frame systems.

The research methods utilized in this report include field monitoring and testing of bridges with lean-on bracing as well as parametric finite element analyses to provide data that provide insight into the refinement of lean-on bracing design methodologies. The report has been divided into 12 chapters. Following this introductory chapter, a review of the literature and pertinent background information is provided in Chapter 2. Results from the field instrumentation and testing of three bridges with lean-on bracing are provided in Chapter 3. The results from the field monitoring and tests provided valuable data for the validation of FEA models of lean-on bracing systems, which is summarized in Chapter 4. Chapter 5 provides a rationale behind the inclusion of lean-on bracing to reduce brace stresses under live load to improve fatigue performance. The next four chapters provide results from the parametric investigation on specific aspects related to lean-on bracing behavior. Chapter 6 outlines the results of the investigation targeted at recommendations related to the layout of cross-frames in lean-on bracing applications. While there are multiple components that comprise the total system stiffness, the results from computational studies targeting brace stiffness requirements in lean-on applications are covered in Chapter 7. Improvements on the girder in-plane stiffness behavior of both conventional lean-on bracing systems were developed and is summarized in Chapter 8. Chapter 9 focuses on the total system stiffness. The brace strength requirements are then covered in Chapter 10. Finally, Chapter 11 outlines the proposed design methodology for lean-on bracing systems and Chapter 12 provides an overview of the research contributions.

Chapter 2. Background

2.1. Introduction

The limit state of lateral-torsional buckling (LTB) is a critical consideration in steel I-girder bridges. Although the LTB resistance can be improved by increasing the section properties (by way of adjusting the girder proportions), the most efficient means of increasing the resistance is to reduce the unbraced length. For individual girders, the unbraced length is the distance between bracing locations, which often varies during the erection process. Effective bracing can be achieved by controlling the lateral movement of the compression flange (lateral bracing) or by controlling the twist of the section (torsional bracing). This chapter outlines the past research that is most pertinent to the present study. Although lateral bracing will be briefly reviewed, the most common form of bracing in steel girder applications are either cross-frames or diaphragms, which are categorized as torsional braces since these elements restrain girder twist. Therefore, the primary focus of this report is directed at torsional bracing provided by cross-frames or diaphragms.

The following sections provide background information on the dual criteria for stiffness and strength of braces. Pertinent solutions for determining the lateral-torsional buckling resistance are presented, as well as expressions for the brace stiffness and strength requirements, with an emphasis placed on recent research developments. Current bracing design provisions are discussed, followed by an overview of lean-on bracing adaptations to these provisions developed by Helwig and Wang (2003). The final section is dedicated to potential areas of investigation regarding the applicability of the presented background information to the current research project.

2.2. Lateral Torsional Buckling

As depicted previously in Figure 1-1, LTB involves a lateral translation of the compression flange and a twist of the girder. The buckling behavior is often characterized as occurring between the brace locations. However, depending on the specific systems, the buckled shape may include either occur between the brace locations or along the entire system length, which are discussed in the following sections.

2.2.1. Lateral-Torsional Buckling of I-Shaped Girders

The first mode of buckling is the buckling of an unbraced section, or buckling between brace points as exhibited in Figure 2-1.

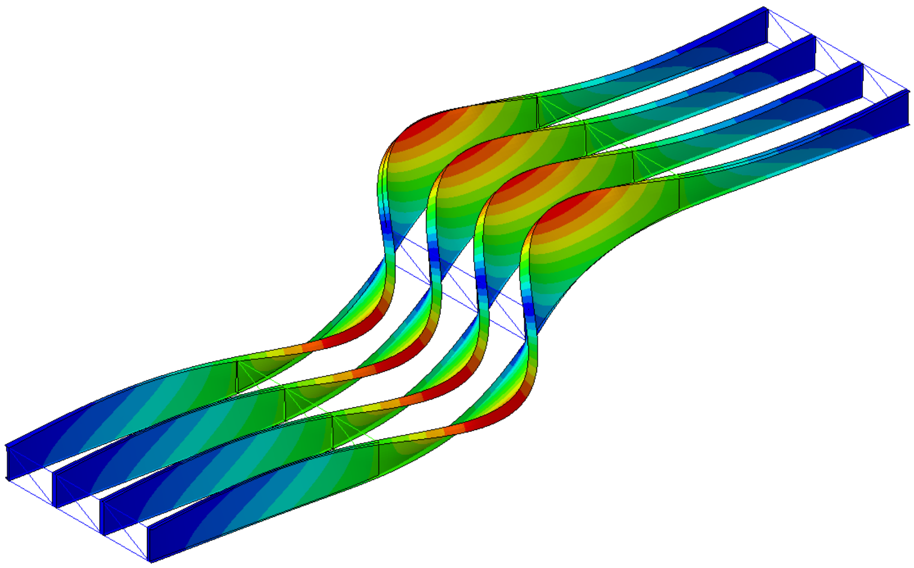

Figure 2-1. Girder System Buckling between Brace Points

Timoshenko and Gere (1961) provide the following elastic solution for a doubly-symmetric section with warping stiffness subjected to uniform moment along the unbraced length, which is given by Equation 2.1.

$$M_{cr} = \frac{\pi}{L_b}\sqrt{EI_yGJ + \frac{\pi^2 E^2 C_w I_y}{L_b^2}} \qquad 2.1$$

Where:

M_{cr} is the buckling moment

L_b is the unbraced length

E is the modulus of elasticity

I_y is the weak-axis moment of inertia

G is the shear modulus of elasticity

J is the torsional constant

C_w is the torsional warping constant, $\frac{I_y h_0^2}{4}$ for a doubly-symmetric I-shaped sections

h_0 is the distance between flange centroids

The two terms under the radical in Equation 2.1 each represent a different aspect of the torsional stiffness. The first term is referred to as the St. Venant torsional resistance and is related to the uniform torsional stiffness. The second term is related to the non-uniform torsional stiffness and is referred to as the warping torsional resistance. In the original derivation of Equation 2.1, Timoshenko stated that twist and lateral deformation were restrained at the ends of the unbraced length; however, only the boundary condition of zero twist was actually enforced in the derivation. Therefore, solely preventing the twist of the cross-section results in effective bracing against LTB. Bracing can also be achieved by stopping the lateral deformation of the compression flange (lateral bracing), which also essentially stops the twist of the section since the lateral deformation of the compression element generally leads to twist of the section.

As stated above, Equation 2.1 was derived for the case of uniform moment loading. When the loading applied to the beam produces non-uniform moment loading, the buckling capacity can be significantly larger than that given by Equation 2.1. Although solutions can be derived for specific load cases, the benefits of moment gradient in design are typically accounted for by using moment gradient factors denoted by the variable (C_b). There are a variety of C_b factors available to approximate the benefits of moment gradient. Expressions for C_b are provided in AASHTO LRFD (2020) and AISC . Equation 2.2 is the equation found in AASHTO LRFD Appendix A6, and Equation 2.3 is the specification provided in AISC Chapter F for C_b.

$$C_b = 1.75 - 1.05\left(\frac{M_1}{M_2}\right) + 0.3\left(\frac{M_1}{M_2}\right)^2 \leq 2.3 \qquad 2.2$$

Where:

M_1 is the smaller end moment

M_2 is the larger end moment

Equation 2.2 is intended to be applied to straight-line moment diagrams and the AASHTO Bridge Design Specifications (BDS) has included a number of rules for determining the values of M_1 and M_2 so that the expression can be used for "general" moment diagrams. These rules are not covered in this report since there is a great deal of work ongoing to incorporate more accurate C_b factors. The 10th edition of the AASHTO BDS will incorporate the expression used in the AISC specification, as well as additional solutions for non-prismatic girders in the Appendix. One option for non-prismatic girders makes use of a form of the AISC Cb for singly-symmetric sections as well as a method of converting the non-prismatic section to an effective prismatic section (Reichenbach *et al.*, 2020).

Equation 2.3 is independent of the shape of the moment diagram and as noted below makes use of the absolute value of all moments.

$$C_b = \frac{12.5M_{max}}{2.5M_{max}+3M_A+4M_B+3M_C} \qquad 2.3$$

Where:

M_{max} is the absolute value of the maximum moment within the unbraced segment (L_b)

M_A is the absolute value of the moment at the quarter point of the unbraced segment

M_B is the absolute value of the moment at the centerline of the unbraced segment

M_C is the absolute value of the moment at the three-quarter point of the unbraced segment

2.2.2. System (Global) Lateral-Torsional Buckling

The system, or global, mode of buckling has been studied based upon work originally documented by Yura et al. (2008). The work related to system buckling and was initiated following the collapse of the Marcy Pedestrian bridge, which was a single cell steel tub girder with no top lateral truss. However, following the study of the behavior of the tub girder bridge, a number of problems were identified on farrow I-girder bridges.

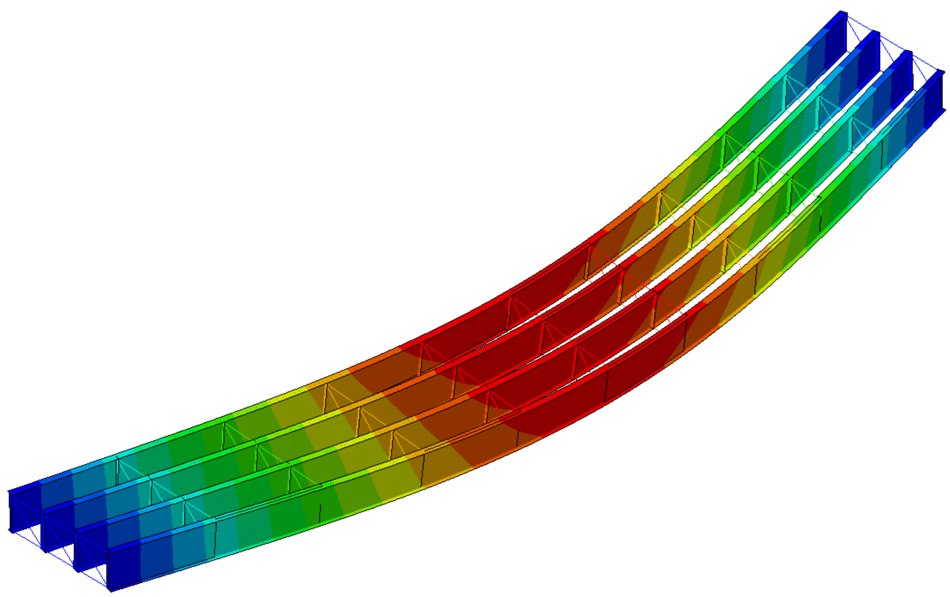

Figure 2-2. Girder System Globally Buckling

System LTB occurs when the girder system is interlinked by braces, such as cross-frames, and the overall system buckles as a unit as illustrated by Figure 2-2. This mode often becomes more critical than conventional LTB (buckling between brace points) in narrow girder systems with larger L/W ratios where L= the span and W= the girder system width. Yura et al. (2008) developed an expression for the elastic global buckling resistance of a doubly-symmetric twin I-girder system, which is shown in Equation 2.4:

$$M_g = \frac{\pi^2 SE}{L^2}\sqrt{I_y I_x} \qquad 2.4$$

Where:

M_g is the elastic global buckling resistance

S is the spacing between the two exterior girders

L is the span length

I_y is the weak-axis moment of inertia of a single girder

I_x is the strong-axis moment of inertia of a single girder

This expression assumes a simply supported, prismatic system. Although Yura et al. (2008) included a slightly more complex solution which included both St. Venant and Warping terms, the St. Venant term does not significantly impact the behavior. Neglecting this term produces the simple expression shown in Equation 2.4. Although the solution was derived for doubly-symmetric sections, when considering singly-symmetric sections, I_y in Equation 2.4 can be replaced with I_{eff} as defined by Equation 2.5 (Yura *et al.*, 2008):

$$I_{eff} = I_{yc} + \frac{t}{c} I_{yt} \tag{2.5}$$

Where:

I_{yc} is the lateral moment of inertia of the compression flange

I_{yt} is the lateral moment of inertia of the tension flange

t is the distance from the centroid of the tension flange to the neutral bending axis

c is the distance from the centroid of the compression flange to the neutral bending axis

Equation 2.4 was originally introduced into the interim AASHTO specifications in 2015. An upper limit of 50% of the value given by Equation 2.4 was adopted into AASHTO due to the potential issues related to second-order effects that could lead to large deformations and 2nd order forces (Sanchez and White, 2012). For cases with moments exceeding 50% of M_g, changes in the girder sections or additional bracing were necessary. Subsequently, bridge owners found systems that had previously been constructed with no problems could not be constructed with the new provisions. Therefore, additional work was conducted by Han and Helwig (2016, 2020) considering the effects of girder continuity, imperfections and non-prismatic sections. Their work led to the following expression:

$$M_{gs} = C_{bs} M_g = C_{bs} \frac{\pi^2 SE}{L^2} \sqrt{I_{eff} I_x} \tag{2.6}$$

Where:

M_{gs} is the modified elastic global buckling resistance

C_{bs} is the system mode moment gradient factor:

1.0 for simply supported or partially erected continuous girder systems

2.0 for fully erected continuous girder systems

In addition to the moment gradient factors, the work in Han and Helwig (2016, 2020) raised the limit on the design moment (M_u) to 70% of M_{gs}, which is the current limit in AASHTO LRFD (2020). The increase was justified by Han and Helwig (2016, 2020) based on the assumed critical imperfection versus the more likely value in erected girder systems with cross-frames fully installed. The critical shape is often assumed to include a lateral sweep of the compression flange with no sweep in the tension flange; however, such an imperfection would not generally be permissible with cross-frames installed. The more likely imperfection of a girder system with cross-frames installed consists of a "pure sweep" imperfection, which is much less sensitive to second-order amplification. While the primary focus of the work in this report is related to effective cross-frame design with lean-on applications, the system mode of buckling can occur in many systems and will be shown in subsequent results. The next section of this report is focused on stability bracing requirements for I-shaped girders.

2.3. Stability Bracing Requirements

Bracing systems are important structural elements in steel I-girder bridges. These systems provide resistance to lateral-torsional buckling (LTB) in straight girder systems by reducing the unbraced length of its members. The stage at which LTB is typically most critical is during either the erection of the members or the placement of the concrete bridge deck. Although construction of the bridge deck is usually the most critical stage, the condition during erection may also be critical. During this time, frequent situations arise when not all of the bracing is installed, leading to larger unbraced lengths as compared to the case during deck construction. In both cases, the non-composite steel girders must resist all construction loading. The braces also aid in resisting the torsion applied to the girders due to the eccentric loading of deck overhang construction. In addition, the cross-frames help to distribute any lateral loads, such as wind loads, across the structure.

This section provides background information on the general bracing needs of I-girders as well as an introduction to the development of the current stability bracing requirements of both torsional and lateral bracing systems.

2.3.1. General Bracing Requirements

The reality that stability braces need to have both adequate stiffness and strength was first demonstrated by Winter (1960). Winter utilized a model consisting of a column and lateral bracing system, which was comprised of perfectly straight rigid links that were hinged at the points of bracing. The lateral bracing was represented as a spring with stiffness measured in units of force per unit displacement. Winter's model provided a simple means of determining the "ideal brace stiffness," which can be defined as the minimum required brace stiffness to force a perfectly straight member to buckle between the braced locations. Another benefit of this model was that the effects of imperfections could readily be investigated. Winter's work demonstrated that when accounting for imperfections, the stiffness required to control brace forces and member deformations was higher than that of the ideal stiffness. As a result, most bracing provisions currently recommend using two times the ideal stiffness. The assumption is that if twice the ideal stiffness is used, then deformations will be limited to the initial imperfection imposed. In general, stability-induced forces within the brace are directly related to the magnitude of the initial imperfection (Yura, 2001). Although Winter's work focused on lateral bracing systems, the dual criteria of stiffness and strength are valid for all stability bracing systems, including torsional beam bracing.

The imperfection that produces the largest brace force generally will have one less "wave" than the unbraced section's buckled shape. For example, with one intermediate brace, the critical imperfection is generally a half-sine curve, while for two intermediate braces the critical imperfection is generally a full sine curve, etc. (Helwig and Wang, 2003).

The initial imperfection assumed in the development of the current AISC design provision expressions is an assumption based on allowable fabrication and construction tolerances for girder out-of-straightness, as established by the AISC Code of Standard Practice (2017). The effect of initial imperfections on torsional bracing was studied by Wang and Helwig (2005). They demonstrated that, in bridge girders, the critical imperfection (i.e., the imperfection that maximizes force demands on the braces) usually involves a lateral sweep of the compression flange, with the tension flange remaining straight. This effectively produces an initial twist of the cross-section. As a result of that research, the initial out-of-straightness of the compression flange is assumed to be $\frac{L_b}{500}$. If the tension flange is assumed straight, the resulting initial imperfection (twist), as defined in AISC (2017), is:

$$\theta_0 = \frac{L_b}{500h_0} \qquad 2.7$$

Where:

L_b is the unbraced length of the girder section

The initial imperfection, θ_0, in Equation 2.7 comes from work documented in Wang and Helwig (2005) that demonstrated the critical shape imperfection involves a lateral translation of the compression flange at the brace location while the bottom flange remains straight. In addition to the critical shape imperfection, Wang and Helwig (2005) also demonstrated the critical location of the imperfections. In general, the largest brace force is created when the maximum twist occurs in the cross frame located near the point of maximum moment. A typical imperfection that was used in the studies is shown in Figure 2-3. The imperfection was modified slightly to provide a slight asymmetry to the shape, similar to the work recommended by Prado and White (2015) and also used by Liu and Helwig (2020) in a study related to torsional brace strength requirements.

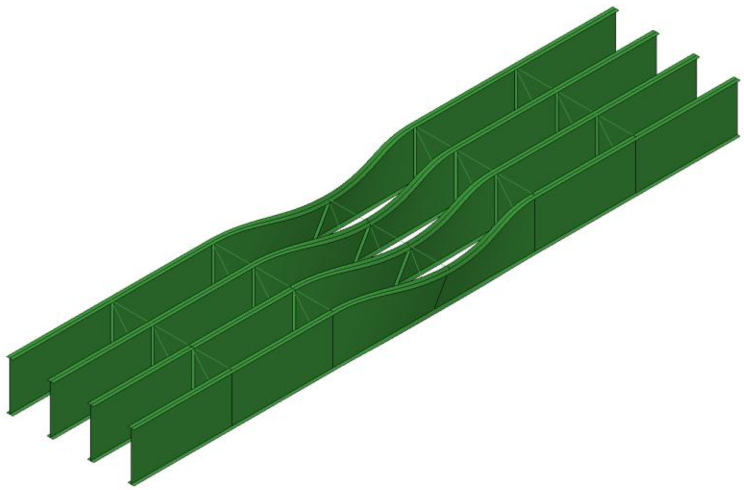

Figure 2-3. Exaggerated Shape of Critical Imperfection Located in Maximum Moment Region

While the goal of an effective stability bracing system is for the girder to buckle between the brace points, narrow girder systems are susceptible to the system buckling mode discussed in the previous sections (Yura *et al.*, 2008; Han and Helwig, 2016) and incorporated into the AASHTO Bridge Design Specifications (BDS) The imperfections utilized by Han and Helwig provided guidance for the current study. While the studies focusing on critical brace forces generally used an imperfection similar to that shown in Figure 2-3, in some cases, the behavior of the system mode was studied, and the imperfections from Han and Helwig were of interest.

The fundamental necessity of beam stability bracing is to resist the tendency of the girder to twist. This can be accomplished by providing adequate torsional and/or lateral bracing. The subsequent sections provide the background on the current torsional and lateral bracing requirements as well as introduce some recent developments that point toward new provisions that are likely to be adopted in the future.

2.3.2. Torsional Bracing Requirements

Taylor and Ojalvo (1966) quantified the buckling capacity of a doubly-symmetric beam with continuous torsional bracing under uniform moment loading:

$$M_{cr} = \sqrt{M_0^2 + \bar{\beta}_b E I_y} \tag{2.8}$$

Where:

M_0 is the buckling capacity of the beam with no intermediate (between supports) bracing (equivalent to M_{cr} from Equation 2.1 using full beam span length, L)

$\bar{\beta}_b$ is the continuous torsional brace stiffness

Further research by Yura (1992, 2001) expanded the applicability of this equation to consider discrete torsional braces, moment gradient, load position, singly-symmetric sections, and the impact of cross-sectional distortion:

$$M_{cr} = \sqrt{C_{bu}^2 M_0^2 + \frac{C_{bb}^2}{C_T} \bar{\beta}_T E I_{eff}} \leq M_y \; or \; M_{bp} \qquad 2.9$$

Where:

C_{bu} is the C_b factor corresponding to a beam with no intermediate braces

C_{bb} is the C_b factor corresponding to a beam fully braced at intermediate brace locations

C_T is the top flange loading modification factor:

1.0 for centroidal loading

1.2 for top flange loading

$\bar{\beta}_T$ is the equivalent effective continuous torsional brace stiffness = $\beta_T * \frac{n}{L}$

β_T is the torsional stiffness provided by a single brace

n is the number of intermediate braces

L is the span length

M_y is the yield moment (this can be replaced by the plastic moment capacity)

M_{bp} is the buckling capacity of the girder when buckling occurs between the brace points

By rearranging Equation 2.9, the ideal stiffness for continuous torsional bracing can be obtained as shown in Equation 2.10.

$$\bar{\beta}_{Ti} = (M_{cr}^2 - C_{bu}^2 M_0^2) \frac{C_T}{C_{bb}^2 E I_{eff}} \qquad 2.10$$

Adjusting for discrete torsional bracing, the ideal stiffness can now be written in terms of the continuous torsional bracing stiffness, as shown in Equation 2.11.

$$\beta_{Ti} = \frac{\bar{\beta}_{Ti} L}{n} \qquad 2.11$$

In the bracing provisions of Appendix 6 of the AISC Specification (2017), the buckling capacity of the unbraced beam (M_0) is conservatively neglected. Taking this into account and substituting Equation 2.10 into Equation 2.11 results in Equation 2.12 for the ideal stiffness of a discrete torsional brace:

$$\beta_{Ti} = \frac{C_T L M_{cr}^2}{n E I_{eff} C_b^2} \qquad 2.12$$

Finally, assuming top flange loading ($C_T = 1.2$) and adjusting for twice the ideal stiffness by setting the buckling capacity (M_{cr}) equal to the factored design moment (M_u) results in Equation 2.13 for required brace stiffness as shown in AISC (2017):

$$\beta_{Treq} = \frac{2.4 L M_u^2}{\varphi n E I_{eff} C_b^2} \qquad 2.13$$

Where:

φ is 0.75 (LRFD)

Assuming that the brace stiffness is sufficient to limit the deformation to the initial twist, the relationship between the brace stiffness and brace moment can be described by Equation 2.14.

$$M_{br} = \beta_{Treq}\theta_0 = \frac{2.4 L M_u^2}{\varphi n E I_{eff} C_b^2}\frac{L_b}{500 h_0} \qquad 2.14$$

The use of twice the ideal stiffness works well for columns, but for beams stabilized by torsional braces, recent work by Liu and Helwig (2020b) found that a higher stiffness was required to limit the deformation to that of the initial imperfection. The recommendation of their research was to increase the stiffness requirement for torsional bracing to three times the ideal stiffness. The 2022 AISC Specification increased the required torsional brace stiffness to three times β_{ideal}, resulting in a constant of 3.6 instead of 2.4. The AASHTO bracing provisions permit two times β_{ideal} (resulting in expressions identical to Equations 2.13 and 2.14) provided the depth of the torsional brace is at least 80% of the beam depth.

Expressions based upon a moment of the stiffness times the initial imperfection such as that shown in Equation 2.14 are similar to past editions of AISC. In the 2017 AISC Specification, strhength provisions for M_{br} were changed to two percent of the beam design moment based off of work by Prado (2015). However, this approach was found to produce unconservative brace strength estimates in many cases was recently found to be unconservative in many cases (Liu and Helwig, 2020). Therefore, the 2022 AISC strength provisions returned to a required torsional brace strength equal to the stiffness times the initial imperfection similar to what was shown in Equation 2.14.

Therefore, to summarize the current 2022 AISC brace provisions require a stiffness equal to 3 x beta ideal (constant of 3.6 instead of 2.4 in Equation 2.13) and a strength requirement equal to the stiffness x the assumed initial imperfection ($L_b/500h_o$). The 10th edition AASHTO bracing provisions for required strength and stiffness are identical to the AISC specification for torsional brace depths less than 80% of the beam web depth. Provided a brace depth of at least 80% of the beam depth is utilized, the 10th Ed. AASHTO bracing provisions require a stiffness of twice the ideal stiffness (constant of 2.4 in stiffness equation) and a strength equal to the stiffness x the assumed initial imperfection ($L_b/500h_o$).

2.3.3. Lateral Bracing Requirements

While the last section focused on the requirements for braces that restrain the twist of the section, an alternative approach to effective bracing is to provide bracing that restrains lateral displacement of the compression flange. Thus, beam bracing is typically characterized as either torsional bracing or lateral bracing. While discrete torsional braces such as cross-frames are traditionally utilized in bridge applications, lateral bracing is also sometimes used during construction or in the completed bridge. For example, erectors may choose to provide lateral bracing in the form of guy cables. In addition, flange level lateral trusses are often used for bracing to restrain wind loads. The 10th edition AASHTO bracing provisions also permit lateral braces form sources like the trusses to be used to reduce the stiffness requirements of the torsional beam bracing.

Lateral braces, as the name suggests, restrain out-of-plane lateral displacement of the compression flange, thereby forcing the beam to buckle between the respective brace points. Lateral bracing systems in bridge applications are categorized as either relative (also referred to as panel) bracing or discrete (also referred to as point or nodal) bracing. Lateral truss systems that restrain a compression flange are the primary example of relative bracing.

The strength of a beam braced laterally by discrete or continuous bracing is given by Equation 2.15 (Yura, 1992).

$$M_{cr} = \sqrt{\left[(C_{bu}M_0)^2 + \left(C_{bb}P_{yc}h_0\right)^2 A_d\right](1 + A_d)} \qquad 2.15$$

Where:

M_{cr} is the strength of a beam braced laterally by discrete or continuous bracing

C_{bu} is the C_b factor assuming the beam is unbraced

M_0 is the uniform moment buckling solution

P_{yc} is the beam compressive flange force $= \frac{\pi^2 EI_{yc}}{L^2}$

A_d is the bracing factor $= L\sqrt{\frac{.17\overline{\beta_L}}{C_L P_{yc}}}$

C_L is the loading factor

$1 + \frac{1.2}{n}$ for top flange loading

1.0 for centroid or uniform moment loading

n is the number of discrete braces

I_{yc} is the out-of-plane moment of inertia of the compression flange

d is the beam depth

L is the span length

J is the St. Venant torsional constant

The M_{cr} equation can be rearranged to solve for the required effective continuous lateral brace stiffness, $\bar{\beta}_L$. Then, the required discrete brace stiffness, β_L, can be found by rearranging Equation 2.16:

$$\bar{\beta}_L = \frac{\beta_L \times (\#\ discrete\ braces)}{\alpha L} \qquad 2.16$$

Where:

β_L is the discrete lateral brace stiffness

α is 0.75 for one midspan brace or 1.0 for two or more braces

Based on the assumption that the brace stiffness is sufficient to limit the deformations to the assumed value of $\frac{L_b}{500}$, the required strength of a discrete lateral bracing system is calculated using Equation 2.17 (Yura, 2001):

$$F_{br} = \frac{0.01 C_L C_d M_f}{h_0} \qquad 2.17$$

Where:

C_d is the modification factor for reverse-curvature bending given by Equation 2.18

M_f is the maximum factored beam moment along the length of the span

A modifying factor for double curvature of 1.0 is used for beams in single curvature. For beams with inflection points along the span, i.e. double-curvature, Equation 2.18 is used (Yura, 2001):

$$C_d = 1 + \left(\frac{M_s}{M_L}\right)^2 \qquad 2.18$$

Where:

M_s, M_L are maximum moments causing compression in the top and bottom flanges as shown in Figure 2-4.

The lateral beam bracing formulations in the AISC Specification (2022), assume top flange loading and therefore take $C_L = 2.0$. In addition, instead of using the expression shown in 2.18, the AISC provisions simply use C_d = 2.0 if the beam is subjected to reverse curvature. A lateral brace is required on each flange on either side of inflection points since both flanges are subjected to compression.

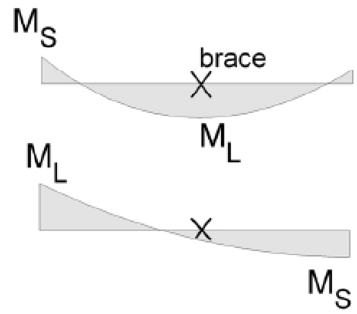

Figure 2-4. Maximum Moment Locations for C_d. Adapted from Yura, 1992

2.3.4. Combined Bracing Effect

Yura (1992) suggests that combined torsional and lateral bracing is more effective than torsional or lateral bracing alone. Combining the equations for lateral and torsional bracing (Equations 2.9 and 2.15) using linear superposition results in a conservative approach.

Tran (2009) found through elastic eigenvalue buckling studies that bracing stiffness interactions vary depending on the sign of the bending moment. Light lateral bracing in combination with torsional bracing was found to be most effective in reducing torsional bracing demands.

Prado (2015) built on the work done by Tran (2009) and agrees with the linear superposition proposed by Yura (1992) for positive moment cases, but suggests that negative moment cases require that the torsional brace stiffness be twice the nodal lateral stiffness value. In the case where the laterally-braced top flange is in tension and the bottom flange is in compression, the upper lateral brace provides negligible benefit. Additionally, the torsional brace effectively becomes a lateral brace to the bottom compression flange, which increases the minimum torsional bracing stiffness requirement. However, this increase was found to be unlikely to exceed the minimum required lateral stiffness.

Trahair and Nethercot (1984) developed a more complicated equation that offers greater accuracy for combined lateral and torsional bracing for doubly-symmetric beams subjected to uniform moment. This approach will be utilized in this study.

2.4. Traditional Cross Frame Design

As outlined in the previous section, effective stability bracing systems must satisfy both stiffness and strength requirements. While the previous section highlighted the stiffness and strength requirements of the torsional bracing system, the system stiffness is a function of a number of different components. This section focuses on the torsional bracing requirements considering the different components for conventional bracing applications.

2.4.1. Torsional Bracing System Stiffness

The total system stiffness for torsional bracing is primarily comprised of three components, including: the brace stiffness, in-plane girder stiffness, and cross-section distortional stiffness. Like many stability bracing systems, the total stiffness is governed by the expression for springs in series. The total stiffness of a torsional bracing system can therefore be expressed using the following expressions (Yura, 1992):

$$\beta_T \geq \beta_{Treq'd} \qquad 2.19$$

$$\frac{1}{\beta_T} = \frac{1}{\beta_b} + \frac{1}{\beta_g} + \frac{1}{\beta_{sec}} \qquad 2.20$$

Where:

β_T is the total brace stiffness of the torsional system

β_b is the stiffness of the brace

β_g is the in-plane girder stiffness

β_{sec} is the stiffness of the cross section related to cross sectional distortion

Equation 2.20 indicates that β_T is less than the smallest of the three individual stiffness components, which are assumed to interact as springs in series. From this relationship, it is evident that an otherwise stiff cross-frame can be adversely affected by poor in-plane girder stiffness or significant distortional effects in the girder webs. Thus, the overall stiffness of a torsional brace is effectively limited by the most flexible component in Equation 2.20.

In design, the required torsional brace stiffness, β_{Treq}, is found by using expressions such as those provided in Equation 2.13. To serve as an adequate brace, the cross frame and its connections shall be designed and detailed such that β_T exceeds β_{Treq}. Satisfying this requirement, in addition to the corresponding strength requirements, ensures that a cross frame or diaphragm can act as a suitable brace point and, in turn, enhance the LTB resistance of the girder.

2.4.1.1. Torsional Brace Stiffness, β_{br}

The most common form of bracing in steel bridge applications are the use of torsional braces consisting of cross-frames or diaphragms to ensure adequate LTB resistance. Without the stiffness contribution of braces, the girders will deform in a "racking" shape, as shown in Figure 2-5.

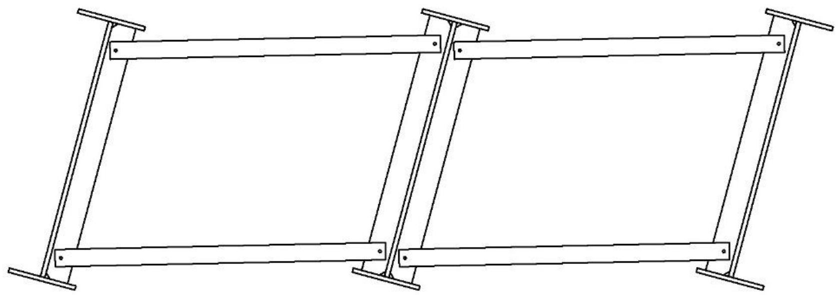

Figure 2-5. Racking Deformation Caused by no Torsional Bracing

Different cross-frame geometries are utilized such as X-shapes, K-shapes, and occasionally Z-shapes. (Figure 2-6) X-type braces work well with deep girders, such as in built-up I-girder bridges, while K-type braces or diaphragms may be better suited for shallower girders. It is recommended that the angle of the diagonals are configured with a slope close to a 45-degree angle with the bottom strut. Significantly flatter or steeper slopes often reduce the effectiveness of the brace. The torsional stiffness (i.e., the stiffness response of the brace when subjected to an in-plane moment) of the brace can be estimated based on an idealized truss model (Yura, 2001; Helwig and Wang, 2003). As an example, Equation 2.21 is used to estimate the torsional brace stiffness of a Z-type cross-frame or a tension-only X-type cross frame, for which the compression diagonal is considered ineffective at resisting loads. Equation 2.22 and 2.23 provide the expressions for X-type and K-type cross frames assuming the members can support compression.

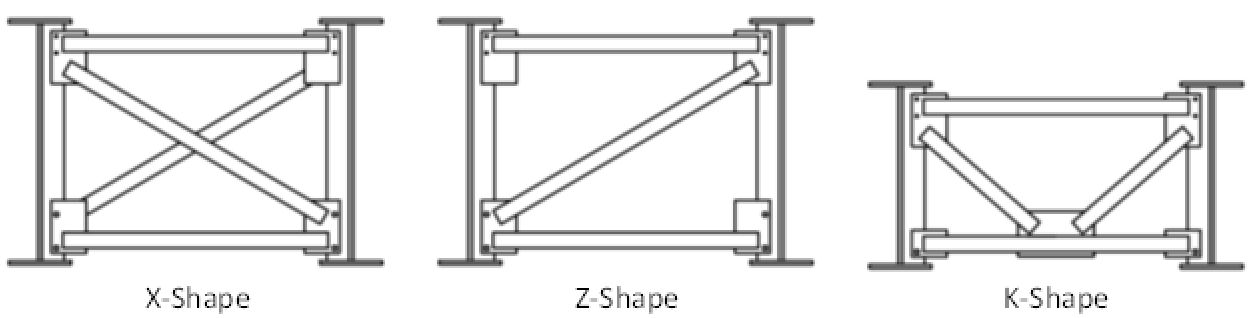

Figure 2-6. Various Forms of Cross-Frames

In many cases, cross-frames are constructed with slender angle sections whose compression load-carrying capacity is negligible.

$$\beta_{b,Z} = \frac{ES^2h_b^2}{\frac{2L_d^3}{A_d}+\frac{S^3}{A_h}} \qquad 2.21$$

$$\beta_{b,X} = \frac{ES^2h_b^2A_d}{L_d^3} \qquad 2.22$$

$$\beta_{b,K} = \frac{2ES^2h_b^2}{\frac{8L_d^3}{A_d}+\frac{S^3}{A_h}} \tag{2.23}$$

Where:

S is the girder spacing

h_b is the depth of the cross-frame

L_d is the length of the cross-frame diagonal members

A_d is the cross-sectional area of the cross-frame diagonals

A_h is the cross-sectional area of the cross-frame struts

The derivation of expressions such as Equation 2.21 are based on a truss analogy which relies on the axial stiffness of the strut and diagonal members of the cross-frame. Although not explicitly presented, the inherent flexibility of the connections should also be considered in the evaluation of the overall brace stiffness, similar to what is done for cross-section distortional effects or in-plane girder flexibility.

For many cross-frame applications, single-angle or tee sections are attached to connection or gusset plates along only one leg or flange, respectively. This, in turn, introduces an eccentric load path through the connection that can significantly impact the stiffness of the brace. In lieu of a more refined assessment of these softening effects, AASHTO LRFD (2020) recommends a simple reduction factor based on experimental and analytical studies conducted by Battistini et al. (2013, 2016) and Wang (2013). For stability bracing applications during construction, a reduction factor of 0.65 is recommended. Based upon recommendations in Reichenbach et al. (2021) a reduction factor of 0.75 is recommended for the cross-frames in the composite structure when evaluating behavior such as live load induced forces for evaluating fatigue performance. These reduction factors can be applied to the cross-sectional area of the diagonals and struts in the development of Equation 2.21. This reduction factor was calibrated to represent these softening effects for a wide range of common cross-frame configurations, connections, and member sizes. Alternatively, similar accuracy was achieved by modelling the cross-frame members as beam elements and specifying the eccentricity of the angle or WT member directly in a 3D model of the bridge during construction or in-service (Park et al. 2023).

2.4.1.2. In-Plane Girder Stiffness, β_g

The in-plane (i.e., vertical) flexural stiffness of the bridge girders themselves contribute to the overall stiffness of the torsional bracing system. The stiffness contribution of the girders was first shown in twin-girder systems (Helwig, Yura and Frank, 1993). As shown in Figure 2-7, when the girders are subjected to a twist, the internal moment in the cross-frame is equilibrated by vertical shear forces acting at the ends of the brace. The vertical shear forces on the adjacent girders cause one girder to deflect upwards and the other to deflect downwards leading to a rigid body rotation.

These deformations reduce the effectiveness of the brace. With a wider system, this displacement is reduced, as demonstrated by the four-girder system shown in the figure.

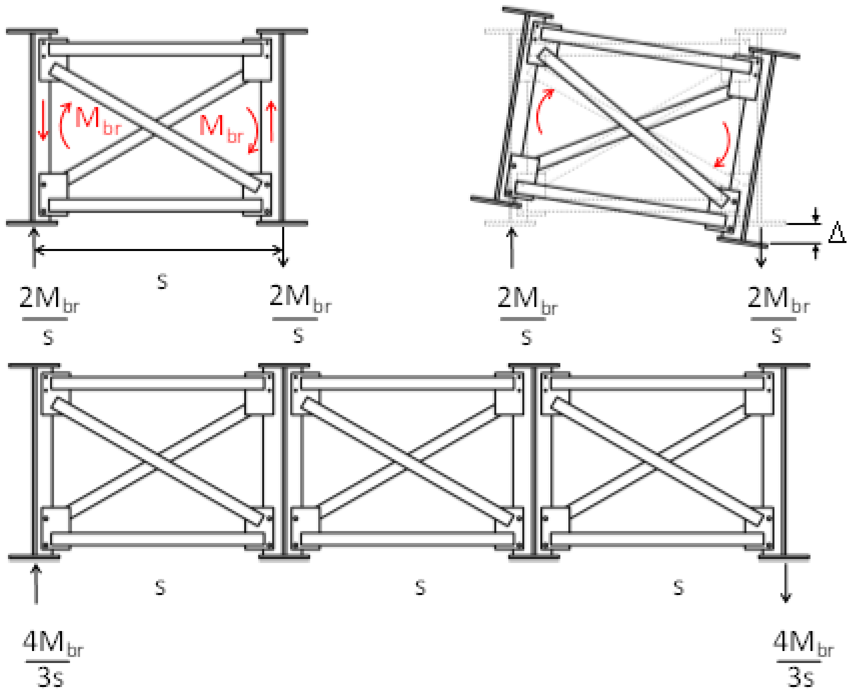

Figure 2-7. In-Plane Girder Stiffness

This behavior was quantified for a twin-girder system in Equation 2.24 (Helwig, Yura and Frank, 1993):

$$\beta_g = \frac{12s^2EI_x}{L^3} \qquad 2.24$$

Where:

I_x is the in-plane moment of inertia of the girder

L is the span length

For a framing system with more than two girders, Equation 2.25 is instead used (Yura, 2001; Helwig and Yura, 2015):

$$\beta_g = \frac{24(n_g - 1)^2 s^2 E I_x}{n_g L^3} \qquad 2.25$$

Where:

n_g is the number of girders in the system

The in-plane girder stiffness contribution is most critical in narrow systems, such as two or three-girder bridges, and is tied to the system buckling mode, which was discussed in Section 2.2.2 (Yura *et al.*, 2008; Han and Helwig, 2016). If β_g is less than β_{Treq}, full bracing cannot be achieved regardless of the stiffness of the brace that is utilized. From a buckling perspective, the system mode will control over buckling between the brace points. As noted earlier, design guidance for the system failure mode has been incorporated into AASHTO LRFD (2020). However, it is not currently included in AISC (2017) because narrow systems are not frequently found in building applications, such that this stiffness component is comparatively large relative to the other components identified in Equation 2.20. Consequently, the failure mode is not likely to govern for bracing design applications in buildings, except in cases such as walk-ways or other narrow girder systems that mimic highway bridge applications.

Due to limitations with respect to accounting for the stiffness multiple girders and unconservative results produced with Equation 2.25, an update was proposed to the in-plane girder stiffness by Fish in 2021. A final version was released by Fish et al. (2025) alongside an update to the global buckling moment capacity. These updated expressions are shown in Equation 2.30 and 2.31.

$$M_{gs,2025} = C_{bs}\frac{\pi^4 sE}{(KL)^2}\sqrt{I_{eff}I_x\alpha_x} \qquad 2.26$$

$$\beta_{g,2025} = \frac{\pi^4 EI_x s^2 \alpha_x L_{b,avg}}{(KL)^4} \qquad 2.27$$

Where:

K is an effective length factor used to account for warping restraint added by modifications to the bridge system such as lateral trusses.

α_x is the system warping stiffness factor given in Equation 2.28.

$L_{b,avg}$ is the average unbraced length within the span given in Equation 2.29.

$$\alpha_x = \frac{\left(n_g^2 - 1\right)}{12} \qquad 2.28$$

$$L_{b,avg} = \frac{L}{n+1} \qquad 2.29$$

Table 2-1. System Warping Stiffness Factor Values

Number of Girders	System Warping Stiffness Factor
2	1
3	4
4	10
5	20
6	35
7	56
8	84
9	120
10	165

2.4.1.3. Cross-Section Stiffness, β_{sec}

If the braces are relatively shallow compared to the girder depth, the effects pf distortion that are related to the stiffness of the cross-section, β_{sec}, may have a significant effect. For rolled shape applications with either unstiffened or full-depth web stiffeners, Yura derived the following equation (1992, 2001):

$$\beta_{sec} = \frac{3.3E}{h_0}\left(\frac{(N+1.5h_0)t_w^3}{12} + \frac{t_s b_s^3}{12}\right) \qquad 2.30$$

Where:

N is the contact length of the torsional brace (i.e. width of the brace along the girder length)

h_0 is the height of the web

t_w is the thickness of the web

t_s is the thickness of the stiffener

b_s is the width of the stiffener

Since many bracing systems may have negligible "contact length," N may be taken as zero in Equation 2.30, resulting in the expression given in Equation 2.31 (Helwig and Yura, 2015). This form is included in AISC Appendix 6:

$$\beta_{sec} = \frac{3.3E}{h_0}\left(\frac{(1.5h_0)t_w^3}{12} + \frac{t_s b_s^3}{12}\right) \quad 2.31$$

The first term in the equation accounts for the effective moment of inertia for the part of the web assumed to participate in the distortion, and the second term accounts for the moment of inertia of the stiffener, taken about the centroid of the web. For built up sections that often have more slender webs than rolled sections, Equations 2.30 and 2.31 may not adequately represent the cross-sectional stiffness. In these cases, the webs can be divided into regions above the brace and below the brace using the following expressions for β_{sec} (Yura, 2001):

$$\beta_{sec} = \frac{1}{\frac{1}{\beta_{top}} + \frac{1}{\beta_{bot}}} \quad 2.32$$

$$\beta_{top} = \frac{3.3E}{h_0}\left(\frac{h_0}{h_{top}}\right)^2\left(\frac{1.5h_{top}t_w^3}{12} + \frac{t_s b_s^3}{12}\right) \quad 2.33$$

$$\beta_{bot} = \frac{3.3E}{h_0}\left(\frac{h_0}{h_{bot}}\right)^2\left(\frac{1.5h_{bot}t_w^3}{12} + \frac{t_s b_s^3}{12}\right) \quad 2.34$$

Only the region outside of the brace depth contributes to the cross-sectional distortion. Because most cross-frames in bridge I-girder applications are relatively deep with respect to the girder depth, the cross-section stiffness component tends to be a large value, such that it is not usually a significant concern in Equation 2.20. Language in the 10th Edition of AASHTO (2020) for stability bracing allows β_{sec} to be taken as infinity for braces deeper than 80% of the web depth. This provision recognizes the minimal impact of cross-sectional braces for relatively deep braces since the portion of the web above and below the brace is relatively small and doesn't distort significantly.

2.4.2. Torsional Bracing System Strength

In addition to stiffness requirements, the bracing also must satisfy strength requirements to effectively prevent LTB of a bridge girder. The forces in the cross brace are found based on the required moment in the brace, M_{br} that is calculated using a formulation such as that shown in Equation 2.14. The brace moment can be idealized as a force couple so that forces in the cross-frame members can be determined. The relationship between the torsional brace moment and forces induced in cross-frames are depicted in Figure 2-8 for X-frames in either a tension only cross-frame or a compression system, as well as for K-frames.

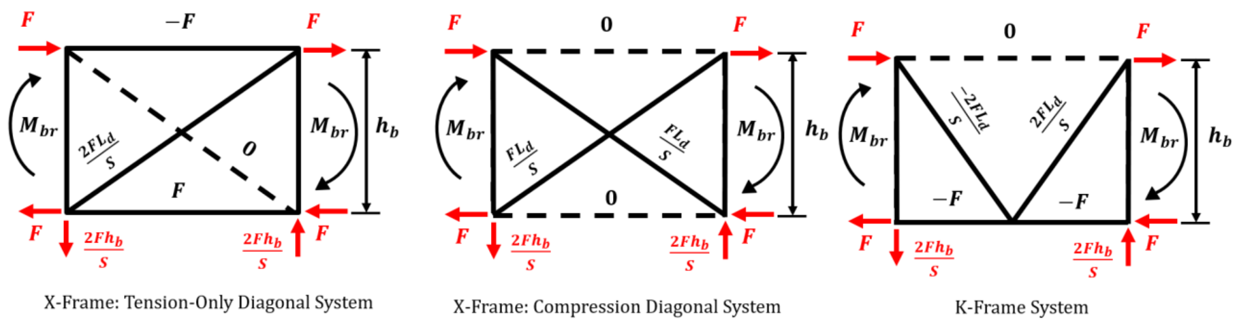

Figure 2-8. Idealized Cross-Frame Forces

As discussed previously, the AASHTO 10th Edition bracing provisions required twice the ideal stiffness for cross-frames at least equal to 80% of the girder depth, thich will generally be the case. Provided that adequate stiffness is provided, the resulting girder twist is equal to the initial imperfection, θ_0 and the resulting bracing moment is $\beta_T\theta_0$. This relationship is reflected by Equation 2.35.

$$M_{br} = \beta_T\theta_0 = F_{br}h_b \qquad 2.35$$

The applied force couple in the brace results from the brace moment required to restrain girder twist. The couple is a linear function of the required stiffness and an assumed initial imperfection (Helwig and Wang, 2003):

$$F_{br} = \frac{M_{br}}{h_b} = \frac{\left[\frac{0.024M_rL}{nC_bL_b}\right]}{h_b} \qquad 2.36$$

Where:

F_{br} is the force in the brace

β_T is the bracing system stiffness

h_b is the height of the brace

θ_0 is the initial twist, or initial imperfection, of the girder

From Equation 2.36, the force in each member can be estimated by evaluating the cross-frame as an idealized truss subjected to a moment, or a resolved force couple at the top and bottom nodes of the truss. As shown in Figure 2-8, for a tension-only system, the force in the struts is equal to F_{br} in compression, and the force in the tension diagonal is given by Equation 2.37 (Helwig and Wang, 2003):

$$F_d = \frac{2F_{br}L_d}{s} \qquad 2.37$$

Where:

L_d is the length of the cross-frame diagonal member

s is the spacing between the girders

After the stability-related member forces are calculated in accordance with Figure 2-8, cross-frame members can be sized for adequate strength. Note that the stability bracing forces in cross-frames are to be treated as any other load case such as wind or live load force effects in cross-frames. As such, the stability bracing forces can and should be combined with other concurrently acting load cases via linear superposition.

2.4.3. Lateral Bracing System Stiffness

Much like torsional braces, lateral braces must possess adequate strength and stiffness to provide a suitable brace point for a beam or girder. It is important to note that discrete lateral bracing is most effective when placed as close to the compression flange as possible, keeping in mind that in reverse-curvature bending, lateral bracing must be attached to both flanges. Largely based on the work of Winter (1960) that investigated column buckling, Yura (1992, 2001) developed a simple design approach to estimate these stiffness and strength requirements. As such, the required stiffness of a lateral beam brace is estimated using Equation 2.38, where $P_f C_b$ can be approximated by $\frac{M_f}{h_0}$ (AISC, 2022):

$$\beta_L^* = \frac{2N_i P_f C_b C_L C_d}{L_b} \; or \; \frac{2N_i M_f C_L C_d}{h_0 L_b} \qquad 2.38$$

Where:

N_i is $4 - \frac{2}{n}$ or a coefficient depending on the number of braces within the span as provided in Table 2-2

P_f is the equivalent elastic buckling capacity of the compression flange $= \frac{\pi^2 E I_{yc}}{L_b^2}$

C_L is the top flange factor, as defined in Equation 2.39

It was recognized that the required brace stiffness was a function of the number of intermediate braces provided along the length of the beam. Yura (1992, 2001) developed an accurate approximation of these effects (i.e., a definition for N_i), which is given in Table 2-2. It is important to note that this equation is analogous to the ideal stiffness formulation developed for the lateral bracing of columns (Winter, 1960). In general, an increase in the number of braces results in an increase of the ideal brace stiffness.

Table 2-2. Brace Coefficient used in Equation 2.38

Number of Evenly Spaced Braces	Exact value of N_i	Approximate Value of $N_i = 4 - \frac{2}{n}$
1	2	2
2	3	3
3	3.41	3.33
4	3.63	3.5
Many	4	4

Helwig et al. (1997) found that if certain circumstances mitigate the effects of load height (i.e., tipping restraint or benefits of intermediate bracing), then a flange loading modification of 1.0 may be used as in the case of centroidal or uniform moment loading. However, for top flange loading without mitigating factors, C_L is given as Equation 2.39 (Yura, 1992), and alternatively may be conservatively assumed to be 2.0 (AISC, 2022).

$$C_L = 1 + \frac{1.2}{n} \tag{2.39}$$

Where:

n is the number of discrete braces

2.4.4. Lateral Bracing System Strength

The top and bottom struts of a cross-frame may be classified as a lateral bracing system. The forces in cross-frame members are discussed in Section 2.4.2. For a tension-only diagonal system, or Z-frame, the forces in the struts are equal to $F_{br} = M_{br}/h_b$ in compression, and the forces in the tension diagonal can be calculated using Equation 2.37. Then, the cross-frame members can be sized for adequate strength.

2.5. Lean-On Bracing Design

The lean-on bracing system was first suggested for skewed bridges to help minimize the magnitudes of live load-induced forces. Additionally, the reduction in the number of cross-frames can result in a significant reduction in material and fabrication costs, as these are typically the most expensive components per unit weight on steel bridges due to complexities in fabrication and erection. A schematic was shown previously in Figure 1-2 that demonstrated the lean-on concepts by selectively removing cross-frame from a given line in place of top and bottom struts that provide a load path to lean girders in a given line on the cross-frame. Fewer cross-frames also generally results in fewer complex details that must be inspected on routine bridge inspections, resulting in less inspection time. Figure 2-9 shows the lean-on bracing applied in an implementation application in TxDOT study 5-1772.

Figure 2-9. Lean-on Bracing in Lubbock Texas Implementation Study (TxDOT Project 5-1772)

As shown in the figure, torsional braces (i.e., cross-frames) provide the primary source of stability for the girders across the width of the bridge. In general terms, the top and bottom struts in the adjacent girder bays of a continuous brace line effectively "lean-on" the full torsional braces to stabilize these neighboring bridge girders.

The top and bottom struts are then tasked with transferring the forces developed in the adjacent girders. This is analogous to the shear force that stabilizing columns in a frame must resist when adjacent columns lean on it for stability. Thus, the full cross-frames in a bracing line are subjected to increased demands for both stiffness and strength requirements to adequately stabilize more than two girders across the bridge width, as described in the next section.

Although lean-on concepts were initially proposed for systems with significant support skew, the approach can also be used for girder systems with normal supports. A typical bracing layout utilizing lean-on concepts is shown in Figure 2-10 and Figure 2-11 for a straight, three-span continuous bridge with normal supports. In skewed bridges, it has been shown to be advantageous to place the first cross-frame transversely in a given bracing line so as to position the brace as far from the support as possible (Romage, 2008). In these systems, cross-frames near the supports should be placed near the exterior girders that correspond to the acute angle of the skewed support. To maximize the in-plane stiffness of the girder system, the braces should be spread out across the full bridge width to fully engage the girder system. Near midspan, the use of a line of cross-frames across the full width of the system helps to engage all the girders for this purpose.

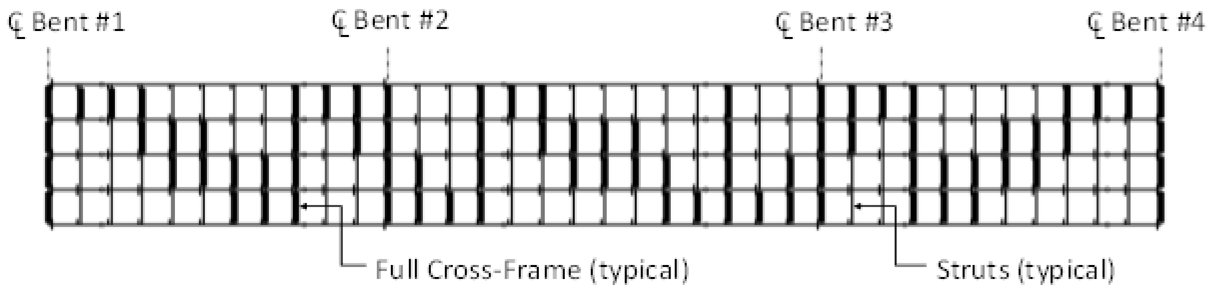

Figure 2-10. Typical Lean-On Bracing Layout

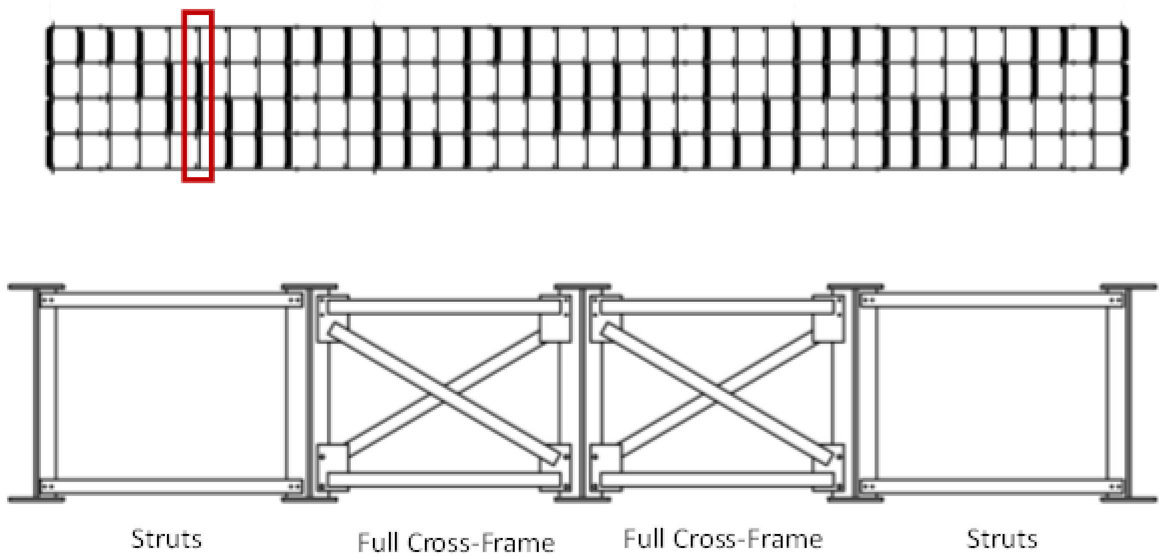

Figure 2-11. Lean-On Bracing Detailed Layout

Overall, there is a lack of understanding and clear guidelines detailing the most appropriate and effective application of lean-on bracing, particularly in more complex framing systems. The following sections discuss the major findings from the previous research related to lean-on bracing. Most of the lean-on work to date has focused primarily on the torsional bracing aspects of the system, and very little research has focused on the lateral bracing components of a lean-on system.

2.5.1. Torsional Bracing System Stiffness for Lean-On Applications

In terms of the required stiffness requirements outlined previously in Section 2.3, past studies have been conducted to approximate the increased demands on cross-frames when included in a lean-on bracing system. Some refinement has been made to the torsional system stiffness calculations to account for lean-on bracing applications. Modifications have been recommended for the brace stiffness and in-plane girder stiffness that can be used with the expression for springs in series given previously in Equation 2.20.

2.5.1.1. Torsional Brace Stiffness, β_{br}

When lean-on applications are utilized for cross-frames, the stiffness of the torsional brace, as expressed in Equation 2.21, is modified to consider the location of the brace relative to the lean-on bays. The cross-frame stiffness for a tension-only diagonal system was revised by Helwig and Wang (2003) to consider the number of girders per cross-frame, n_{gc}. Romage (2008) modified the cross-frame stiffness depending on the relative location of the bracing line on the bridge. Equation 2.40 is used for the brace stiffness component of braces located in interior bays, and Equation 2.41 is used for braces located in exterior bays.

$$\beta_{br} = \frac{Es^2 h_b^2}{\frac{n_{gc} L_d^3}{A_d} + \frac{s^3 \left(\frac{n_{gc}}{2}\right)^2}{A_h}} \quad 2.40$$

$$\beta_{br} = \frac{Es^2 h_b^2}{\frac{n_{gc} L_d^3}{A_d} + \frac{s^3 \left(n_{gc}-1\right)^2}{A_h}} \quad 2.41$$

Where:

n_{gc} is the number of girders per cross-frame

The original formulation that was derived for use in Helwig and Wang (2003) was focused on cross-frame lines with a single cross-frame located at the extreme end of the cross-frame. The expression has been misinterpreted in some applications when more than one cross-frame is positioned in a given line. Developing improved guidance on the stiffness and strength behavior of the lean-on applications to avoid misinterpretation of the expressions is a major goal of the research documented in this study. The refined expression is discussed in 0.

2.5.1.2. In-Plane Girder Stiffness, β_g

Helwig and Wang (2003) recommended the reduction of the in-plane girder stiffness by 50% when utilizing lean-on bracing as compared to a system only utilizing traditional torsional bracing concepts, as expressed in Equation 2.42. It is assumed that a lean-on system would have an in-plane girder stiffness between that of a twin-girder system and of a traditional cross frame layout, and finite element analysis solutions showed reasonable correlation with the 50% reduction. However, this equation can potentially be adjusted for increased precision.

$$\beta_g = \frac{12\left(n_g-1\right)^2 s^2 EI_x}{n_g L^3} \quad 2.42$$

Fish et al. (2025) did not propose any updates to Equation 2.42 as lean-on bracing systems were outside the scope of the research paper. Due to the fundamental issues with the equation that

Equation 2.42 was based upon, the in-plane girder stiffness of lean-on bracing systems will be addressed later in this report.

2.5.2. Torsional Bracing System Strength for Lean-On Applications

Similar to the stiffness, the strength of the cross-frame will vary with its location along the bridge. To find the tension force in the cross-frame diagonal, Equation 2.43 may be used. Equations 2.44 and 2.45 may be used to find the compressive force in the struts in interior bays and bays closer to supports, respectively. The member forces for a four-girder system, where F denotes F_{br}, are shown in Figure 2-12.

$$F_d = \frac{n_g F_{br} L_d}{N_c S} \qquad 2.43$$

$$F_{s,int} = \frac{n_g F_{br}}{2N_c} \qquad 2.44$$

$$F_{s,ext} = \left(n_g - 1\right) F_{br} \qquad 2.45$$

Where:

n_g is the number of girders stabilized in the brace line under consideration

N_c is the number of cross-frames at each brace line

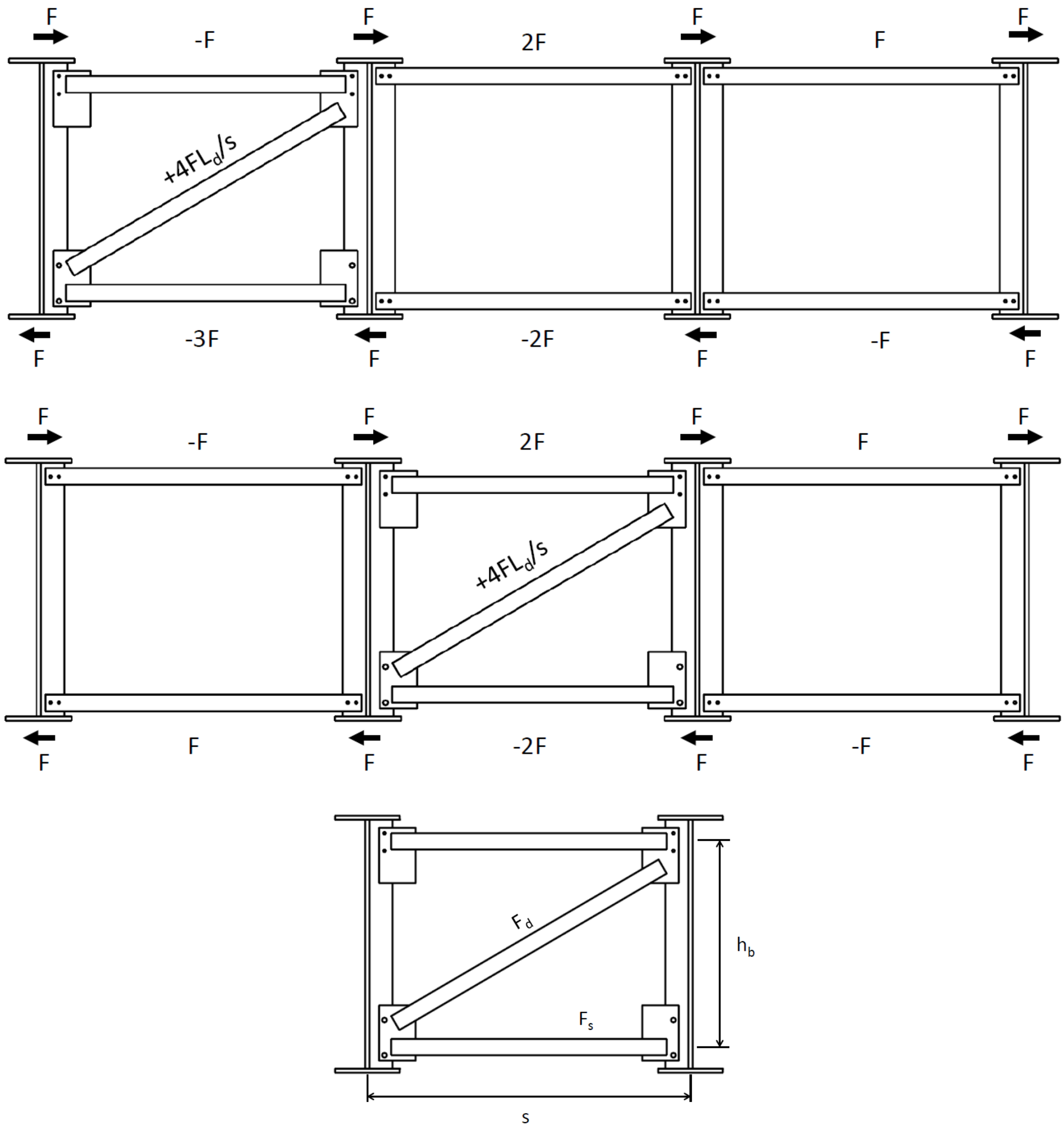

Figure 2-12. Torsional Brace Forces

Chapter 3. Field Instrumentation and Monitoring

3.1. Identification of Existing Lean-On Bridges

In an effort to identify existing bridge designs utilizing lean-on bracing, as well as to gather information about the experiences of bridge engineers with existing design guidance, the research team conducted interviews and released an electronic survey in the first few months of 2021. Three Texas Bridges utilizing lean-on bracing, SH 105, FM1902B, and IH35 E, were identified in addition to the bridge in Lubbock, Texas of which the research team was already familiar.

Engineers that were engaged in recent lean-on design applications provided information regarding the issues with interpreting and applying existing lean-on expressions in the design of a bridge over the Brazos River on SH 105. The lean-on system was designed primarily using the existing design expressions as developed by Helwig and Wang (2003). As a result of discussions with the engineers involved in the design, there were a few specific points of difficulty (specifically regarding the application of the current design expressions):

1. The role/implementation of multiple cross-frames within a given bracing line
2. Impact of girder continuity
3. Effect of non-prismatic girder cross-sections

Based upon uncertainties in the potential behavior of the bridge during construction, the design team revisited their original analysis and design. During this process, concerns were raised about the stability of the system during deck casting. Due to the girders and cross-frames having already been fabricated, coupled with the simplistic nature of the existing design expressions, the design team conducted detailed finite element analyses of the system to confirm that the bridge possessed sufficient stability during construction.

Another application of lean-on bracing was the bridge at FM 1902B on Chisholm Trail Parkway south of Ft. Worth, Texas. The designer provided information from an electronic survey documenting the experience with lean-on bracing. The bridge was designed using the FEA program LARSA. Lean-on bracing was chosen for the purpose of handling heavy skew and minimizing fatigue. The designer utilized the Steel Bridge Design Handbook (Helwig and Yura, 2015) and previous project documents to complete the design.

Lean-on bracing was also used on an overpass to IH35 E south of downtown Dallas. The lean-on system was designed primarily using finite element analysis (FEA). With proper modelling decisions, a 3D model, inherently accounts for the impact of many of the parameters not yet fully accounted for in the original design expressions as developed by Helwig and Wang (2003). The existing design expressions, however, were used as a “check” of the FEA results.

The survey received responses from several states, including engineers from Texas, North Carolina, Arkansas, Wisconsin, Pennsylvania, Florida, Virginia, Connecticut, Tennessee, Illinois, Alaska, and Kentucky. Of these responses, only a few had completed lean-on bracing projects and, fewer still, had designed bridges while primarily utilizing the existing design expressions. Concerns were raised by those who had completed lean-on bracing projects about how to appropriately calculate the brace stiffness at different locations within the structure.

In response to a question about the reason for choosing lean-on bracing for their project, the primary reason identified was the benefit in heavy skew scenarios followed by economy and facilitating erection, ending with fatigue. There were other reasons mentioned including: bridge widening and controlling deflection differentials. Designers utilized TxDOT report 0-1772 (Helwig and Wang, 2003), the Steel Bridge Design Handbook (Helwig and Yura, 2015), previous project documents, and class notes to aid in the design process, but survey respondents noted that designing lean-on bracing required similar or more effort relative to conventional bracing.

Regarding the responses from those who had not been a part of a lean-on bracing design project, all desired additional insight into lean-on bracing design concepts. However, many of the respondents noted the lack of confidence in lean-on bracing from government DOTs and practicing engineers due to the following reasons:

1. A formal procedure for designing all types of bracing;
2. A dependence on knowing a contractor's erection plan and the discrepancies between an assumed and desired erection sequence; and,
3. Lack of coverage in the AASHTO Bridge Design Specifications.

Although the research team continued the effort to identify a lean-on bridge currently in construction phases, no active projects were identified that coincided with the duration of the research project. As such, the team moved forward with the field instrumentation of two completed Texas bridges. A brief background on prior instrumentation of a lean-on bracing system and the instrumentation of the SH 105 Brazos River Bridge and the Chisholm Trail bridge. In addition, the research team had access to data from a field monitoring study on the first lean-on bridges constructed in Texas. That data came from TxDOT Project 5-1772 on bridges in Lubbock, Texas. Data gathered from the field instrumentations was used to validate models to be utilized in parametric studies on lean-on bracing, and findings are discussed in Chapter 4.

3.2. Lubbock Bridge

3.2.1. Background

The 19th Street West Bound Bridge in Lubbock, TX, was instrumented as part of TxDOT Project 5-1772,which was the implementation study for Project 0-1772, Cross-Frame and Diaphragm Behavior in Bridges with Skewed Supports. Romage (2008) provides a detailed discussion of the sensor layout for the project, where the instrumented cross-frames were chosen based on the critical design cases. The critical locations were the intermediate brace near the support and the braces closest to midspan, due to the girder moments and bracing layout. The lean-on equations discussed in Chapter 2 were used to size the cross-frame members, and the controlling angle size was used throughout the structure. It is important to note that this bridge has a 60-degree skew, resulting in different critical cases compared to a non-skewed bridge.

These governing cases resulted in the instrumentation of the cross-frames designated in Figure 3-1. Because a given bracing line consists of bays with cross-frames and bays with only top and bottom struts, special designations need to be used to present the bracing layout. The cross-frames (designated X#), struts (designated S#), and girders (designated G#) were instrumented with strain gages, as shown in Figure 3-2 and Figure 3-3. The # following each member designator provides a designator for the strut number or cross-frame number. Tilt sensors were used to measure girder rotations at locations labeled “TS,” and laser distance meters were used to measure global deflections at locations designated A through K. “M” and “D” are used to designate multiplexers and dataloggers used for data acquisition. The laser distance meters provide distance measurements used to estimate girder deflections with reading accurate to 1/32 in. Readings at each location are taken with the bridge unloaded and with the trucks in position, and the girder deflection is determined from the difference. Three readings are taken and averaged to obtain each measurement. The elastic strain readings from the sensors were used to determine the stresses/forces in the cross-frames during deck placement and during a live load test after the deck had cured.

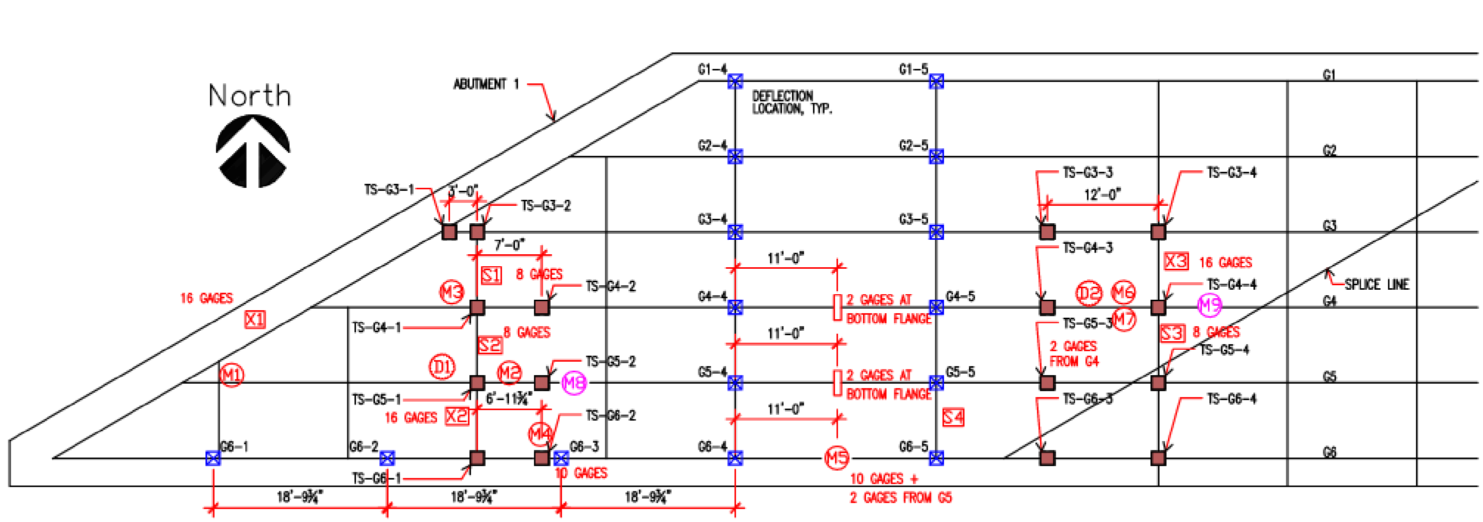

Figure 3-1. Instrumentation Plan for 19th Street Westbound Bridge

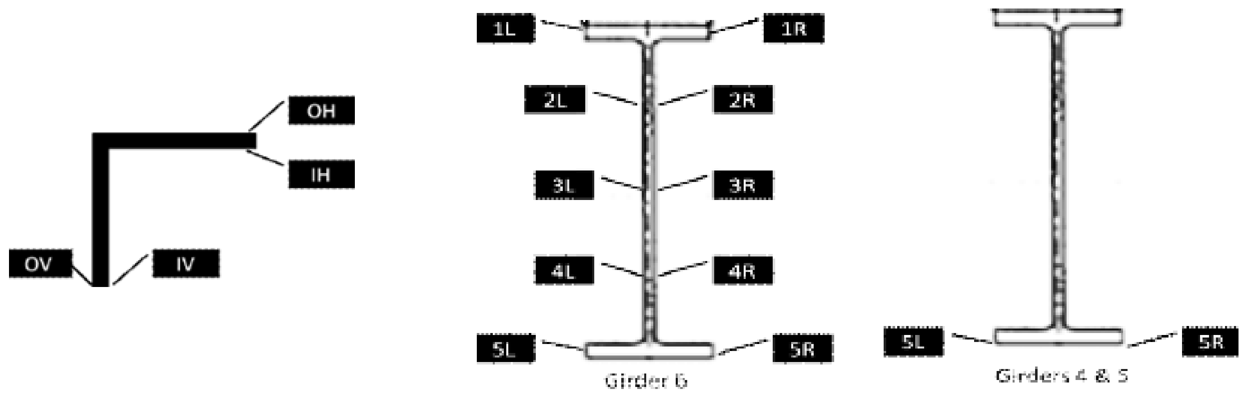

Figure 3-2. (a) Brace Angle and (b) Girder Gage Locations for 19th Street Westbound Bridge

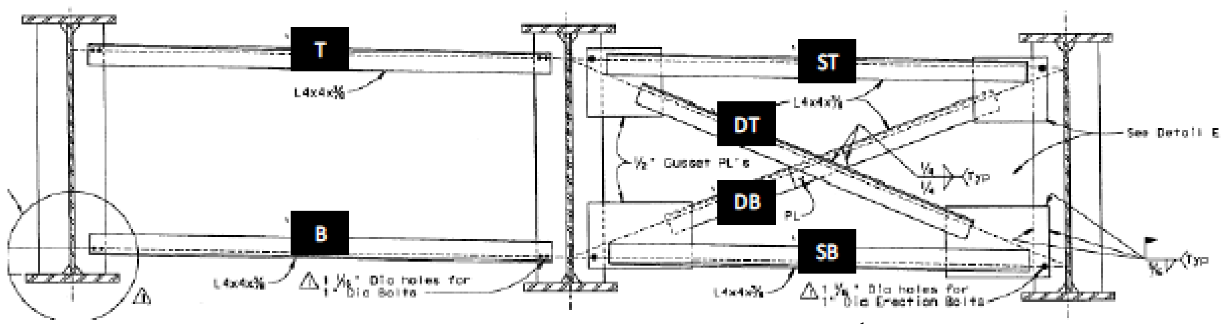

Figure 3-3. Strut and Cross Frame Strain Gage Locations for 19th Street Westbound Bridge

3.2.2. Data Archive

Two cross-frame lines (CFL) were instrumented on the Lubbock Bridge: CFL #3 and CFL #7. Construction and live load data were collected for these cross frames (Romage, 2008). During construction, a timeline for the pour is estimated based on field notes, and the assumed rate is 48 feet per hour over approximately 6 hours.

Live load testing occurred in several stages due to the significant number of cases tested, which can be subdivided by gridline number and truck positioning. The gridlines were positioned every 20 feet perpendicular to the longitudinal axis of the bridge, as shown in Figure 3-4. In total, there were 24 gridlines. The trucks were positioned in 6 different configurations with schematics provided in Appendix G. Lubbock Bridge Live Load Testing Layouts Romage (2008):

- Staggered ahead station
- Staggered behind station
- Side-by-side south
- Side-by-side north
- End-to-end south
- End-to-end central

For a preliminary analysis, the research team on this project focused on the gridline subset with the largest axial forces, Grid #7.

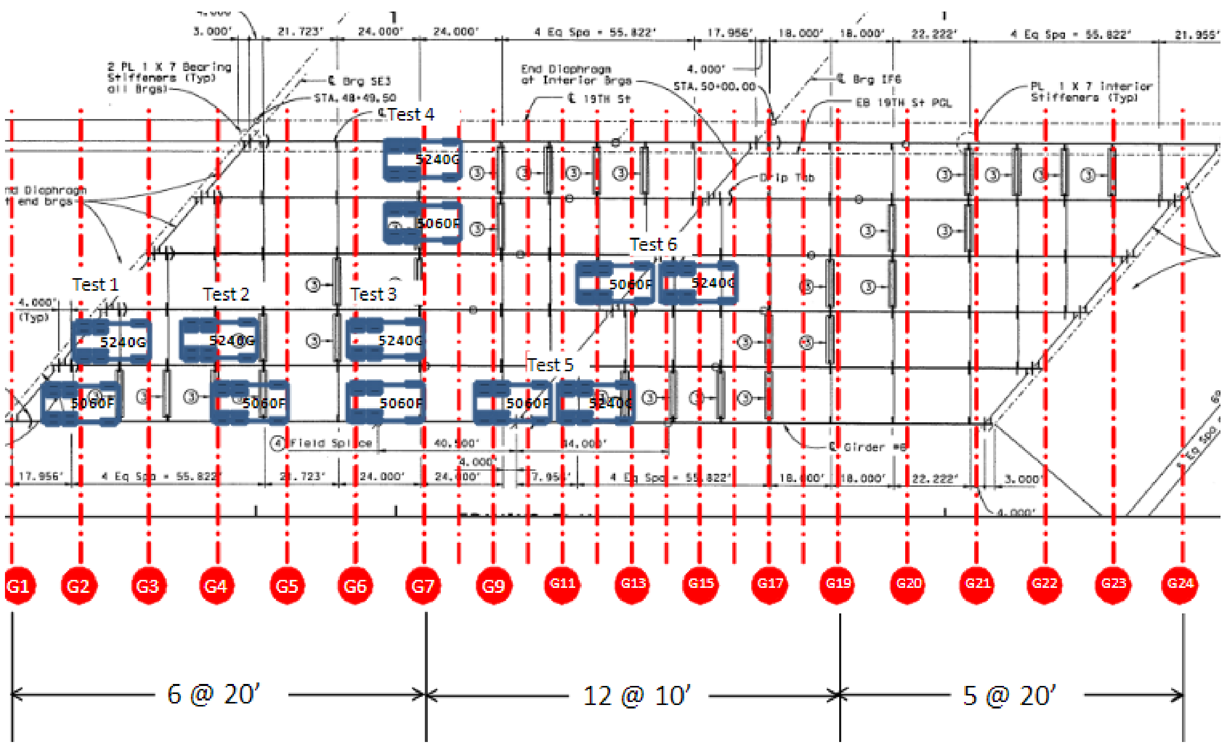

Figure 3-4. Grid and examples of truck positions utilized for the Lubbock Bridge (Romage, 2008).

3.3. SH 105 Brazos River Bridge

3.3.1. Overview

The bridge on SH 105 at the Brazos River is a three-span steel plate girder structure utilizing lean-on bracing, with prestressed concrete girder approach spans. A plan view of the three steel spans (denoted 6, 7, and 8) are shown in the framing plan in Figure 3-5, and a typical transverse section is shown in Figure 3-6. The spans are 234 feet, 300 feet, and 234 feet, respectively. The bridge is a five-girder system, with each bay braced by a full cross-frame (denoted by a thicker line in the framing plan) or struts (denoted by a thinner line). The bracing layout of span 8 is a mirror image of span 6.

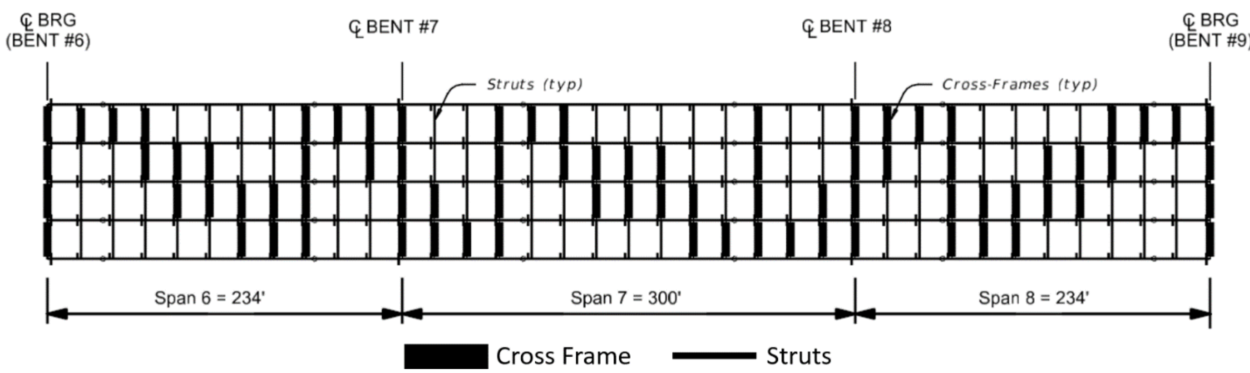

Figure 3-5. SH 105 Bridge Steel Framing Plan

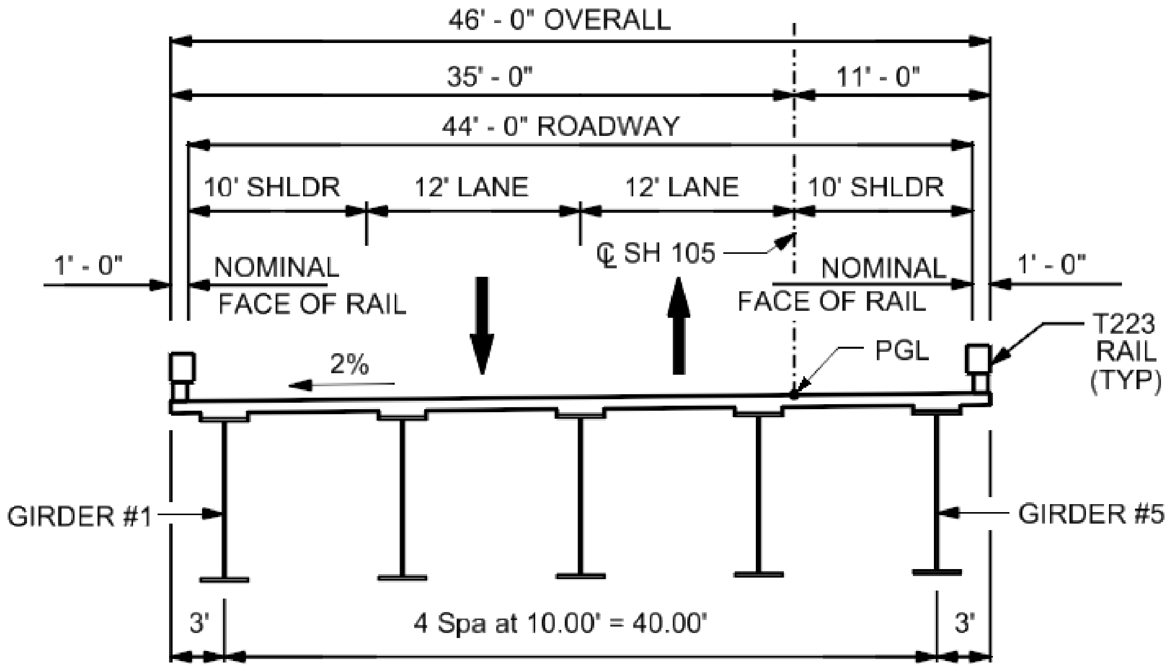

Figure 3-6. Typical Transverse Section on SH 105 Bridge

Prior to instrumentation, the research team visited the SH 105 bridge to inspect the site for accessibility. Figure 3-7 and Figure 3-8 are photographs taken by the research team on September 24, 2020. As shown in the pictures, Spans 7 and 8 cross over the Brazos River, and as such, are not conveniently accessible. Span 6, however, extends over a flat grassland, which allowed for a simpler method of accessing the bridge members for instrumentation.


Figure 3-7. SH 105 Bridge Span 7-8

Figure 3-8. SH 105 Bridge Span 6

3.3.2. Sensor Layout

The purpose and scheme for the instrumentation of the bridge on SH 105 at the Brazos River is similar to that of the 19th Street Westbound Bridge discussed in the previous section. Measurements from strain gages were utilized for determining the force distribution in select girders, cross-frames, and struts. Girder displacements were also measured in order to quantify global behavior.

To determine an efficient placement of the strain gages, a preliminary analysis to estimate the girder moments and global displacements were considered, as differential vertical movement of the girders induces cross-frame and strut forces. As a result, locations of relatively high positive bending moment were selected. For this continuous end span, relatively large positive moments (and vertical deflections) occur approximately in the range of 25-55% of the span length from the exterior support. Therefore, bridge cross-sections within this portion of the span were selected. Other motivating factors for the instrumentation locations included the number and position of the cross-frames. The finalized strain gauge layout for Span 6 of the SH 105 bridge is shown in Figure 3-9, and the layout for the girder displacement readings is shown in Figure 3-10. Girder deflections were determined with a laser distance meter using the same method applied in the Lubbock Bridge load testing discussed in the last section. Cross frame line 5 was chosen because it is close to midspan, while line 3 was selected to compare the behavior of cross frames centered in the cross section as compared to near the edge.

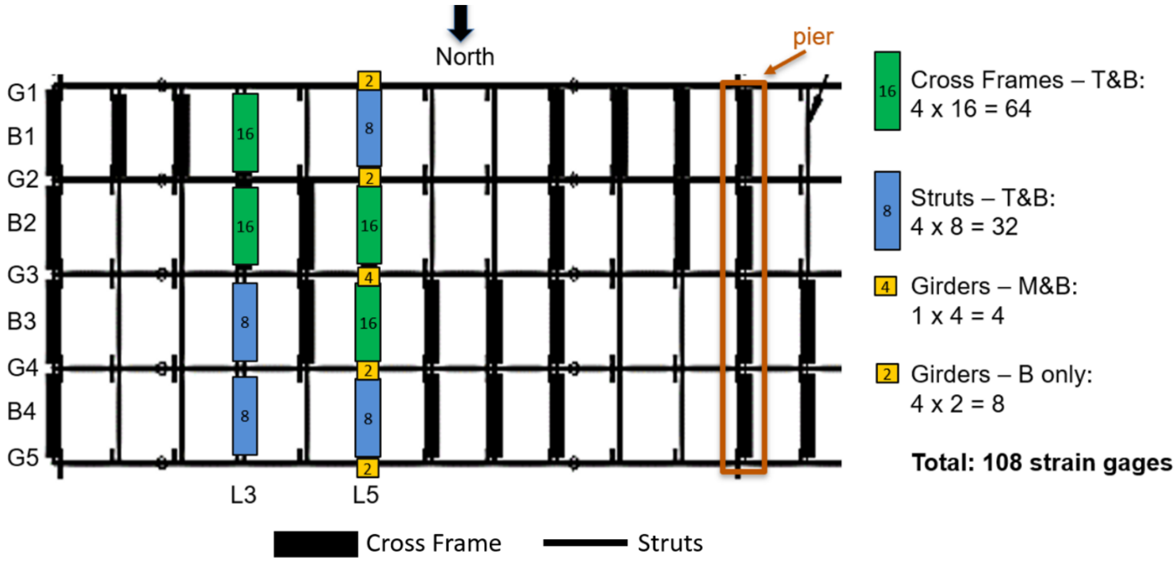

Figure 3-9. SH 105 Bridge Span 6 Strain Gauge Layout

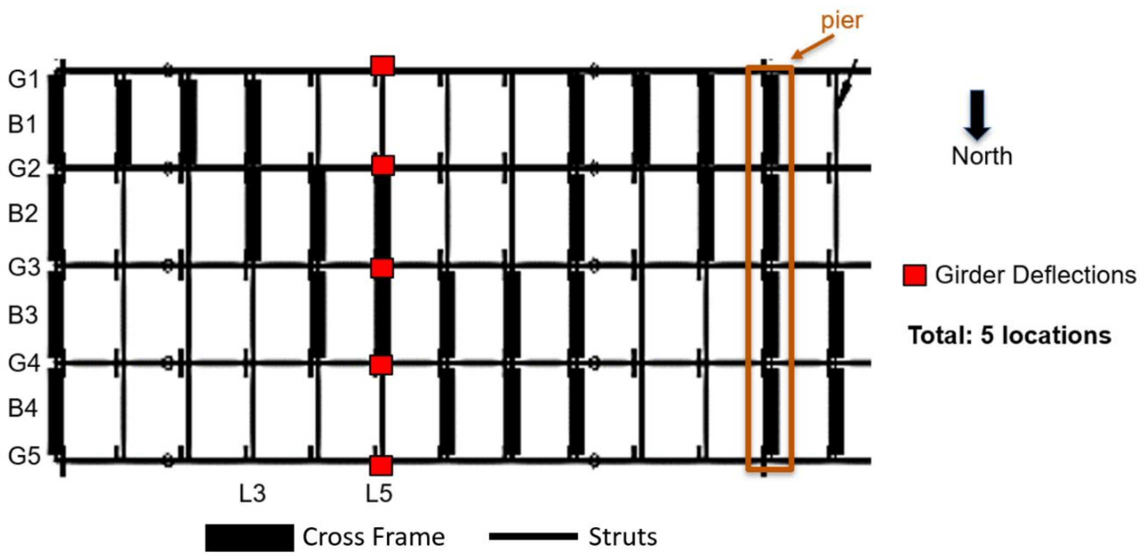

Figure 3-10. SH 105 Bridge Span 6 Girder Displacement Layout

A more granular look at the sensor layout for each member type is provided below. These sensor placements are again similar to the locations used on the 19th Street Westbound Bridge discussed in the last section. Each cross-frame is composed of angles, so four strain gages were required to accurately capture out-of-plane behavior and twist for each member cross section. As such, the conventions "OH" for outer horizontal, "IH" for inner horizontal, "OV" for outer vertical, and "IV" for inner vertical describe the sensor placement on each angle. A visual representation of the location of the four strain gauges on each angle is shown in Figure 3-11.

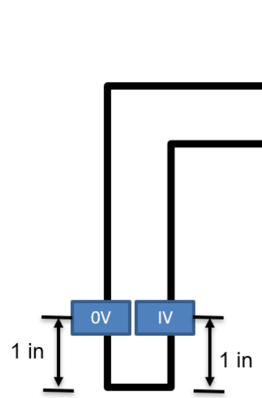

Figure 3-11. Strain Gage Placement on Angles

During field instrumentation, a slight revision was made to the sensor positioning on the top struts. With the deck in place, access to the top of the top strut was overly difficult. Instead of placing the OH strain gauge as indicated in Figure 3-11, this sensor was placed as indicated in Figure 3-12 for all top struts.

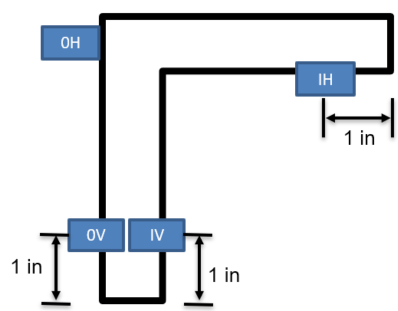

Figure 3-12. Revised Strain Gauge Placement on Top Struts

The top struts were instrumented to obtain a measure of the role of the composite bridge deck, and to observe the lateral force distribution between the cross-frames and lean-on bays. The composite bridge deck represents a relatively rigid element, and the forces in the top struts should be small. This meant each instrumented cross-frame required 16 strain gauges, while each instrumented lean-on bay required eight strain gauges. The labeling convention is shown in Figure 3-13, where "ST" denotes strut, top; "SB" denotes strut, bottom; "XT" denotes cross-frame, top; and "XB" denotes cross-frame, bottom.

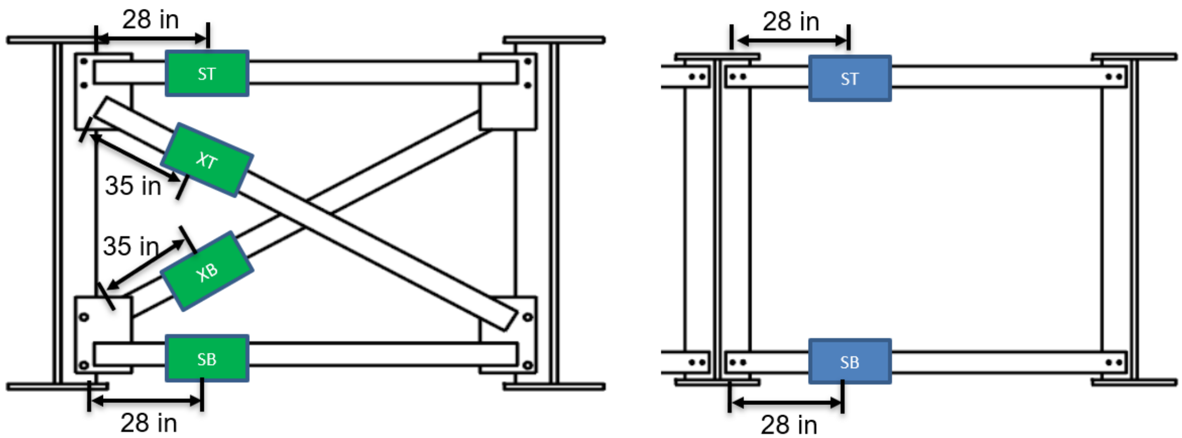

Figure 3-13. Strain Gage Placement on Cross-Frames and Struts

To capture global behavior, each girder was instrumented with two strain gages at the bottom flange, with the center girder instrumented with two additional strain gauges at mid-height. Although this girder instrumentation was not as extensive as on the 19th Street bridge, the SH 105 bridge is not skewed, and thus out-of-plane bending and distortion of the girders were not the primary concern. As shown in Figure 3-14, N and S were used to denote the North and South sides of the girder, with the number 1 designating a flange location and 2 designating a web location.

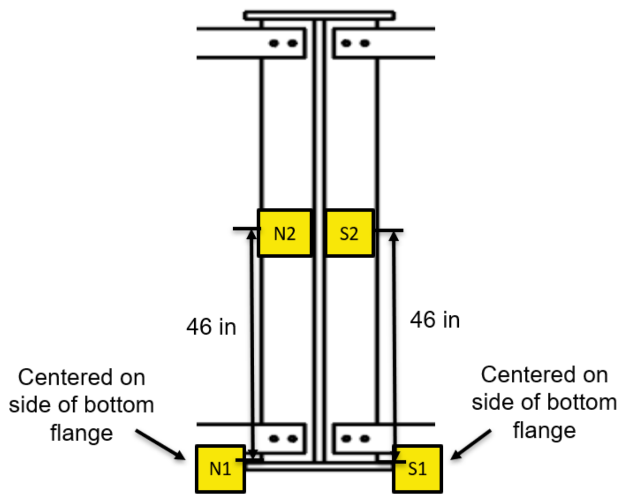

Figure 3-14. Strain Gage Placement on Center Girder

All labeling conventions are provided in Appendix A. SH 105 Bridge Sensor List Conventions, while the full sensor list is located in Appendix B. SH 105 Bridge Sensor List.

3.3.3. Data Acquisition

Two Campbell Scientific CR6 dataloggers (DAQ) and seven Campbell Scientific AM16/32B multiplexers (MUX) were used to collect data from the 108 strain gauges specified in the layout. Each DAQ was coded and powered independently, with DAQ 1 collecting data from MUX 1-4 for cross-frame line 5, and DAQ 2 collecting data from MUX 5-7 for cross-frame line 3. The wiring diagram is shown in Figure 3-15.

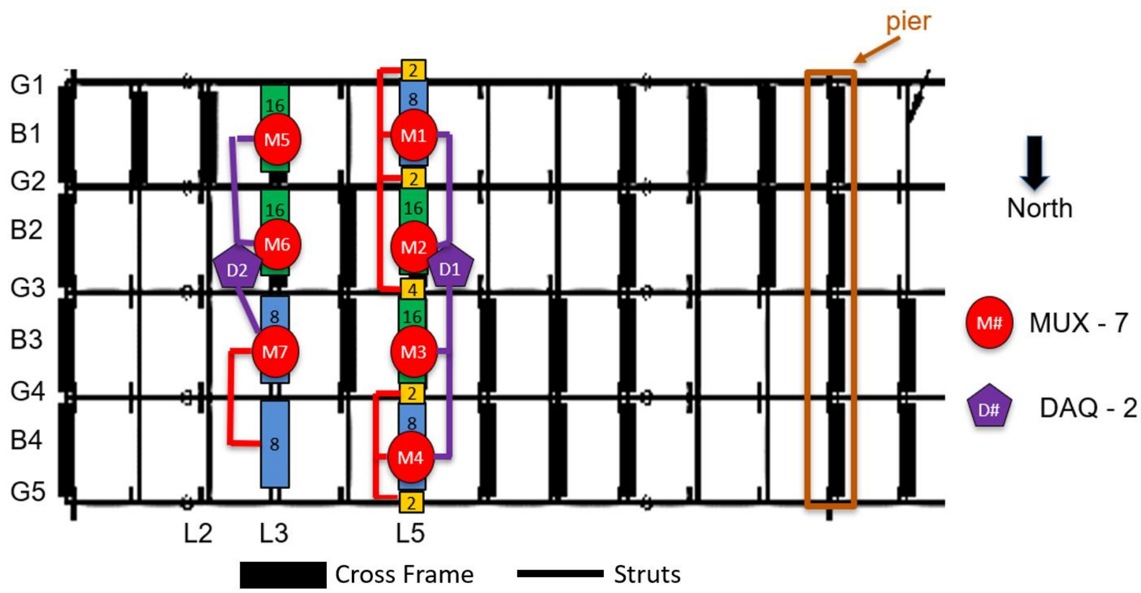

Figure 3-15. SH 105 Bridge Wiring Diagram

Both DAQ were programmed to sample data at 30-second intervals, and timestamps were manually recorded at the start of each load case to allow for continuous data collection as trucks were moves to specific locations and paused to collect data. The data was sampled a minimum of 5 times for each loading and unloading position to allow for stable readings to be taken, and select sensors were monitored throughout the test to ensure values were properly recorded.

3.3.4. Live Loading

Before live load testing could occur, load case patterns were determined based on the position of the cross frame lines instrumented. Identifiers were provided on the deck using spray paint and duct tape to assist in positioning the trucks into the proper position for each load case. The load case patterns are provided in Appendix C. SH 105 Bridge Live Load Testing Layout, along with actual truck positions during these load cases.

Truck loading was conducted on July 13, 2021, using four trucks loaded with sand/gravel. Prior to testing, each truck was measured and weighed using two vehicle scales. The scales provided a measure of the wheel loads and were positioned in front of each select wheel and the truck drove onto the scale. measurements for each truck are shown in Figure 3-16, while the axle weights are listed in Table 3-1.

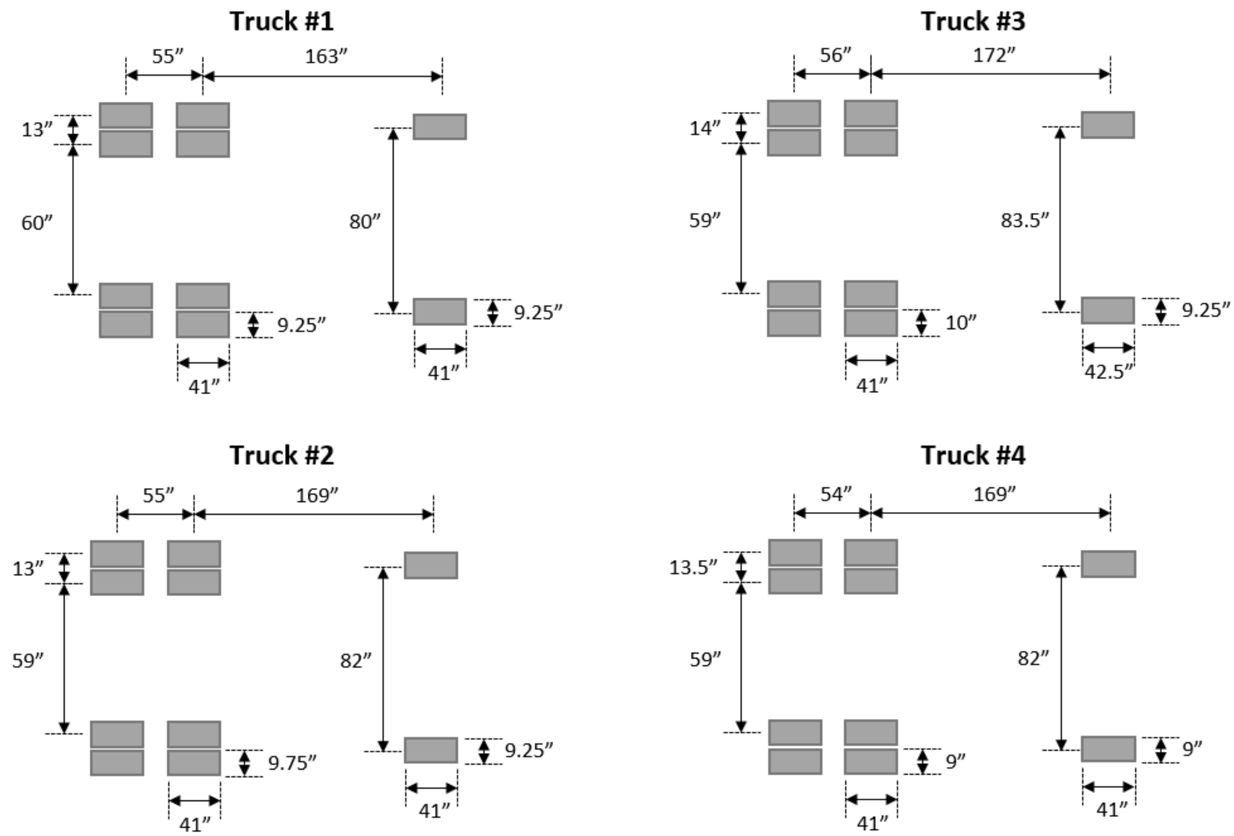

Figure 3-16. Truck Measurements Collected During Live Load Testing

Table 3-1 Truck Weights as Measured During Live Load Testing

Truck #	Steer Axle (lb)	Forward Drive Axle (lb)	Backward Drive Axle (lb)	Gross Vehicle Weight (lb)
1	11250	16800	16000	44050
2	12050	20450	19900	52400
3	12200	19850	19900	51950
4	12650	21650	20600	54700

Each truck was labelled with a number to keep track of the position of each truck during each test. The numbers were attached on the rear of each truck and also on the front bumper, as shown in Figure 3-17.

Figure 3-17. Truck Setup for Load Case #1

During testing, the following four-step process was followed for the nine load cases tested:

1. Collect unloaded deflection at midspan and strain measurements for five minutes.
2. Position trucks into desired load case.
3. Collect loaded deflection at midspan and strain measurements for five minutes. Collect truck distances from the ideal location using measure tape (Figure 3-18).
4. Remove trucks from the span.

After testing was complete, the duct tape markers for positioning trucks were removed from the deck, and all trucks were cleared of any markings.

Figure 3-18. Measuring the Distance between Trucks

3.4. Chisholm Trail Bridge at FM1902

3.4.1. Overview

The FM 1902B Overpass at Chisholm Trail Parkway is a six-girder bridge located in Johnson County, Texas, south of Ft. Worth, that is in use for the Chisholm Trail Parkway toll road. The girders are spaced at 10 feet, and each side of the bridge has a 4-foot overhang. The bridge consists of three spans of 180.5 feet, 235 feet, and 195 feet for a total length of 611 feet. The bridge has a width of 58 feet and has a 45-degree skew at the supports. The use of lean-on bracing resulted in a replacement of 155 of the 203 intermediate cross-frames with lean-on struts, a reduction of approximately 76%. The frames are spread out across the width, as shown in Figure 3-19.

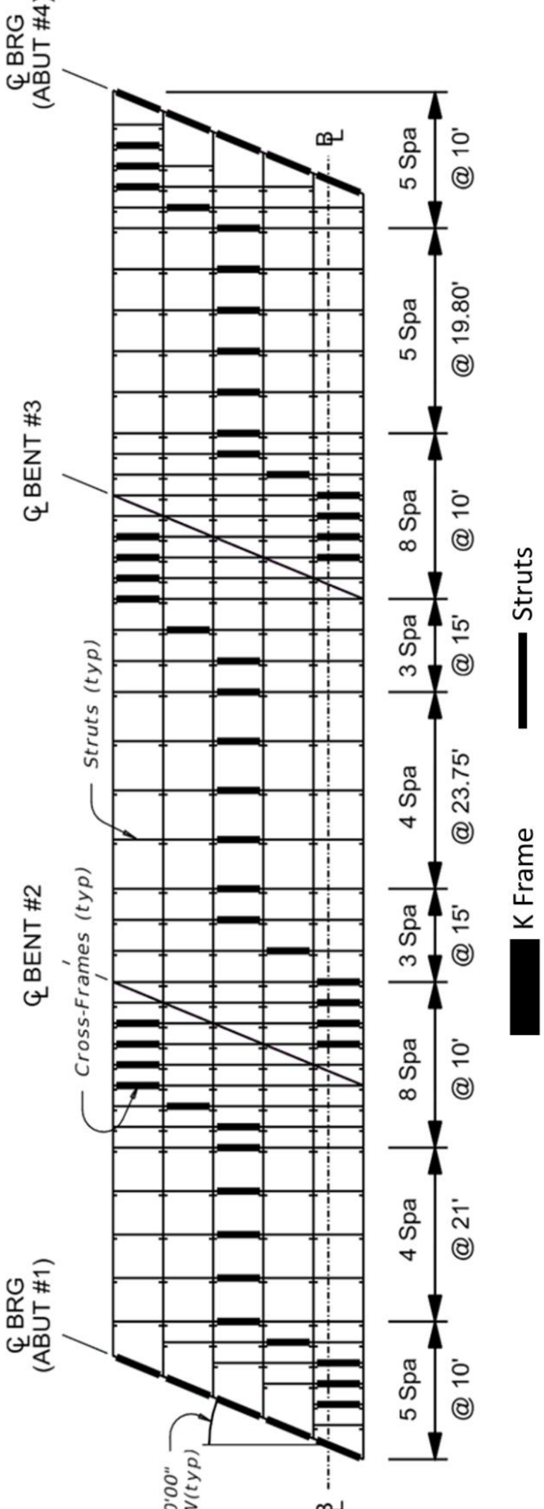

Figure 3-19. Chisholm Trail Pkwy at FM1902B: Framing Plan

A typical transverse section of the bridge is shown in Figure 3-20. The Chisholm Trail bridge has an interior barrier that separates north and southbound traffic, which was recognized by the researchers as a factor impacting live load testing by limiting load cases across the width of the bridge.

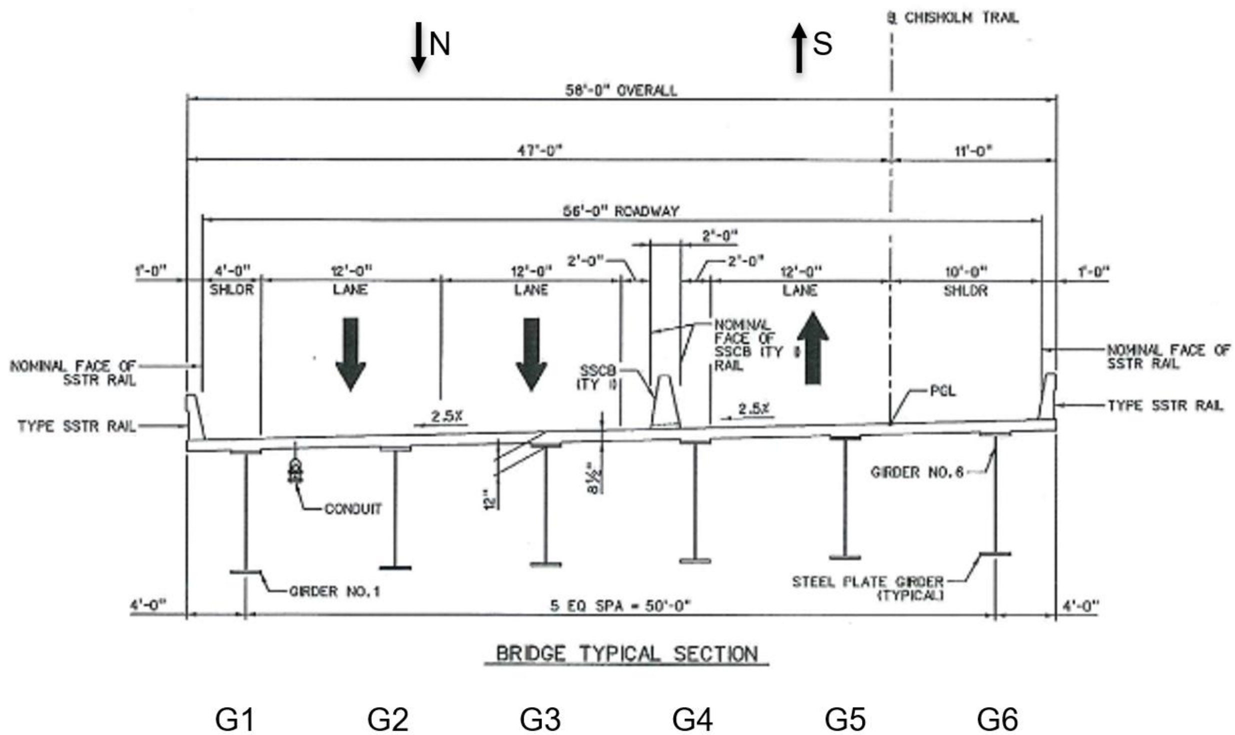

Figure 3-20. Chisholm Trail at FM1902B: Typical Transverse Section

During a site visit, the research team was able to determine that both Spans 1 and 3 were accessible to instrumentation from beneath the bridge without the need for traffic closures. The flat grass areas under these spans are ideal for access during instrumentation and are shown in Figure 3-21. The research team selected Span 1.

Figure 3-21. Chisholm Trail Bridge Spans

3.4.2. Sensor Layout

The instrumentation plan of the Chisholm Trail bridge was based on adding sensors to two key locations: midspan and near the interior pier. Inspired by the results of the SH 105 and the 19th Street Westbound Bridges, the midspan sensors and deflections were placed to capture the effect of the high positive bending moment and maximum bridge deflection. Sensors placed at the interior pier were used to collect data on the effect of the system's skew and unique cross-frame detailing on the pier.

The research team used 128 strain gauges, which was the maximum number possible. This was limited by the number of available data acquisition systems, as well as the time-sensitive nature of the instrumentation. Figure 3-22 illustrates the final strain gauge layout for the Chisholm Trail bridge, while the locations for deflection measurements are shown in Figure 3-23. The deflection readings were determined with the laser distance meter in the same way as for the Lubbock and SH 105 Bridges.

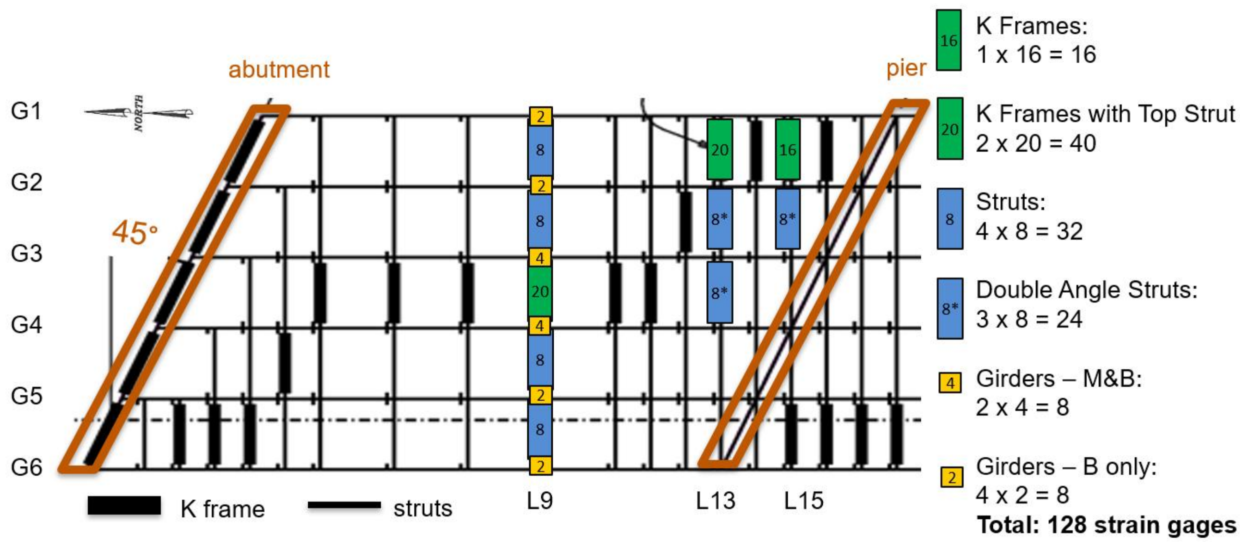

Figure 3-22. Chisholm Trail Bridge Span 1 Strain Gauge Layout

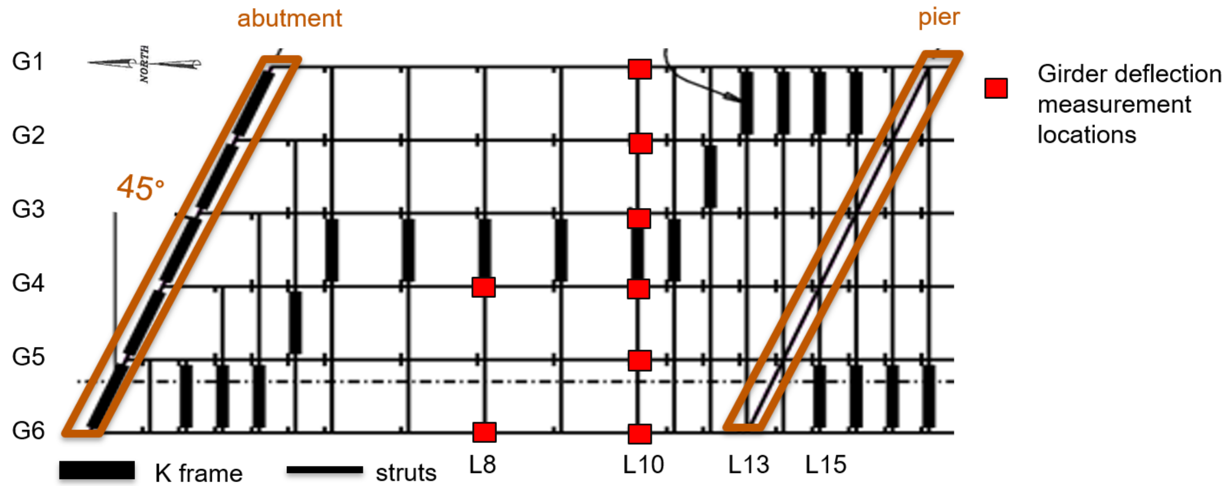

Figure 3-23. Chisholm Trail Span 1 Girder Displacement Layout

As discussed in the section outlining the instrumentation plan for the SH 105 bridge, the typical convention for each sensor is "OH" for outer horizontal, "IH" for inner horizontal, "OV" for outer vertical, and "IV" for inner vertical. Numbers are added to the double angle members to further distinguish sensor locations.

Figure 3-24 displays the sensor locations on the double angle top and bottom struts. Due to the detailing on these members, the double angle members are assumed to act as as a built-up member with a concentric connection and only four total sensors were used. The sensor location on the horizontal was selected based on accessibility.

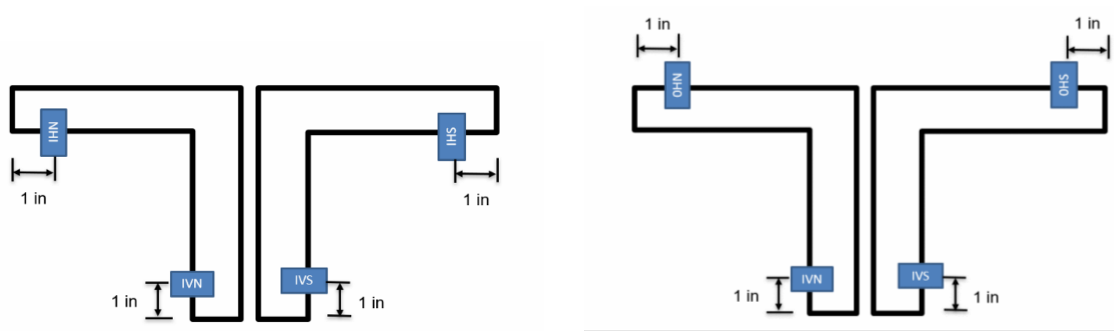

Figure 3-24. Chisholm Trail Double Angle Top and Bottom Strut Strain Gauge Placement

Figure 3-25 displays the sensor locations on single-angle top and bottom struts. The sensor location on the horizontal was based upon accessibility and were similar to the selected locations for the on SH 105 Bridge.

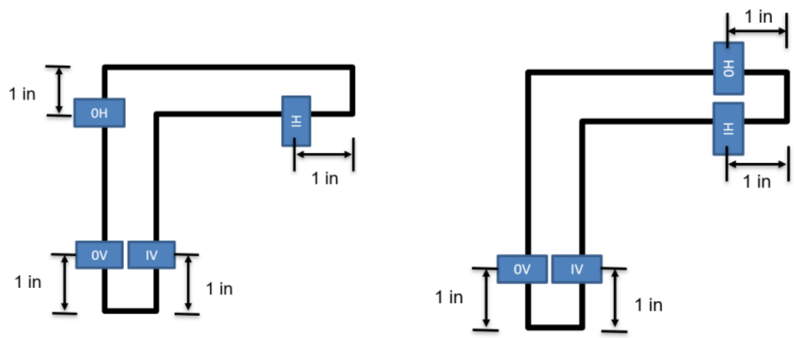

Figure 3-25. Chisholm Trail Single Angle Top and Bottom Strut Strain Gauge Placement

Similar to the SH 105 Bridge, the labeling convention is shown in Figure 3-26, where "ST" denotes strut, top; "SBE" denotes strut, bottom east; "SBW" denotes strut, bottom west; "XT" denotes cross-frame, top; and "XB" denotes cross-frame, bottom. Two of the three instrumented K-frames include a top strut sensor set for a total of 20 sensors (16 for the third K-frame). Each lean-on bay has eight sensors.

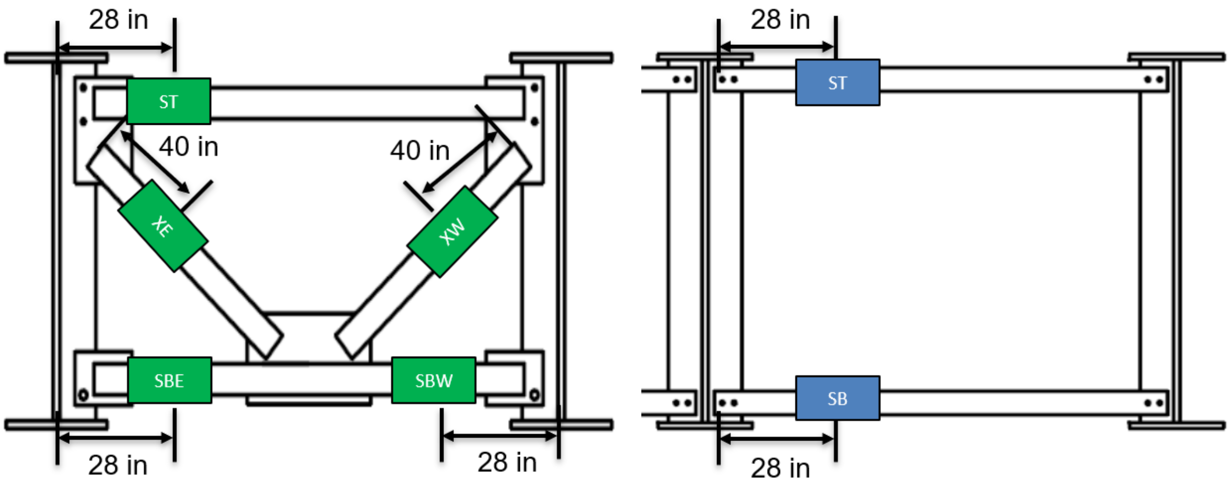

Figure 3-26. Chisholm Trail Strain Gage Placement on Cross-Frames and Struts

Girder sensor locations remain unchanged from Section 3.3.2. All labeling conventions can be found in Appendix D, while the full sensor list is given in Appendix E.

3.4.3. Data Acquisition

Data acquisition for the Chisholm Trail bridge was similar to the systems used for collecting data from the SH 105 Bridge. Two Campbell Scientific CR6 dataloggers (DAQ) and eight Campbell Scientific AM16/32B multiplexers (MUX) were used to collect data from the 128 strain gauges specified in the layout. Each DAQ were coded and powered independently, with DAQ 1 collecting data from MUX 1-4 (cross-frame line 8), and DAQ 2 collecting data from MUX 5-8 (primarily cross-frame lines 13 and 15). The wiring diagram is shown in Figure 3-27.

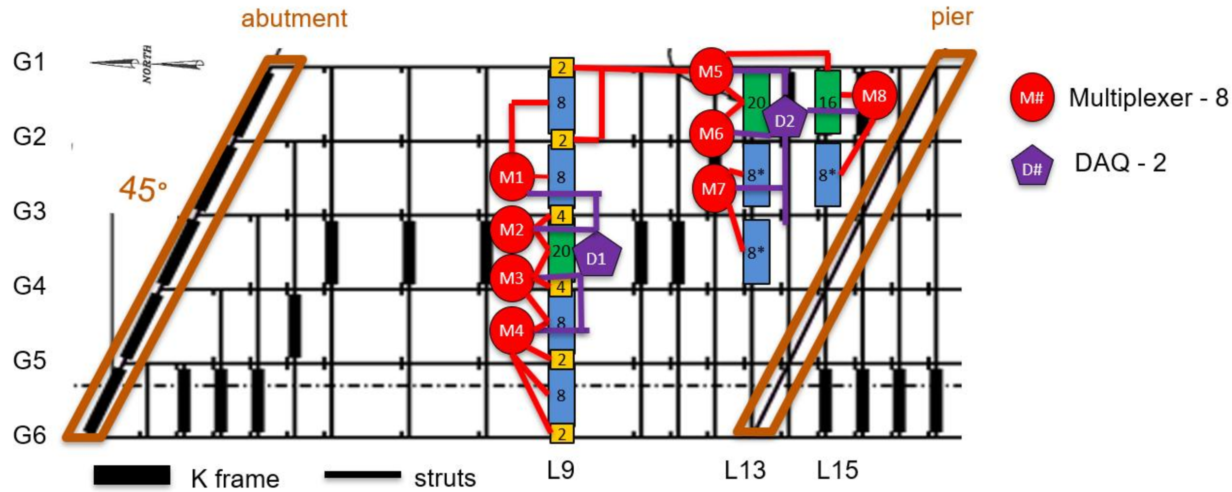

Figure 3-27. Chisholm Trail Strain Gage Placement on Cross-Frames and Struts

3.4.4. Live Loading

The live load cases for the Chisholm Trail Bridge were selected based upon preliminary Finite Element Analyses (FEA), data collected during the testing of the Lubbock bridge, and the position of the instrumented cross frame lines. Appendix F includes all live load cases for the Chisholm Trail Bridge.

Live load testing was conducted on November 14, 2021, utilizing four trucks supplied by TxDOT. Trucks were measured via tape measure and weighed using two vehicle scales. Measurements are displayed in Figure 3-28, and axle weighs are listed in Table 3-2. To avoid data contamination from other bridge traffic, the researchers worked with the toll authority to have the bridge shut down to traffic for approximately three hours. The traffic was diverted from the toll road via detour.

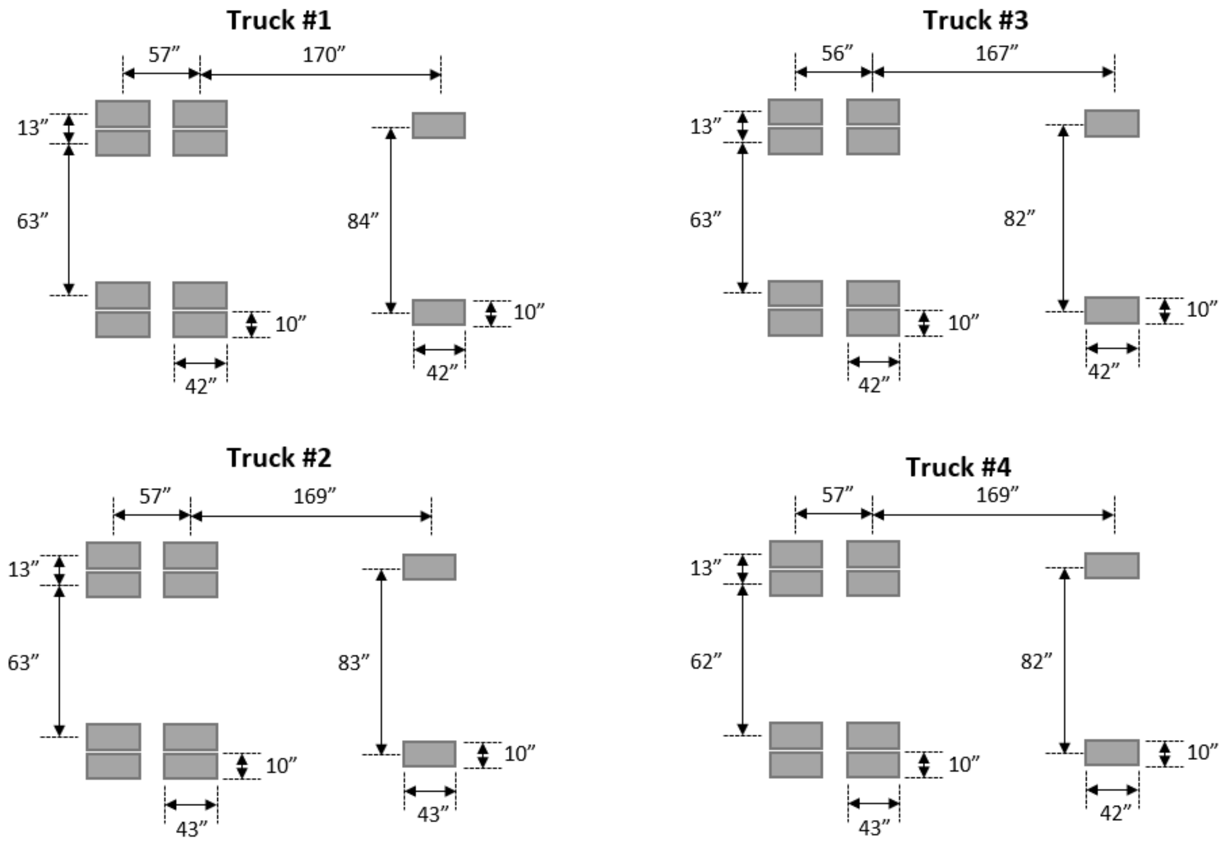

Figure 3-28. Truck Dimensions for Live Load Testing of the Chisholm Trail Bridge

Table 3-2 Truck Weights for Live Load Testing of the Chisholm Trail Bridge

Truck #	Steer Axle (lb)	Forward Drive Axle (lb)	Backward Drive Axle (lb)	Gross Vehicle Weight (lb)
1	11000	15800	16050	42850
2	11750	14200	14800	40750
3	11200	14700	15100	41000
4	11100	14500	14650	40250

Figure 3-29. Load Case 4 on the Chisholm Trail Bridge

After labelling the trucks to keep track of their positions, live load testing occurred using the same four-step procedure previously discussed:

1. Collect unloaded deflection at midspan and strain measurements for five minutes.
2. Position trucks into desired load case.
3. Collect loaded deflection at midspan and strain measurements for five minutes. Collect truck distances from the ideal location using measure tape.
4. Remove trucks from the span.

In total, six load cases were completed for the Chisholm Trail Bridge. Upon completion of the testing, all markings and duct tape were removed from the bridge.

3.5. Data Processing

3.5.1. Strain Gauge Readings to Axial Forces

In order to convert the measured strains from the cross-frames into axial forces and stresses, a linear regression procedure outlined in Helwig and Fan (2000) Appendix B was used. The cross-frames were made up of angle sections. According to the mechanics of thin-walled structures, no warping stresses are induced in these cross-sections when members are subjected to torsional moments. Therefore, longitudinal stresses are caused exclusively by axial force and bending moment and are distributed linearly along the cross-section of the bracing members. The longitudinal stress distribution is described by the following equation:

$$f = a + bx + cy \qquad 3.1$$

Where:

f is the longitudinal stress (determined from Hooke's Law as the measured strain multiplied by the modulus of elasticity E)

x, y are locations on the coordinate system of the cross-section

a, b, c are constants

The Regression Method is used to determine constants b and c using the following equations:

$$I_{11}b + I_{12}c = I_{10} \tag{3.2}$$

$$I_{21}b + I_{22}c = I_{20} \tag{3.3}$$

Where:

$I_{11} = \sum_{i=1}^{n} (x_i - \bar{x})^2$

$I_{22} = \sum_{i=1}^{n} (y_i - \bar{y})^2$

$I_{12} = I_{21} = \sum_{i=1}^{n} (x_i - \bar{x})(y_i - \bar{y})$

$I_{10} = \sum_{i=1}^{n}(x_i - \bar{x})(f_i - \bar{f})$

$I_{20} = \sum_{i=1}^{n}(y_i - \bar{y})(f_i - \bar{f})$

$\bar{x} = \frac{1}{n}\sum_{i=1}^{n} x_i$

$\bar{y} = \frac{1}{n}\sum_{i=1}^{n} y_i$

$\bar{f} = \frac{1}{n}\sum_{i=1}^{n} f_i$

The constant a from Equation 3.1 is then calculated using:

$$a = \bar{f} - b\bar{x} - c\bar{y} \tag{3.4}$$

The axial force in the member can be derived using beam-column theory after the constants in Equation 3.1, are determined. If the origin of the x-y coordinate system passes through the centroid of the cross-section, the axial force is given by:

$$N = aA \tag{3.5}$$

Where:

N is the axial force

A is the cross-sectional area of the member

Detailed sample calculations for this method are included in Appendix H. Axial Force Sample Calculations.

3.6. Deflection Measurements

Deflection readings were measured using laser distance meters from ground level beneath the span. Quick-setting Hydrostone was used to create a level surface in holes dug directly below the reading locations. The laser distance meters were positioned on the hardened Hydrostone surface next to a marked location to ensure consistency in the readings. Upon taking a measurement, the meters collected three rounds of data from each position. Readings were taken with each bridge loaded and unloaded between each truck position. During post-processing, these three data points were averaged and rounded to the nearest unit able to be collected by the strain gauge. After all data points were averaged, the deflection measured during a load case was subtracted by the deflection measured during the last zeroth case (no load on bridge). The difference in these quantities signified the deflection of the bridge.

Chapter 4. Bridge Model Validation

4.1. Introduction to Model Validation

Parametric finite element modelling was used in the study to develop an understanding of the behavior and to provide comprehensive results that could be used to establish consistent design guidance for lean-on bracing applications. Therefore, accuracy in the modelling methods is critical towards achieving accurate results. It follows that the data from the field monitoring of bridges under construction (Lubbock Bridge) and the completed bridges (Lubbock, SH105, and Chisholm Trail Bridges) were important for model validation. Model validation is comprised of modeling the subject of the experimental data in a finite element analysis program, identifying key validation parameters affecting the results, and determining the minimum complexity of the model required to get representative results of the actual system. The bridges at SH 105, Chisholm Trail, and Lubbock were modeled using ABAQUS (2022) based on field measurements and design drawings. The key validation parameters affecting the results were identified as the support conditions, the deck-barrier stiffness, and the R-factors for the cross-frame members. The identification of these parameters led to adjustments to the model's element structure, mass distribution, and material properties. These adjustments led to the completion of high-fidelity models of SH 105, Chisholm Trail, and Lubbock bridges being developed. The results produced by the SH 105 and Chisholm Trail bridge models were representative of the results captured in the in-situ condition. Conversely, uncertainty in the loading conditions of the Lubbock bridge provided some difficulty to validation by the research team.

4.2. Model Validation Parameters

In order to refine a modeling approach to be used in future parametric studies, it is necessary to first develop accurate models of the bridges that were instrumented and loaded. Several variables were considered and tested in the validation of the bridge models. These variables most notably include the support conditions of the bridge, the modulus of elasticity of the bridge deck and rails, and R-factors applied to the braces in order to account for connection eccentricity. The following sections explain the significance of each of these components in detail, as well as the parameter ranges that were considered in the model validation.

4.2.1. Support Conditions

The TxDOT standard details specify five types of elastomeric bearing details for bridges: end fixed (EF), end expansion (EE), interior fixed (F), interior expansion (E), and end sliding (ES). The end and interior specify the location of the elastomeric bearing along the bridge length with respect to the end or interior piers of bent caps. An end bearing is at a simple support (such as an abutment), while an interior bearing is generally placed at a pier where the girder is continuous over the support.

As shown in Figure 4-1, fixed bearings include a bolt hole that tends to restrict translation at the bearing. Expansion bearings have slotted holds that tend to allow moving in the direction of the slot. Some bearings accommodate translations through the shearing of an elastomer, while other bearings accommodated translations through sliding and generally make use of reduced friction with materials such as polytetrafluoroethylene (PTFE).

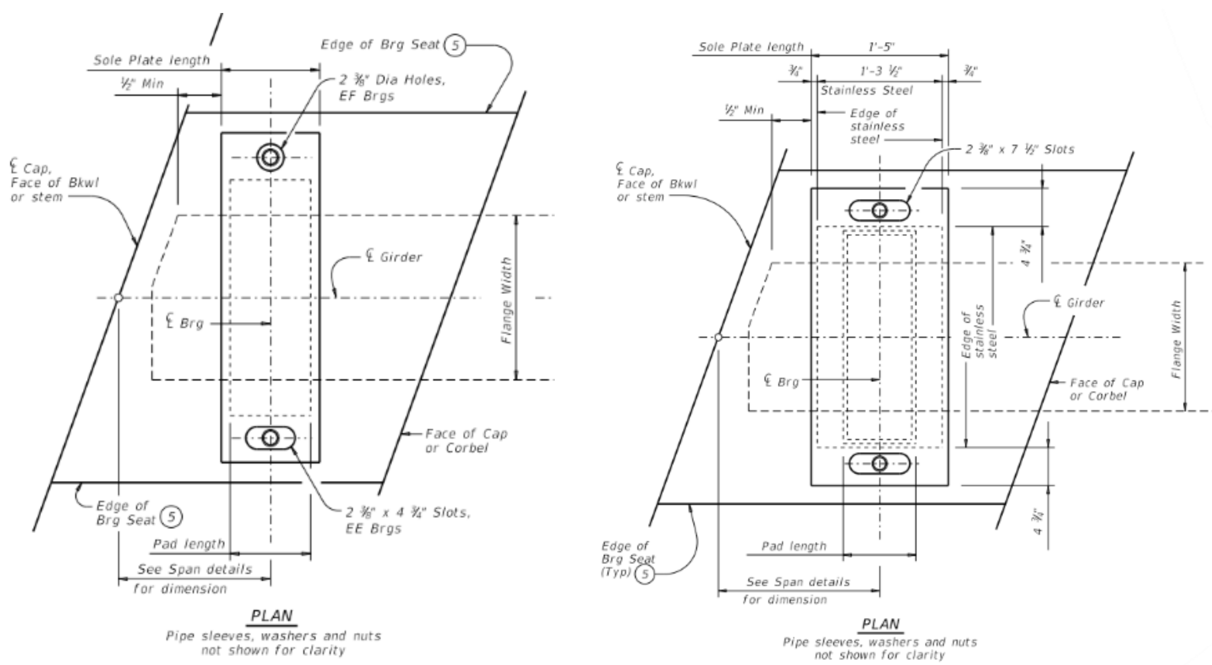

Figure 4-1. Fixed Support Detail (A) and Sliding Support Detail (B)

With an understanding of the behavior of these bearing details in mind, simplified support configurations were designed and tested by Han (2016) and Belivanus (2016). Han proposed that elastomeric bearings could be modeled as a combination of springs and rollers. The approximate spring stiffness was determined using *4.1* (Han, 2016).

$$k_{bearing} = \frac{GA}{h_{rt}} \tag{4.1}$$

Where:

$k_{bearing}$ is the spring stiffness

G is the shear modulus for an elastomeric bearing (~ 0.1 ksi)

A is the plan area of the bearing

h_{rt} is the total elastomer height

From *4.1*, the bearing stiffnesses for every support of each instrumented bridge in the present study were evaluated and are shown in Table 4-1.

Table 4-1. Bearing Type and Approximate Spring Stiffness for Each Instrumented Lean-On Bridge

	SH-105		**Chisholm Trail**		**Lubbock**	
	Type	$\boldsymbol{k_{bearing}}$	***Type***	$\boldsymbol{k_{bearing}}$	***Type***	$\boldsymbol{k_{bearing}}$
Abutment #1	ES7	$10.7\ \frac{k}{in}$	ES4	$8.2\frac{k}{in}$	ES3	$7.1\frac{k}{in}$
Abutment #2	EE7	$8.3\frac{k}{in}$	ES4	$8.2\frac{k}{in}$	ES3	$7.1\frac{k}{in}$
Interior Bent	E9, F9	$11.7\ \frac{k}{in}$	F7, E7	$10.4\frac{k}{in}$	F6	$9.4\frac{k}{in}$

Computational validation studies were conducted with various approximations between the bearing stiffness, restricting movements in the X, Y, and Z translational displacement, and altering the region of application of the boundary conditions. The test cases were as follows:

1. Single node application and all supports the same;
2. Single node application and supports varied based on detail;
3. Element edge application and all supports the same;
4. Element edge application and supports varied based on detail; and,
5. Element edge application, supports varied based upon detail, and springs instead of rollers on select bearing types.

Visual representations of each support case are included in Figure 4-2 and Figure 4-3. Flexible springs or rigid pin supports are indicated in the figure in the longitudinal (z), lateral (x), and/or vertical (y) directions.

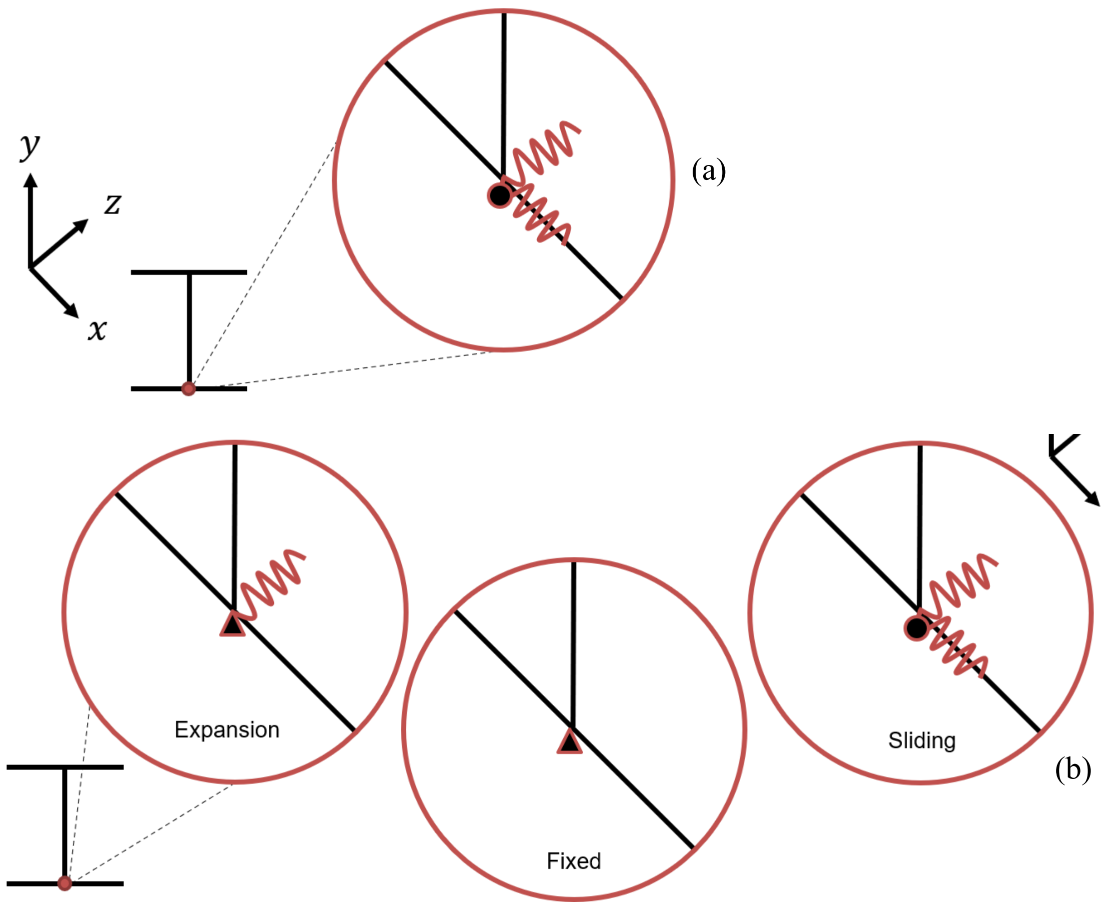

Figure 4-2. Support Approximation Model Cases 1 (a) and 2 (b)

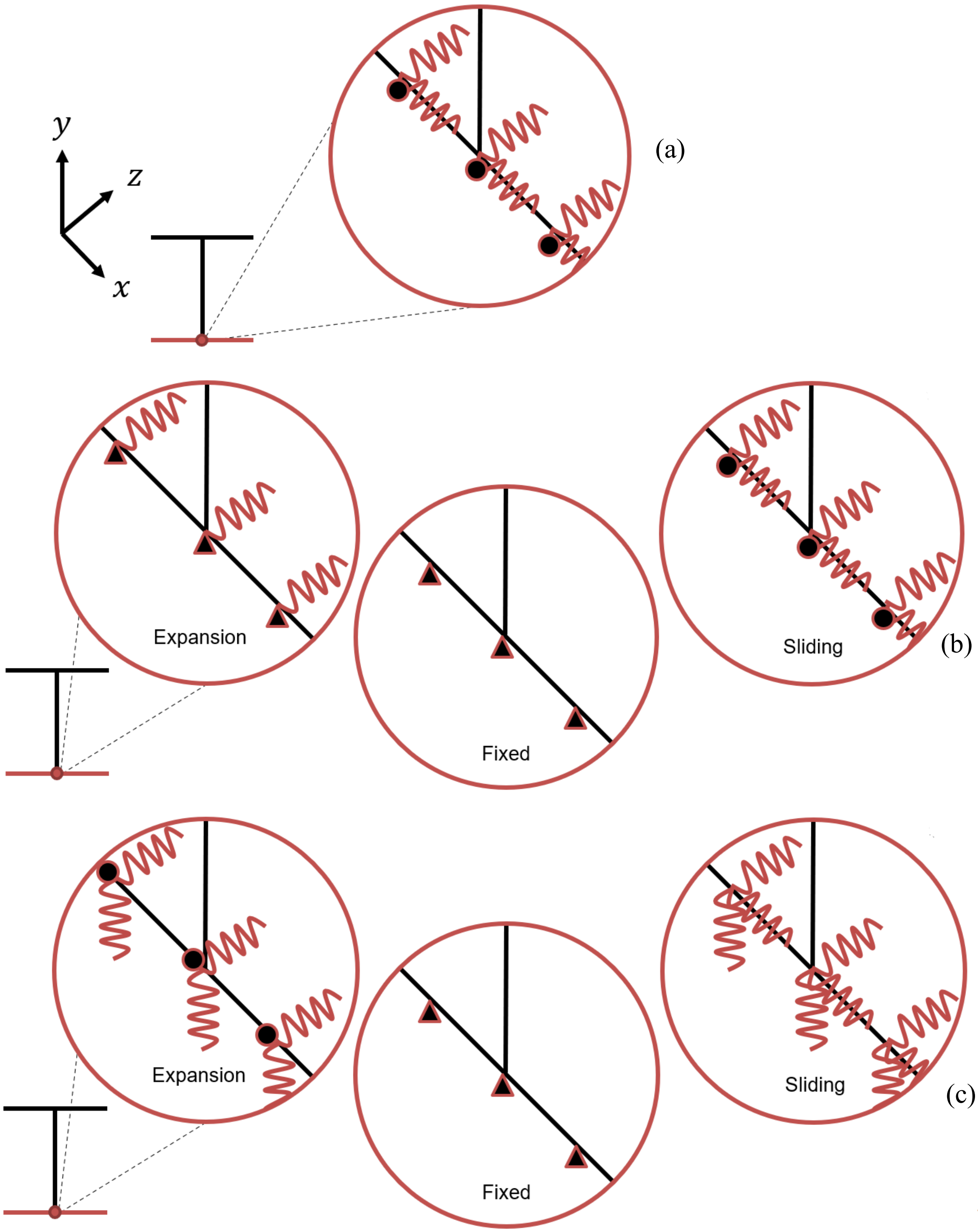

Figure 4-3. Support Approximation Model Cases 3 (a), 4 (b), and 5 (c)

For validation purposes, the spring stiffness at each support was altered during testing based on an amplification factor. Thus, values of the spring stiffness were augmented by a set percentage of the initial value. The results were processed using *4.2*. Test Case 4 offered the highest fidelity to the field results in comparison to the other support condition models and was therefore used in the validation models.

$$\frac{A_{factor} \cdot k_{bearing}}{k_{bearing}} \rightarrow \frac{k_A}{k_{bearing}} \quad 4.2$$

Where:

$k_{bearing}$ is the spring stiffness

k_A is the augmented spring stiffness

A_{factor} is the augment factor

4.2.2. Deck Modulus of Elasticity

The concrete components of each bridge contribute a significant component of the total system stiffness. Two of the most common metrics for defining concrete behavior are compressive strength (f'_c) and modulus of elasticity (E_c). The required compressive strength and concrete type are typically prescribed in the design drawings. The Young's modulus of elasticity is used to quantify the resistance of a material to tensile deformation, otherwise described as the stiffness of the material. The equation for the modulus of elasticity provided in AASHTO is included in 4.3.

$$E_c = 33{,}000\ K_1 w_c^{1.5} \sqrt{f'_c} \quad 4.3$$

Where:

E_c is the modulus of elasticity in ksi;

K_1 is a correction factor for the aggregate, usually taken as 1.0;

w_c is the unit weight of concrete in kcf; and,

f'_c is the compressive strength of concrete in ksi.

A similar equation is provided in ACI (2019) for normal-weight concrete. However, this equation was derived from the stress-strain curves of concrete and corresponds to the slope of the line drawn from a stress of zero to 0.45 f'_c . Because this equation does not depend upon the aggregate type, mixture proportions, or age of the concrete, there may be scatter in the data (2019).

$$E_c = 57{,}000\sqrt{f'_c} \quad 4.4$$

Where:

E_c is the modulus of concrete in psi; and

f'_c is the compressive strength of concrete in psi.

For completed bridges in this investigation, 4.4 was used to calculate an expected modulus of elasticity. An approximate range of ±1000 ksi from the expected modulus was considered in the analysis to ensure the most accurate value was used. It is important to note that in these models, the stiffness contribution of the concrete deck and rails is also affected by the rigidity of the connections. Increases in the connection stiffness may result in a higher validation modulus, while flexibility in the connections may cause a reduced modulus in the model, both of which can play an important role in correlating the accuracy of the model with measured data.

For bridges in construction, findings from Topkaya et al. (2004) were applied for guidance on the stiffness contribution of wet concrete. Topkaya et al. (2004) showed that concrete stiffness increases significantly faster than strength, with 90% stiffness but only 45% strength achieved after 22 hours. No data was taken within the first 4 hours of curing. Since approximately 30% stiffness was achieved at 4 hours, the researchers tested values from 0 to 30% of the calculated modulus of elasticity predicted with Eq. 2.4 for the stiffness of freshly placed concrete during deck placement.

4.2.3. R-Factors

R-factors are stiffness reduction factors applied to bracing members with eccentricity caused by connections, as reported in Battistini et al. (2016), Reichenbach et al. (2020), and Park et al. (2022). These members experience flexure due to connection eccentricity in addition to axial force, leading to a reduction in the effective axial stiffness of the members. The use of R-factors to modify the axial stiffness of line elements allow a significant reduction in the complexity of Finite Element Analysis models by enabling designers to simplify their bracing models by utilizing axial loaded elements that can be modeled using truss elements. This is permissible because R-factors apply a reduction in the stiffness of the member by effectively reducing the cross-sectional area or elastic material modulus of a member. Due to the stiffness of these elements being calculated directly using a combination of Young's Modulus and cross-sectional area, reducing either the area or the material modulus directly reduces the member stiffness.This in turn reduces the complexity required to model bridges, process the data, and reduces computation time, as truss elements are much simpler to model compared to the alternative of shell elements.

NCHRP Report 962 (M. Reichenbach et al., 2021) and Report 1045 (Park et al., 2022) provide R-factors for analysis. The R-factor for cross-frames is 0.75 (a 25% reduction in stiffness) for a constructed bridge and 0.65 (a 35% reduction in stiffness) for a bridge in construction. These reductions can be applied to eccentric X-frame and K-frame members. The authors are not aware of any studies conducted to determine an R-factor for lean-on struts. Since R-factors account for flexibility from the connection eccentricity, members with concentric connections have R=1.0. For the purposes of the research project, a range of 0.5 to 1 was used to determine the R-factors for structural systems that utilize lean-on struts. The methodologies applied in this research are consistent with those reported in Reichenbach et al. 2021 and Park et al. 2022.

4.3. Model Validation Procedures

ABAQUS (2022) was used to develop detailed models of the bridges. In order to test the variables described previously, a Python script was developed to efficiently build and analyze hundreds of models with varied parameters. The following sections discuss the details of the ABAQUS modeling procedures, Python scripting logic, and the objective functions used in MATLAB to determine the highest-fidelity model.

4.3.1. Overview of Modeling Practices (ABAQUS)

On top of the already discussed support condition approximations in Section 2.2, modeling bridges required several approximations and modeling decisions. Key modeling decisions and methodologies are listed below:

1. The deck, barriers, girders, and stiffeners are modeled using shell elements. Linear (S4) and quadratic (S8R) shell elements were used and evaluated. The mesh size was limited to 6 inches.
2. Bracing members were modeled using a single linear truss element (T3D2), and the cross-sectional area was reduced by an appropriate R-factor.
3. The deck and barrier are merged as a single part.
4. The ends of the braces are each terminated at a point along the girder web.
5. The deck-barrier and girder interact via a tie interaction.
6. Mass was distributed along each element to minimize errors in the cross-sectional properties of the shell elements.
7. Haunch depth was considered in the mass distribution. Haunch was calculated based on the thickest top flange.
8. Breaks/joints in the bridge curbs and barriers simulated by detaching elements at measured intervals with a 1-inch gap between them to represent system stiffness more accurately.
9. Although the barriers tended to taper along the height, these members were modeled as a rectangular cross-section with an average thickness.

4.3.2. Overview of Parametric Study Code (Python)

Parametric studies require a large number of bridge models to be produced with numerous variations in overall bridge geometry and cross-sectional properties. To facilitate the modeling and minimize errors from modeling, python scripting to generate the models provides and efficient means of capturing the wide range of parameters.

ABAQUS CAE allows the use of Python scripting to automate model construction, analysis execution, and data output. Capitalizing on this technology, the research team created a Python script that builds a desired bridge, analyzes that bridge, and returns relevant analysis data. The script reads an input file with various bridge parameters (see appendix for full details), such as bridge geometry, load patterns, and analysis settings. These inputs then inform the script and enable the script to create a bridge model according to the input specifications.

By using this script and varying input parameters, the research team can analyze a variety of bridge permutations in an efficient manner. While the development and evaluation of a robust Python script requires significant effort at the outset of the parametric program, the benefits of a validated script significantly improve the quality of the overall investigation since the research team can focus on the processing and interpretation of the output data.

4.3.3. Objective Functions (MATLAB)

The datapoints from the models were compared with measured values for the girder displacements in order to validate the support conditions and concrete modulus of elasticity. Models of each bridge were built and analyzed using ranges of values for the stiffness of the support conditions and the modulus of elasticity. In order to determine the most accurate combination of values for the support conditions and modulus, the displacement of the girders in the model was compared with the measured values for several truck load cases. In order to effectively compare these values, an equation for a square root sum of squares objective function was used, as shown below. The resulting value represents the total sum of the error from every data point measured in inches.

$$obj = \sqrt{\sum_{t=1}^{T}\sum_{n=1}^{n_g}\left(\Delta_{exp_{tn}} - \Delta_{model_{tn}}\right)^2} \qquad 4.5$$

Where:

T is the number of load cases considered

n_g is the number of girders

Δ_{exp} is the experimental girder deflection (in)

Δ_{model} is the model girder deflection (in)

4.4. SH 105 Brazos River Bridge Model Validation

4.4.1. Introduction to SH 105 Bridge Model Validation

The geometry of the SH 105 at Brazos River bridge and layout of instrumentation were discussed in Section 3.3. This section provides the steps that were utilized to validate the FEA model based on field measurements.

4.4.2. Validated Model Results

In order to validate an ABAQUS model of the SH 105 bridge, displayed in Figure 4-4, emphasis was placed on the spring and deck stiffness parameters. Parametric studies were run in order to determine the effect of the elastic modulus of the deck, elastic modulus of the bridge rails, and the support conditions. The test range of the elastic modulus was 1000 ksi to 5000 ksi in increments of 100 ksi. The bearing stiffness was adjusted based on a normalization of the default values in increments of 10% of the base value within a range of 80% to 120%. After analysis of the results, the models were determined to be insensitive to the modulus of the barrier and insensitive to the spring stiffness value. Overall, the displacement results were primarily affected by the deck modulus. The range of objective function values can be seen in Figure 4-5, with an optimum deck modulus of 5200 ksi and 100% spring stiffness. Plots of the girder deflections for this model are shown in Figure 4-6 - Figure 4-9. The agreement between measured and predicted values are reasonable and well within the resolution of the laser distance meter used to measure displacement, which was 1/16″.

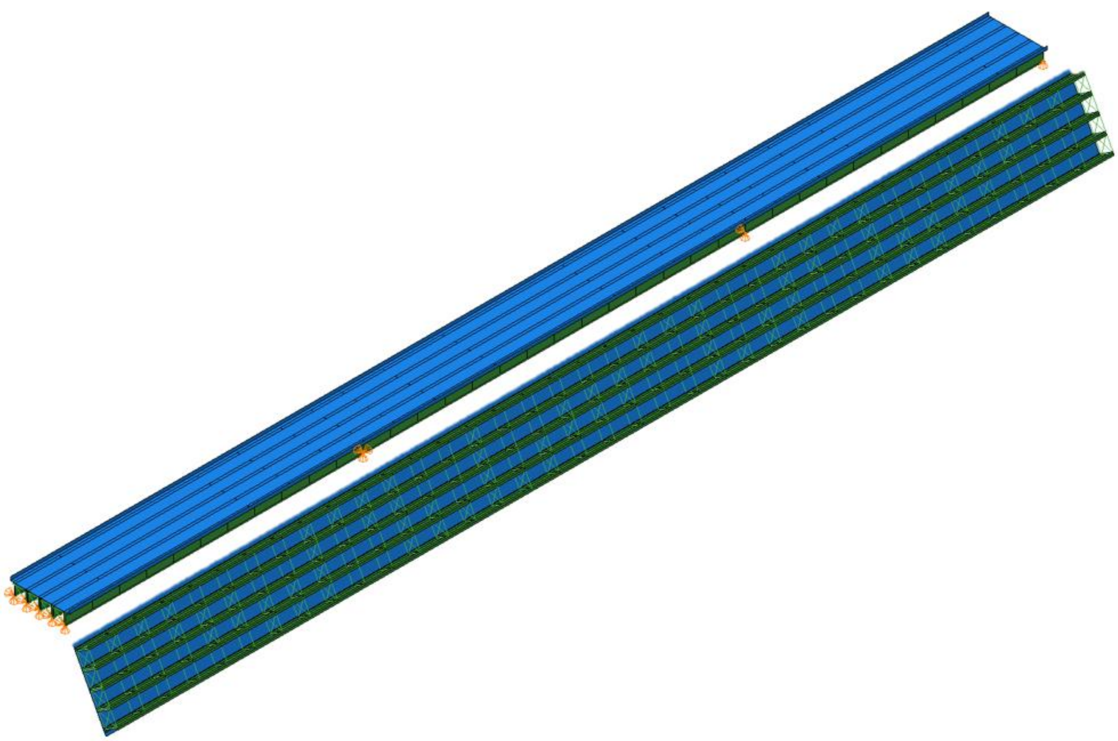

Figure 4-4. Model of SH 105

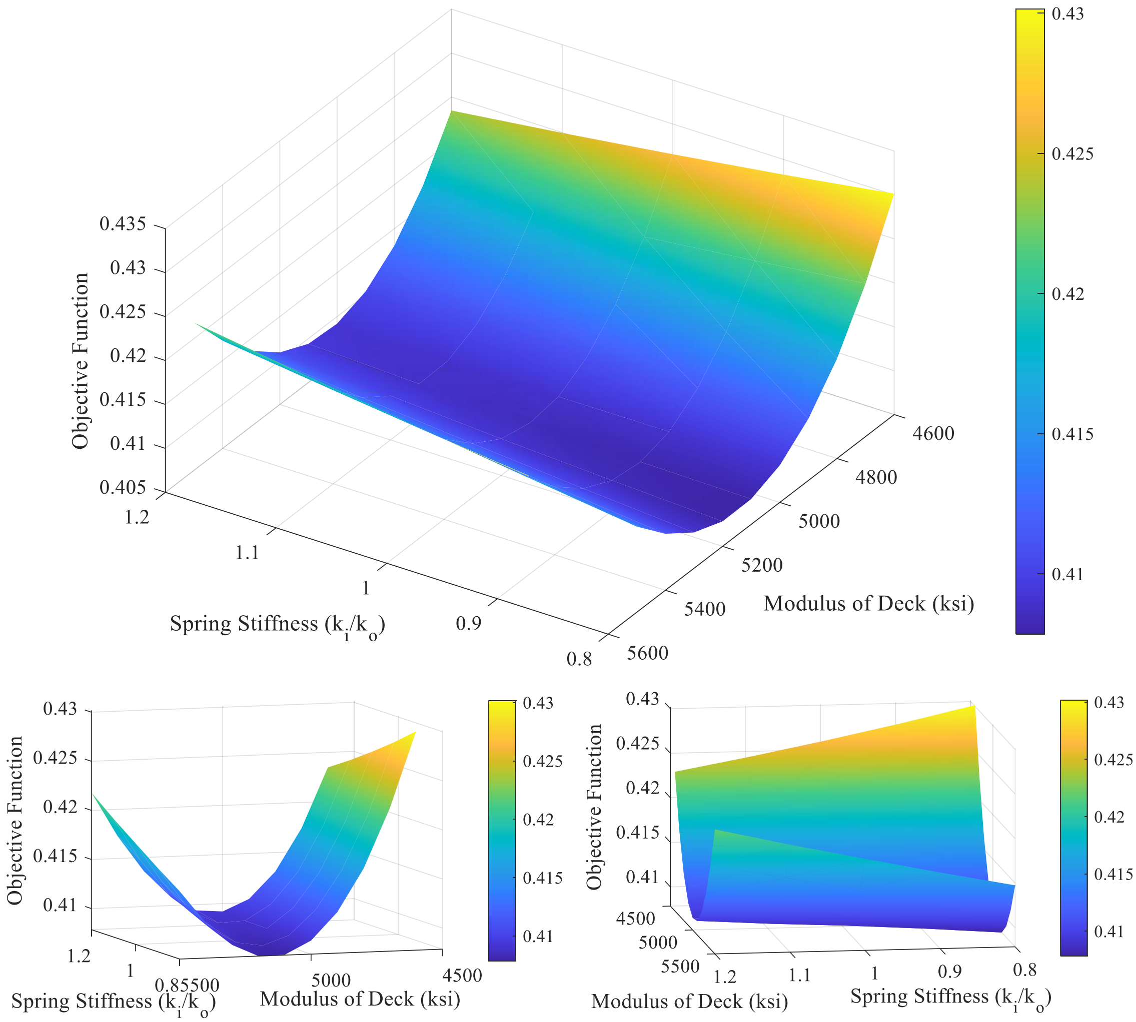

Figure 4-5. SH 105 Spring and Deck Stiffness Objective Function

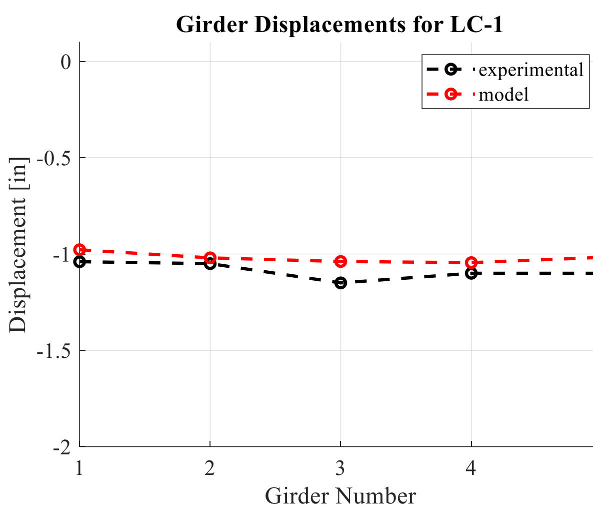

Load Case 1 Displacements [in]			
G	Experimental	Model	Exp/Model Difference
1	-1.04	-0.98	0.06
2	-1.05	-1.02	0.03
3	-1.15	-1.04	0.11
4	-1.10	-1.04	0.06
5	-1.10	-1.02	0.08
		Average	0.07

Figure 4-6. SH 105 Bridge Girder Displacements Load Case 1

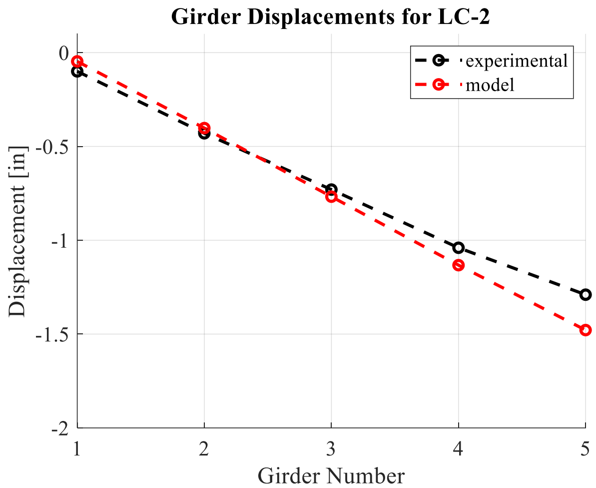

Load Case 2 Displacements [in]			
G	Experimental	Model	Exp/Model Difference
1	-0.10	-0.05	0.05
2	-0.43	-0.40	0.03
3	-0.73	-0.77	0.04
4	-1.04	-1.13	0.09
5	-1.29	-1.48	0.19
		Average	0.08

Figure 4-7. SH 105 Bridge Girder Displacements Load Case 2

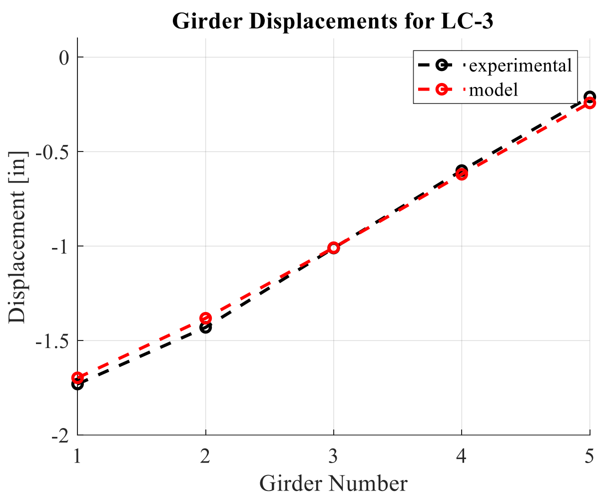

Load Case 3 Displacements [in]			
G	Experimental	Model	Exp/Model Difference
1	-1.73	-1.70	0.03
2	-1.43	-1.38	0.05
3	-1.01	-1.01	0.00
4	-0.60	-0.62	0.02
5	-0.21	-0.24	0.03
		Average	0.03

Figure 4-8. SH 105 Bridge Girder Displacements Load Case 3

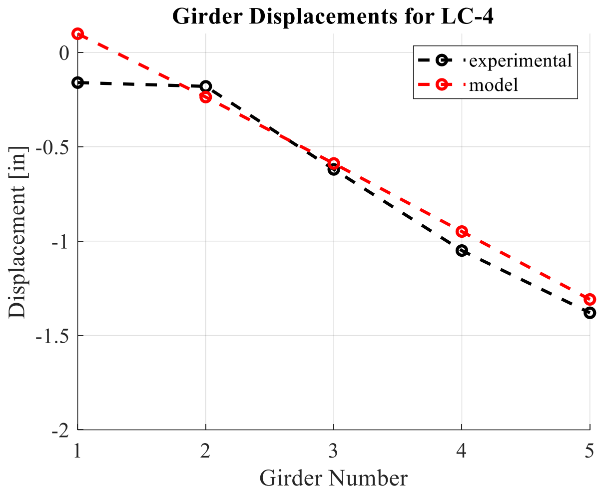

Load Case 4 Displacements [in]			
G	Experimental	Model	Exp/Model Difference
1	-0.16	0.10	0.26
2	-0.18	-0.24	0.06
3	-0.62	-0.59	0.03
4	-1.05	-0.95	0.10
5	-1.38	-1.31	0.07
		Average	0.10

Figure 4-9. SH 105 Bridge Girder Displacements Load Case 4

4.5. Chisholm Trail Bridge at FM1902

4.5.1. Introduction to Chisholm Trail Bridge Model Validation

The FM 1902B Overpass at Chisholm Trail Parkway is a completely constructed six-girder bridge located in Johnson County, Texas, south of Ft. Worth. The bridge geometry and instrumentation were discussed in Section 3.4.

4.5.2. Validated Model Results

The validation of the Chisholm Trail bridge was conducted similarly to the SH 105 bridge model. However, there are two key differences between the two bridges. The Chisholm Trail bridge has a large barrier in the middle of the deck and utilizes some double-angle members, as shown in Figure 4-10, while SH 105 does not. The interior barrier greatly affected the stiffness of the system and thus was a major focus in the stiffness validation. The parametric studies varied the elastic modulus of the deck, the elastic modulus of the barrier, and the stiffness of the support conditions. The range of the elastic modulus tested was 1000 ksi to 5000 ksi. The spring stiffness was adjusted based on a normalization of the default values in increments of 10% of the base value from 80% to 120%. Similar to the findings from SH 105, the behavior of the model was found to be insensitive to the spring stiffness value, and the base approximation was acceptable. Unlike the SH 105 model, however, both the modulus of the deck and barrier influenced system performance. The analysis of the system was conducted with variations of the modulus of the deck and barrier/rails from 2000 to 5000 ksi in increments of 750 ksi. The objective function results are provided in Figure 4-11. The modulus of the deck with the best correlation is shown to be 4250 ksi, and the modulus of the barrier and rails is 5000 ksi. The resolution of the laser distance meter used to measure displacement is 1/16″, and many of the model values are within or close to that tolerance.

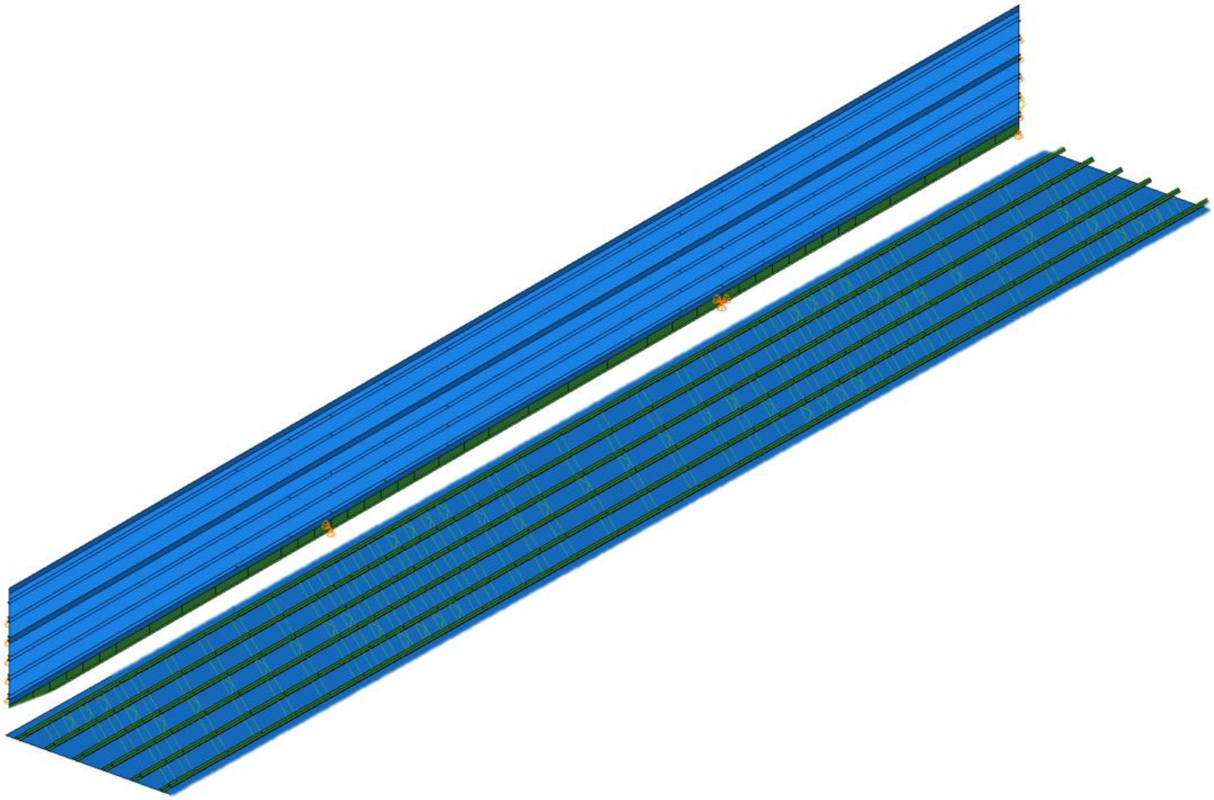

Figure 4-10. Model of Chisholm Trail Bridge

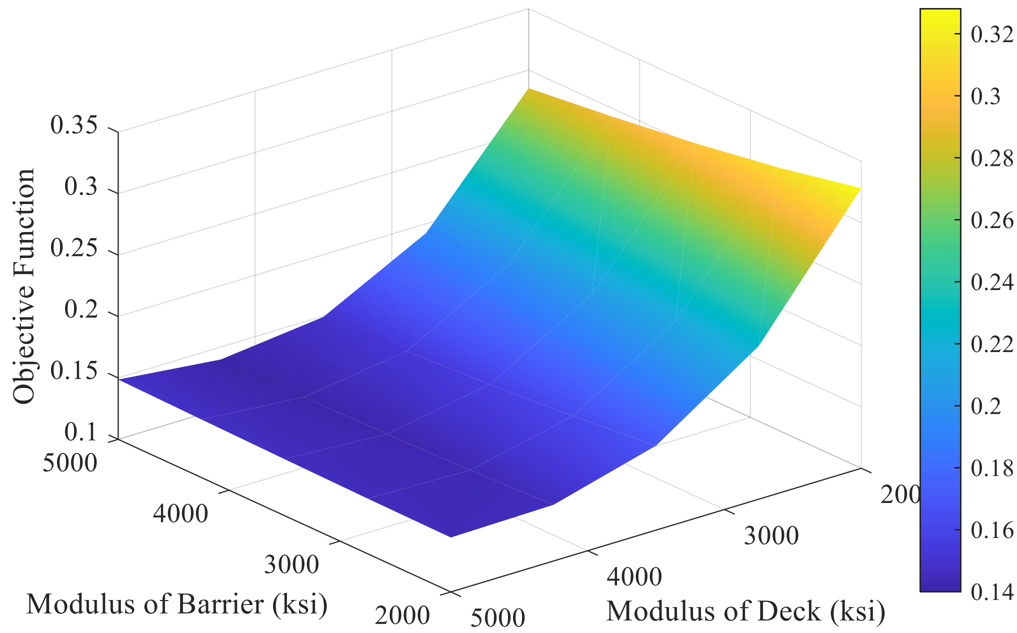

Figure 4-11. Chisholm Trail Deck and Barrier Stiffness Objective Function

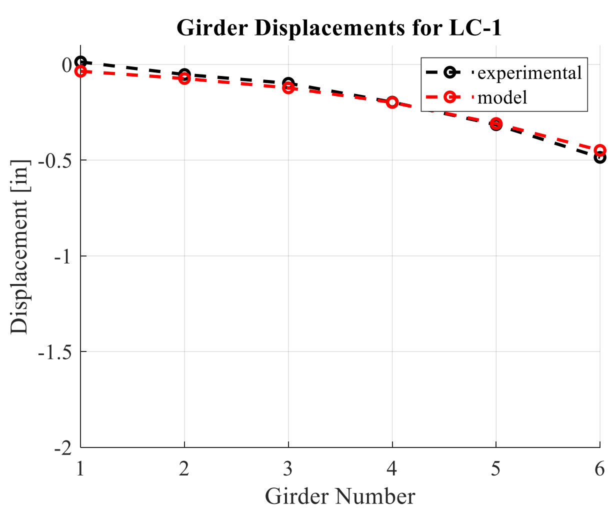

Load Case 1 Displacements [in]			
G	Experimental	Model	Exp/Model Difference
1	0.01	-0.04	0.05
2	-0.05	-0.07	0.02
3	-0.10	-0.12	0.02
4	-0.20	-0.20	0.00
5	-0.31	-0.31	0.01
6	-0.49	-0.45	0.04
		Average	0.02

Figure 4-12. Chisholm Trail Girder Displacements Load Case 1

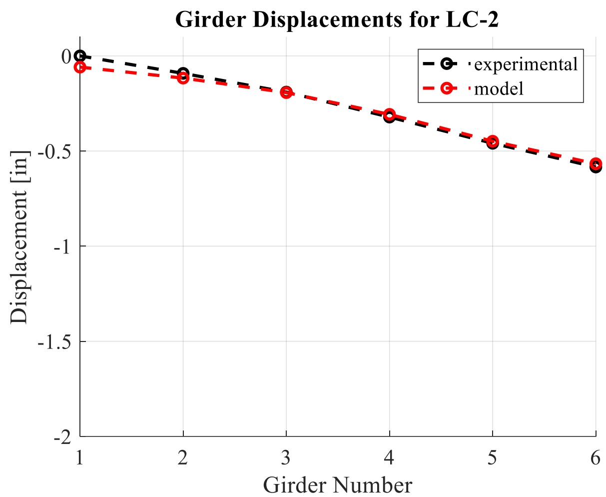

Load Case 2 Displacements [in]			
G	Experimental	Model	Exp/Model Difference
1	0.00	-0.06	0.06
2	-0.09	-0.12	0.02
3	-0.19	-0.19	0.00
4	-0.32	-0.31	0.01
5	-0.46	-0.45	0.01
6	-0.58	-0.57	0.02
		Average	0.02

Figure 4-13. Chisholm Trail Girder Displacements Load Case 2

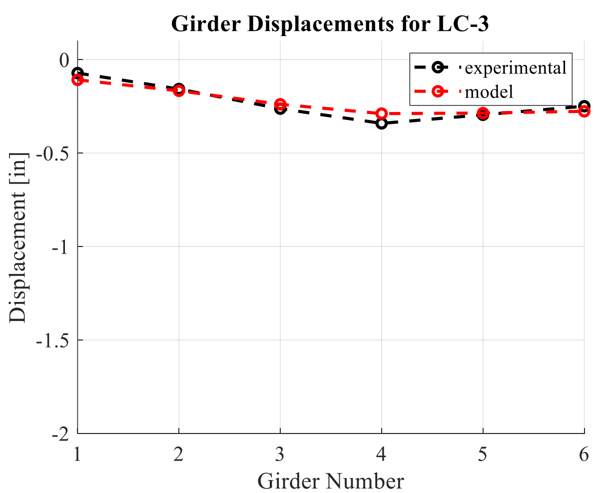

Load Case 3 Displacements [in]			
G	Experimental	Model	Exp/Model Difference
1	-0.07	-0.11	0.04
2	-0.16	-0.17	0.01
3	-0.26	-0.24	0.02
4	-0.34	-0.29	0.05
5	-0.30	-0.29	0.01
6	-0.25	-0.28	0.03
		Average	0.03

Figure 4-14. Chisholm Trail Girder Displacements Load Case 3

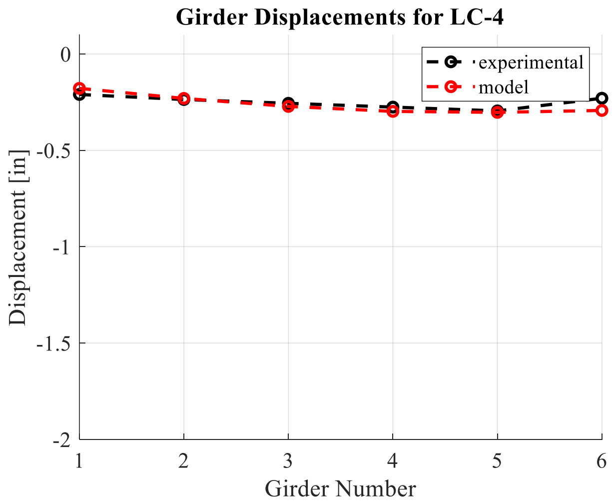

Load Case 4 Displacements [in]			
G	Experimental	Model	Exp/model Difference
1	-0.21	-0.18	0.03
2	-0.24	-0.23	0.01
3	-0.26	-0.27	0.02
4	-0.28	-0.30	0.02
5	-0.30	-0.30	0.01
6	-0.23	-0.29	0.06
		Average	0.02

Figure 4-15. Chisholm Trail Girder Displacements Load Case 4

4.6. Lubbock Bridge Model Validation

4.6.1. Overview of Lubbock Bridge

The 19th Street West Bound Bridge in Lubbock, TX, was instrumented as part of TxDOT Project 0-1772 Cross-Frame and Diaphragm Behavior in Bridges with Skewed Supports. The bridge has a 60-degree skew, resulting in different critical cases compared to a non-skewed bridge. The bridge has three spans and six girders across the width. Data for this bridge was recorded for the lean-on bracing during the deck pour, as reported by Romage (2008). The data from this bridge is very valuable to the present study since no bridges with lean-on bracing were identified that are under construction during the life of this study. Romage (2008) provides a detailed discussion of the sensor layout for the project, and a summary is provided in Section 3.2. Sensor readings from the deck pour were used for model validation.

4.6.2. Field Instrumentation and Testing

The instrumentation plan utilized for testing the Lubbock bridge is discussed in Section 3.2. Two cross-frame lines were instrumented: one in the support region and one at the midspan of the bridge. Three lean-on strut sets and two cross-frames were instrumented with strain gauges.

As previously stated, the Lubbock data is currently the only data set available for lean-on bracing during construction. The data includes several hours of deck pour, which was the focus of the validation. Unlike SH 105 and the Chisholm Trail bridge, modeling construction requires the consideration of the loads applied by overhangs, screed, scaffolding bridges, and concrete. Figure 4-16 is a picture taken during the deck pour highlighting these construction components.

Figure 4-16. Lubbock Bridge During Deck Pour (Romage, 2008)

Based upon the field notes (Romage, 2008), a deck pour timeline was constructed and is shown in Figure 4-17. Gaps in the field notes prevented a full timeline from being prepared. There was some uncertainty in the timeline; however, the focus of the validation readings are based upon the readings with no concrete and the changes when all of the concrete was placed on te bridge. Therefore, the timeline is not a major factor in the resulting data. Figure 4-17 provides an overview of the deck casting sequence. The concrete placement started on the West end of the bridge and progressed across the positive moment region. Around 7am. Concrete was placed of the support region at the East end of the bridge to prevent uplift. The casting then proceeded from the span on the West end of the bridge towards the East end with a continuous deck casting sequence.

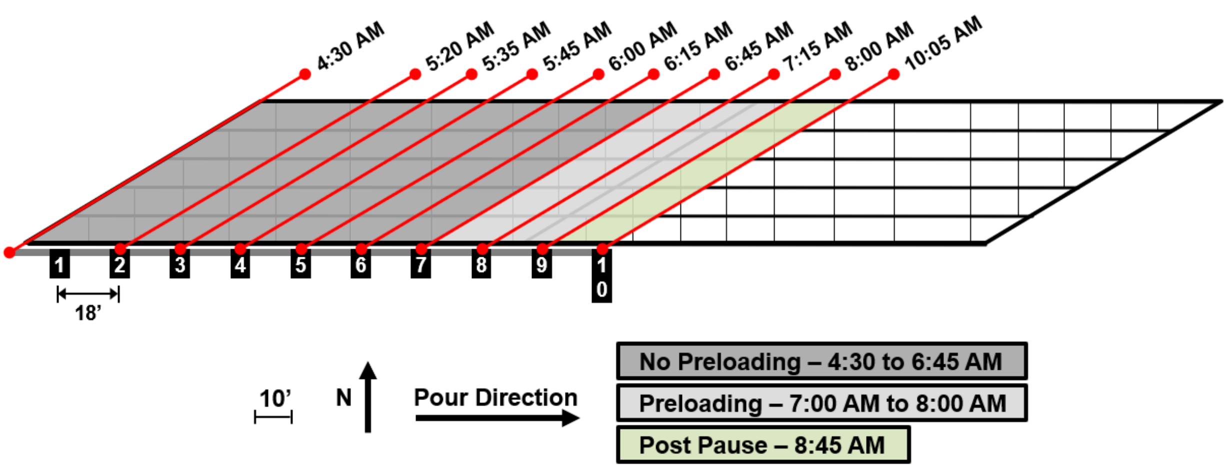

Figure 4-17. Deck pour sequence timeline created by research team for reference based on field notes during Lubbock instrumentation.

A mockup of the applied loads for the construction condition are shown in Figure 4-18 based upon the field notes from the instrumentation and typical construction values. The overhangs were placed every 72".

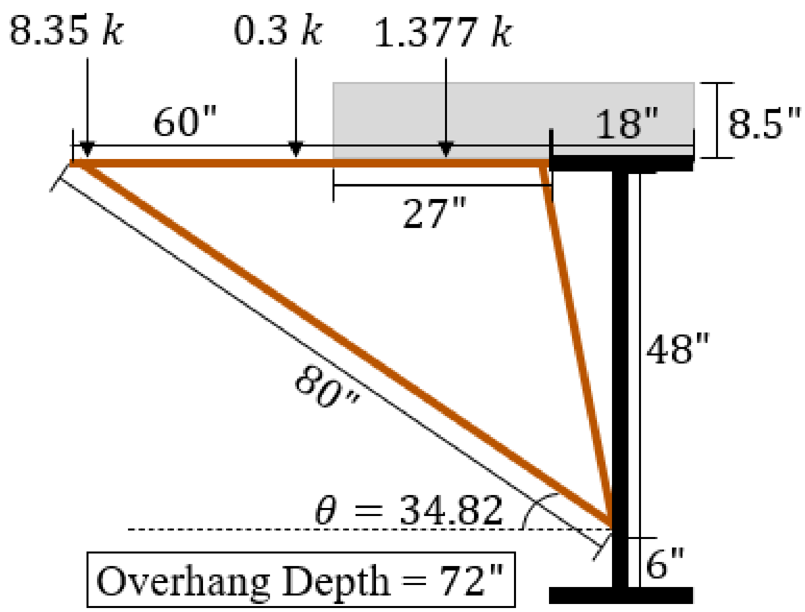

Figure 4-18. Overhang loading to be applied during construction based on field notes.

The horizontal loads applied to the girders at each overhang brace can be categorized by the source of the load:

- The concrete (C) contributed 0.5 kips.
- The screed (S) contributed 12.5 kips.
- The first bridge (B1) contributed 6.2 kips.
- The second bridge (B2) contributed 3.3 kips.

Based upon the field notes, these loads were applied at the following positions relative to each other and to the skew of the system as shown in Figure 4-19. The exact position of these components was not measured throughout the deck pour. As such, the research team used the estimated rate of the deck pour and consistent spacing based on the initial few hours of field notes.

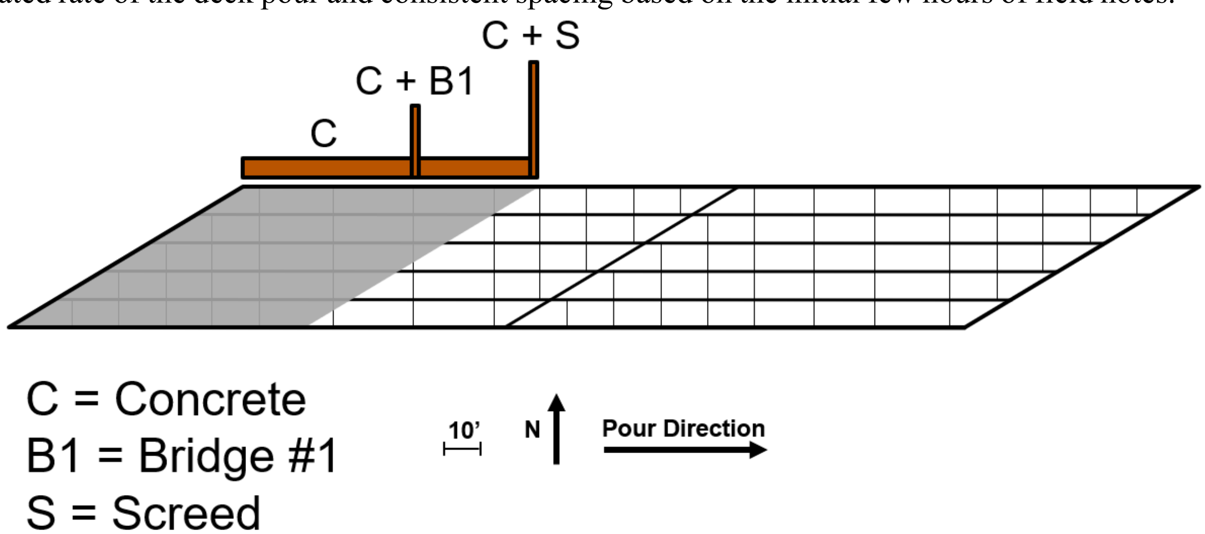

Figure 4-19. Overhang load positions of screed and deck pour bridges.

The Lubbock model was designed to fit the 6:00 AM deck pour condition based upon the previously stated modeling assumptions and can be seen in Figure 4-20. The figure illustrates all of the potential locations for the overhang forces based on the overhang bracket positions. However, only brackets in the deck pour region were given load magnitudes. The self-weight of the concrete was included in the concrete properties.

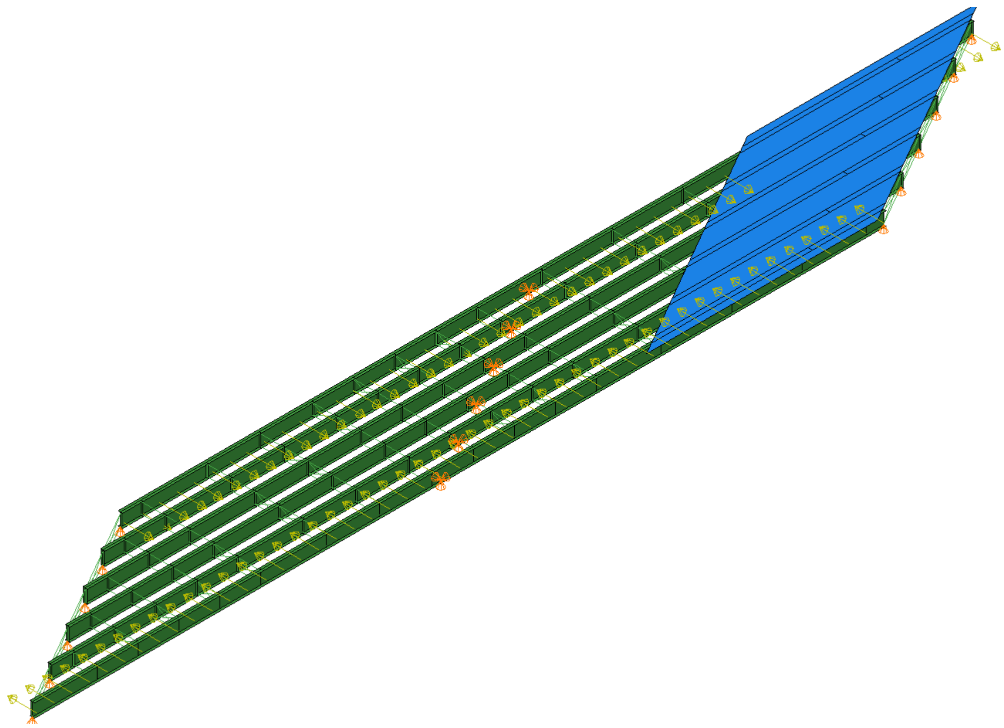

Figure 4-20. Lubbock Model used for Validation

4.6.3. Validated Model Results

The research team conducted a parametric study varying the R-factor for lean-on bracing from 0.4 to 0.6 for both the lean-on struts and full cross-frames, and modulus of the deck (0 to 200 ksi). The results demonstrated the best settings involved a lower stiffness of 36 ksi was preferred, but the results were generally insensitive to the R-factor.

However, the reason the results were indifferent to the R-factor was due to the conflicting behavior of the two cross-frames instrumented in the model. When the results of one cross-frame line improved, the results of the other cross-frame line strayed further from the experimental results. Figure 4-21 highlights this by showing relatively comparable results in CFL #7 at the loss of comparable results in CFL #3.

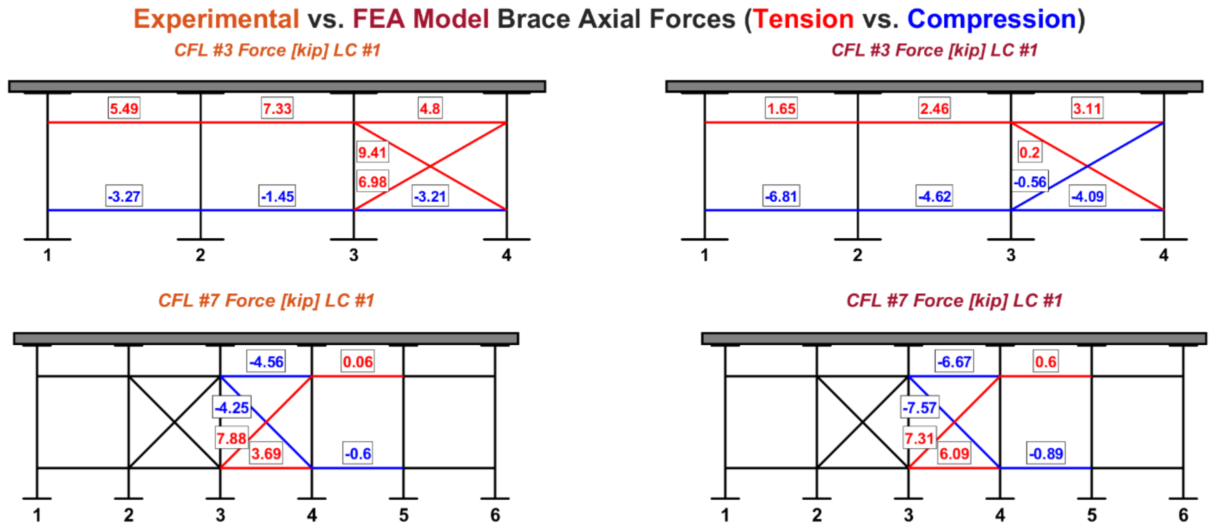

Figure 4-21. Results from 6:00 AM Model

The research team attempted to adjust the model by introducing a linear concrete stiffness distribution and manipulating the support conditions. These alterations did little to change the conflicting results. Based on the validation of SH 105 and Chisholm, the research team concluded that the uncertainty in the loading and deck pour timeline was likely the cause of the discrepancy and was not something the research team could overcome by altering the model. Thus, the research team concluded that the modelling decisions based upon the data from the three bridges had good to reasonable agreement.

4.7. Application of Methodology in Future Analyses

The general modeling procedure discussed in Section 4.3.1 for 3D finite element analyses, as implemented in the Python scripts, played an important role in the parametric investigation. The Python scripting was used to create models in Chapter 5, which presents results on a detailed study considering different lean-on bracing cross-frame layout schemes for both normal and skewed bridge systems. The purpose of the study is to identify optimal layouts that can be recommended for designers for certain bridge geometries. 0 focuses on an analytical study to develop stiffness and strength estimates for various cross-frame layouts in a single line of bracing. A study for the individual cross-frame line stiffness was applied as a means of confirming the analytical derivations. The 3D modeling procedure was based around the utilization of ABAQUS (2022), a general finite element analysis program, to model bridge systems in order to obtain and verify stiffness quantities. The research team used two analysis procedures: eigenvalue buckling and nonlinear geometric large displacement analyses reflecting the impact of imperfections.

Eigenvalue buckling analysis is a first order static analysis method utilized to determine the stiffness and moment capacity of bridge systems. When a valid model is analyzed using this approach, the model provides an estimate of the critical buckling load (eigenvalue) along with the buckled shape (eigenvector)

For bridge applications, the eigenvalues and eigenvectors can be used to determine the critical buckling moment, buckling mode type (global, local, or between brace points), and stiffness required to reach those values. The brace stiffness that comes from an eigenvalue buckling analysis is related to the ideal stiffness, which was discussed in Chapter 2. The research team used eigenvalue buckling analyses to verify the brace stiffness and quantify factors to in-plane girder stiffness and global lateral torsional buckling moment capacity expressions. These analyses were also used to determine the behavior of lean-on layouts, lateral trusses, and support skew.

Nonlinear geometric analysis is a method by which a specified imperfection is applied to the system to represent the effects of out-of-straightness and twist associated with geometric tolerances. For the purposes of this report, nonlinear geometric imperfection was utilized to verify stiffness components and quantify layout effects. Chapter 2 provided a discussion of critical shape imperfections from previous studies. The recommendations from the previous studies were utilized to define the imperfection about the cross-frame line that was most likely to be critical.

Chapter 5. Live Load Stress Response of Lean-on Systems

One of the major benefits of using lean-on bracing is the reduction in live load induced stresses, specifically in skewed systems. Most cross-frames are comprised of single angle members, which fit into the AASHTO fatigue classification of E′, which is the worst detail in terms of performance. In these cases, a reduction in live-load induced stresses is highly desirable, particularly in bridges with skewed supports. A measure of the advantages of lean-on bracing can be obtained by comparing the behavior of a bridge with conventional bracing versus lean-on bracing as a with truck loading on the composite girder systems. For this purpose, a bridge with geometry consistent with the Lubbock bridge was utilized, considering both conventional and lean-on bracing. Using the HS20 design fatigue truck from AASHTO, various load paths were analyzed across the example bridge. The analysis was conducted using a linear static analysis to estimate forces in various cross-frames on the bridge. This section provides an overview of the behavior of the bridge with the different bracing layouts in terms of the live load induced stresses in the bracing.

The influence surface represents the axial force distribution of a selected bracing member as a function of a concentrated load applied at any longitudinal and transverse locations on the bridge deck. Figure 5-1 provides an example influence surface of the members of a single X-frame in the modeled bridge considering conventional bracing. While the influence surface represents the behavior of a structural member for a load applied at any location on the deck, a specific grid is generally used to generate the influence surface. For this example, the simulated truck load was applied at 60 points across the width of bridge. The yellow highlight represents the cross-frame that was selected for this example.

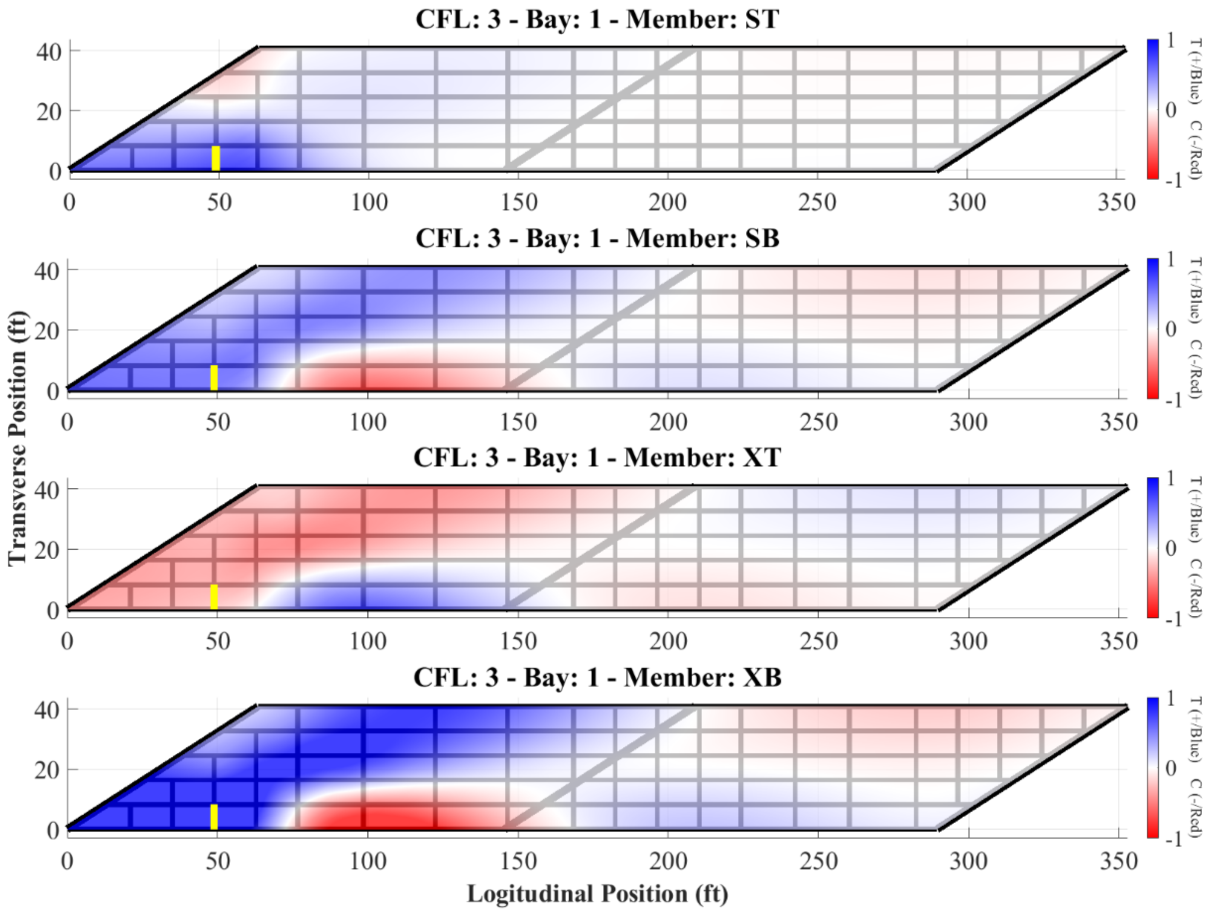

Figure 5-1. First Bridge Example using Conventional Layout Axial Force (kip) Influence Surface

The influence surface of the conventional system can be compared directly with that of the lean-on system which is shown in Figure 5-2. Overall, there is a reduction in the cross-frame member stresses. Additionally, the top strut features the greatest change in stress distribution, being in compression instead of tension.

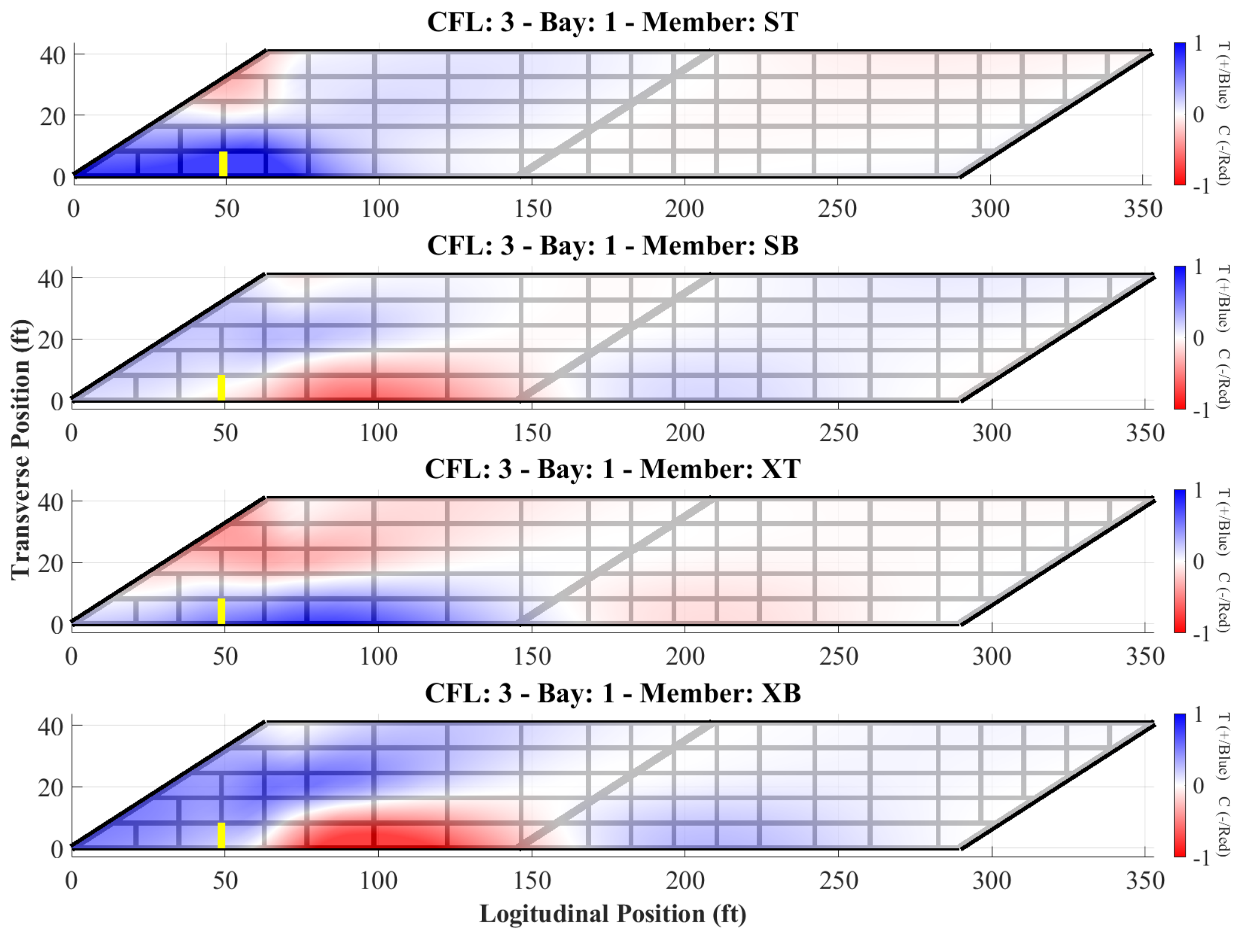

Figure 5-2. 1st Bridge Example using Lean-on Layout Axial Force (kip) Influence Surface

Another way to examine the results of an influence surface is by selecting the loading of a particular path of the truck. In this case, a truck loading path, illustrated in Figure 5-3, along the bottom half of the bridge was selected.

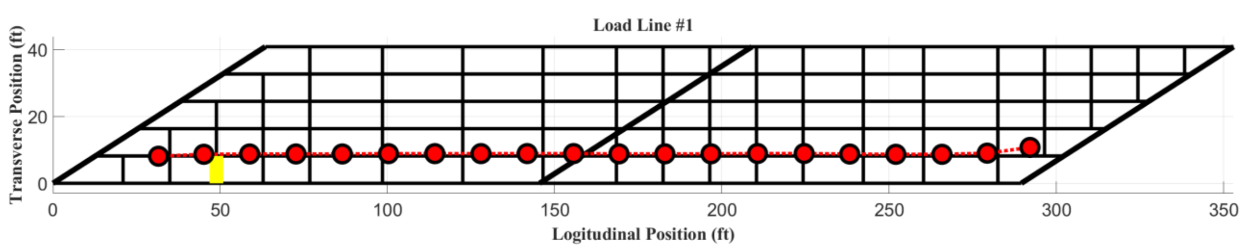

Figure 5-3. Example Truck Path

Here the stresses for each brace member can be directly compared at specific load points as shown in Figure 5-4.

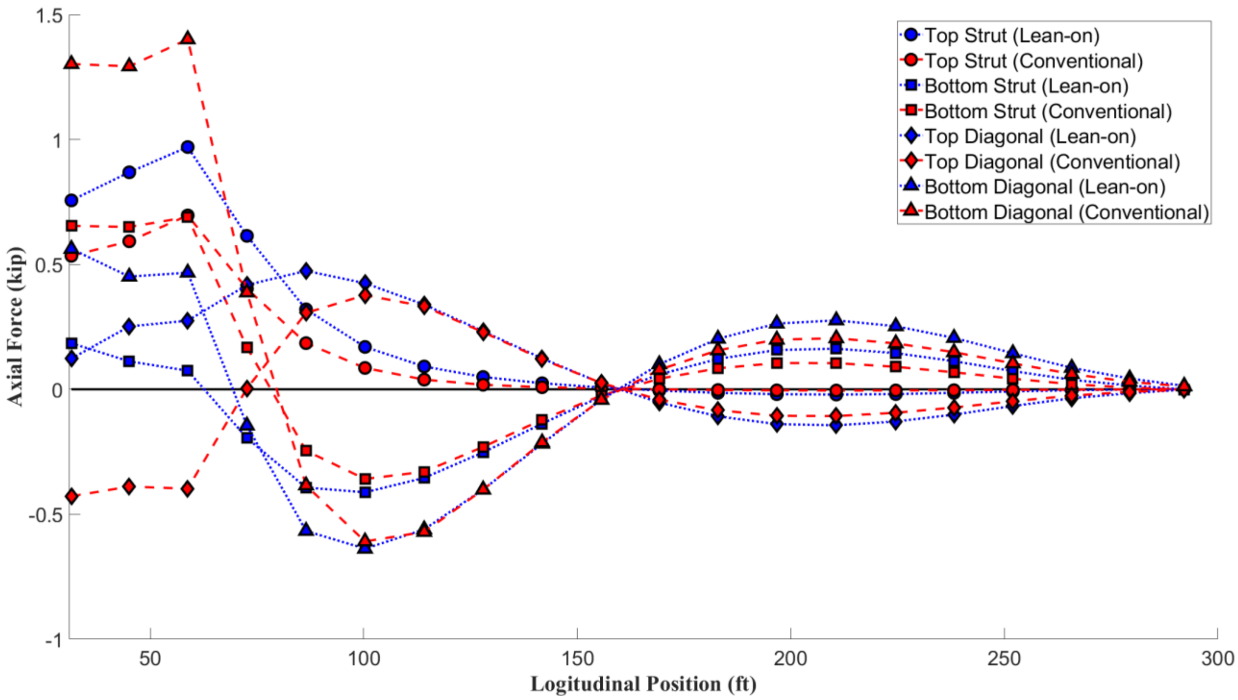

Figure 5-4. Comparison of Brace Stress along Truck Path for 1st Bridge Example

The results in Figure 5-4 highlight how the use of lean-on bracing can reduce the axial forces induced in the cross-frame members. This reduction in axial forces improves fatigue performance which is a primary advantage of lean-on bracing.

Another advantage to the use of lean-on bracing is the reduction in the number of bracing members in the bridge, which therefore reduces inspection requirements. For the example bridge model, this reduction can be seen in Figure 5-5. The lean-on version of the bridge has 216 total bracing members whereas the conventional system had 320 bracing members. Overall, this means that less bracing members experience fatigue stresses.

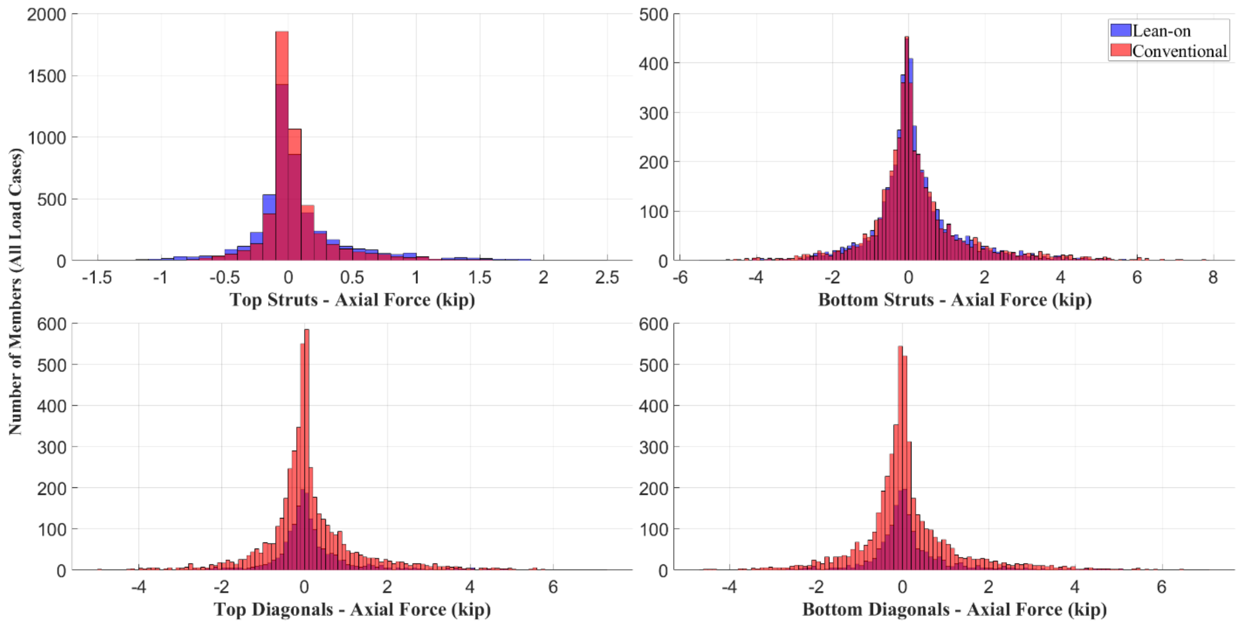

Figure 5-5. Comparison of Envelope Axial Force Distribution for 1st Example Model

A similar distribution can be found by running a second example bridge using the system geometry of SH 105. The results for the conventional and lean-on layouts are shown in Figure 5-6. Overall, the nonskew bridge generally had a magnitude lower forces than the heavily skewed bridge, emphasizing that cross-frame fatigue is primarily a concern skewed systems.

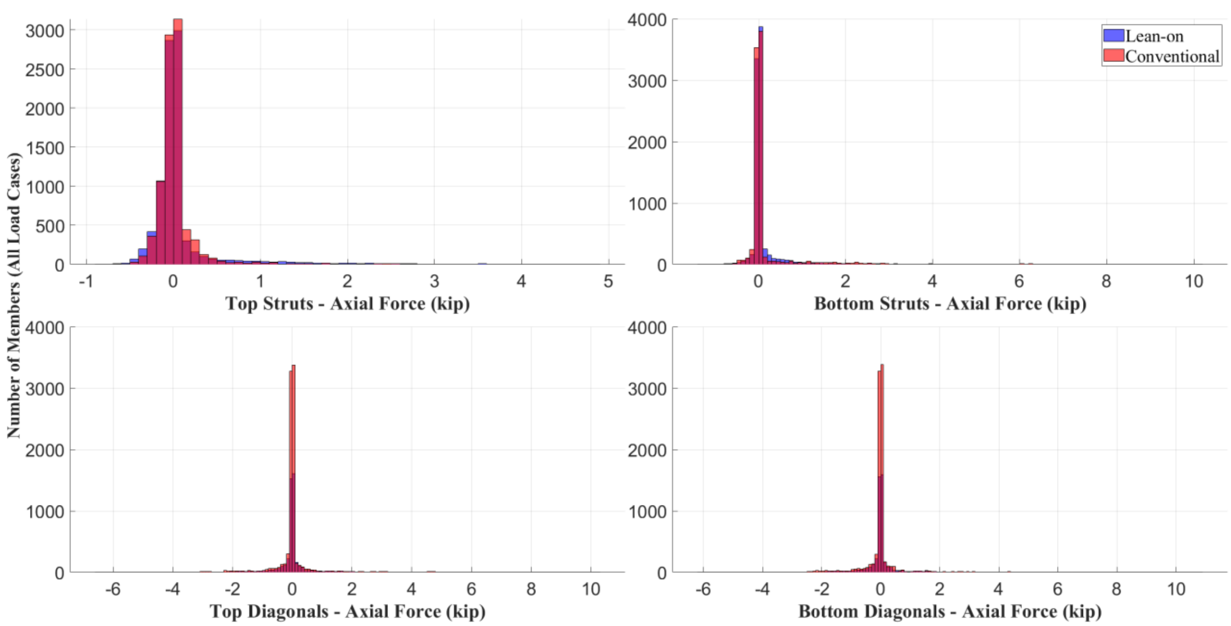

Figure 5-6. Comparison of Envelope Axial Force for 2nd Example Model

Chapter 6. Configuration of Cross-Frame System in Lean-on Systems

The research investigation included several studies investigating the stiffness behavior with lean-on bracing. The investigations included both eigenvalue buckling analyses as well as nonlinear geometrical analyses on imperfect systems. Eigenvalue buckling analyses provide insight in the ideal stiffness behavior of the system as well as the controlling buckling modes. Nonlinear geometrical analyses provide insight into the behavior in terms of brace forces and deformational behavior. The term "layout-study" refers to parametric investigations focused on the structural behavior based upon positioning of cross-frames along the length and width of the bridge.

The initial studies consisted of eigenvalue buckling analyses that provided an indication of the effectiveness of various lean-on configurations. Subsequent studies considered the behavior by isolating the brace stiffness component and included both eigenvalue buckling analyses and nonlinear geometric analysis on imperfect systems. As is discussed later in the chapter, the studies demonstrated that different buckling modes resulted depending on the geometry and bracing utilized for specific problems. In some instances, the controlling mode shapes involved buckling between the brace points at critical locations on the structure as discussed and illustrated in Chapter 2.2. In other cases, the controlling buckling mode resembled a half-sine curve mode that is labeled as a global mode. Based upon the results from the study, observations are made regarding the optimal layout, which was used to develop the final recommendations on the cross-frame layout.

Due to the significant number of parameters and geometries possible with lean-on bracing, refining the number of layouts was a difficult process. The parametric studies were therefore conducted in three phases. The purpose of Phase 1 was to identify lean-on configurations that were likely to be the most efficient and consisted of two steps within the phase. Step 1 consisted of "preliminary studies" to eliminate ineffective layouts. Step 2 consisted of an increased focus in the investigation of lean-on configurations to target the most effective candidate layouts for consideration in the subsequent analysis phases.

Phases 2 and 3 generally consisted of studies that isolated the bracing components so that design solutions for each component could be developed. More specifically, Phase 2 focused on determining solutions reflective of the behavior related to the cross-frame stiffness for different lean-on configurations. The Phase 2 studies demonstrated the ideal distributions based upon the controlling buckling mode shapes. In Phase 3, the impact of the lean-on configuration on the in-plane girder stiffness was studied. The studies built off of the Phase 1 studies that primarily focused on systems with normal supports since the optimal lean-on layout was not as clear. The Phase 3 investigation was used to develop a "layout factor" that reflected the impact of lean-on bracing on the in-plane stiffness component. For systems with skewed supports, the optimal locations for the full cross-frames are more apparent and are discussed later in the chapter. Phase 2 and 3 consisted of detailed investigations on the most efficient systems identified in Phase 1. The Phase 2 and 3 investigations consisted of analyses on systems that allowed individual components of the bracing system (i.e. brace stiffness versus in-plane stiffness) to be considered so that design formulations for different lean-on components could be developed.

6.1. Phase 1: Initial Layout Study

The implementation of lean-on bracing into a design requires the specification of a layout of the cross-frames and lean-on struts. Due to the number of possible permutations, selection of the optimal layout is often not clear. The effective brace stiffness of each cross-frame line and the in-plane girder stiffness of the system are inter-related, and the relationship between these two components of the system stiffness must be developed.

The research team considered several possible bracing configurations and compared the relative performance of each layout. The initial layout study was conducted in two steps: 1) a preliminary investigation considering a wide array of layouts and 2) and a more detailed series of analyses on the most effective lean-on configurations. Figure 6-1 shows the layout of cross-frames that were considered in each step. The Conventional Layout (cross-frames in every bay) was included as a baseline case for the purposes of comparison for the lean-on configurations. Step 1 included a total of 6 lean-on configurations that were each given a name that reflected the distribution of full cross-frames based upon a plan view of the bridge span. Following Step 1, three of the bracing geometries tended to underperform and were therefore removed from consideration. Step 2 focused on the remaining three configurations that showed the best efficiency. The failure mode, buckling capacity, and minimum brace area corresponding to the ideal stiffness were recorded from the eigenvalue buckling analyses.

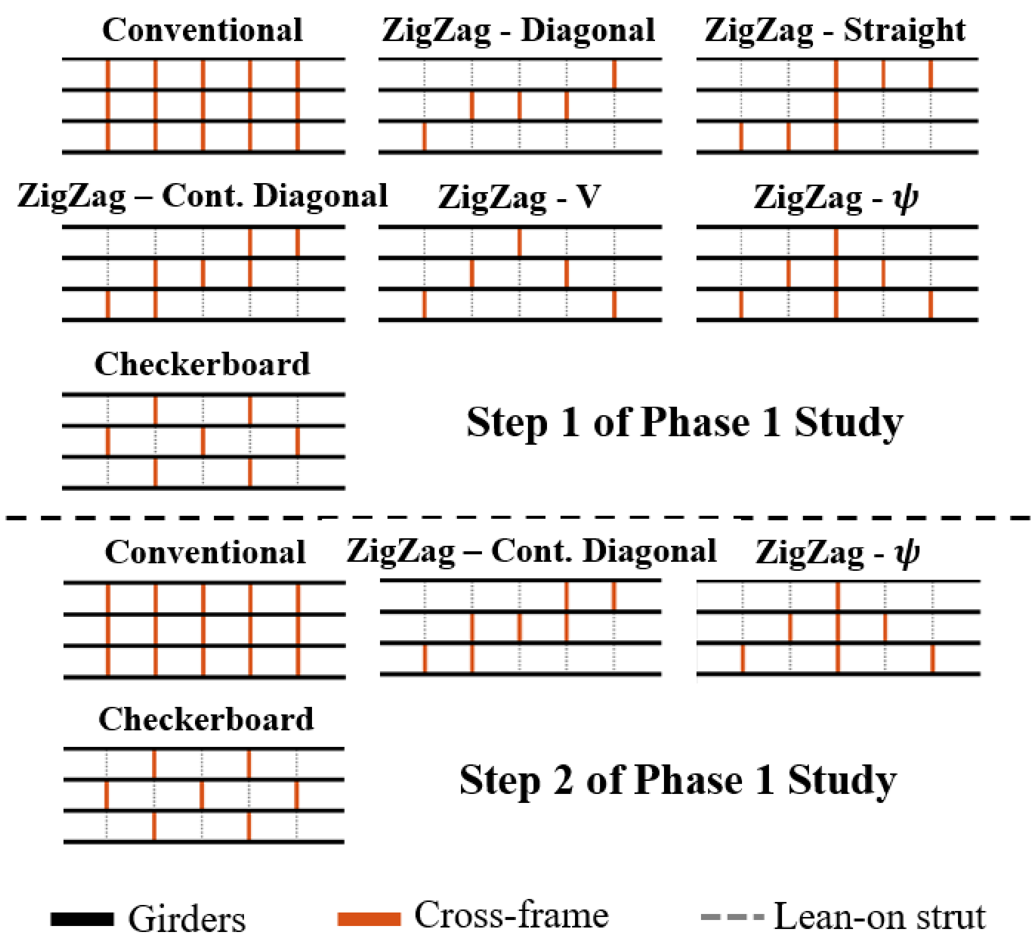

Figure 6-1. Configurations Considered in Preliminary (Step 1) and Initial Layout Study (Step 2)

The Phase 1 study made use of bridge systems that had either 4 or 5 girders along the bridge width. The girders were spaced at either 10′ or 12′ on center. The bridges with normal supports had span lengths of either 150′ or 250′ and the cross-sections are shown in Figure 6-2. The sections were proportioned using ratios of the span/depth and girder-depth/flange-width that are commonly used in design. The girder span-to-depth ratio was 25 for single-span bridges and 35 for continuous-girder systems. Girder cross-sections with a girder-depth to flange-width ratio ranging between 4 and 6 were evaluated. The ratio of 6 represents the extreme limit in the AASHTO BDS whereas the ratio of 4 is better representative of girder proportions often found in practice. Single- and two-span continuous bridges were studied with spacings between brace lines of either 25′ or 40′. Girder systems with flange-level lateral trusses included in the exterior bays of each span were also considered. However, due to the lack of relevancy to the layout study, the results for the lateral trusses are discussed in Appendix L. Phase 1 Lateral Truss Results. As noted earlier in the chapter, support skew was not considered in the initial (Phase 1) study, which included a total of 512 bridges.

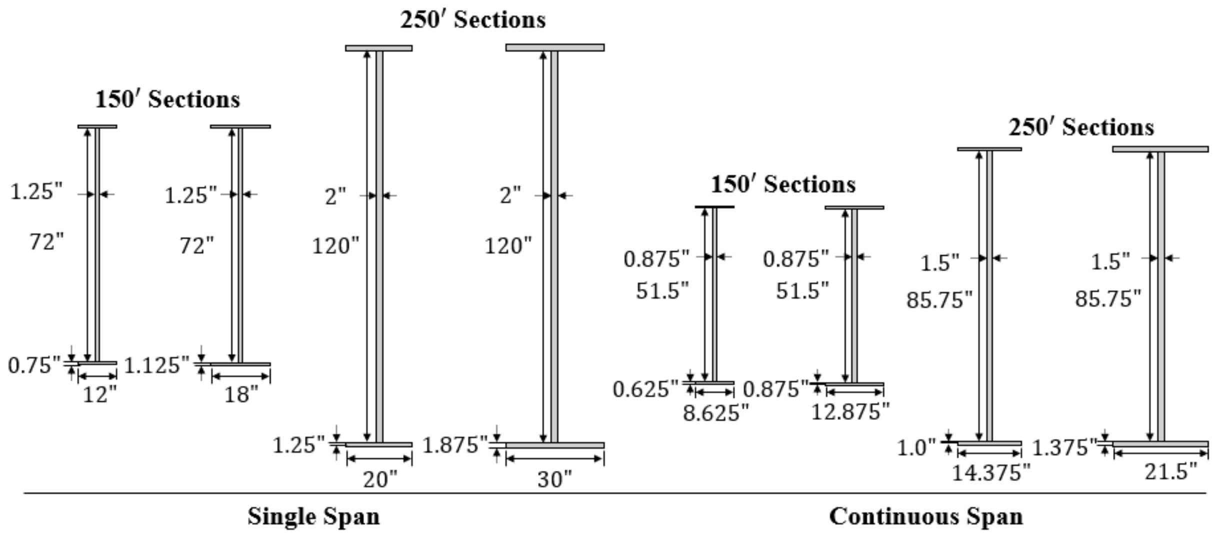

Figure 6-2. Girder Sections Used for Bridges in Initial Parametric Study

The effectiveness of the lean-on bracing configurations evaluated based upon the performance relative to the conventional bracing configurations (no lean-on bracing). These comparisons were conducted by examining the maximum moment capacity and the minimum brace area required leading to buckling between the bracing lines with uniformly distributed loads for the lean-on systems relative to the conventional bracing configuration. The uniformly-distributed load produced a non-uniform moment akin to the moment produced during a deck pour. The maximum brace area evaluated was limited to 5 in^2 which coincides with the maximum size recommended in the TxDOT standard details. From a detailing perspective, this maximum size would result in an angle size of approximately L6x6x5/8 with an R-factor reduction of 0.65 applied. For example, the area of an L6x6x5/8 is 7.13 in^2. Applying the reduction factor of 0.65, the modelled area is 0.65 x 7.13 in^2 = 4.63 in^2 < 5 in^2. While this level of detail was not utilized in the analysis – this provides an indication of the approximate size of the angle that might be chosen. In the analysis, specific brace areas were utilized that would need to reflect the reduction factor in actual applications. For each bridge, data was collected from the eigenvalue buckling analyses using the following brace areas (in^2): 5.00, 3.75, 2.5, 1.25, 0.50, 0.375, 0.250, 0.125, 0.1, 0.075, 0.050, 0.025, and 0.005, which results in a total of 6,656 datapoints. The areas less than 1 in. are obviously not practical in actual application and were utilized only to provide an indication of the behavior as a function of the brace stiffness.

The ideal brace stiffness is often referred to as the minimum brace stiffness required for the main member to buckle between the bracing lines. However, such a definition can be difficult to determine in a general girder system due to moment gradient and other sources of warping restraint that may develop at the brace locations. The potential warping restraint can vary significantly based on several factors. Therefore, multiple criteria were used to determine the ideal brace stiffness. The ideal brace stiffness was determined by either the minimum stiffness resulting in a mode shape corresponding to buckling between the brace points or the brace stiffness to reach the moment capacity from Timoshenko's buckling equation using the spacing between bracing lines. Additionally, a single-girder eigenvalue buckling analysis for each unbraced length and cross-section was conducted to ensure there was no major discrepancy between the model and calculations.

The main metric used to compare the configurations is the average minimum brace area obtained from the eigenvalue buckling analyses. Lower averages indicate an improvement in the system performance. The average minimum brace area for each layout is listed in Table 6-1. As expected,, the lean-on layouts required greater areas for the cross-frame members to reach the ideal stiffness compared to the conventional case. Additionally, the areas required varied significantly between lean-on layouts in the single span models. Based on the analyses, ZigZag - ψ and Checkerboard generally required the least brace area for single and continuous systems, respectively.

Table 6-1. Minimum Average Brace Area of Layouts Compared to Conventional Bracing for Systems with No Lateral Trusses

Layout	**Single Span – No LT**		**Continuous Span – No LT**	
	$\bar{A}_{br}$	$\frac{\bar{A}_{br,lean}}{\bar{A}_{br,conventional}}$	$\bar{A}_{br}$	$\frac{\bar{A}_{br,lean}}{\bar{A}_{br,conventional}}$
Conventional	3.18	1.00	1.71	1.00
ZigZag – Continuous Diagonal	3.64	1.14	2.41	1.41
ZigZag – ψ	3.38	1.06	2.45	1.44
Checkerboard	3.80	1.19	2.40	1.41

The Phase 1 study highlighted general trends regarding the performance of various lean-on layouts. However, the Phase 1 study lacked isolation of the factors affecting the performance of lean-on layouts that are necessary to develop design guidance. In light of this, the research team devised a series of studies to better grasp each factor in isolation including 1) the assessment of the impact of the layout on the brace stiffness and in-plane girder stiffness in isolation, 2) the derivation and verification a new in-plane girder stiffness layout factor, and 3) quantifying the behavior of lean-on bracing in systems with skewed supports. The study documenting the isolation of layout effects on brace stiffness is covered in Phase 2 of the layout study in the next section.

6.2. Phase 2: Layout Effect Study with Isolated β_{br}

The Phase 2 studies focused on the impact of the cross-frame stiffness component for various lean-on systems on the buckling behavior of the girder system. A number of different configurations were considered in the Phase 2 studies to investigate the impact of the bracing layout on the resulting buckling mode. Therefore, many of the configurations that are discussed in this section vary significantly from those cases outlined in Table 6.1 from the last section. However, the results from these analyses are important for understanding the characteristics of the lean-on bracing configuration that is utilized with respect to the lateral and longitudinal distribution of the cross-frames in a given span. A major goal of the Phase 2 investigation was isolating and quantifying the interaction of the layouts and stiffness components.

As noted in Chapter 2, the total system stiffness is a function of the stiffness of the brace, the in-plane stiffness of the girders, and the cross-sectional stiffness to control distortion. Because the focus of these analyses was specifically on the cross-frame bracing component, modelling decisions were selected so that the cross-sectional distortion component, β_{sec}, and in-plane stiffness component, β_g, could be effectively treated as "infinitely" stiff and therefore having insignificant impact on the overall behavior. To eliminate the effects of the cross-sectional distortion component, full depth cross-frames were utilized. To eliminate the effects of the in-plane stiffness, a relatively wide girder spacing was used. By removing these two stiffness components from the problem, the stiffness of the cross-frames and struts distributed throughout the span could be the isolated.

Girder systems with varying geometries were analyzed to ensure the in-plane girder stiffness was sufficiently large to be treated as an infinitely stiff component. Based upon a sensitivity analysis, the threshold for stiffness components to be considered as effectively infinite is approximately 10 to 11 times the ideal stiffness. All the proposed girder system dimensions were above or at the threshold as shown in Table 6-2.

Table 6-2. Bridge Parameters and Calculated β_g Compared to $\beta_{T,ideal}$

Girder Spacing	**Total width of girder system**	**Span Length**	**Number of Cross Frame Lines**	**Unbraced Length**	$\boldsymbol{\beta_{g,eq,2025}}$	$\boldsymbol{\beta_{br,eff,FEA}}$	$\boldsymbol{\frac{\beta_g}{\beta_{T,ideal}}}$
$(\boldsymbol{S})$	$(\boldsymbol{W_g})$	**(L)**	$(\boldsymbol{n_c})$	$(\boldsymbol{L_b})$	$\left(\frac{kip-in}{rad}\right)$	$\left(\frac{kip-in}{rad}\right)$	
80′	320′	150′	5	25′	10,278,000	229,000	45
40′	160′	150′	5	25′	2,569,000	228,000	11

Based upon the results from the preliminary study summarized in Table 6.2, the in-plane girder stiffness could be considered infinitely stiff with a spacing of either 40 or 80 ft; however, a value of 80 ft. was utilized. Since the values of the cross-sectional stiffness and the in-plane girder stiffness were effectively infinite, the expression for springs in series given previously in Equation 2.20, dictates that the total system stiffness is only a function of the stiffness of the braces.

By relating the ideal stiffness directly with the brace stiffness, the research team was able to investigate the interaction between adjacent bracing lines. If bracing lines acted independently, layouts would exhibit no effect on the brace stiffness requirements of the girders. Thus, the brace stiffness requirement would solely be based on the girder geometry and the applied moment, as demonstrated in Figure 6-3. Based on conventional understanding, the provided brace stiffness is dependent on the position, member sizes, and number of cross-frames in a cross-frame line. Henceforth, cross-frames lines with the same number of cross-frames, member sizes, and cross-frame positioning are referred to as equivalent stiffness bracing lines.

Fish et al. (2025), focused on the effective bracing as a function of the number of cross-frames along a given cross-frame line for conventional bracing systems. The effective bracing factor is given in Equation 6.3 and can be applied to the brace stiffness expression as shown in Equation 6.4. A similar approach is desirable for lean-on systems.

$$C_{nc,x,k} = 1 + \frac{n_g - 2}{n_g + 1.75} \tag{6.1}$$

$$\beta_{br,eff} = C_{nc,x,k}\beta_{br} \tag{6.2}$$

The first step in determining the impact of lean-on struts on the bracing behavior is to determine the minimum brace area corresponding to buckling between the brace points in the stiffness isolated conventional system. The minimum brace area corresponds to the ideal stiffness and was used as a point of reference. A starting point for the ideal stiffness comes from a bracing system with conventional bracing. To buckle between the brace points, a girder must have all brace points (cross-frame lines) achieve the ideal stiffness. Once the ideal stiffness is determined using a conventional bracing system, the system can be reanalyzed with some of the conventional cross-frame lines replaced by equivalent stiffness bracing lines with lean-on struts. As the girder cross section is constant and therefore the moment corresponding to buckling between the brace points is the same, the ideal stiffness and thus brace stiffness requirement is the same. The minimum brace area of these new bracing lines can then be determined and is equal to the ideal stiffness of the lean-on configuration. The overall process is summarized in Figure 6-3.

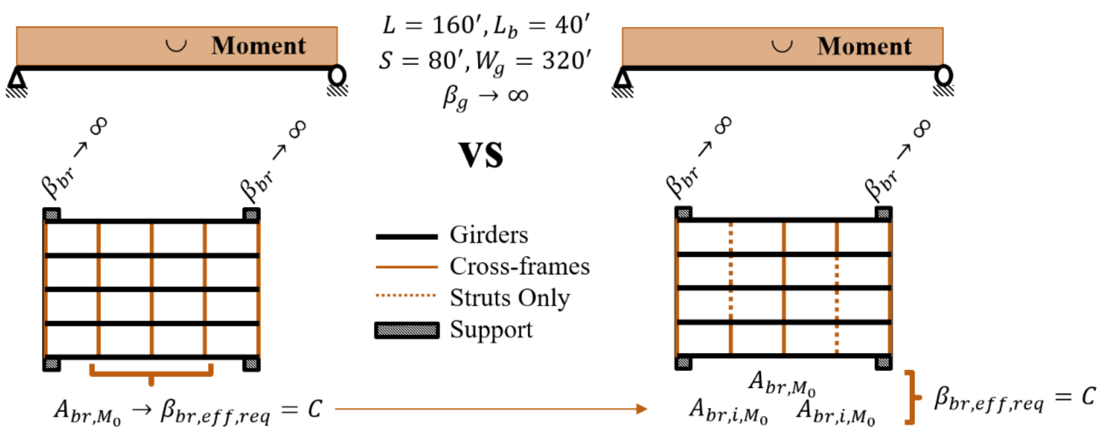

Figure 6-3. Process Used to Isolate the Individual Cross-Frame Line Stiffnesses for Isolated System

The research team analyzed various layouts utilizing equivalent stiffness bracing lines after collecting the corresponding ideal stiffness from a conventional bracing configuration. The configurations shown in Figure 6-4 correspond to the layouts analyzed for a 5-girder system. The thick dark grey lines at or near the middle of each span demonstrate a full bracing line at the ideal stiffness. These full bracing lines existed to maintain the in-plane girder stiffness and consequently ensure that the in-plane girder stiffness did not significantly influence the solution. The thick orange lines and thin dotted grey lines were cross-frames and lean-on struts, respectively, whose stiffness were varied to find the ideal stiffness condition (buckling between the brace points). The aim of these configurations was to determine the effects of cross-frame number and position on the effective brace stiffness of a cross-frame line with lean-on bracing.

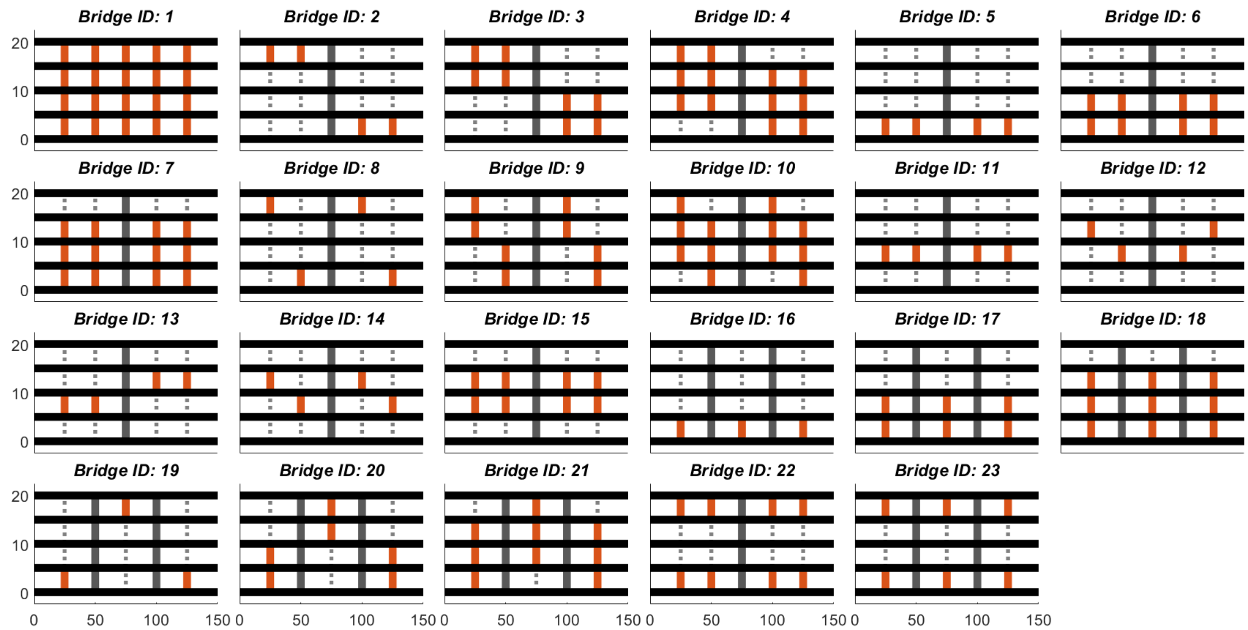

Figure 6-4. Girder Layouts Used in the Layout Effect Parametric Study

The totality of the parametric study conducted is summarized in Table 6-3 and comprises the results of 135 bridge systems. The systems analyzed can be subdivided into systems with only internal cross-frames and systems with cross-frames extending from the exterior. The purpose of studying internal versus external cross frames was to understand the fundamental buckling behavior as a function of the cross-frame layout.

Table 6-3. Total List of Layouts Per Number of Girders Varied in Layout Effect Parametric Study

# of Girders	# of Layouts Total	# of Layouts with only Internal Cross-frames	# of Layouts with Cross-frames Extending from the Exterior
7	52	24	28
6	37	14	23
5	23	5	18
4	16	1	15
3	7	0	7

The variation in $A_{br,min}$ at the corresponding ideal stiffness produced by differences in bracing line orientation is provided in Table 6-4. The range in the variation was dependent on geometrical factors such as the number of girders due to the increase in possible permutations of cross-frames and lean-on struts. The maximum variation was approximately 30% with an outlier occurring in the 7-girder internal only cross-frame layout. In summary, β_g was likely locally compromised due to the low torsional rigidity across the width of the system.

Table 6-4. Variation in minimum brace area of equivalent stiffness lines.

Layouts with:	**Cross-frames Extending from the Exterior**					**Only Internal Cross-frames**		
# of Girders	**7**	**6**	**5**	**4**	**3**	**7**	**6**	**5**
Variation in Minimum Brace Area Grouped by Equivalent Stiffness Bracing Lines $\left(\frac{A_{br,lean,max}}{A_{br,lean,min}}\right)$	1.29	1.24	1.20	1.18	1.14	1.59	1.25	1.18
	1.19	1.20	1.18	1.20		1.24	1.22	1.00
	1.21	1.22	1.16	1.00		1.10	1.20	
	1.23	1.18	1.01			1.12	1.09	
	1.19	1.02				1.09		
	1.03					1.01		

The data in Table 6-5provides typical examples of the results obtained from the eigenvalue buckling analyses of these isolated systems. The term "isolated system" reflects that the total system stiffness is only a function of the stiffness of the cross-frames. Overall, the results demonstrated that different permutations of the orientation of the same cross-frame line altered the minimum required brace area needed to obtain buckling between the brace points (ideal stiffness). These results indicate that the effective brace stiffness of a bracing line is dependent on the layout of the system as well as the number, size, and position of cross-frames in the specific bracing line.

Table 6-5. Examples of Differences in Brace Performance of Equivalent Bracing Lines

Exterior Cross-frame Layout	$\frac{A_{br,lean}}{A_{br,lean,min}}$	**Interior Cross-frame Layout**	$\frac{A_{br,lean}}{A_{br,lean,min}}$
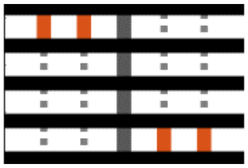 **Case 1**	1.02	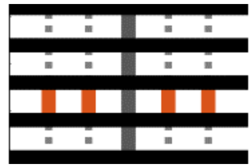 **Case 6**	1.18
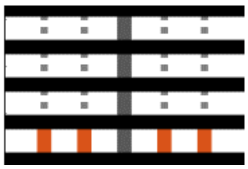 **Case 2**	1.20	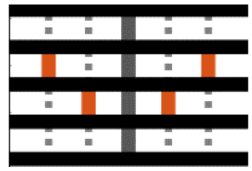 **Case 7**	1.17
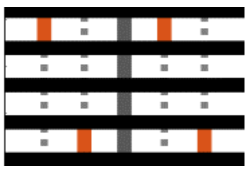 **Case 3**	1.07	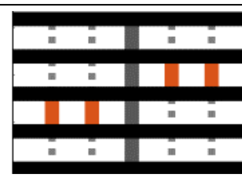 **Case 8**	1.00
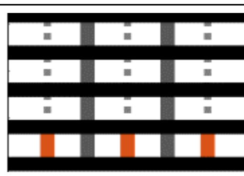 **Case 4**	1.20	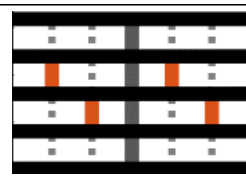 **Case 9**	1.07
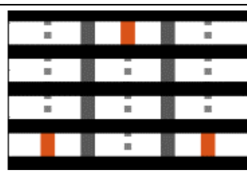 **Case 5**	1.00		

The ratio of $A_{br,lean}/A_{br,lean,min}$ that is tabulated represents the efficiency of the system with values of unity representing optimum behavior. Using the examples in Table 6-5 for reference, the lean-on bracing lines performed best when the distribution of cross-frames was equal and opposite about the axes of symmetry of the bridge. Additionally, cross-frames in adjacent bracing lines in direct contact such as Case 5 and 8 in Table 6-5 show an increase in the efficiency of the braces. This behavior can be categorized in terms of two layout effects that were valuable when selecting recommended configurations for cross-frames in Section 6.4:

1. Global layout effect
2. Local layout effect

The discussions of global and local effects are based upon observations in the behavior of the 135 bridge systems with various cross-frame distributions. The global layout effect is categorized based on the global distribution of the cross-frames, as illustrated in Figure 6-5. The distribution should be centered about the axes of symmetry with respect to the bracing system, aiming for opposite sections of the bridge to have equal cross-frame distributions. Cross-frames biased to one side of the bridge, such as Figure 6-5A, result in reductions in the bracing behavior. The bias is reflected in the location of the centroid of the bracing that is offset from the centroid of the girder system. For a given cross-frame size, biases in the distribution lead to lower overall stiffness and a reduction in the maximum moment capacity. Therefore, the preferred configuration leads to the centroid of the cross-frames in the overall system to coincide with the centroid of the bridge system as depicted in Figure 6-5B.

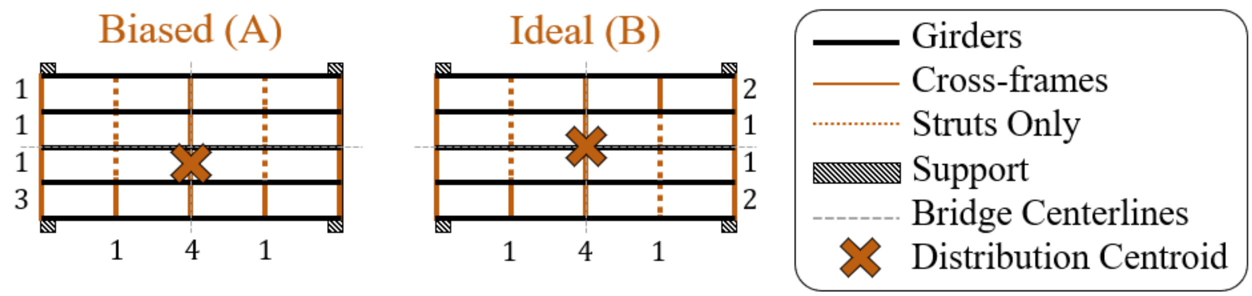

Figure 6-5. Illustration Covering the Source of the Global Layout Effect

As noted earlier, the girder system may buckle between adjacent bracing lines (local scale) or by a half-sine curve within the span (global scale). Therefore, local layout effects are categorized based on the interaction between adjacent bracing lines, which is highlighted in Figure 6-6. The five-girder system results in 4 bays between adjacent girders. Considering local effects, adjacent bracing lines that have cross-frames in the same bay provide a greater stiffness than cross-frames in different bays. For a given cross-frame size, a configuration that fails to link or pair cross-frames in consecutive bracing lines results in a lower maximum moment capacity and alters the displacement distribution (maximum displacement is no longer about a critical geometric imperfection). As is discussed later in this chapter, these layout effects cause susceptibility to amplification of geometric imperfections. The cases shown in Figure 6-6 represent extremes in the behavior. For example – the paired layout shown in Figure 6-6A is not likely ideal when other factors such as the in-plane stiffness are considered. In this case, shifting the cross-frame in intermediate bracing line 2 to the 2nd bay from the bottom may be better overall behavior when all cases are considered. However, extreme cases such as the unpaired cases shown in Figure 6-6B generally result in very poor behavior with regards to local effects. The combination of local and global layout effects were used to develop recommended cross-frame configurations for various geometries and are discussed in more detail in Section 6.4.

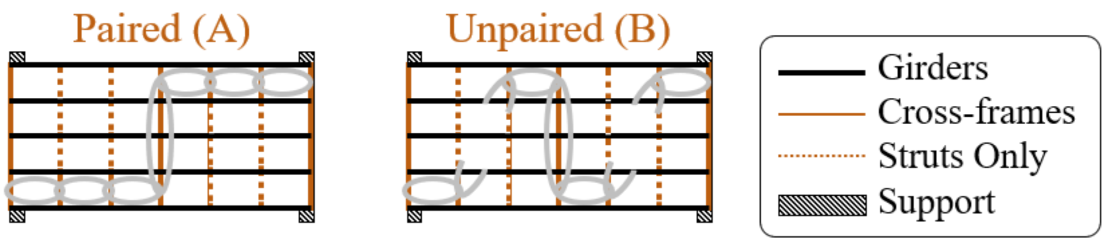

Figure 6-6. Illustration Covering the Source of the Local Layout Effect

The layout effects can be further highlighted by examining the displacements and member stresses of bridge systems with poor local or global layouts with cross frames proportioned to provide the ideal stiffness by conducting a nonlinear geometric analysis on an imperfect system. The bracing configurations selected from those shown previously in Figure 6-4 are Bridge IDs: 1, 8, and 19. Bridge 1 is the conventional layout. Bridge 8 has a poor distribution with respect to local layout effects, while Bridge 19 results in a bias of the bracing leading to global effects as shown in Figure 6-7. Both of these distributions generally reduce the maximum moment capacity (maximum load proportionality factor, LPF), however, the local effects with Bridge 8 are specifically poor and can cause a significant increase in the member stresses and changes in the final displaced shape.

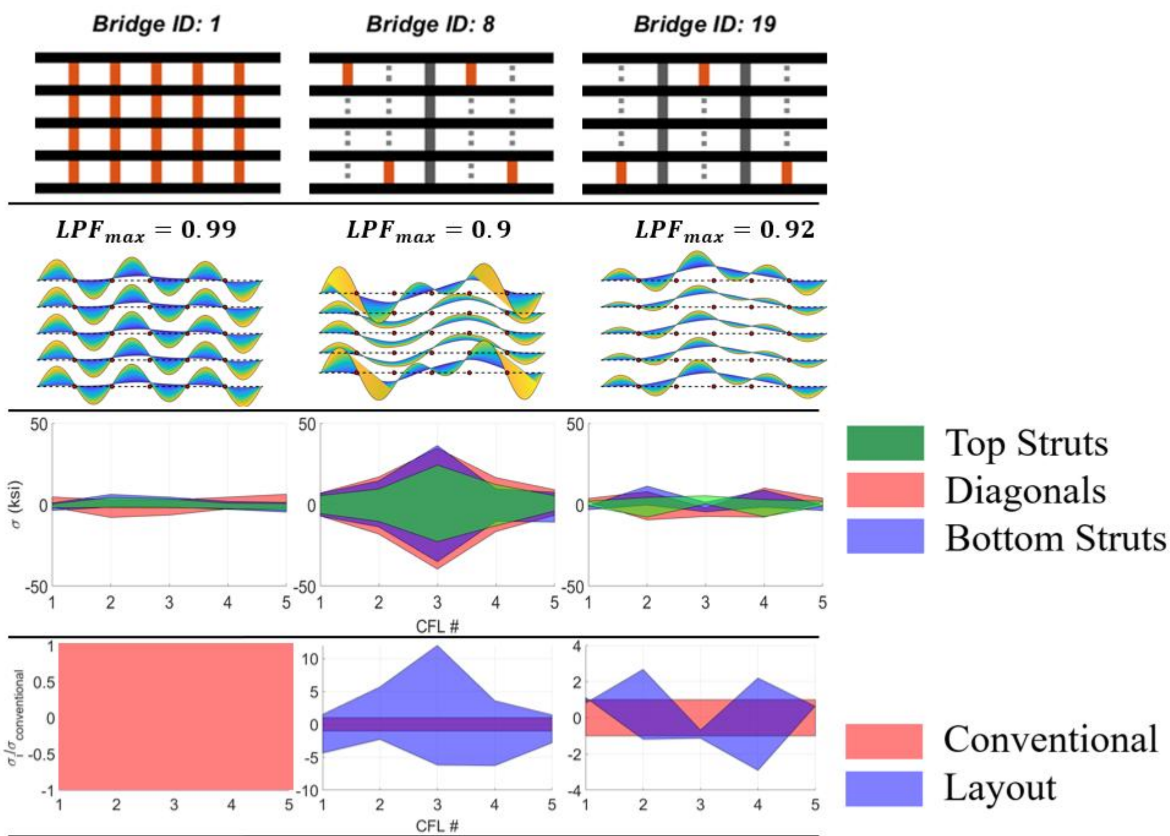

Figure 6-7. Maximum Layout Brace Stress Envelope for Multiple Layouts

Configurations with several girders leaning on a cross-frame positioned in the exterior bay tend to increase the required cross-frame sizes. Figure 6-8 demonstrates this effect. There is a full line of cross-frames at midspan and lean-on layouts in the other bracing lines. The figure includes a graph with the total volume of diagonal members on the vertical axes (normalized by the volume for a conventional layout). The horizontal axis represents the number of cross-frames per line in the lean-on bracing lines. The lines in the graph show bridges with 3 to 7 girders. A series of figures are shown to the left of the graph for the specific case of 5 girders, which is represented by the gray line in the graph. Therefore, the case with 5 girders has 3 data points ranging from 1 brace per line to 3 braces per line (4 braces per line would represent conventional bracing for the 5-girder system). The graph on the top is for an unbiased layout, while the graph on the bottom represents the extreme biased layout where all cross-frames extend from one side of the bridge. Relative to conventional bracing, for a given number of cross-frames per line, the wider girder systems result in more girders leaning on the cross frames in a given line and the resulting volume of diagonals is larger. Providing more cross-frames in each line leads to improved behavior with the total volume of diagonals required lower than cases with fewer cross-frames per line. Comparing the top curve to the bottom curve, the unbiased layout leads to improved behavior in the system with significant reductions in the total volume of diagonals required.

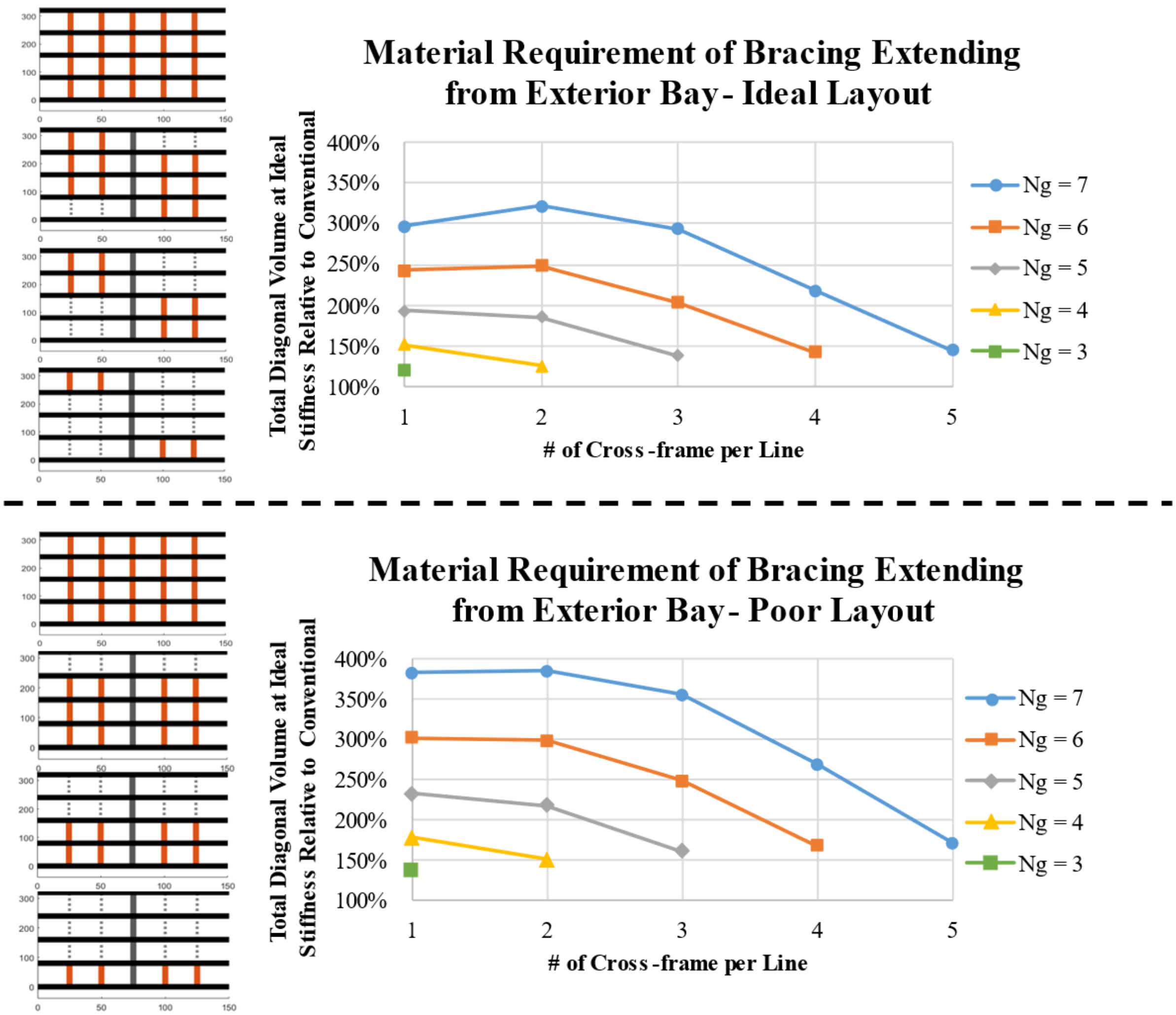

Figure 6-8. Global Layout Effect and Number of Adjacent Leaning Girders on Bracing Material Requirements

Thus, minimizing the number of adjacent leaning girders results in improvements in material efficiency. Designers should focus on layouts that minimize the number of adjacent leaning girders that utilize bracing lines such as the ones illustrated in Figure 6-9. These bracing lines reached the ideal stiffness within 20% of the material used in the conventional cross-frame line. Configurations such as those shown in Figure 6-9 are representative of configurations such as the checkerboard layout. However, while adding additional cross-frames in a given line does reduce the "volume" of the diagonals, the impact of adding cross-frames needs to be compared with respect to fabrication costs and potential fatigue stresses, particularly for girders with skewed supports – which are discussed later in Section 6.3.

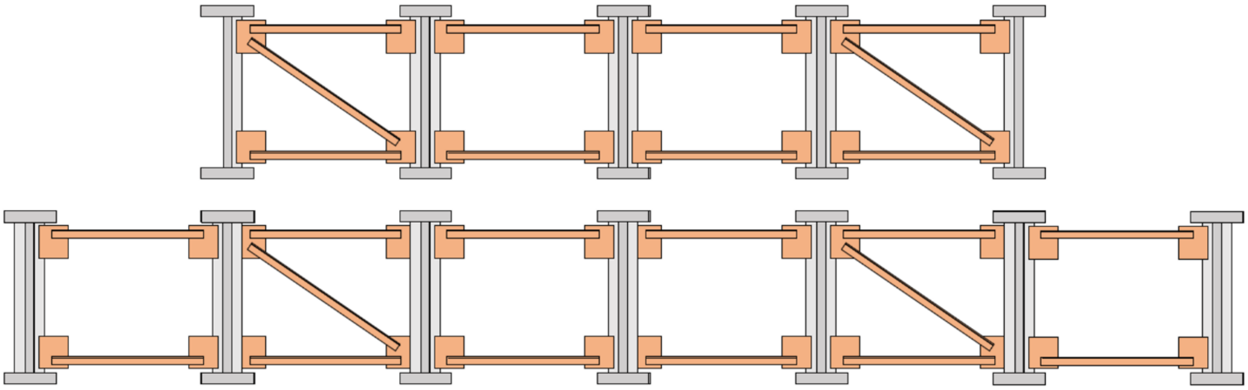

Figure 6-9. Effective Lean-On Cross-Frame Line for Reducing Brace Area Requirements

The results outlined in this section emphasize the need to link corresponding bracing lines, distribute cross-frames about the axes of symmetry of the girder lines, and minimize the number of adjacent leaning girders. The identified layout effects are considered in Section 6.4 that focuses on the recommended layouts as a function of bridge geometry. Additional considerations include the required moment capacity, brace efficiency, and susceptibility to critical geometric imperfections.

These layout effects also provided insight into the reasons specific configurations, shown in Figure 6-10, covered in Phase 1 performed better relative to one another. For example, the ZigZag – Diagonal was outperformed by ZigZag – Continuous Diagonal due to the improved linkage of bracing lines and reduction of the local layout effect. The Checkerboard performance variability may be tied to local layout effects and the minimization of the number of leaning girders. ZigZag – ψ, on the other hand, likely performed as well as it did due to having a full cross-frame line at the maximum moment region.

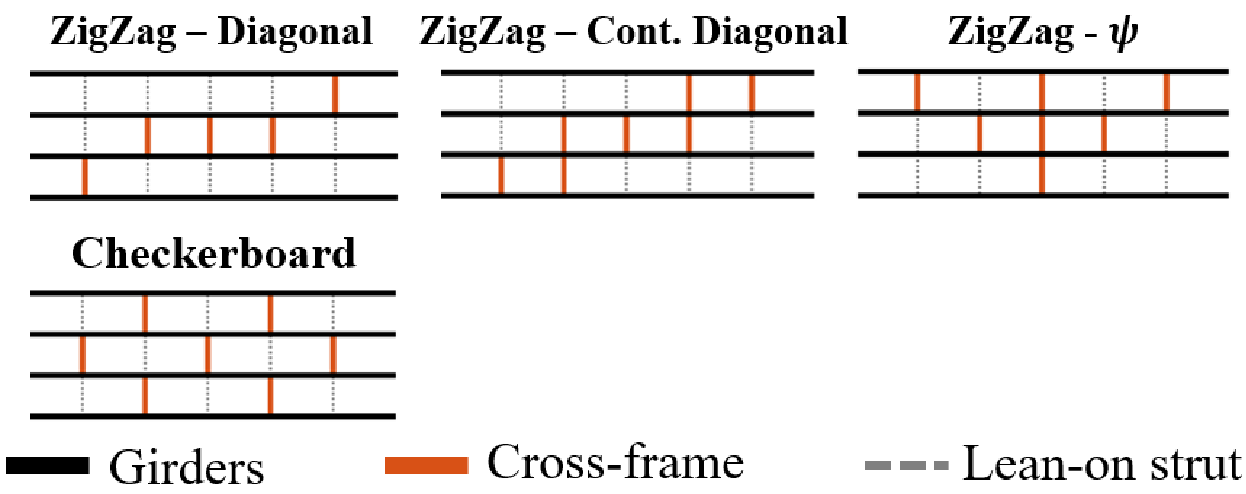

Figure 6-10. Highlighted Layouts for Behavior Comparison

The next section of this report is focused on the behavior of the in-plane girder stiffness for lean-on configurations. A similar concept that was utilized in this section is applied in which large brace areas are utilized with common girder spacing.

6.3. Phase 3: Layout Effect Study with Isolated β_g

Reductions in the effective in-plane girder stiffness was previously observed when lean-on bays were introduced to the system (Helwig and Wang, 2003). Helwig and Wang 2003 made comparisons using the expression for the in-plane girder stiffness that was derived in 1993 for twin girders and extended to systems with more than 2 girders. However, Fish (2021) showed that the original in-plane girder stiffness expression led to increasing errors for larger numbers of cross-frame lines relative to FEA solutions. The updated expression derived by Fish (2021) and later verified in Fish et al. (2025), considered the effects of multiple girders and the stiffness of multiple inline cross-frames. Based upon the improved behavior with the 2025 in-plane girder stiffness, the recommendation of using the 50% reduction on the in-plane girder stiffness expression developed by (Helwig and Wang, 2003) was considered in the present study.

Similar concepts utilized in the Phase 2 studies were applied in Phase 3 in terms of isolating the in-plane girder stiffness, β_g, by maximizing the β_{br} component to an effective value of infinity. The process was achieved by increasing the area of the bracing members to levels where β_{br} was greater than approximately 10 to 11 times the ideal stiffness of the system, $\beta_{T,ideal}$. As noted earlier, studies were conducted that found reaching this (10~11 $\beta_{T,ideal}$) level of bracing sufficiently reduced the impact of the specific stiffness component.

The formulation of the proposed β_g expression from Fish et al. (2025) is derived based upon a modified expression for the system buckling (M_g). As such, a layout factor, referred to as C_{LO}, that encompasses the effects of cross-frame configurations on M_g, is squared and applied to the β_g expression. By using such a factor, the intricate complexities of layout effects can be summarized with a reduction that provides good accuracy with FEA solutions. Thus, the objective of the study was to discover a conservative yet reasonable lower-bounded factor for bridges with both normal and skewed supports. The layout factor evaluated from the FEA, $C_{LO,FEA}$, is defined in Equation 6.3 and can be applied to the $M_{g,2025}$ and $\beta_{g,2025}$ (Equation 2.30 and 2.31) as shown in Equations 6.4 and 6.5:

$$C_{LO,FEA} = M_{g,lean-on}/M_{g,conventional} \tag{6.3}$$

Where:

$M_{g,lean-on}$ is the global lateral torsional buckling capacity of the lean-on system analyzed.

$M_{g,conventional}$ is the global lateral torsional buckling capacity of the conventional system analyzed.

$$M_{gs,2025} = C_{LO,FEA}C_{bs}\frac{\pi^2 sE}{(KL)^2}\sqrt{I_{eff}I_x\alpha_x} \tag{6.4}$$

$$\beta_{g,2025} = C_{LO,FEA}^2\frac{\pi^4 EI_x s^2\alpha_x L_{b,avg}}{(KL)^4} \tag{6.5}$$

The variables considered in the parametric study are shown in Table 6-6. Note that the transition between parallel and perpendicular bracing in skewed systems occurs at 20 degrees, which coincides with the cross-frame detailing requirements in the AASHTO BDS (2024). The four sections utilized in Fish et al. (2025) were reused in the present studies and are displayed in Figure 6-11. The girder spacing of 5′ was used to reduce the in-plane girder stiffness such that the global lateral torsional buckling mode dominated the behavior.

Table 6-6. Bridge parameters varied in system stiffness behavior parametric study.

Bridge Parameters	**Values**
Gider Spacing	[5′]
Number of Girders	[4,5,6,7]
Unbraced Length	[25′]
Span Length	[150′, 200′]
Section #	[1,2,3,4]
Skew	[0°, 20°, 30°, 60°]

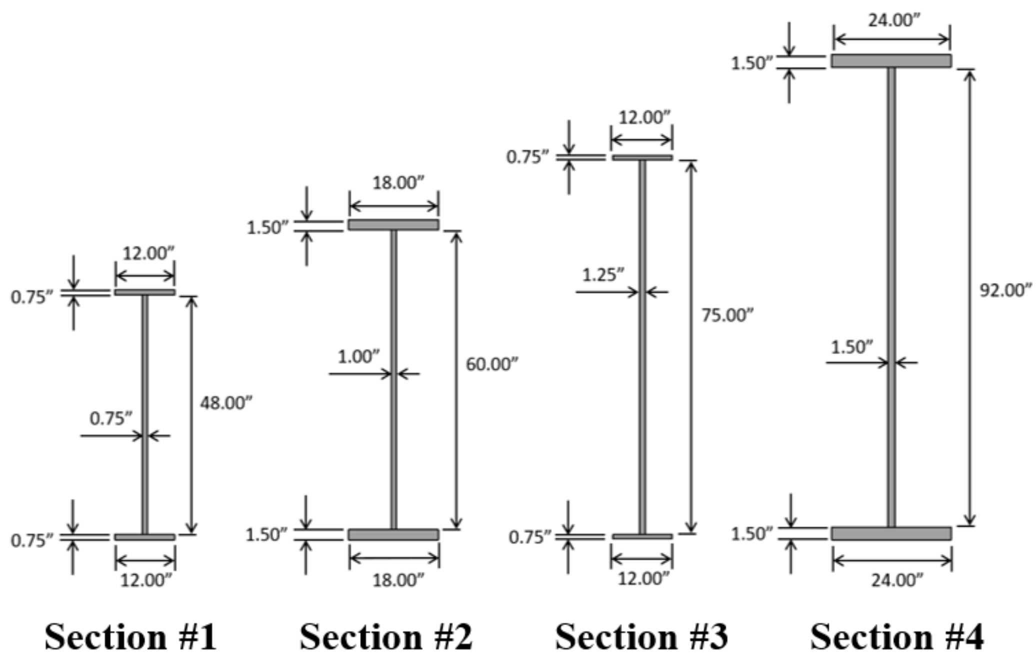

Figure 6-11. Sections used in Isolated β_g Layout Effect Study (Fish et al., 2024)

Four configurations were utilized from Phase 1 of the parametric studies. In addition, a new layout, labeled as "X", was introduced for bridges with normal supports. The investigated layouts are shown in Figure 6-12. Small adjustments were made to the configurations based on the initial bracing condition and the Phase 2 studies that isolated the β_{br} layout study to ensure proper cross-frame line pairing and constructability.

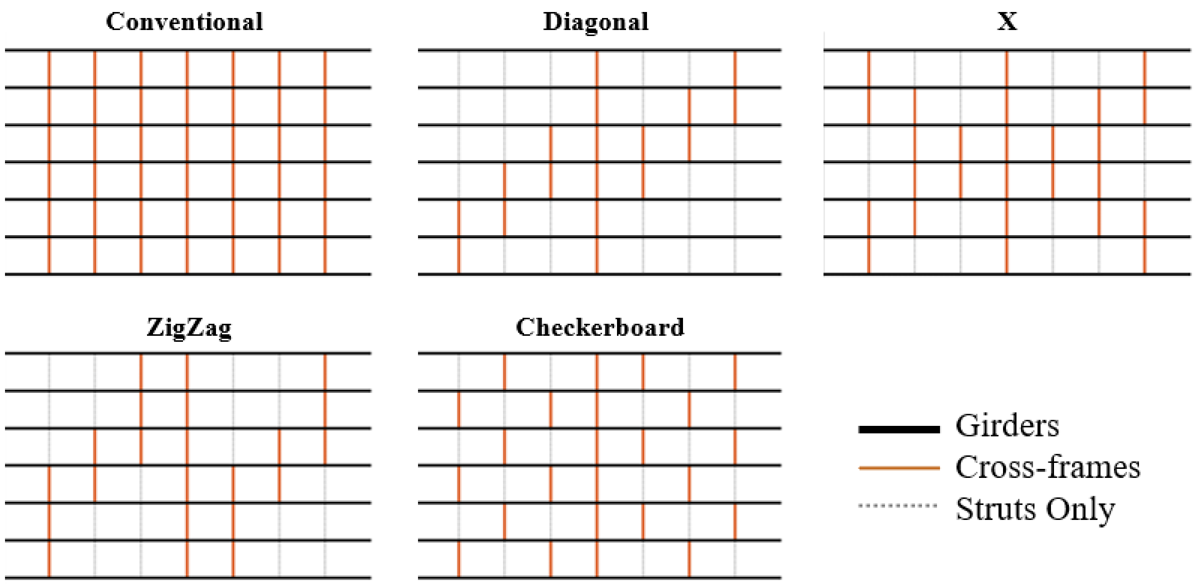

Figure 6-12. Nonskew Layouts Analyzed in Layout Study

The two lean-on layout candidates for skewed systems: diagonal and checkerboard are illustrated in Figure 6-13. These layouts minimize the number of cross-frames near the supports, thereby reducing truck-induced forces for improved fatigue performance. In addition, the layouts can aide in ease of erection by enabling more pliable cross-frame lines for fit-up. For the analyzed bridges, the spacing between bracing lines was reduced by half in the support region to mimic the designs observed in the Lubbock and Chisholm Trail bridges. As is later discussed and shown in Figure 6-17, using a uniform brace spacing can lead to larger unbraced lengths near the supports due to restrictions based on detailing of the cross-frame line that frames into the fascia girder near the supports. Helwig and Wang (2003) recommended to offset the first bracing line by 4-5 ft. to avoid congestion and large live-load induced forces. By introducing non-uniform spacing, the models had unbraced lengths that were less than or equal to the maximum unbraced length specified.

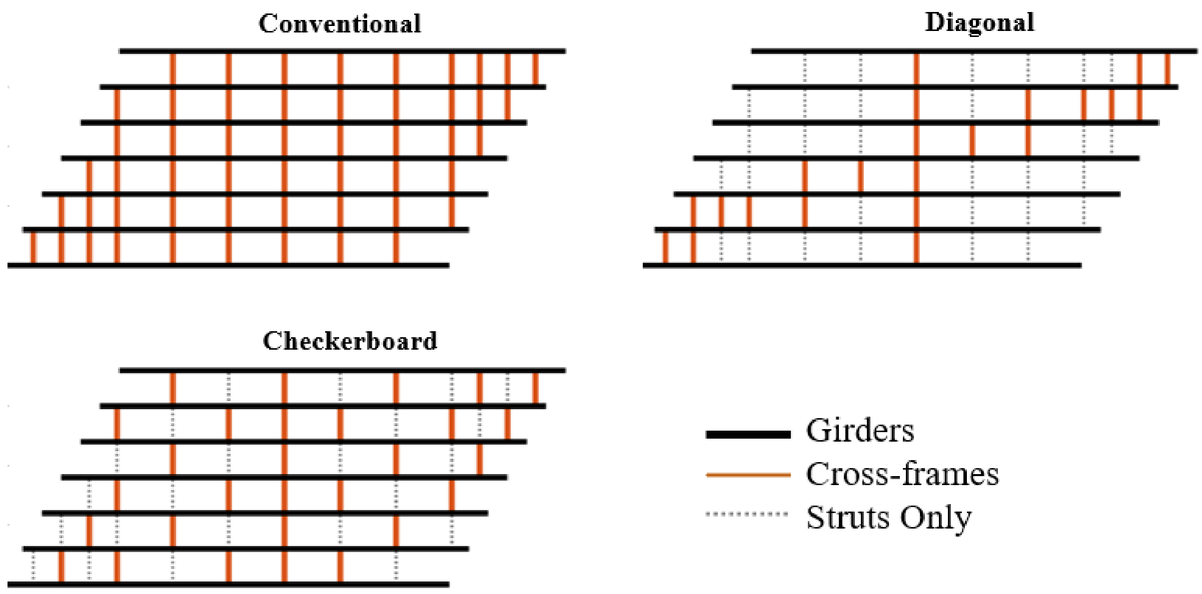

Figure 6-13. Skew Layouts Analyzed in Layout Study

Before examining the eigenvalue buckling results of the parametric study, C_{LO} as previously defined, is a reduction factor that accounts for the reduction in system torsional rigidity due to the implementation of lean-on bracing. By definition, C_{LO} will always be less than one in a lean-on system. The $(C_{LO})^2$ is used for β_g following the derivation proposed by Fish et al. (2025).

The eigenvalue buckling results for systems with normal supports are shown in Figure 6-14. The y-axis is representative of the applicable reduction value for M_g in Figure 6-14(A) and for β_g in Figure 6-14(B). The values for C_{LO} were determined from the FEA solutions so that exact agreement was achieved between the FEA solutions and Eqs. 6.4 and 6.5 for M_g and β_g. Due to the large number of geometries considered, there is obviously a range of values of C_{LO} determined from the various model geometries; however, the range is not that large. The data bins on the x-axis represent the bracing layout as well as the number of girders. The eigenvalue buckling results demonstrated a C_{LO} of approximately 0.95 ($C_{LO}^2 = 0.9$) was sufficient coupled with layout-specific recommendations to cover reductions in the β_g associated with lean-on bracing configurations. The recommendations are as follows:

- As a general rule, lean-on bracing should not be used with bridges with only 3 girders since there is very little savings in eliminating braces. An exception to this would be the removal of individual cross-frames framing in near a support in a heavily skewed bridge. In this case, the number of removed braces is very small and has little impact on the stability performance.

- The checkerboard layout should be limited to cases with 4 or 5 girders since wider systems become dominated by local layout effects.

- The diagonal layout should not be utilized for bridges with normal supports, ZigZag should be used instead (see Figure 6-12).
- The X-layout should not be used for systems with less than 6 girders, as using the layout would lead to situations that either include too many cross-frames (effectively conventional) or too few cross-frames (poor distribution of cross-frames to maximize lean-on bracing). These extreme scenarios lead to the large variation in $C_{LO,FEA}$ shown in Figure 6-14.

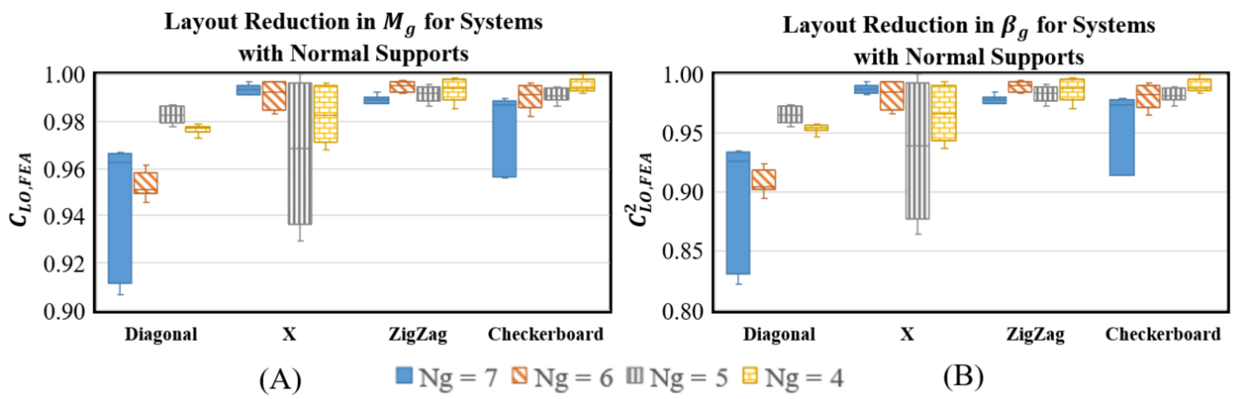

Figure 6-14. C_{LO} (A) and C_{LO}^2 (B) Effect on Systems with Normal Supports

From a stability perspective, girder systems with skewed supports tend to have improved stability behavior, meaning that the required stiffness of cross-frames systems are reduced compared to bridges with normal supports. The improved stability due to skewed supports can be idealized as the bracing behaving as both a lateral bracing system and a torsional bracing system. This behavior is depicted in Figure 6-15, which highlights how the cross-frame lines frame back to the supports. Because the bracing lines connect to adjacent girders at different locations along the length, the skew effects can be idealized by shifting the girders to a normal configuration. The braces therefore behave as a combined lateral and torsional system leading to improved efficiency. Thus, the system experiences similar benefits to having flange-level lateral trusses, which lead to increased warping stiffness which can be captured with an effective length factor, K. However, before the K-factors are discussed, the C_{LO} factors for systems with skewed supports and lean-on bracing are examined.

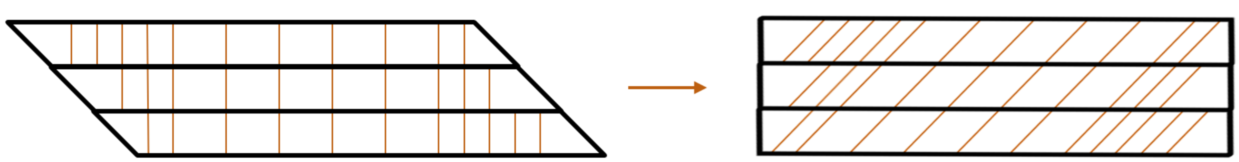

Figure 6-15. Normalized Skew System

Figure 6-16, shows the FEA solutions related to the C_{LO} factors for bridges with skewed supports. The results demonstrates that the lean-on bracing applications in skewed systems generally experience a greater reduction compared to their normal counterparts. These results are likely due to the increased number of cross-frame lines and the locations of those cross-frame lines in the support regions. A C_{LO} of 0.85 ($C_{LO}^2 = 0.73$) provides a reasonable lower bound of the behavior. However, the reduction in the C_{LO} value should not be confused with a less stable system for girders with skewed supports. bridges with support skew experience improved stability. Although the C_{LO} for skewed systems results in a reduction compared to bridges with normal supports, the improved warping stiffness in the bridges results in improved behavior. This effect is handled with an effective length factor as outlined below. The resulting effective length factor substantially improves the stability behavior of bridges with skewed supports relative to systems with normal supports.

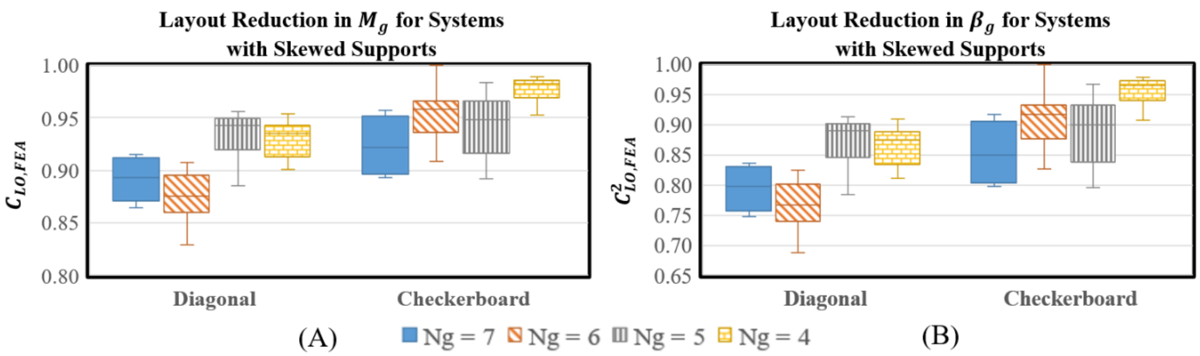

Figure 6-16. C_{LO} (A) and C_{LO}^2 (B) Effect on Skewed Systems

Based upon the FEA solutions, a range of K-factors are displayed in Figure 6-17A for a variety of skewed systems from the parametric studies. The meaning of the gap designation will be defined in subsequent paragraphs and is illustrated Figure 6-18. The skew angles range from 20 degrees to 60 degrees. Overall, the K-factors are primary affected by the severity of the skew angle and cross-frame line implementation. Large skew angles lead to improved warping resistance and smaller K-factors. However, even 20 degree skew angles lead to K-factors significantly less than unity. Because the in-plane girder stiffness is a function of $1/L^4$, the impact of the K-factor is substantial as shown in Figure 6-17B.

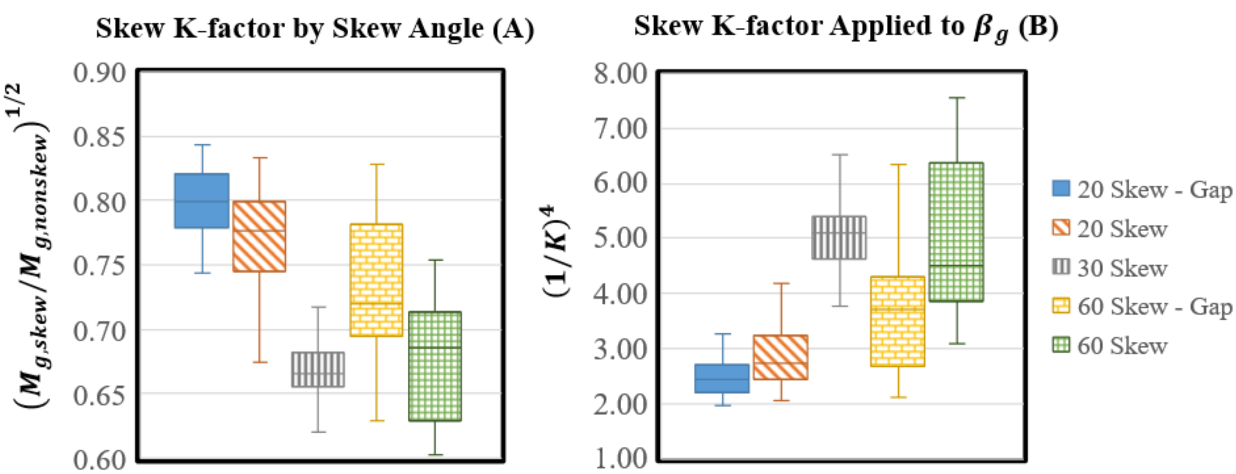

Figure 6-17. Skew System K-factors and Effect of K-factors on β_g

As previously mentioned, the K-factors shown in Figure 6-17 for skewed systems are primarily governed by two factors:

1. The severity of the support skew.
2. The number of girders braced by the cross-frame lines near the support region.

Both factors are directly involved in the amount of warping restraint provided to the system as both factors determine the extent that the girders are framed back to the supports. The further into the span the girders are framed back towards the supports and the greater the number of girders framed into the supports, the greater the warping restraint. The gap cases, which are illustrated in Figure 6-18, lack cross-frame lines that brace all the girders near the support region. As such, these cases have less warping restraint and a lower K-factor. Gaps in the cross-frame lines may also cause larger unbraced lengths than expected in the exterior girder.

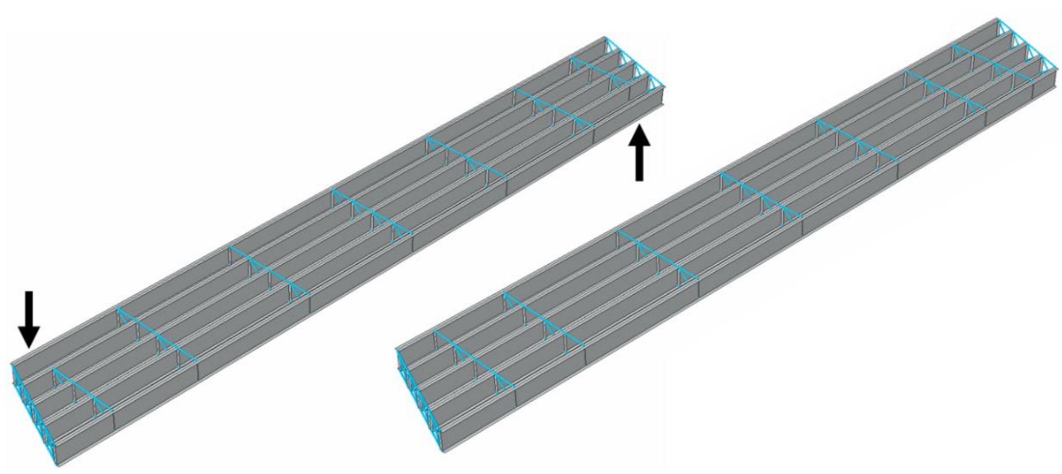

Figure 6-18. Gap Model vs. Regular Model of Skewed System

The data in Figure 6-17 emphasizes the variance that can occur with the cross-frame line placement in the support region. As such, designers relying on the warping restraint given by skewed supports should ensure the cross-frame lines frame back towards supports (outside of the support buffer) and connect all girders. Overall, the effect on M_g and β_g requires the effect of both the K and C_{LO} factors to be combined, which is shown in Figure 6-19. Note that the red dashed line signifies the lean-on recommendation, and the red dotted line signifies the conventional recommendation.

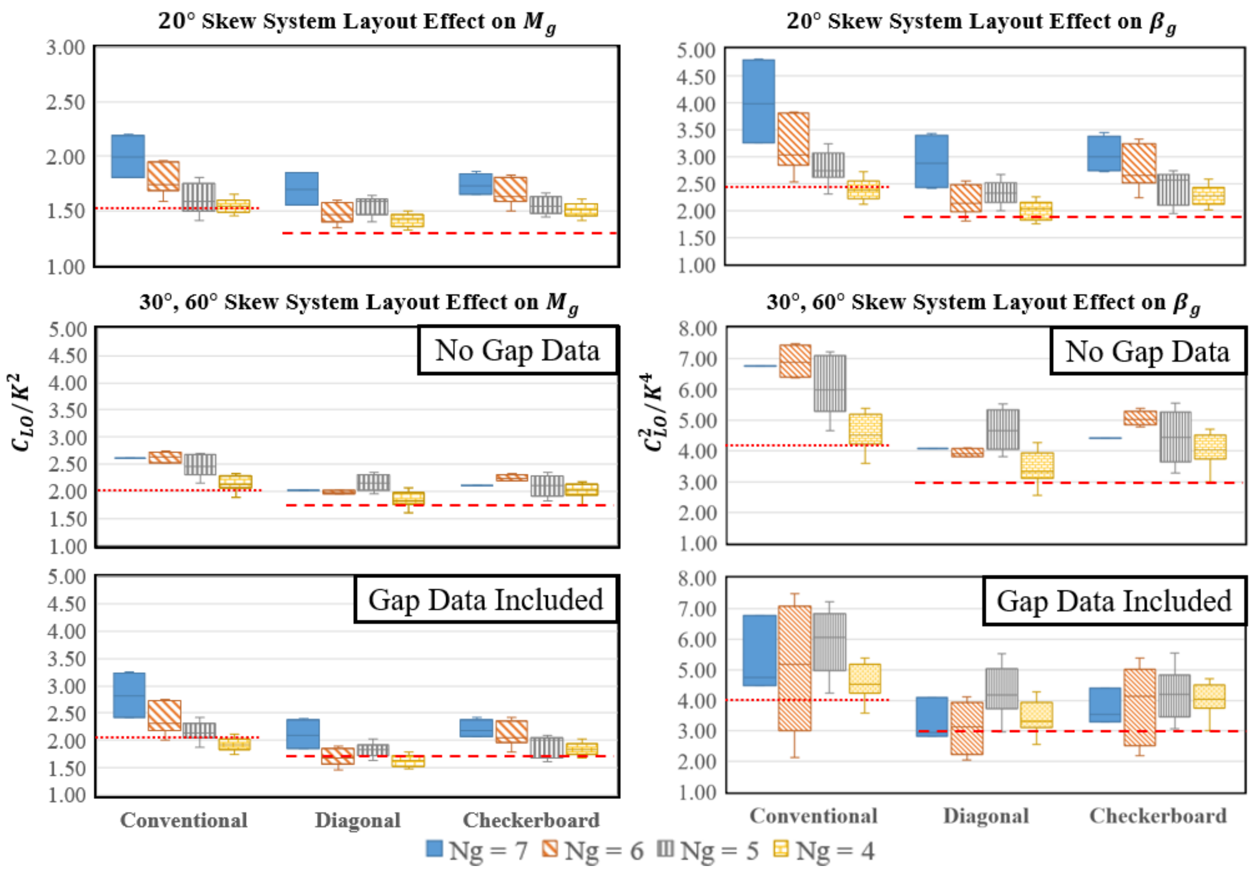

Figure 6-19. C_{LO} and K-factor Effect on $M_{g,2024}$ and $\beta_{g,2024}$

Using the data illustrated in Figure 6-19, a list of recommendations has been made for various bridge geometries. The recommendations are listed in Table 6-8 and Table 6-9. Of note, the gap cases for the 60° skew cases (most notably $N_g = 6$) were ignored for the final recommendations. These cases produced values that were outliers to the general trends discovered in the study due to the gap causing a larger unbraced length in the exterior girders than other cases. Improving the distribution of cross-frames eliminates this outlier, so these cases were not considered for the recommendations, but highlight that designers need to mind the gap in skewed designs.

Table 6-7. Lean-on β_g and M_g Recommendations

Skew Angle ($\boldsymbol{\theta}$) in Degrees	**Layout**	$\boldsymbol{C_{LO}}$	$\boldsymbol{K}$	**Effective $\boldsymbol{M_g}$ ($\boldsymbol{C_{LO}/K^2}$)**	**Effective $\boldsymbol{\beta_g}$ ($\boldsymbol{C_{LO}^2/K^4}$)**
$\theta < 20$	Conventional	1.00	1.0	1.00	1.00
	Lean-on	0.95		0.95	0.90
$20 > \theta \leq 30$	Conventional	1.00	0.8	1.56	2.44
	Lean-on	0.85		1.33	1.76
$\theta \geq 30$	Conventional	1.00	0.7	2.04	4.16
	Lean-on	0.85		1.73	3.01

These recommendations produce conservative estimates based on a combined effect utilizing a conservative lower bounded layout factor counterbalanced with the semi-conservative K-factor. Overall, quantifying the warping restraint provided by the support region and layout reduction provides a significant increase in the capacities used in the design process of skewed systems.

6.4. Summary of Layout Recommendations

To ensure the optimal placement of cross-frames in layouts, the research team has defined five overarching rules to optimum layout design. Overall, designers using leaning layouts must:

1. Ensure that cross-frames are equally distributed about the bridge centerlines.
2. Ensure all cross-frame lines are linked with girder pairs.
3. Ensure a cross-frame is included in every bay such that no bay is fully leaning along the span.
4. Ensure the number of adjacent leaning girders never exceeds a maximum of three in each cross-frame line.
5. Ensure a full cross-frame line is installed at the midspan of the bridge in order to facilitate erection and maximize the vertical warping stiffness of the girders. Diaphragms should be included at the supports.

Table 6-8 and Table 6-9 present the typical layout designs for nonskew and skew systems using the five rules above. Each layout is given design limits and relevant notes about their application. ZigZag and X have a minimum number of bracing lines (CFLs) that must be present to ensure development of the full layout.

Table 6-8. Recommended Lean-on Layouts for Bridge Systems with Support Skew ≤ 20°

Layout		# of Girders (# of CFLs)	Notes
ZigZag	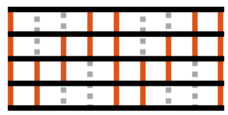	4 to 5 (≥7)	Optional layout for narrow systems
Checkerboard	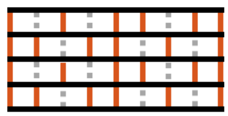	4 to 5 (any number)	Preferred layout for narrow systems
X	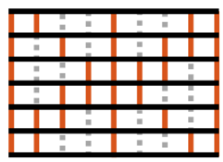	≥6 (≥5)	Preferred layout for wide systems

Due to the possible permutations of skewed systems caused by the variation of skew angle, span length, and bridge width present in design, a consideration for systems with clusters of leaning struts has been introduced for the diagonal layout in Table 6-9. In the event more than 6 sets of leaning struts are present in adjacent bracing lines, the installation of an additional cross-frame is recommended to preserve system stiffness behavior.

Table 6-9. Recommended Lean-on Layouts for Bridge Systems with Support Skew > 20°

Layout		# of Girders	Notes
Diagonal	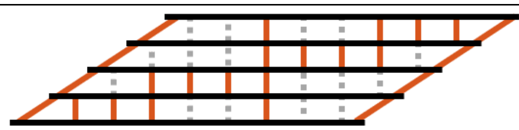 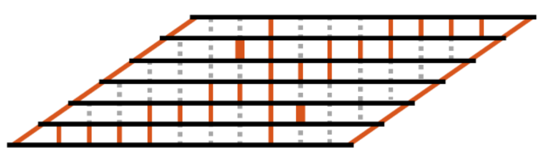	≥4	Preferred layout for skewed systems Additional cross-frames installed as needed to reduce clusters of leaning girders in clear span and also aid in stability during erection
Checker-board	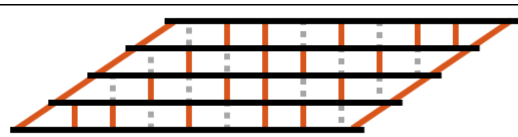	4 to 5	Optional layout for skewed systems

The configurations displayed above adhere to the five rules of layout design with one exception, checkerboard. Checkerboard does not fully hold to rule 2: ensure all cross-frame lines are linked with girder pairs. Due to the local layout effects, checkerboard loses efficiency in systems with a high number of girders and is thus limited to 5 or less (unless in the case of <5 CFLs). In accordance with the girder restrictions, the use of lean-on layouts should not be attempted for narrow girder systems (<3 girders) due to reductions in β_g. β_g typically controls narrow systems.

Lean-on struts may be used sparingly in conventional systems to minimize live load stresses and facilitate erection near supports with little impact on system behavior. These instances should be limited to ~10% of the total bays and multiple lean-on bays should not be placed in the same cross-frame line. The proper usage of lean-on struts in a conventional system is illustrated in Figure 6-20. As stated in Chapter 6.3, cross-frames, excluding diaphragms, should not be installed within $4'$ of the supports in consideration of fatigue stresses.

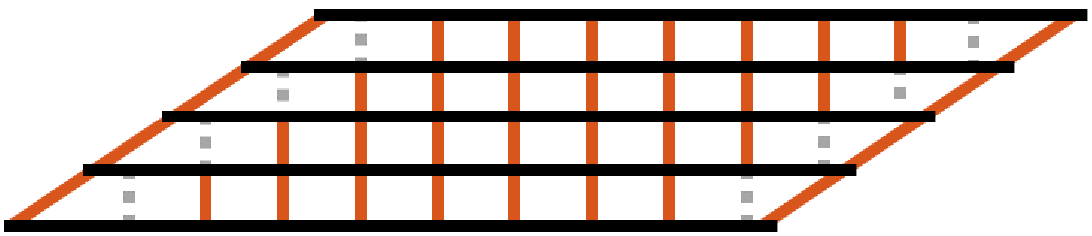

Figure 6-20. Example of Conventional System using Lean-on Bracing Strategically

Chapter 7. Lean-On Brace Stiffness Behavior

In the previous lean-on bracing studies outlined in Chapter 2, analytical equations were developed for the stiffness of a conventional cross-frame as well as expressions for lean-on applications with a single cross-frame in the exterior bay of the bracing line. These equations are limited in their scope of application by the number, type, and position of the cross-frame. In order to provide solutions appropriate for a wider range of applications, the research team developed expressions for the stiffness of lean-on bracing lines applicable for cases with any number of cross-frames. The new expressions are applicable for cross-frames with Z-, X-, or K-frame geometries in various positions along the bracing line.

Following this introduction, Section 7.1 provides stiffness derivations for single cross-frames as well as a lean-on bracing lines with one cross-frame with a single diagonal (Z-shaped) cross-frame. In a similar fashion, Section 7.2 provides stiffness expressions for X- and K-frame braces. The focus in Sections 7.1 and 7.2 consist of the virtual work method to evaluate the stiffness or individual cross-frames as well as simple lean-on bracing lines with a single cross-frame. In Section 7.3, the MATLAB (MathWorks, 2025) Symbolic Solver is utilized to evaluate the stiffness since the method can be easily extended to a wider range of bracing line geometries to develop the best approach applicable for the structural system. While Sections 7.1-7.3 are directed at the stiffness of a single bracing line, in reality, the individual bracing lines are not truly isolated. Instead, adjacent bracing lines tend to interact and therefore the behavior needs to consider the lateral and longitudinal distribution bracings. Therefore, in Sections 7.4 and 7.5, the behavior of cross-frame lines in 3D systems are considered to develop expressions that reflect the interaction between bracing lines along the span length. Section 7.6 summarizes the stiffness design recommendations for lean-on systems. While the behavior of true lean-on bracing systems are best represented by the results presented in Sections 7.4 and 7.5, the results in Sections 7.1 through 7.3 provide insight into the mechanisms of lean-on bracing and tend to demonstrate the incremental development of the design approach.

7.1. Virtual-Work Derivations for Z-Shaped Cross-Frame Bracing Lines

This section begins with an overview of the stiffness expressions for conventional bracing as well as the lean-on applications discussed in Chapter 2. Two particularly relevant derivations are covered for the brace stiffness: i) a single cross-frame with a twin girder system, and ii) a bracing line with a single cross-frame and lean-on struts for a system with more than two girders. The focus of Section 7.1 is for Z-shaped cross-frames.

7.1.1. Twin Girder System Derivation

Yura (2001) developed expressions for the torsional brace stiffness of torsional braces with Z-, X-, or K-shaped geometries. As noted above, this subs-section (Section 7.1) is focused on Z-shaped cross-frames. For a Z-shaped member with a single diagonal, the diagonal will generally be controlled by compression and must have adequate buckling resistance for the design forces. However, the Z-shaped cross-frame derivation is also applicable to cross-frames with two diagonals in which an engineer may conservatively neglect the compression diagonal due to the relatively low buckling strength of single-angle members that are frequently used for the braces. Such a cross-frame is often referred to as a tension-only diagonal system. The ensuing discussion focuses on the derivation for the Z-shaped system. In the derivation, the cross-frame is idealized as a truss with concentrically loaded members. The method of virtual work can be used to derive the expression. Torsional braces provide stability by imparting a restraining torque to the girders that essentially is represented by the force couples Fh_b that develop at both ends of the cross-frame depicted in Figure 7-1. The force couple Fh_b, is essentially the "brace moment".

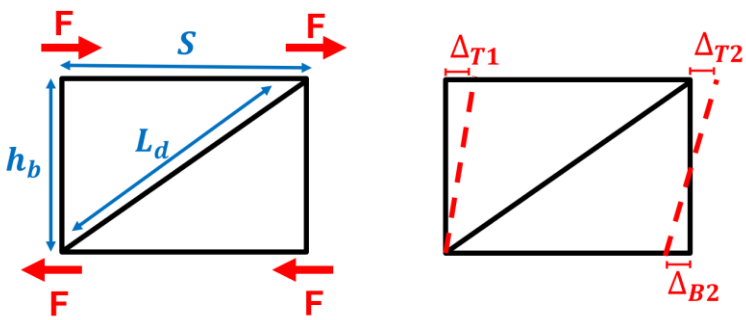

Figure 7-1. Twin Girder Brace Stiffness Idealization

The stiffness of a torsional brace is related to the brace moment and the resulting twist (θ) that results due to the axial deformations in the cross-frame members, for which Equation 7.1 and Equation 7.2 are combined leading to Equation 7.3. The deformation Δ in Equation 7.3 denotes relative lateral deformation between the top and bottom of the cross-frame and is related to the twist of the girder by $\theta = \Delta/h_b$.

$$M = Fh_b \tag{7.1}$$

$$\beta_{br} = \frac{M}{\theta} \tag{7.2}$$

$$\beta_{br} = \frac{Fh_b^2}{\Delta} \tag{7.3}$$

Where:

M is the moment from the stability-induced force couple;

F is the element of the force couple, which for stiffness calculations is assumed to be a unit load applied at the top and bottom of the cross-frame in the directions shown;

h_b is the depth of the cross-frame;

θ is the rotation of the girder;

Δ is the relative lateral displacement of the girder at the top and bottom of the cross-frame ($\Delta_{T2} + \Delta_{B2}$ in Fig. 7-1).

The value of Δ can be evaluated using the method of virtual work, resulting in Equation 7.4 for β_b. This equation represents the stiffness of a Z-shaped cross-frame, which agrees with the expression presented in Yura (2001) that was presented in Eq. 2.21. Yura (2001) also presents similar derivations for X-type and K-type cross-frames, that were presented in Eqs. 2.22 and 2.23.

$$\beta_{br,Z} = \frac{h_b^2 S^2 E}{\frac{2L_d^3}{A_d} + \frac{S^3}{A_s}} \qquad 7.4$$

Where:

S is the girder spacing

E is the modulus of elasticity

L_d is the length of the cross-frame diagonal members

A_d is the cross-sectional area of the cross-frame diagonals

A_s is the cross-sectional area of the cross-frame struts

From Equation 7.4, it is evident that the stiffness of the brace is a function of the axial stiffness of the individual members when the cross-frame is subjected to equal force couples on either end. Although not explicitly presented, the inherent flexibility of the connections should also be considered in the evaluation of the overall brace stiffness.

As noted in Chapter 2, single-angle or tee sections are often used for the cross-frame members and are attached to gusset plates, which results in eccentric connections relative to the centroid of the angle or tee section. The eccentricity of the cross-frame member is also often impacted by the thickness of the connection plate (stiffener connecting the cross-frame to the girder). The eccentricity results in bending of these members in addition to the axial shortening. Therefore, relative to the stiffness calculations that led to Equation 7.4 or from an analysis using truss elements to model the cross-frames, the bending associated with the eccentric connections leads to a reduction in stiffness as covered in Battistini et al. (2013, 2016) and Wang (2013). The stiffness reduction can be approximated with a fixed reduction factor, R. The AASHTO LRFD (2020) recommends an R-value of 0.65 during construction and 0.75 in the completed bridge as developed in Reichenbach et al. (2020) and Park et al. (2022). The R-factor can be applied to the cross-sectional area of the diagonals and struts in a computer analyses or stiffness equations. This reduction factor was calibrated to represent the softening effects for a wide range of common cross-frame configurations, connections, and member sizes based upon the results of extensive parametric FEA studies.

7.1.2. Original Lean-On Bracing Derivation

Similar to the stiffness of a single cross-frame developed by Yura (2001), Helwig and Wang (2003) derived a generalized equation for the brace stiffness contribution in a lean-on bracing system that reflected the bracing load path of a series of adjacent girders restrained by top and bottom struts with a single cross-frame in the outer-bay of the bracing line similar to the system depicted in Figure 7-2. The expression is given by Equation 7.5. As denoted by the subscript "Z" on the stiffness, the cross-frame in the derivation was assumed to be a Z-Frame with a single diagonal contributing to the stiffness.

$$\beta_{br,Z} = \frac{h_b^2 S^2 E}{\frac{n_g L_d^3}{A_d} + \frac{S^3}{A_s}\left(n_g - 1\right)^2} \qquad 7.5$$

Where:

n_g is the number of girders across the width of the system. In Helwig and Wang (2003) this was referred to as n_{gc}, which is the number of girders per cross-frame; however, since only one cross-frame in the outer bay was assumed in the derivation, this is the number of girders. The other terms are as defined previously.

The method of virtual work can be used to account for the axial shortening of the struts and diagonals based upon the respective forces in the individual members. As an example, the idealization of a four-girder system is shown in Figure 7-2 in which each vertical line represents a girder across the width of the bridge. The free-body diagram shows the accumulation of forces that develop assuming that each girder across the width of the bracing line buckles and requires a restraining moment of Fh_b. Therefore, starting from the right end of the bracing line (farthest away from the cross-frame), the strut forces and deformations accumulate along the width of the system. In such a derivation with lean-on bracing, the girder that is the farthest from the cross-frame is essentially the "critical girder" since the lateral deformations at the top and bottom of the brace are the largest due to the accumulation of the total axial deformations of all of the struts. For example, Δ_{B4} in Figure 7-2 includes the axial deformations of all 3 bottom struts in the bracing line such as $\Delta_{B4} > \Delta_{B3} > \Delta_{B2}$. A similar relationship exists for the deformations Δ_{T4} along the top struts of the bracing line.

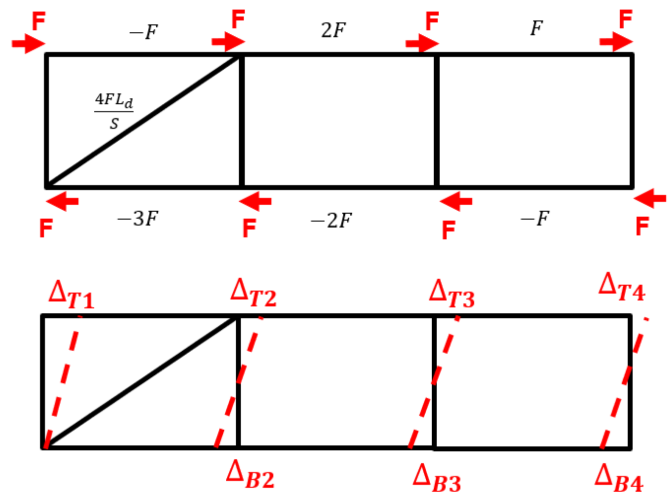

Figure 7-2. Lean-On Bracing Stiffness Idealization

Considering Equation 7.5, the calculated brace stiffness of this system is shown in Equation 7.6.

$$\beta_{br}(n_g = 4, n_c = 1) = \frac{h_b^2 S^2 E}{\frac{4L_d^3}{A_d} + \frac{9S^3}{A_s}} \tag{7.6}$$

The expression in Equation 7.5 has been used in some designs for lean-on systems with more than one cross-frame was provided in a given bracing line. Due to the definition for n_{gc} in Helwig and Wang (2003) which was the number of girders per cross-frame, the vague definition of the variable has led designers to simply divided the number of girders by the number of cross-frames. Although such an interpretation seems logical based upon the definition of the variable, this application is incorrect and was not the intended application of the expression.

Another limitation of the lean-on bracing stiffness and strength from Helwig and Wang (2003) is that only the Z-shaped cross-frame was considered in the derivation. Derivations for X-type and K-type cross-frames improve the applicability to a wider range of systems. In the following sections, the model validation process, derivation, and validation of lean-on bracing stiffness equations for K-frames and full X-frames are discussed. Treatments are subsequently given that reflect cases where more than one cross-frame is provided in a given line and the cross-frames can be located anywhere along the bracing line. However, the basic derivation in the next section begins by assuming a single cross-frame is provided in the outside bay of the bracing line, similar to the assumption utilized in Helwig and Wang (2003). More complex arrangements are considered later in this chapter.

7.2. Virtual Work Derivations for X- and K-Type Cross-Frame Bracing Lines

While the last section is focused on lean-on bracing with Z-type cross-frames, this section presents derivations of the lean-on stiffness equations considering X-type and K-type systems. Modifications for lean-on applications with multiple cross-frames are discussed in Section 7.3.

7.2.1. Two-Dimensional Model Validation

To provide validation of the derived expressions, cross-frame systems with the same assumptions as previous derivations were first considered (Yura, 2001; Helwig and Wang, 2003, Gasser (2024), Bjelland 2024). In addition to analytical derivations, SAP2000 was used to model the cross-frame line as a two-dimensional truss system and provide validation of the derived-stiffness expressions. The fundamental assumption for truss members is that elements are subjected to pure (concentric) axial force. The girder cross-sections were assumed to be rigid, and the cross-frame line was simply supported with lateral unit loads applied at the top and bottom of each girder to create a force couple on both ends of the cross-frame, as depicted in Figure 7-3.

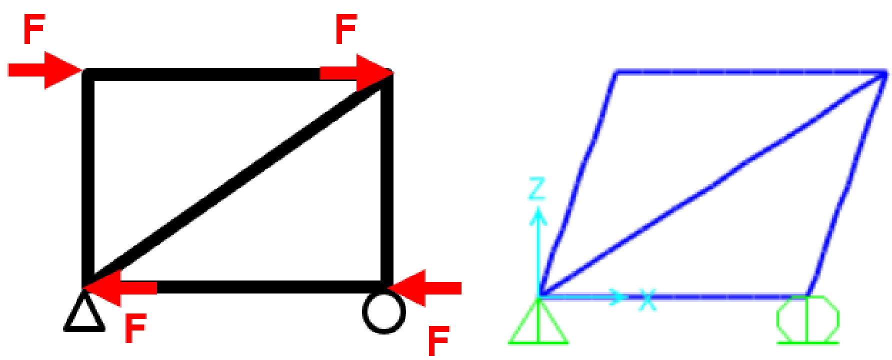

Figure 7-3. Twin Girder Tension Model Idealization and Deformed Shape

The equation for the brace stiffness based on the Z-frame model (tension-only diagonal system) is given by Equation 7.4 (Yura, 2001). In order to calculate the stiffness of the model, Equation 7.3 was used, with the value of Δ indicating the sum of the respective displacements at the top and bottom of the right girder in Figure 7-3. In the computer models, the elastic modulus of 29,000 ksi was used for the cross-frame members, and a relatively stiff elastic modulus of 29,000,000 ksi was utilized for the girder cross-sections to essentially eliminate the effects of cross-sectional distortion. A number of different geometries were considered. However, the computer models for the presented results made use of cross-frame members with an area of 6.45 in^2, a girder spacing (S) of 96 inches, and a cross-frame depth (h_b) of 76 inches. The stiffness of the computer model was 2,185,000 kip-in/rad, which agrees with the Z-frame stiffness model given in Equation 7.4 and provides validation of the derived expression.

7.2.2. Lean-On with K-Frames

A good starting point for assessing the stiffness and strength behavior for systems with lean-on bracing and K-frames is Yura's (2001) derivation for a K-frame with a twin-girder system. The behavior of K-frames that provide stability to adjacent girders are idealized with the force couples shown in Figure 7-4. With such a loading, the diagonals for the K-frame experience equal magnitudes of force; however, one diagonal is in tension and the other is in compression. The basic assumptions utilized for the Z-frame model idealization discussed in the last section apply. Figure 7-4 depicts the K-frame with force couples on either end and identifies the geometry of the brace.

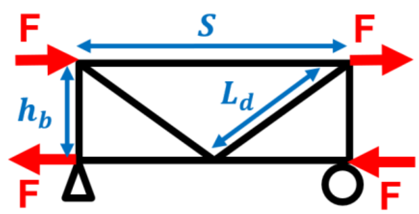

Figure 7-4. Twin Girder K-Frame Idealization

The force distribution of the system is shown in Figure 7-5. Although the top strut is a zero-force member, the actual member must be included since it maintains that the flanges of adjacent girders move in the same direction, which is important to the buckling behavior of the girders. Therefore, K-frame details without the top strut are not recommended in practice.

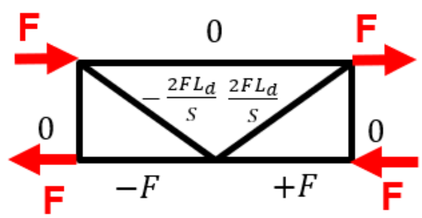

Figure 7-5. Twin Girder K-Frame Real Force Distribution

While the K-frame is subjected to force couples at both ends, the impact of the virtual unit forces at the top and bottom of the K-frame are considered separately and superimposed in the virtual work method. These virtual forces are used to evaluate the lateral deflection at the top right of the K-frame (Δ_{T2}) and the lateral deflection at the bottom right of the K-frame (Δ_{B2}) as was shown earlier in Fig. 7-1. The results for the virtual work of a unit force applied to the top of the right girder (T2) are shown in Figure 7-6.

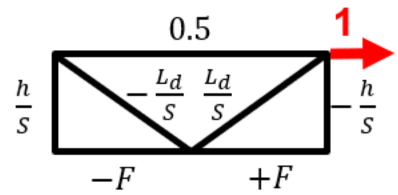

Figure 7-6 Twin Girder K-Frame Virtual T2 Force Distribution

The virtual work forces for a unit force applied to the bottom of the right girder (B2) are shown in Figure 7-7.

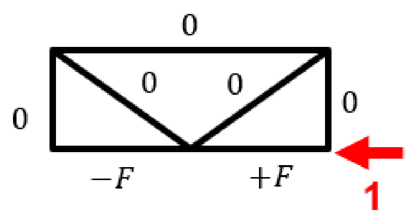

Figure 7-7 Twin Girder K-Frame Virtual T2 Force Distribution

The resulting displacement calculations are included in Table 7-1. For example, the increment of the component of Δ_{T2} for a given member is found by multiplying the length of the member by product of the real force and the $F_{virtual,T2}$ virtual force at the node of interest for the T2-deflection, and dividing by the product of the member area and the modulus of elasticity of the member $[F_{real}F_{virtual}]L/AE$. In a similar fashion, the component of Δ_{B2} for a given member is found using $F_{virtual,B2}$ in the calculation. For the purposes of sign convention, positive force values indicate tension, while negative values indicate compression. The last two columns represent the contribution of the deflection component for the deflection of interest. The total deflection component is found by summing the deflection components.

Table 7-1. Virtual Work Calculations for Two Girders and One K-Frame

Member	**Length**	**Area**	F_{real}	$F_{virtual,T2}$	$F_{virtual,B2}$	Δ_{T2}	Δ_{B2}
Top Strut	S	A_s	0	0	0	0	0
Left Bottom Strut	$S/2$	A_s	F	1	-1	$\frac{FS}{2A_sE}$	$-\frac{FS}{2A_sE}$
Right Bottom Strut	$S/2$	A_s	$-F$	0	-1	0	$\frac{FS}{2A_sE}$
Left Diagonal	L_d	A_d	$-\frac{2FL_d}{S}$	0	0	0	0
Right Diagonal	L_d	A_d	$\frac{2FL_d}{S}$	$\frac{2L}{S}$	0	$\frac{4FL_d^3}{S^2A_dE}$	0

For example, from the table of forces, the total relative displacement between the top and bottom of the brace is given by:

$$\Delta = \Delta_{T2} + \Delta_{B2} = \frac{4FL_d^3}{S^2 A_d E} + \frac{FS}{2A_s E} \quad 7.7$$

The two components for Δ_{B2} cancel one another and they were not included in Equation 7.7. This displacement can be used in Equation 7.7 to evaluate the stiffness of K-frame in a twin girder system.

7.2.2.1. Force Distribution for Lean-On System with K-frames

For the case with twin girders and a single K-frame, the brace is subjected to equal force couples on both ends. However, in a lean-on system with an unequal number of girders on either side of the K-frame, the force couples are different on the two sides of the brace. For the examples outlined in this section, the K-frame is positioned on the far-left bay of the bracing line so that the force couple on the right side of the K-frame is larger than that on the left. The forces vary based on the number of girders (effectively the number of lean-on bays) in the system. The distribution for one K-frame and one lean-on bay is shown in Figure 7-8. A comparison between Figure 7-8 and Figure 7-5 demonstrates that the top strut is not a zero-force member when the force couples on both ends are different. The unbalanced lean-on effects result in a net force in the top chord of the K-frame.

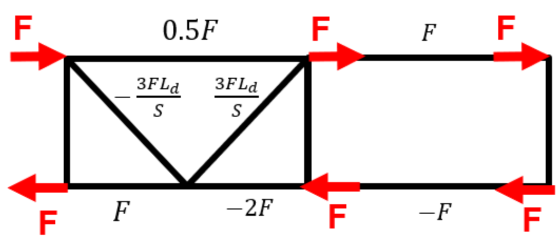

Figure 7-8 Force Distribution for One K-Frame and Three Girders

The distribution for one K-frame and two lean-on bays is shown in Figure 7-9.

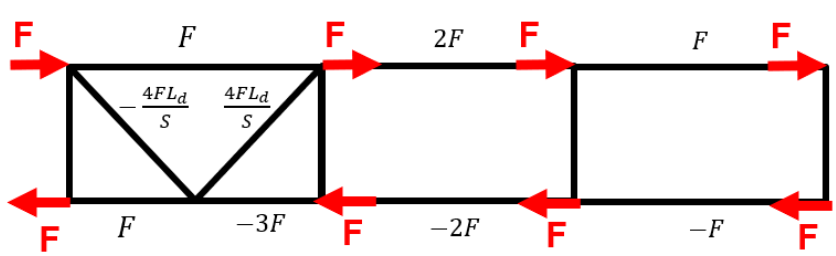

Figure 7-9 Force Distribution for One K-Frame and Four Girders

The general form of the force distribution is shown in Figure 7-10.

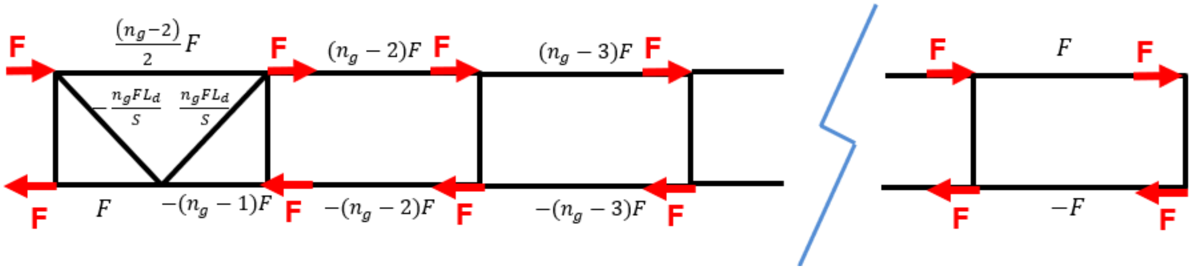

Figure 7-10 Generalized Lean-On K-Frame Force Distribution

7.2.2.2. K-Frame Lean-On Virtual Work Calculations

Virtual work calculations were completed for systems with one K-frame and three or four girders. Although the models considered the girders to have rigid cross-sections, in SAP models with a girder modulus of 29,000 ksi as opposed to 29,000,000 ksi, the difference in the calculated displacement was less than 1%. The calculations are shown in Table 7-2 and Table 7-3. As noted earlier, for lean-on systems the girder that is the farthest away from the brace in the bracing line experiences the largest deformation and, therefore, that girder is critical from a stiffness perspective. Therefore, in the evaluation of the relative deformation between the top and bottom of the brace, the deformation, Δ, is based upon the critical girder. For example, considering the 3-girder system, the "*i*" values in Table 7-2 denote the panels/bays between girder lines where the deflection component applies. For example, *i* = 1 means the bay with the cross-frame, while *i* = 2 means the bay with the two struts for the 3-girder problem.

Table 7-2. Virtual Work Calculations for Three Girders and One K-Frame

Member	**Length**	**Area**	$\boldsymbol{F_{real}}$	$\boldsymbol{F_{virtualT3}}$	$\boldsymbol{F_{virtualB3}}$	Δ_{Ti}	Δ_{Bi}
Top Strut (i = 1)	S	A_s	0.5F	0.5	0	$\frac{FS}{4A_sE}$	0
Left Bottom Strut (i = 1)	$S/2$	A_s	F	1	-1	$\frac{FS}{2A_sE}$	$-\frac{FS}{2A_sE}$
Right Bottom Strut (i = 1)	$S/2$	A_s	$-2F$	0	-1	0	$\frac{FS}{A_sE}$
Left Diagonal (i = 1)	L_d	A_d	$-\frac{3FL}{S}$	$-\frac{L}{S}$	0	$\frac{3FL_d^3}{S^2A_dE}$	0
Right Diagonal (i = 1)	L_d	A_d	$\frac{3FL}{S}$	$\frac{L}{S}$	0	$\frac{3FL_d^3}{S^2A_dE}$	0
Lean-On Bottom Strut 1 (i = 2)	S	A_s	$-F$	0	-1	0	$\frac{FS}{A_sE}$
Lean-On Top Strut 1 (i = 2)	S	A_s	F	1	0	$\frac{FS}{A_sE}$	0

The total displacement of the critical girder in a three-girder system is given by Equation 7.8, which sums up the deflection components for the two bracing bays, Δ_{Ti} and Δ_{Bi}, in Table 7-2.

$$\Delta = \Delta_{T3} + \Delta_{B3} = 6\frac{FL_d^3}{S^2A_dE} + \frac{13}{4}\frac{FS}{A_sE} \qquad 7.8$$

Table 7-3. Virtual Work Calculations for Four Girders and One K-Frame

Member	Length	Area	F_{real}	$F_{virtual,T4}$	$F_{virtual,B4}$	Δ_{Ti}	Δ_{Bi}
Top Strut (i = 1)	S	A_s	F	0.5	0	$\frac{FS}{2A_sE}$	0
Left Bottom Strut (i = 1)	$S/2$	A_s	F	1	-1	$\frac{FS}{2A_sE}$	$-\frac{FS}{2A_sE}$
Right Bottom Strut (i = 1)	$S/2$	A_s	$-3F$	0	-1	0	$\frac{3FS}{2A_sE}$
Left Diagonal (i = 1)	L_d	A_d	$-\frac{4FL_d}{S}$	$-\frac{L_d}{S}$	0	$\frac{4FL_d^3}{S^2A_dE}$	0
Right Diagonal (i = 1)	L_d	A_d	$\frac{4FL_d}{S}$	$\frac{L_d}{S}$	0	$\frac{4FL_d^3}{S^2A_dE}$	0
Lean-On Bottom Strut 1 (i = 2)	S	A_s	$-2F$	0	-1	0	$\frac{2FS}{A_sE}$
Lean-On Top Strut 1 (i = 2)	S	A_s	$2F$	1	0	$\frac{2FS}{A_sE}$	0
Lean-On Bottom Strut 2 (i = 3)	S	A_s	$-F$	0	-1	0	$\frac{FS}{A_sE}$
Lean-On Top Strut 2 (i = 3)	S	A_s	F	1	0	$\frac{FS}{A_sE}$	0

The total displacement of the critical girder in a four-girder system is given by Equation 7.9.

$$\Delta = \Delta_{T4} + \Delta_{B4} = 8\frac{FL_d^3}{S^2A_dE} + 8\frac{FS}{A_sE} \qquad 7.9$$

7.2.2.3. Generalized Lean-On Stiffness Equation with One K-Frame

A generalized displacement equation was determined for lean-on applications with one K-frame based on the virtual-work calculations discussed previously. The expression for the relative deformation between the top and bottom of the brace (Δ) is given by Equation 7.10.

$$\Delta = 2n_g\left(\frac{FL_d^3}{S^2A_dE}\right) + \left[\frac{1}{4}(n_g - 2) + \frac{n_g - 1}{2} + (n_g - 1)(n_g - 2)\right]\left(\frac{FS}{A_sE}\right) \qquad 7.10$$

Where the first term corresponds to the displacements of the diagonals in the K-frame, the second term corresponds to the displacements in the struts of the cross-frame. The equation was further simplified to the form shown in Equation 7.11.

$$\Delta = 2n_g\left(\frac{FL_d^3}{S^2A_dE}\right) + \left[n_g^2 - \frac{9}{4}n_g + 1\right]\left(\frac{FS}{A_sE}\right) \quad 7.11$$

Equation 7.11 was validated using a SAP model with six girders and one K-frame, with both the equation and the model computing a critical displacement of 0.0149 inches for the values included in Section 7.2. The resulting stiffness equation is given by Equation 7.12.

$$\beta_{br,K} = \frac{ES^2h_b^2}{2n_g\frac{L_d^3}{A_d}+(n_g^2-\frac{9}{4}n_g+1)\frac{S^3}{A_s}} \quad 7.12$$

7.2.3. Lean-On with X-Frames

The Z-frame models discussed in Section 7.2 can be used for models with a single diagonal. However, as mentioned in that section, the Z-frame model is also applicable to "tension-only diagonal" models in which the compression diagonal is conservatively neglected. However, if the compression diagonal has adequate compression capacity to support the induced force without buckling, the tension-only diagonal representation of an X-system can significantly underestimate the stiffness. Therefore, in lean-on systems, the designer may wish to consider both diagonals and the contribution of the second diagonal member to accurately quantify the stiffness of the brace in a lean-on system needs to be considered. Yura (2001) developed a "compression system" model which accounted for both X-frame diagonals. In an X-system with equal force couples on either side, the top and bottom struts are zero-force members. However, similar to the K-frame lean-on system discussed in the last section, when more girders are positioned on one side than the other of a full X-frame, the force couples are different and the top and bottom struts are generally not zero-force members. Therefore, in the derivation of the stiffness for an X-system in lean-on applications, the top and bottom struts develop forces and must be considered in the stiffness expression.

7.2.3.1. Lean-On Real Force Distribution

The idealization of a lean-on bracing line with one X-frame is an indeterminate system, so the derivation for a precise expression is heavily reliant on pattern recognition in comparisons between models. Similar force paths as the Z-frame and K-frame were observed, with slightly different proportions. The force distribution for one X-frame and one lean-on bay is shown in Figure 7-11.

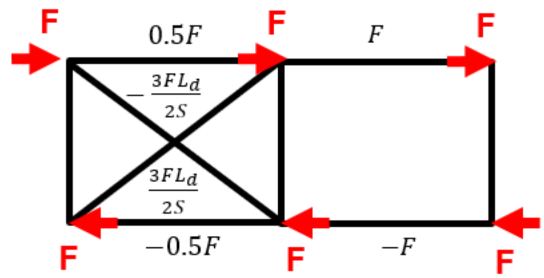

Figure 7-11 Force Distribution for One X-Frame and Three Girders

The distribution for one X-frame and two lean-on bays is shown in Figure 7-12.

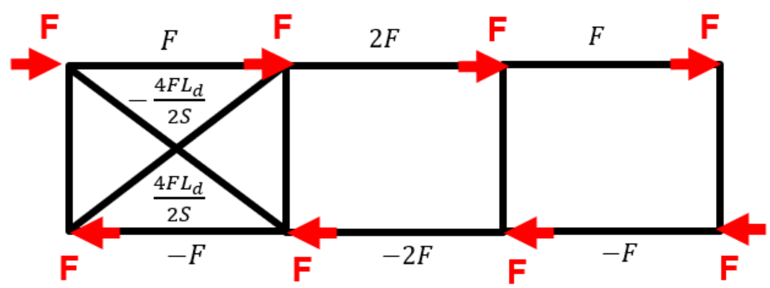

Figure 7-12 Force Distribution for One X-Frame and Four Girders

The general form of the X-frame force distribution is shown in Figure 7-13.

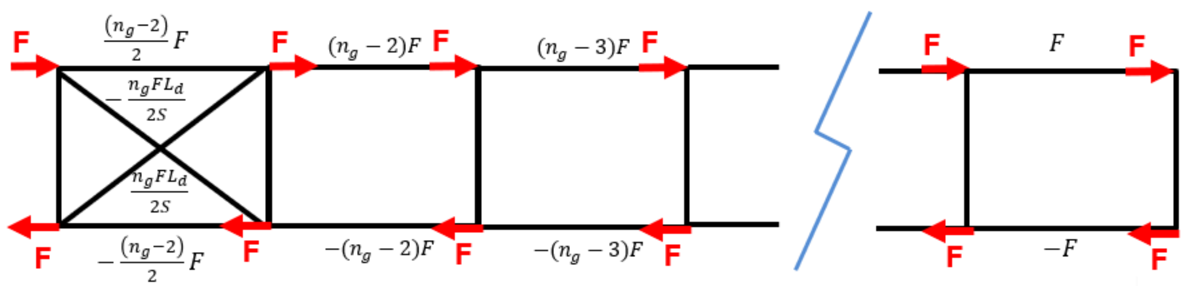

Figure 7-13 Generalized Lean-On X-Frame Distribution

7.2.3.2. Lean-On Virtual Work Calculations

Virtual work calculations were completed for systems with one X-frame and three or four girders, assuming the full X-frame was in an outer bay. The member axial forces for the virtual-force cases were obtained by applying a unit load to the appropriate model, and the values were converted into ratios of L, S, A_d, and A_s. As in the previous derivations, the torsional stiffness of the system is assumed to solely come from the torsional bracing. The calculation summary for a three-girder system is shown in Table 7-4, and the calculation summary for a four-girder system is shown in Table 7-5. As outlined in the last section, the values of "i" in the table represent the bracing bay that the members are located. The increment of the deformation at the top and bottom of the bracing panels is given in the last two columns.

Table 7-4. Virtual Work Calculations for Three Girders and One K-Frame

Member	Length	Area	F_{real}	$F_{virtual,T3}$	$F_{virtual,B3}$	Δ_{Ti}	Δ_{Bi}
Top Strut (i = 1)	S	A_s	$\frac{1}{2}F$	$\frac{1}{3}$	$\frac{1}{6}$	$\frac{1}{6}\frac{FS}{A_sE}$	$\frac{1}{12}\frac{FS}{A_sE}$
Bottom Strut (i = 1)	S	A_s	$-\frac{1}{2}F$	$\frac{1}{3}$	$-\frac{5}{6}$	$-\frac{1}{6}\frac{FS}{A_sE}$	$\frac{5}{12}\frac{FS}{A_sE}$
Top Diagonal (i = 1)	L_d	A_d	$-\frac{3FL_d}{2S}$	$-\frac{1}{3}\frac{L_d}{S}$	$-\frac{1}{6}\frac{L_d}{S}$	$\frac{1}{2}\frac{F}{S^2A_dE}$	$\frac{1}{4}\frac{FL_d^3}{S^2A_dE}$
Bottom Diagonal (i = 1)	L_d	A_d	$\frac{3FL_d}{2S}$	$\frac{2}{3}\frac{L_d}{S}$	$-\frac{1}{6}\frac{L_d}{S}$	$\frac{FL_d^3}{S^2A_dE}$	$-\frac{1}{4}\frac{FL_d^3}{S^2A_d}$
Lean-On Bottom Strut 1 (i = 2)	S	A_s	$-F$	0	-1	0	$\frac{FS}{A_sE}$
Lean-On Top Strut 1 (i = 2)	S	A_s	F	1	0	$\frac{FS}{A_sE}$	0

The total displacement of the critical girder in a three-girder system is the deformation in the 3rd girder given by Equation 7.13.

$$\Delta = \Delta_{T3} + \Delta_{B3} = \frac{3}{2}\frac{FL_d^3}{S^2A_dE} + \frac{5}{2}\frac{FS}{A_sE} \qquad 7.13$$

Table 7-5. Virtual Work Calculations for Four Girders and One K-Frame

Member	Length	Area	F_{real}	$F_{virtualT3}$	$F_{virtualB3}$	Δ_{Ti}	Δ_{Bi}
Top Strut (i = 1)	S	A_s	F	$\frac{1}{3}$	$\frac{1}{6}$	$\frac{1}{3}\frac{FS}{A_sE}$	$\frac{1}{6}\frac{FS}{A_sE}$
Bottom Strut (i = 1)	S	A_s	$-F$	$\frac{1}{3}$	$-\frac{5}{6}$	$-\frac{1}{3}\frac{FS}{A_sE}$	$\frac{5}{6}\frac{FS}{A_sE}$
Top Diagonal (i = 1)	L_d	A_d	$-2\frac{FL_d}{S}$	$-\frac{1}{3}\frac{L_d}{S}$	$-\frac{1}{6}\frac{L_d}{S}$	$\frac{2}{3}\frac{FL_d^3}{S^2A_dE}$	$\frac{2}{6}\frac{FL_d^3}{S^2A_dE}$
Bottom Diagonal (i = 1)	L_d	A_d	$2\frac{FL_d}{S}$	$\frac{2}{3}\frac{L_d}{S}$	$-\frac{1}{6}\frac{L_d}{S}$	$\frac{4}{3}\frac{FL_d^3}{S^2A_dE}$	$-\frac{2}{6}\frac{FL_d^3}{S^2A_dE}$
Lean-On Bottom Strut 1 (i = 2)	S	A_s	$-2F$	0	-1	0	$2\frac{FS}{A_sE}$
Lean-On Top Strut 1 (i = 2)	S	A_s	$2F$	1	0	$2\frac{FS}{A_sE}$	0
Lean-On Bottom Strut 2 (i = 3)	S	A_s	$-F$	0	-1	0	$\frac{FS}{A_sE}$
Lean-On Top Strut 2 (i = 3)	S	A_s	F	1	0	$\frac{FS}{A_sE}$	0

The total displacement of the critical girder in a four-girder system is given by Equation 7.14.

$$\Delta = \Delta_{T4} + \Delta_{B4} = 2\frac{FL_d^3}{S^2 A_d E} + 7\frac{FS}{A_s E} \qquad 7.14$$

7.2.3.3. Generalized Lean-On Stiffness Equation with One X-Frame

A generalized displacement equation was determined for lean-on with one X-frame based on the virtual work calculations discussed previously. This expression is given by Equation 7.15.

$$\Delta = \frac{1}{2}n_g\left(\frac{FL_d^3}{S^2 A_d E}\right) + \left[\frac{1}{2}(n_g - 2) + 2n_g(n_g - 1) - n_g(n_g + 1) + 2\right]\left(\frac{FS}{A_s E}\right) \qquad 7.15$$

Where the first term corresponds to the displacements of the diagonals in the X-frame, the second term corresponds to the displacement of the top strut of the cross-frame, the third term corresponds to the displacement of the bottom strut of the cross-frame, and the last term corresponds to the cumulative displacements of the top and bottom struts in lean-on bays. The equation may be further simplified to the form shown in Equation 7.16.

$$\Delta = \frac{1}{2}n_g\left(\frac{FL_d^3}{S^2 A_d E}\right) + \left[n_g^2 - \frac{5}{2}n_g + 1\right]\left(\frac{FS}{A_s E}\right) \qquad 7.16$$

Equation 7.16 was validated using a SAP model with six girders and one X-frame, with both the equation and the model computing a critical displacement of 0.0145 inches for the girder and brace parameters outlined in Section 7.2. The resulting stiffness equation is given by Equation 7.17.

$$\beta_{br,X} = \frac{ES^2 h_b^2}{\frac{1}{2}n_g\frac{L_d^3}{A_d} + (n_g^2 - \frac{5}{2}n_g + 1)\frac{S^3}{A_s}} \qquad 7.17$$

7.3. General Bracing Line Stiffness Formulation

The virtual work method (VWM) provides an effective means of determining the brace-stiffness expressions for simple bracing line configurations but requires considerable extrapolation for general cases of lean-on applications. The reason for this is the VWM requires the truss system to be solved upwards of three times to calculate the displacement at the selected girder. These solutions require the use of the method of joints or sections to analyze the truss. Due to this increased complexity, computational investigations using finite element models provide a more efficient means of studying more complex systems.

The finite element method (FEM) is used due to the method's flexibility and ability to model numerous systems with relative computational ease. However, similar to the VWM, large systems often become complex, requiring the solution of numerous systems of equations. These operations are simplified with computational solvers. While the FEM approach may not be viewed as an efficient approach when closed-form solutions are desired - with modern symbolic solvers in applications such as MATLAB (MathWorks, 2025), using FEM for algebraic solutions provides an effective means of developing general solutions. The following section summarizes the application of the FEM approach to generate closed-form expressions that build off of the VWM expressions and can be used to develop viable simplifications for applications of bracing a system of girders in a given span.

FEM solutions are based on the assembly of a global stiffness matrix and force vector using the degrees of freedom of each node. For truss systems, the force vector consists of the applied forces acting on each degree of freedom. The global stiffness matrix is assembled using local stiffness matrices in reference to the individual elements and the applicable degrees of freedom forming the FE model. These local stiffness matrices are added to the global stiffness matrix based on the degrees of freedom of the nodes in each element. For planar (2D) truss elements, the local stiffness matrix is given in 7.18 (Greenlee, 2010).

$$\boldsymbol{k} = \frac{AE}{L}\begin{bmatrix} \cos^2(\theta) & \cos(\theta)\sin(\theta) & -\cos^2(\theta) & -\cos(\theta)\sin(\theta) \\ \cos(\theta)\sin(\theta) & \sin^2(\theta) & -\cos(\theta)\sin(\theta) & -\sin^2(\theta) \\ -\cos^2(\theta) & -\cos(\theta)\sin(\theta) & \cos^2(\theta) & \cos(\theta)\sin(\theta) \\ -\cos(\theta)\sin(\theta) & -\sin^2(\theta) & \cos(\theta)\sin(\theta) & \sin^2(\theta) \end{bmatrix} \tag{7.18}$$

Where:

$\boldsymbol{k}$ is the local stiffness matrix of the 2D truss element.

A is the cross-sectional area of the 2D truss element.

L is the length the 2D truss element.

E is the Young's modulus of the 2D truss element.

θ is the angle of rotation of the 2D truss element from the global x-axis.

The system of linear equations, demonstrated in 7.19, is solved using linear-algebra techniques after removing linearly dependent terms (Greenlee, 2010).

$$\boldsymbol{K\delta} = \boldsymbol{F} \tag{7.19}$$

Where:

$\boldsymbol{K}$ is the global stiffness matrix of the entire system.

$\boldsymbol{\delta}$ is the global displacement vector of the entire system.

$\boldsymbol{F}$ is the global force vector of the entire system.

The displacements can be referenced from the system solution by examining the displacement vector. These values can also be used to determine the stress (force) and strain in the truss elements applying Hooke's Law ($\sigma = E\varepsilon$). The stress is given in terms of the global coordinates in 7.20 (Greenlee, 2010).

$$\boldsymbol{\sigma} = \frac{E}{L}\{-\cos(\theta) \quad -\sin(\theta) \quad \cos(\theta) \quad \sin(\theta)\}\boldsymbol{\delta} \tag{7.20}$$

Where:

$\boldsymbol{\sigma}$ is the global stress vector of the entire system.

With this basic understanding of planar trusses, a symbolic solver can be used to determine the stiffness properties of each bracing configuration. To match the virtual-work solution, the girders (vertical elements) are assumed to be rigid relative to the struts and diagonal members (horizontal elements). To replicate this, rollers are placed at the top nodes to restrict vertical deflections ($\Delta_y = 0$) which is consistent with the outcome of the virtual-work solution. Doing this additionally removes any terms related to the vertical members, which represent the girders, in the solutions. An example of a truss system is provided in Figure 7-14.

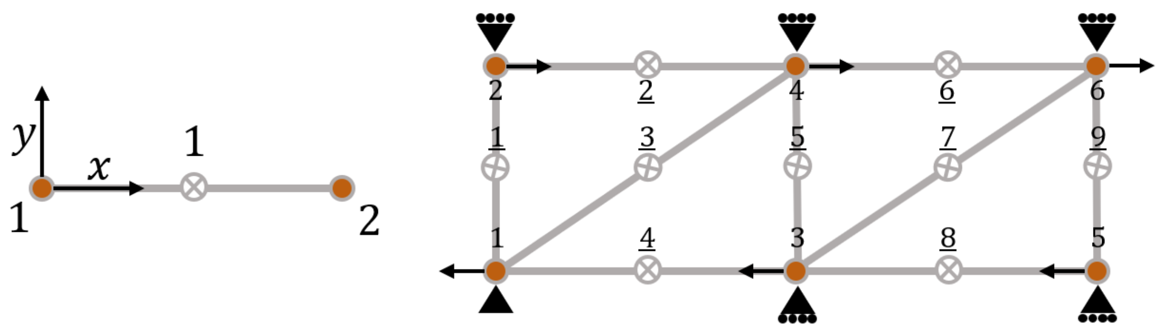

Figure 7-14. Local Truss Element and Example Truss System

The MATLAB (MathWorks, 2025) symbolic solver was used to develop the FEM-based equations. Table 7-6 provides the solutions for several of the systems shown thus far in Chapter 7, exhibiting the robustness of the symbolic solver. Overall, there is perfect agreement between the VW expression from hand solutions and the FEM symbolic solver.

Table 7-6. Comparison of Virtual Work and Finite Element Method Stiffness Solutions

Cases	VWM Δ Eq.	VWM β_{br} Eq.	FEM Δ Eq.	FEM β_{br} Eq.
	$\frac{FS}{A_sE}+\frac{2FL_d^3}{A_dES^2}$	$\frac{ES^2h_b^2}{\frac{S^3}{A_s}+\frac{2L_d^3}{A_d}}$	$\frac{FS}{A_sE}+\frac{2FL_d^3}{A_dES^2}$	$\frac{ES^2h_b^2}{\frac{S^3}{A_s}+\frac{2L_d^3}{A_d}}$
	$\frac{FL_d^3}{A_dES^2}$	$\frac{EA_dS^2h_b^2}{L_d^3}$	$\frac{FL_d^3}{A_dES^2}$	$\frac{EA_dS^2h_b^2}{L_d^3}$
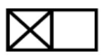	$\frac{3}{2}\frac{FL_d^3}{A_dES^2}+\frac{5}{2}\frac{FS}{A_sE}$	$\frac{ES^2h_b^2}{\frac{5S^3}{2A_s}+\frac{3L_d^3}{2A_d}}$	$\frac{3}{2}\frac{FL_d^3}{A_dES^2}+\frac{5}{2}\frac{FS}{A_sE}$	$\frac{ES^2h_b^2}{\frac{5S^3}{2A_s}+\frac{3L_d^3}{2A_d}}$
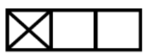	$\frac{2FL_d^3}{A_dES^2}+\frac{7FS}{A_sE}$	$\frac{ES^2h_b^2}{\frac{7S^3}{A_s}+\frac{2L_d^3}{A_d}}$	$\frac{2FL_d^3}{A_dES^2}+\frac{7FS}{A_sE}$	$\frac{ES^2h_b^2}{\frac{7S^3}{A_s}+\frac{2L_d^3}{A_d}}$
	$\frac{FS}{2A_sE}+\frac{4FL_d^3}{A_dES^2}$	$\frac{2ES^2h_b^2}{\frac{S^3}{A_s}+\frac{8L_d^3}{A_d}}$	$\frac{FS}{2A_sE}+\frac{4FL_d^3}{A_dES^2}$	$\frac{2ES^2h_b^2}{\frac{S^3}{A_s}+\frac{8L_d^3}{A_d}}$
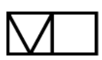	$\frac{6FL_d^3}{A_dES^2}+\frac{13}{4}\frac{FS}{A_sE}$	$\frac{ES^2h_b^2}{\frac{13S^3}{4A_s}+\frac{6L_d^3}{A_d}}$	$\frac{6FL_d^3}{A_dES^2}+\frac{13}{4}\frac{FS}{A_sE}$	$\frac{ES^2h_b^2}{\frac{13S^3}{4A_s}+\frac{6L_d^3}{A_d}}$
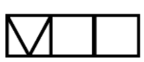	$\frac{8FL_d^3}{A_dES^2}+\frac{8FS}{A_sE}$	$\frac{ES^2h_b^2}{\frac{8S^3}{A_s}+\frac{8L_d^3}{A_d}}$	$\frac{8FL_d^3}{A_dES^2}+\frac{8FS}{A_sE}$	$\frac{ES^2h_b^2}{\frac{8S^3}{A_s}+\frac{8L_d^3}{A_d}}$

With verification of the method with the existing solutions complete, the FEM solver was used to determine generalized expressions for Z-frames, X-frames, and K-frames. These solutions are given in 7.21, 7.22, and 7.23 and the basis of these solutions is provided in Appendix M. Approaches Considered for Brace Stiffness with Greater than One Cross-Frame. Note that these solutions are exact for simple cross-frames lines that are either symmetric and/or have less than 3 torsional braces. The approach provides approximate yet reasonable predictions of the behavior for complex cross-frame layouts. For complex layouts, the solution is generally within 5% of the FEA solution. These solutions represent the entire cross-frame line, so the exact number of girders and cross-frames should be used. The equations are expressed in terms of a factor C_{lean} and the ratio n_g/n_c account for the effects of leaning girders.

$$\beta_{br,line,Z}^{2D} = \frac{ES^2 h_b^2}{\left[\frac{n_g}{n_c}\right]\frac{L_d^3}{A_d} + [C_{lean}]\frac{S^3}{A_s}} \tag{7.21}$$

$$\beta_{br,line,X}^{2D} = \frac{ES^2 h_b^2}{\left[\frac{n_g}{2n_c}\right]\frac{L_d^3}{A_d} + \left[C_{lean} - \frac{n_g}{2n_c}\right]\frac{S^3}{A_s}} \tag{7.22}$$

$$\beta_{br,line,K}^{2D} = \frac{ES^2 h_b^2}{\left[\frac{2n_g}{n_c}\right]\frac{L_d^3}{A_d} + \left[C_{lean} - \frac{n_g}{4n_c}\right]\frac{S^3}{A_s}} \tag{7.23}$$

Where:

n_g is the total number of girders

n_c is the total number of cross-frames in a bracing line

C_{lean} is a rationale number referred to as the lean-on factor associated with the least stiff segment of the bracing line due to leaning girders.

To determine C_{lean}, the bracing line is segmented into different "leaning segments" and is dependent on the least stiff segment of the bracing line which generally corresponds to the maximum number of internal or external leaning girders. Figure 7-15 demonstrates how to determine the number of leaning girders used in the C_{lean} Equations 7.24 and 7.25. There are 9 girders in the cross-section of Figure 7-15 represented by the vertical lines. There are two cross-frames and three "leaning segments" that are classified as either external segments or internal segments. Equation 7.24 was developed from the data analysis from the parametric studies with the operator "*floor*" in the expression indicating to round the parameter down to the nearest integer. Equation 7.25 is a simplification_that can be slightly unconservative yet provides a reasonable degree of accuracy. Furthermore, the expression provides a more direct solution without the need for the "*floor*" operator and thus is recommended for use in design.

For the case of two internal lean-on bays bound by two cross-frames, illustrated in Figure 7-16, the simplification is ~20% unconservative for the strut term. The resulting strut term is 1.25 for the exact method and 1.00 for the simplified method (a 20% relative error). However, when accounting for the influence of the simplifications on the whole expression, the unconservative result is less severe. This can be demonstrated by calculating the stiffness of the bracing system with two internal lean-on bays bound by two cross-frames, again illustrated in Figure 7-16, with both methods; where n_g is 5, n_c is 2, $n_{lean,int}$ is 1, A_d is 5 in^2, A_s is 5 in^2, E is $29000\ ksi$, $S = 120\ in$, $h_b = 80\ in$, and $L_d = 144\ in$. The relative difference in stiffness values is only ~7%. Depending on the spacing and height of the brace, the impact of the strut term changes.

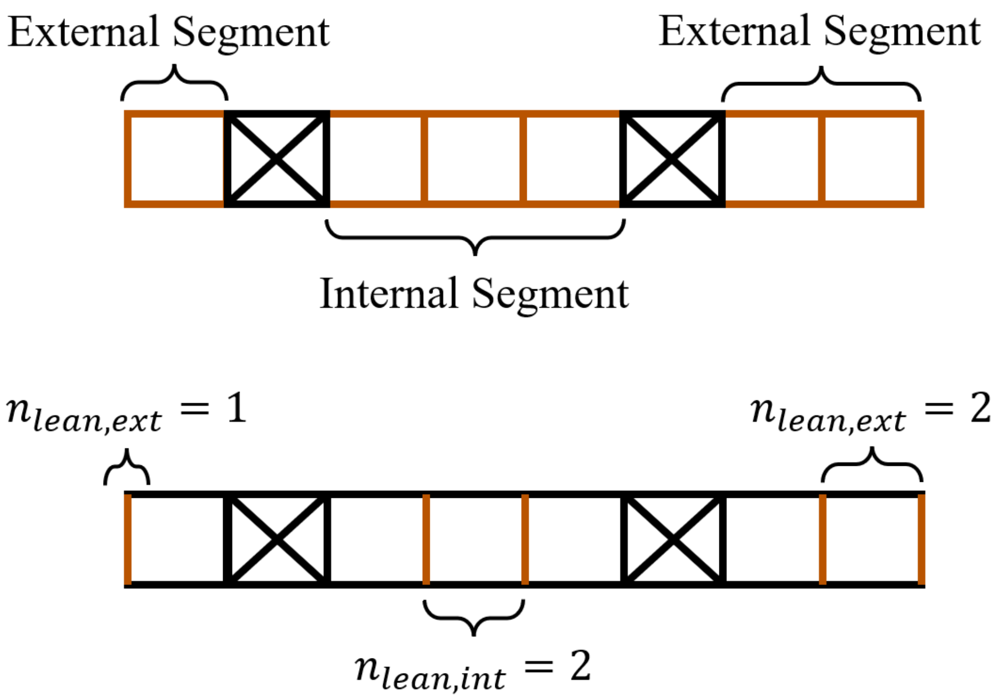

Figure 7-15. Example of Classification of Internal and External Segments and their n_{lean} Values

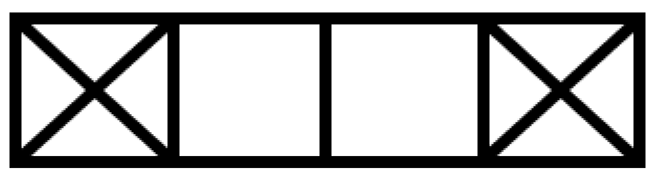

Figure 7-16. Bracing Line with Internal Segment

$$C_{lean} = max\begin{cases} (n_{lean,ext} + 1)^2 \\ floor(1.3975^{n_{lean,int}}) + 1.5n_{lean,int} \end{cases} \quad 7.24$$

$$C_{lean} \approx max\begin{cases} (n_{lean,ext} + 1)^2 \\ (n_{lean,int}/2\ + 1)^2 \end{cases} \quad 7.25$$

Where:

$n_{lean,ext}$ is the maximum number of external leaning girders in the bracing line. Note that this parameter is not the total number of leaning girders, but the maximum number of "external" girders on either side of the cross-frame. This is further explained in the examples below.

$n_{lean,int}$ is the maximum number of internal leaning girders in the bracing line. Note that this parameter is not the total number of leaning girders, but the maximum number of "internal" girders on either side of the cross-frame. This is further explained in the examples below.

For ease of use in future references, the C_{lean} component equations are equated to the constants C_{ext} and C_{int}.

$$C_{ext} = (n_{lean,ext} + 1)^2 \quad 7.26$$

$$C_{int} = floor(1.3975^{n_{lean,int}}) + 1.5n_{lean,int} \approx (n_{lean,int}/2\ + 1)^2 \quad 7.27$$

Where:

C_{ext} and C_{int} are parameters that account for the number of leaning external or internal girders.

When the cross-frame line is symmetric, the value of C_{lean} can be determined with either the full bracing line or by idealizing the bracing line into "simplified" equivalent problems. The 2D representation in Figure 7-16 can be used to illustrate how full bracing lines can be simplified into idealized bracing lines. The bracing lines (left) in Figure 7-17 are of equivalent stiffness to the simplified component bracing line (right). The cases that are "dimmed" simply do not control or are equivalent to the "bolded" case. The central internal leaning bay separates the behavior of the left and right sides of the bracing line. This is only the case for symmetric bracing lines either separated by a central internal leaning bay or in a checkerboard format.

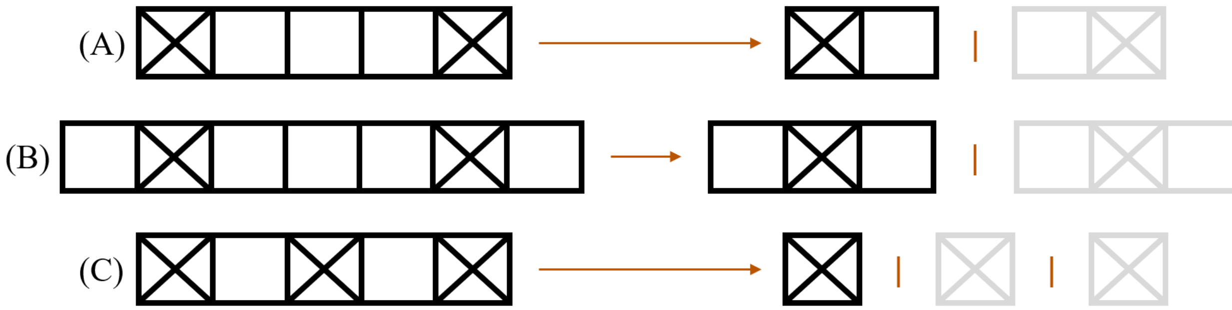

Figure 7-17. Example of Three Bracing Line Simplifications

Using the same geometric values as the previous example (A_d is 5 in^2, A_s is 5 in^2, E is 29000 ksi, $S = 120\ in$, $h_b = 80\ in$, and $L_d = 144\ in$), the bracing expressions can be used to demonstrate the relationship between the bracing lines in Figure 7-17. The evaluations are shown with both the full system (case on the left) and the simplified system (case on the right). Since the cases shown are relatively simple cases, the solutions below are accurate predictions of the FEA solutions:

<u>CASE A:</u> The bracing line in Figure 7-17(A) shows two possible representations for the bracing line consisting of either the "full" bracing line on the left or the simplified bracing line on the right. Considering the full bracing line, the parameters consist of $n_g = 6$, $n_c = 2$, and $n_{lean,int} = 2$ since the two interior girders lean on the outside cross frames. Therefore, $n_g/2n_c = 6/2{\cdot}2 = 3/2$. The value of C_{lean} can be computed using either Eq. 7.24 or 7.25. Using Eq. 7.24, without the "floor" operator, C_{lean} = 4.95. Applying the "floor" operator, the value of C_{lean}= 4. If instead, Eq. 7.25 is utilized, $C_{lean} = \left(n_{lean,int}/2\ +1\right)^2 = 4$.

Alternatively, the simplified system on the right can be utilized to idealize the bracing line that is symmetric about the centerline of the girder system; however, in that case, there is one leaning girder and the idealized system treats that girder as an "exterior" girder relative to the single cross-frame. Therefore, the parameters consist of $n_g = 3$, $n_c = 1$, and $n_{lean,ext} = 1$. For the simplified system the system also has $n_g/2n_c = 3/2$. Again, the value of C_{lean} can be computed with either Eq. 7.24 or 7.25. Using Eq. 7.24, $C_{lean} = \left(n_{lean,ext} + 1\right)^2 = 4$. If instead Eq. 7.25 is utilized, $C_{lean} = \left(n_{lean,ext} + 1\right)^2 = 4$, resulting in identical solutions.

Therefore, for either the full or simplified systems, C_{lean} = 4 and $n_g/2n_c = 3/2$. Using the cross-frame geometry and material properties listed above, Eq. 7.22 can be used to calculate the stiffness of the bracing line as $1{,}515{,}150\,\frac{k-in}{rad}$.

<u>CASE B:</u> The bracing line in Figure 7-17(B) can be represented as a full bracing line with $n_g = 8$, $n_c = 2$, $n_{lean,int} = 2$. and $n_{lean,ext} = 1$. The ratio $n_g/2n_c$ = 2. The value of C_{lean}, needs to consider both the exterior leaners and the interior leaners separately. The

C_{lean} values are evaluated only using the expressions in Eq. 7.25 for simplicity. For the exterior girder, $C_{lean} = (n_{lean,ext} + 1)^2 = 4$. The interior girder has $C_{lean} = (n_{lean,int}/2 + 1)^2 = 4$, and therefore, $C_{lean} = 4$.

Utilizing the simplified system, $n_g = 4, n_c = 1$, and $n_{lean,ext} = 1$. Note that the value of $n_{lean,ext}$ is not the total number of leaning girders, but is instead the maximum number on either side of the cross-frame. In the simplified representation, there is one "external" leaning girder on either side and therefore, $n_{lean,ext} = 1$. The ratio $n_g/2n_c = 2$. The value of C_{lean} from Eq. 7.25 is $C_{lean} = (n_{lean,ext} + 1)^2 = 4$.

Therefore, for either the full or simplified systems, $C_{lean} = 4$ and $n_g/2n_c = 2$. Using the cross-frame geometry and material properties listed above, Eq. 7.22 can be used to calculate the stiffness of the bracing line as $1{,}413{,}250 \frac{k-in}{rad}$.

CASE C: The bracing line in Figure 7-17(C) has $n_g = 6$ and $n_c = 3$ whereas the simplification is $n_g = 2$ and $n_c = 1$. Neither system has any leaning girders since each of the three cross-frames essentially restrain the two adjacent girders, so $C_{lean} = 1$. The values of $n_g/2n_c$ for both the full and simplified systems is 6/6 or 2/2 = 1. Therefore, using $n_g/2n_c = 1$ and $C_{lean} = 1$ along with the cross-frame geometry and material properties given, Eq. 7.22 can be used to calculate the stiffness of the bracing line as $4{,}454{,}670 \frac{k-in}{rad}$.

These idealizations demonstrate how the bracing line can be evaluated with either the full system or can also be idealized as a simplified system. The layouts that were considered essentially produced identical solutions. Due to the symmetry in the systems, both the full and simplified systems could be directly compared and either approach could be used. However, in many cases, the bracing lines are not symmetric and therefore the method with the full bracing line should be used. While these approaches have focused on the behavior of a single bracing line, the bracing line is generally one of many lines along a girder span. In general, there is interaction between the bracing lines in the three-dimensional system, which is the focus of the following section.

7.4. Application of General Brace Stiffness Solutions To Full Bracing Systems

The previous section focused on the stiffness of a given bracing line – which is a 2D representation of a subset of the bracing system. This section is focused on the collective behavior of all of the bracing lines and girders in a given span, which represents the 3D effects of the system. This section is therefore focused on classifying the β_{br} equations for 3D applications to fully account for the collective impact lean-on bracing lines within the girder span to address the system behavior. In general, the brace stiffness equations are equal to or less than the calculated brace stiffness of the 3D models. The discrepancies discussed herein are related to the combination of the vertical and lateral restraints of the girders in a given bracing line that result due to the interaction with the girder flexibility along the entire span. While the cross-sectional slices shown thus far confine the deformations within the bracing line, in reality the girders deflect vertically and transversely. The girders, which were modeled using simple-span boundary conditions, provide some confinement to the rotation of the bracing line. For the system to rotate about the bracing line, the girders must displace along with the bracing line. In 2D, this behavior is akin to lateral and vertical springs at the top and bottom nodes, as illustrated in Figure 7-18.

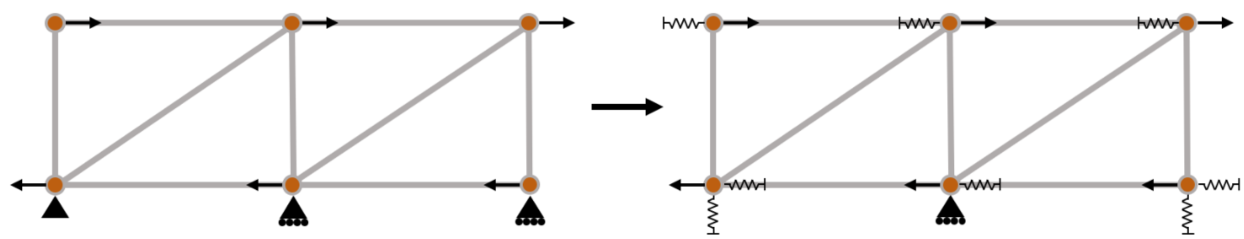

Figure 7-18. Representation of Girder Impact on 2D Model.

The difference in behavior can be further illustrated by comparing the deformed shapes of system models in 2D versus 3D space. The deformed shapes of three models experiencing a "racking" deformation are shown in Figure 7-19. The system that is shown represents a single bracing line located at midspan. For the 3D systems that are considered, the girders were simply supported.

The three different cases represented in Cases A, B, and C include significant variations in the boundary conditions for the bracing line. The racking deformation that is shown occurred due to the loading shown at the top of the figure, which is similar to the force couples used earlier in this chapter to represent the forces imparted on the cross-frames as the girders reach the buckling behavior. Figure 7-19(A) represents the 2D representation of a bracing line that is identical to the models used in the previous sections of this chapter. Figure 7-19(B), represents the 3D system in which the girders are modelled with shell elements so that the entire span is considered and the bracing line is positioned at midspan; however, each of the girders is also vertically restrained at midspan from vertical movement with a "roller support". With the vertical movement restrained at midspan of the 3D model, the racking deformation is relatively similar between the 2D and 3D models. While there is a slightly larger rotation of the fascia girders on either side of the bracing line in Figures 7-18 A and B, the rotation of the girders is relatively uniform across the width of the system. Figure 7-19(C) shows the behavior of the simple span when the vertical restraint is removed from the midspan location. With the vertical restraint removed, the rotation of the system about the bracing line becomes nonuniform, with each brace experiencing a significant difference in the angle of rotation relative to the centroid of the bracing line. The differences between Figure 7-19(B) and Figure 7-19(C) highlight how the racking deformation is coupled with a twist about the bracing line centroid due to the variable vertical and lateral deformation of the girders in three-dimensional space.

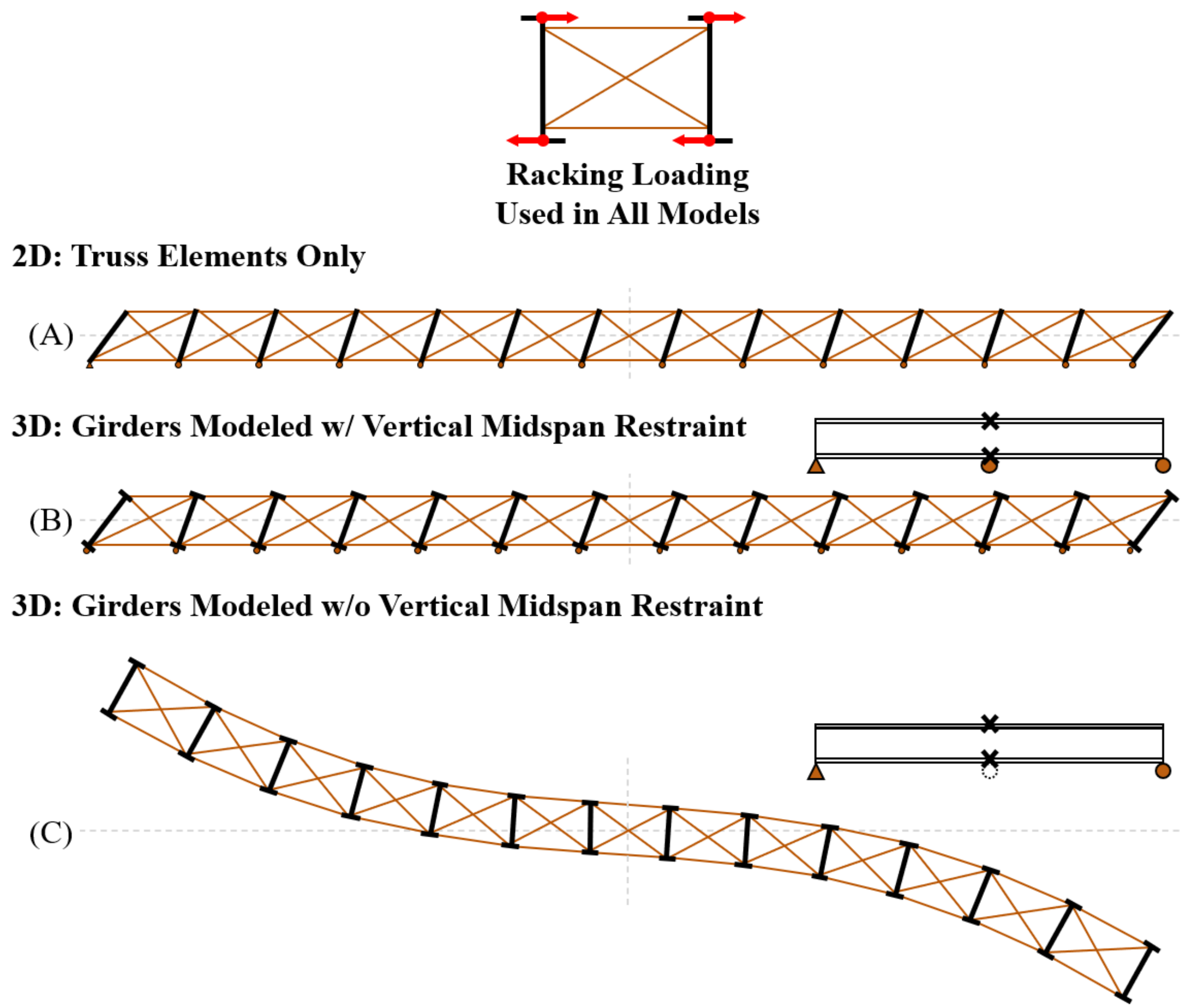

Figure 7-19. Racking in 2D (A) vs. 3D Models with (B) and without (C) Vertical Restraint at the bracing line.

Appendix M provides an overview of the behavior of lean-on bracing lines with more than a single intermediate brace. By analyzing the 3D models of the bracing lines in Appendix M, leveraging the same methods used in Chapter 6.2, the difference between the isolated bracing line in 2D versus the 3D models of the lean-on bracing lines can be quantified. The data in Figure 7-20 shows that the mean of the general solution is ~30% and ~45% conservative for lean-on bracing lines considering the respective cases for Z-frames and X-frames. The behavior with K-frames will likely be similar to X-frames. However, the fundamental idealized behavior of the bracing lines from the 2D models is preserved (Figure 7-17). The behavior indicates a deeper interaction between the braces, leaning struts, and girders than historically recognized.

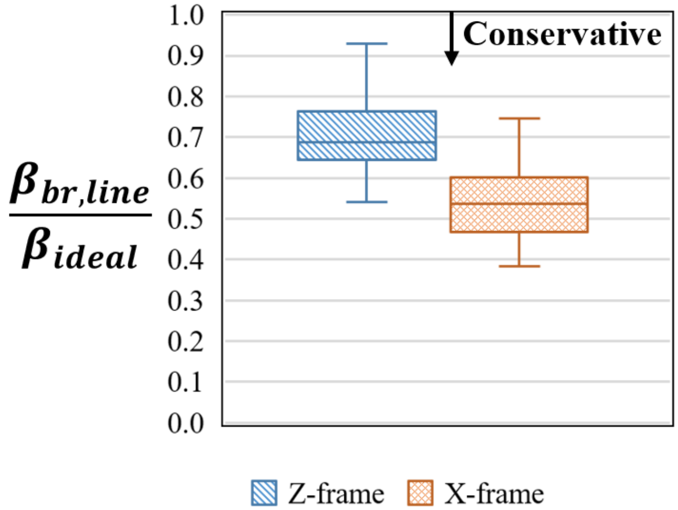

Figure 7-20. Effectiveness of General Equation with or without accounting for Girder Shears

To outline the development of a solution to the numerical discrepancy presented in Figure 7-20, a brief pivot to analyze the behavior of conventional bracing systems is necessary. As mentioned in Chapter 6.3, while developing the improved β_g expression (Fish et al. 2025), a numerical factor applied to the β_{br} was required to represent the true total system stiffness that is consistent with the effective torsional brace stiffness per girder. Cross-frame stiffness expressions were developed and presented by Yura (2001) using a twin girder system, which essentially represents an effective stiffness of half a brace per girder (β_{br}). When more than 2 girders are present in a conventional bracing system the effective stiffness is represented with a factor C_{nc} applied to β_{br} to reflect an effective brace stiffness $\beta_{br,eff}$ representative of the bracing-line stiffness (Fish et al., 2025). The approach of an effective brace per girder ($\beta_{br,eff}$) differs from the methodology presented thus far in this chapter, which has updated the β_{br} expression to include the stiffness of all bracing members in the bracing line. In summary, the two methods evaluated for determining brace stiffness are:

1. Analytically – $\beta_{br,line}$
2. Numerically – $\beta_{br,eff}$

By using the results from 3D FEA, these two methodologies were compared in respect to the number of girders, bracing line configuration, bracing type, girder section, and the ratio of brace height (h_b) to girder spacing (S). The typical result for conventional bracing systems is provided in Figure 7-21. The results in Figure 7-21 compare the relative error between the expressions described thus far: Equation 2.22, Equation 6.2, and Equation 7.22. Note that Equation 6.2 and Equation 7.22 simplify to Equation 2.22 for a single cross-frame. Each curve provides the data for the corresponding bracing line indicated in the legend. The number of girders considered ranged from 2 to 5, which for conventional bracing translates to one through four adjacent cross-frames. These different systems were compared in respect to the S/h_b ratio and relative total system stiffness error.

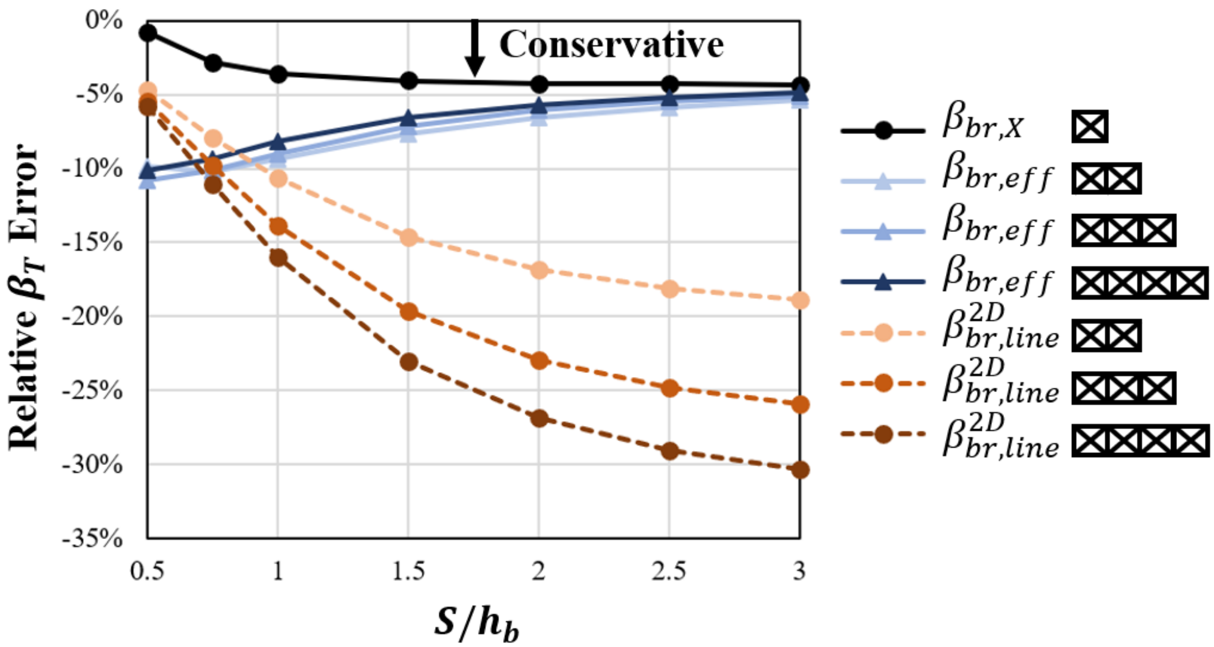

Figure 7-21. Comparison of Brace Stiffness Methods relative to 3D FEA Results for Conventional Bracing Line

The $\beta_{br,line}$ approach provides the best estimate for results of the conventional bracing lines with low S/h_b ratios (<0.75), whereas the numerical $\beta_{br,eff}$ approach is more accurate at higher S/h_b ratios (≥0.75). The reason the $\beta_{br,line}$ expression provides lower (more conservative) estimates of the brace stiffness as the brace widens relative to the depth is due to the shallower inclination of the diagonals which provide less torsional restraint. At high S/h_b ratios, the struts, via the associated term in the stiffness expression, significantly impact the behavior of the full bracing line. Additionally, the $\beta_{br,line}$ expression becomes more conservative as the number of braces in the bracing lines increases. This result is likely tied to the nonuniform rotation about each brace depicted in Figure 7-19(C).

The results in Figure 7-21 provide some context as to the conservative results in Figure 7-20, as those analyses featured S/h_b ratios greater than 3 to prevent the in-plane stiffness component, β_g, from dominating the solution. The wider the system, the larger the in-plane stiffness. In essence, the higher S/h_b ratios increased the $\beta_{br,line}$ error. Further conservatism likely comes from the leaning girders being partially restrained out of plane, which would indicate that C_{lean} is overly conservative (C_{lean} is taken as 1 for conventional bracing).

7.5. General Solution Modifications Necessary for 3D Systems

With the establishment of the behavior related to the S/h_b ratio, the key unknown that is fundamentally required is a resolution of the classification of C_{nc} from Fish et al. (2025), which is applicable to conventional (i.e. not lean-on) bracing. To meet that end, the unique system configuration utilized to determine the numerical $\beta_{br,eff}$ solution was examined. This system configuration, with a very large value of S/h_b of ~16, leads to a simplification in the theoretical $\beta_{br,line}$ solution. By leveraging this simplification, the discrepancy between 2D and 3D solutions was sourced and resolved.

This section provides a transition in the line solutions derived in Section 7.3 for 2D to solutions applicable to general bracing problems. Therefore, a series of transitions are presented throughout this section to develop general equations that account for the interaction between bracing lines along the length of the bridges.

The solutions for $\beta_{br,line}$ were given in 7.21, 7.22, and 7.23. For a system with a large ratio of S/h_b, the length of the diagonal (L_d) and the girder spacing (*S*) are similar in magnitude due to the shallow angle inclination of the diagonal. For K-frames, the spacing approximates to twice the length of the diagonal ($S \approx 2L_d$). By utilizing this simplification and assuming the struts and diagonals have the same cross-sectional area, $\beta_{br,line}$ can be rewritten to solutions nearly equivalent to brace stiffness expressions given in Chapter 2, Equations 2.21, 2.22 and 2.23, with the addition of the lean-on factor C_{lean}. As noted earlier in Section 7.3, the lean-on factor accounts for the impact of the leaning girders on the bracing line stiffness. These special case equations are given in the following expressions:

$$\beta^*_{br,line,Z} = \frac{Eh_b^2 A_d}{\left[\frac{n_g}{n_c} + C_{lean}\right] S} \approx \frac{Eh_b^2 A_d C_{nc,z}}{S} \qquad 7.28$$

$$\beta^*_{br,line,X} = \frac{Eh_b^2 A_d}{C_{lean} S} \approx \frac{Eh_b^2 A_d C_{nc,x,k}}{S} \qquad 7.29$$

$$\beta^*_{br,line,K} = \frac{Eh_b^2 A_d}{C_{lean} S} \approx \frac{Eh_b^2 A_d C_{nc,x,k}}{S} \qquad 7.30$$

Where:

$\beta^*_{br,line,Z}$ represents the simplified 3D FEA stiffness for Z-frames.

$\beta^*_{br,line,X}$ represents the simplified 3D FEA stiffness for X-frames.

$\beta^*_{br,line,K}$ represents the simplified 3D FEA stiffness for K-frames.

Equations 7.28, 7.29, and 7.30 establish why C_{nc} requires two different forms in Fish et al. (2025). The K- and X-frame solutions simplify to the same case whereas the Z-frame solution has the n_g/n_c additional term in the denominator. Another aspect of this solution is that the lean-on factor, C_{lean}, according to the 2D derivation is 1. Thus C_{lean} disappears from the solution unless an assumption is made that C_{lean} is a function of the same behavior as C_{nc}. In essence, these equations highlight how C_{lean} should be interpreted as $1/C_{nc}$ for the conventional case. By accounting for C_{nc} in this way, C_{lean} more accurately represents the bracing line strut behavior for conventional applications.

For clarity, $1/C_{nc,x,k}$ is redefined in Equation 7.31 as the variable C_{ng}, which better reflects that the behavior is closely tied to the relationship between the struts and the number of girders. Due to including the n_g/n_c term in the Z-frame solution, $C_{nc,x,k}$ can be universally used.

$$C_{ng} = \frac{1}{C_{nc,x,k}} = \frac{1}{1 + \frac{n_g - 2}{n_g + 1.75}} = \frac{n_g + 1.75}{2n_g - 0.25} \tag{7.31}$$

By assuming C_{ng} is equal to C_{lean}, the comparison presented in Figure 7-21 can be reframed in Figure 7-22. The combined solution, $\beta^*_{br,line}$, performs better than either $\beta_{br,eff}$ or $\beta^{2D}_{br,line}$, reinforcing that the 2D interpretation of C_{lean} is the source of the discrepancy.

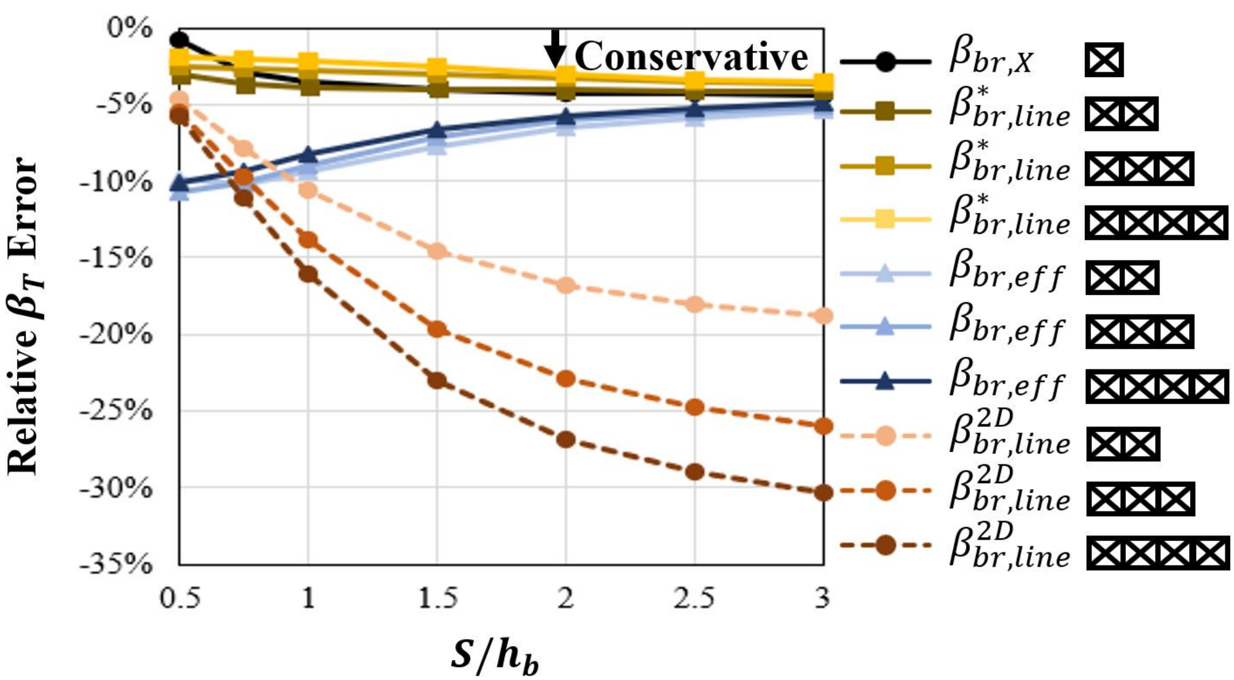

Figure 7-22. Updated Comparison of Brace Stiffness Methods relative to 3D FEA Results for Conventional Bracing Line

Using this framework, the best universal brace stiffness equations can be defined as given in Equations 7.32, 7.33, and 7.34 where C_{strut} replaces C_{lean} to better represent the 3D system behavior.

$$\beta_{br,line,Z}^{3D} = \frac{ES^2h_b^2}{\left[\frac{n_g}{n_c}\right]\frac{L_d^3}{A_d} + [C_{strut}]\frac{S^3}{A_s}} \qquad 7.32$$

$$\beta_{br,line,X}^{3D} = \frac{ES^2h_b^2}{\left[\frac{n_g}{2n_c}\right]\frac{L_d^3}{A_d} + \left[C_{strut} - \frac{n_g}{2n_c}\right]\frac{S^3}{A_s}} \qquad 7.33$$

$$\beta_{br,line,K}^{3D} = \frac{ES^2h_b^2}{\left[\frac{2n_g}{n_c}\right]\frac{L_d^3}{A_d} + \left[C_{strut} - \frac{n_g}{4n_c}\right]\frac{S^3}{A_s}} \qquad 7.34$$

Where:

C_{strut} is the strut efficiency term related to the number of braces, struts, and girders.

Due to the complexity with defining a universal equation for C_{strut} due to the impact of layouts and the large number of possible permutations in bracing lines, the bounds of C_{strut} were pursued using FEA. C_{strut} can be determined numerically by using the high S/h_b ratio case and solving for C_{strut}. The distinctions between the X, K, and Z-frame cases are given in Equations 7.35 and 7.36.

$$C_{strut,FEA,z} = \frac{Eh_b^2A_{d,FEA}}{S\beta_{ideal}} - \frac{n_g}{n_c} \qquad 7.35$$

$$C_{strut,FEA,x,k} = \frac{Eh_b^2A_{d,FEA}}{S\beta_{ideal}} \qquad 7.36$$

C_{strut} is further simplified by distinguishing between conventional and lean-on cases. However, in reality, C_{strut} features granular values depending on how many lean-on struts are introduced in proportion to the number of braces. For design, C_{strut} can be defined by referencing Table 7-7. These numerical factors increase the overall stiffness of the bracing line. With the exception of the full line of bracing recommended near midspan, the typical recommended lean-on bracing lines (see Chapter 6.4) will generally include a total of 1 to 3 full cross-frames in combination with the lean-on struts. These factors are universal and do not depend on the type of brace. The other terms in the $\beta_{br,line}$ correct for the bracing type. Recall from Section 7.3 that C_{ext} and C_{int} are parameters that account for the number of leaning external or internal girders.

Table 7-7. Cases and Values for C_{strut} for $\beta_{br,line}^{3D}$ Expression

System Type	Case	Condition	C_{strut}
Conventional	-	-	C_{ng}
Lean-on	External	$C_{ext} > C_{int}$	$[0.70 - 0.05n_c]C_{ext}$
	Internal	$C_{ext} < C_{int}$	$[0.70 - 0.05n_c]C_{int}$
	Mixed	$C_{ext} = C_{int}$	$[0.85 - 0.05n_c]C_{ext}$

The data from all standard lean-on bracing lines analyzed (148 bracing lines), not including cases that are able to be idealized, are displayed in Figure 7-23. Each box of the box and whisker plot represents a different number of cross-frames (i.e. 2X means two cross-frames) in Figure 7-21(A) and Figure 7-21(B). The y-axis represents the relative error between C_{strut}, which is the same as C_{lean} without corrections, and the FEA results. The comparison highlights how conservative the 2D behavior is. Figure 7-21(A) is the data for lean-on only in external bays whereas Figure 7-21(B) is the data for lean-on only in internal bays. Figure 7-21(C) compares the overall error in C_{strut} depending on whether the lean-on in the external segment, internal segment, or both equally control the stiffness behavior.

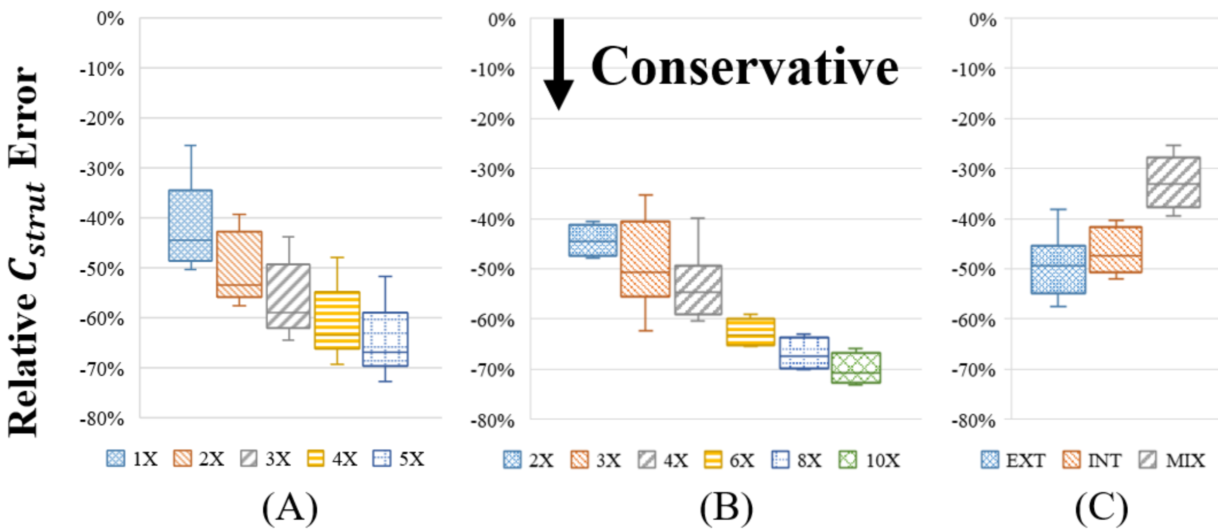

Figure 7-23. C_{strut} error for specific bracing lines with (A) external only lean-on, (B) internal only lean-on, and a summary of (C) both internal only (INT), external only (EXT) lean-on, and a mix of both (MIX).

If the system can be idealized (simplified), as presented in Figure 7-17 and connected examples, the bracing line values for the idealized system should be used as the basis for evaluating C_{strut} and subsequent $\beta_{br,line}^{3D}$ calculation. Using the brace stiffness expression with the values for the full bracing line and not the idealized case may lead to inaccurate results as the idealized bracing system is more representative of the behavior of the bracing line.

The Figure 7-25 represents the distribution of the data, with and without the C_{strut} correction applied. The box and whiskers plots of the data are shown relative to the calculated brace stiffness (A) and error (B). The true stiffness value is β_{ideal}. Overall, $\beta_{br,line}^{3D}$ provides a more accurate and less conservative solution compared to $\beta_{br,line}^{2D}$. The recommended layouts typically have lean-on bracing lines with 1 to 3 braces. The unconservative outliers relative to β_{ideal} in Figure 7-25, generally featured significantly more braces than lean-on bays. These cases have highlighted diminishing returns in the longitudinal restraint and the limitations of a linear approximation. The cases analyzed, due to their girder spacing, also lead to a strut term having a higher than typical weight in the calculation relative to the diagonal term. A typical girder spacing would lead to less error due to the diagonal term having a larger impact on the solution.

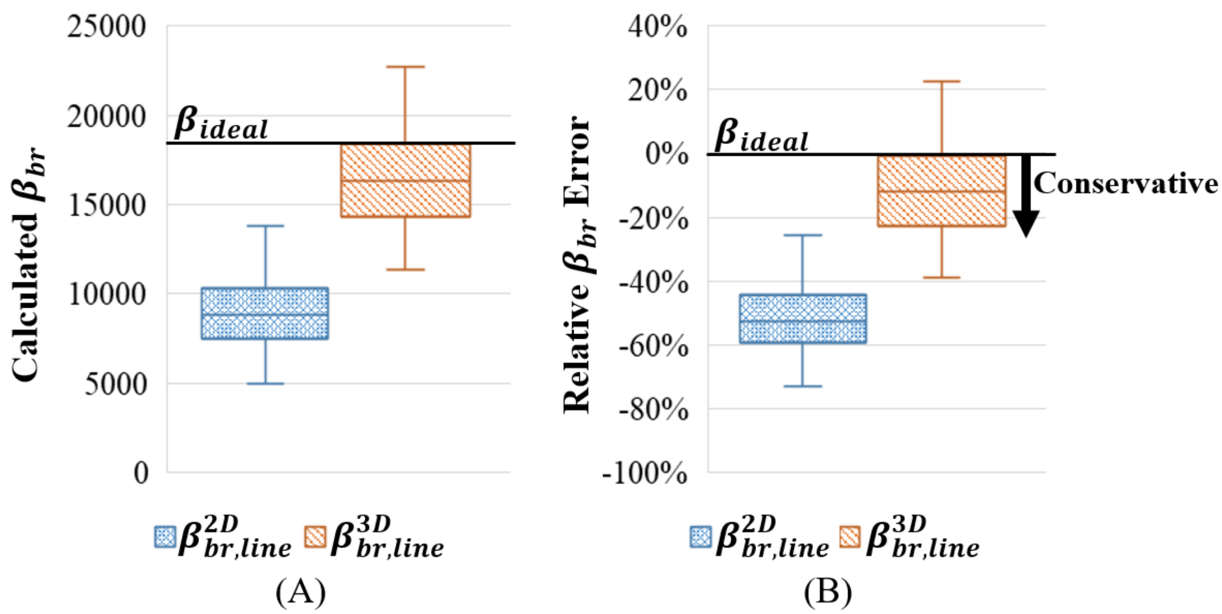

Figure 7-24. Comparison of calculated brace stiffness (A) and relative error (B) between $\beta_{br,line}^{2D}$ and $\beta_{br,line}^{3D}$ for various bracing lines.

7.6. Summary of Design Recommendations

The universal brace stiffness expression, which development was discussed throughout Ch. 7, is shown in Equation 7.37. The values of C_1 and C_2 depend on the bracing type and can be calculated using Table 7-9. C_{strut} depends on the lean-on segments of the bracing line which can be visualized in Figure 7-25. Generally, this only occurs in the case of symmetric bracing lines which are either separated by a central internal leaning bay (cut the bracing line in half) or in a checkerboard format (cut into the repeated brace). C_{strut} can be calculated referencing the cases in Table 7-8 and using Equation 7.37, 7.38, and 7.39.

$$\beta_{br,line} = R \frac{ES^2 h_b^2}{C_1 \frac{L_d^3}{A_d} + [C_{strut} - C_2] \frac{S^3}{A_s}} \tag{7.37}$$

Where:

R is a factor accounting for connection eccentricity (0.65 – during construction when girders are non-composite);

h_b is the height of the brace;

C_{strut} is the strut efficiency term related to the number of girders/braces and leaning girders given in Table 7-8;

C_{ext} is the maximum external leaning girder segment constant given in Equation 7.38;

C_{int} is the maximum internal leaning girder segment constant given in Equation 7.39;

C_1 is a constant term dependent on the bracing type given in Table 7-9;

C_2 is a constant term dependent on the bracing type in Table 7-9;

n_c is the number of cross-frames in the bracing line (or an acceptable idealization);

n_g is the number of girders in the bracing line (or an acceptable idealization);

n_{lean} is the maximum number of grouped leaning girders in the bracing line (or an acceptable idealization) as visualized in Figure 9-1;

A_d is the area of the diagonal braces;

A_s is the area of the top and bottom struts; and,

L_d is the length of a diagonal brace.

Table 7-8. Cases and Values for C_{strut} for $\beta_{br,line}$ Expression

Bracing Line Type	**Case**	**Condition**	$\boldsymbol{C_{strut}}$
Conventional	-	-	$\frac{n_g + 1.75}{2n_g - 0.25}$
Lean-on	External	$C_{ext} > C_{int}$	$[0.70 - 0.05n_c]C_{ext}$
	Internal	$C_{ext} < C_{int}$	$[0.70 - 0.05n_c]C_{int}$
	Mixed	$C_{ext} = C_{int}$	$[0.85 - 0.05n_c]C_{ext}$

$$C_{ext} = (n_{lean,ext} + 1)^2 \tag{7.38}$$

$$C_{int} = \left(n_{lean,int}/2 \ + 1\right)^2 \tag{7.39}$$

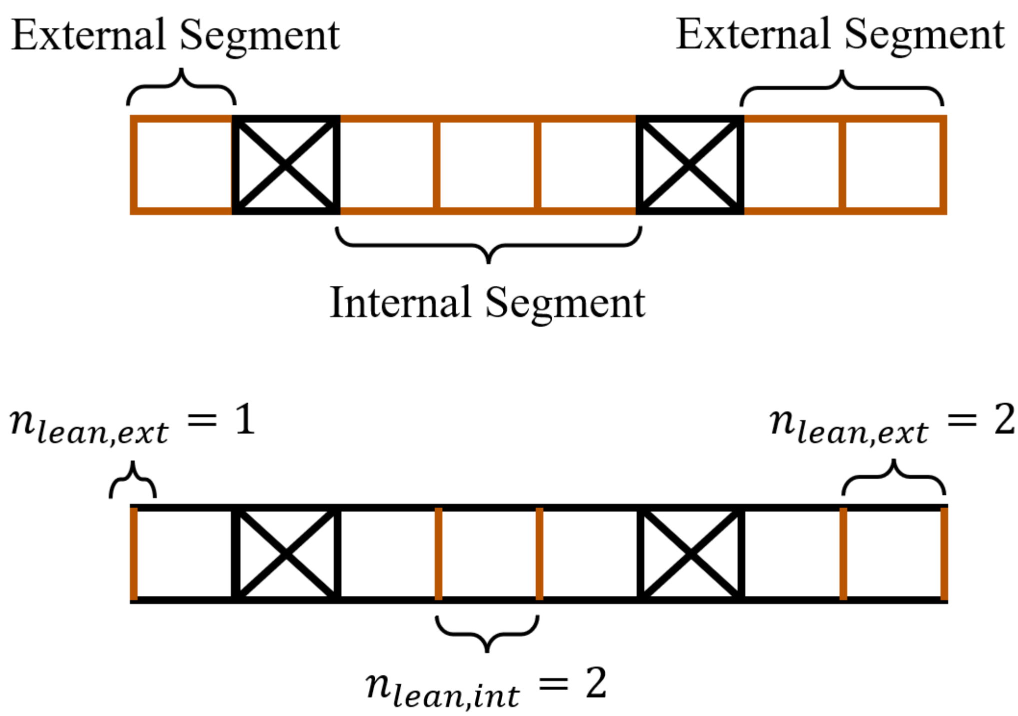

Figure 7-25. Example of Classification of Internal and External Segments and the corresponding n_{lean} Values

Table 7-9. Constants per Brace Type for $\beta_{br,line}$ Expression

Brace Type	C_1	C_2
Z	$\frac{n_g}{n_c}$	0
X	$\frac{n_g}{2n_c}$	$\frac{n_g}{2n_c}$
K	$\frac{2n_g}{n_c}$	$\frac{n_g}{4n_c}$

Chapter 8. Lean-on Bracing Strength Requirements

Effective stability bracing must satisfy both stiffness and strength requirements. The previous chapters focus on the stiffness behavior of the cross-frames. This chapter is directed at the strength requirements for lean-on bracing applications. In general, stability-induced forces are additive to other sources of cross-frame forces (overhang construction, lateral loads on the girders, girder curvature, etc.). This chapter is focused on the forces induced in cross-frames due to stability demands. Updated strength design equations were derived based on the models used to study the stiffness equations for lean-on bracing with the Z-, X-, or K-frames discussed in Chapter 7. The chapter begins by providing an overview of the previously developed expressions and outlines the needs for revisions to the strength requirements. The stability-induced forces are referred to as M_{br}, which represents the restraining torque applied to a single girder by a cross-frame that is providing the stability to the girder system. The stability moment can be idealized as a force couple in the cross-frame such that $Fh_b = M_{br}$, where h_b is the depth of the cross-frame member measured as the distance between the centroidal axis of the top and bottom struts. This is illustrated in Figure 8-1. AASHTO provides expressions for the required brace stiffness and strength and provides expressions that depend on the depth of the brace. For relatively shallow braces compared to the girder depth (brace depth < 75% of girder depth – note the limit was 80% in the 10th edition), AASHTO requires a stiffness that is a multiple of 3 on the ideal stiffness. For deeper braces (brace depth > 75% of girder depth), AASHTO requires a multiple of 2 on the ideal stiffness. The requirements for the multiple of 2 or 3 on the ideal stiffness are based upon limiting the deformation that occurs at the brace to a value of the initial imperfection, $\theta_o = L_b/500h_o$, as outlined in Liu and Helwig (2020) and Han and Helwig (2022) such that the strength requirement is $M_{br} = \beta_T \theta_o$. Because cross-frames are usually nearly full depth (> 75% of the girder depth), the stiffness and therefore based upon the formulation of twice the ideal stiffness and the stability-induced brace strength, M_{br}, is given by Equation 8.1.

$$M_{br} = \frac{2.4L}{nEI_{yeff}}\left(\frac{M_u}{C_b}\right)^2 \frac{L_b}{500h_o} \tag{8.1}$$

Where:

L is the span length

L_b is the length of a diagonal brace member

n is the number of brace lines

I_{yeff} is the effective moment of inertia about the y-axis

E is the modulus of elasticity

h_0 is the distance between flange centroids

M_u is the applied moment

C_b is the moment gradient factor

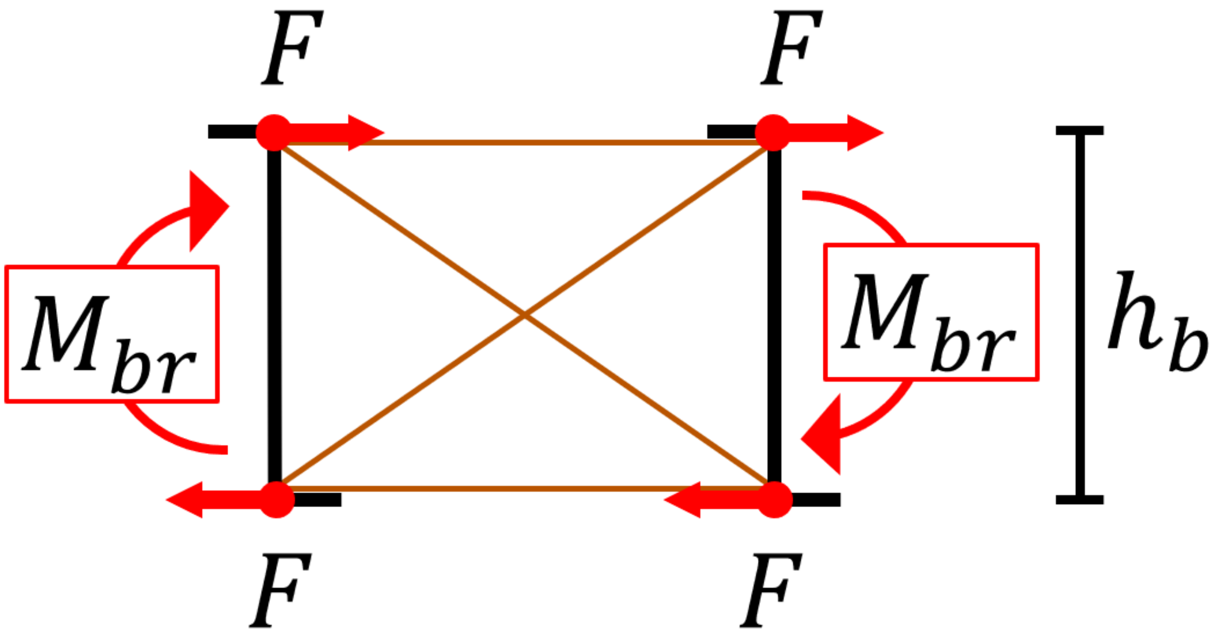

Figure 8-1. Relationship between bracing moment and force couple.

As noted above, the brace moment can be idealized as a force couple and the force component, *F* is calculated using Equation 8.2.

$$F = \frac{M_{br}}{h_b} \qquad 8.2$$

The following subsections outline strength requirements for various cross-frame systems. These expressions are a function of the force couple "F" given by Eqs. 9.1 and 9.2.

8.1. Z-Frame Revised Strength Equations

The previous recommendations that were developed and presented in Helwig and Wang (2003) were outlined in Section 2.5. The previous recommendations were based upon Z-frame systems with very specific layouts of the cross-frames. This section outlines revised expressions. In the revised equations, the coefficients are defined in terms of the same values used in the refined stiffness equation: the number of girders, n_g, the number of cross-frames, n_c, and the maximum number of adjacent lean-on bays, n_{lean}. As noted in the last chapter, lean-on bays that are comprised simply of top and bottom struts provide a load path to lean multiple girders on full cross-frames within the bracing line. As a result – the forces on the cross-frames, in a given bracing line, will vary across the width of the bridge. The maximum forces within a given bracing line are dependent on the controlling segment as shown in Figure 8-2. The forces for the bracing line were determined using the 2D FEM solution developed and validated in Chapter 7.3.

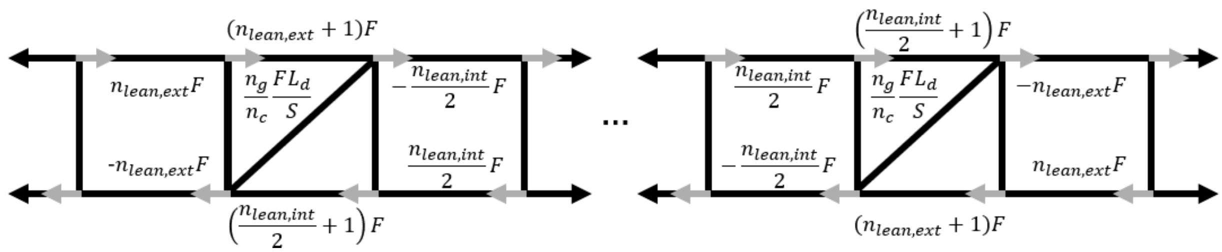

Figure 8-2. Z-Frame Bracing Line Force Distribution

The force requirements for Z-Frames are given by Equations 8.3 and 8.4. These expressions are generally exact relative to a 2D derivation for simple bracing line cases. For more complex bracing lines, such as those discussed in Chapter 7.3, the expressions provide reasonable approximations.

$$F_{d,z} = \frac{n_g}{n_c}\frac{FL_d}{S} \tag{8.3}$$

$$F_{s,z} = \max\begin{cases}(n_{lean,ext}+1)F \\ \left(\frac{n_{lean,int}}{2}+1\right)F\end{cases} \tag{8.4}$$

8.2. X-Frame Revised Strength Equations

Strength equations were developed for X-shaped cross-frames by following a process similar to that used for Z-frames. The generic force distribution for X-frame bracing lines is given in Figure 8-3

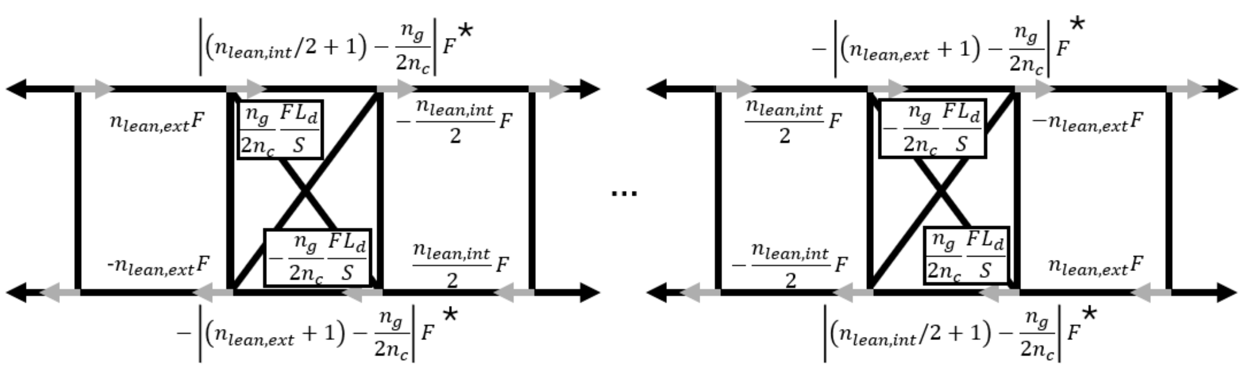

*Depends on which segment controls

Figure 8-3. X-Frame Bracing Line Force Distribution

By taking the maximum force for the diagonals and struts, respectively, the force requirements for X-Frames are given by Equations 8.5 and 8.6. These expressions are generally exact for simple bracing lines and provide reasonable approximations for layouts with increased complexity. Due to the top and bottom strut force distributions becoming discontinuous at the braces, additional equations for the X-frame top and bottom strut are included. These extra expressions generally do not control for lean-on applications. However, they are relevant for the case of conventional bracing ($n_{lean} = 0$).

$$F_{d,x} = \frac{n_g}{2n_c}\frac{FL_d}{S} \tag{8.5}$$

$$F_{s,x} = \max\begin{cases} n_{lean,ext}F \\ \dfrac{n_{lean,int}}{2}F \\ \left|\left(n_{lean,ext}+1\right) - \dfrac{n_g}{2n_c}\right|F \\ \left|\dfrac{\left(n_{lean,int}+1\right)}{2} - \dfrac{n_g}{2n_c}\right|F \end{cases} \tag{8.6}$$

8.3. K-Frame Revised Strength Equations

Similar to the cases demonstrated for Z- and X-frames, the K-frame force distributions depend on the internal and external segments of the system. The force distribution for K-frames is as shown in Figure 8-4.

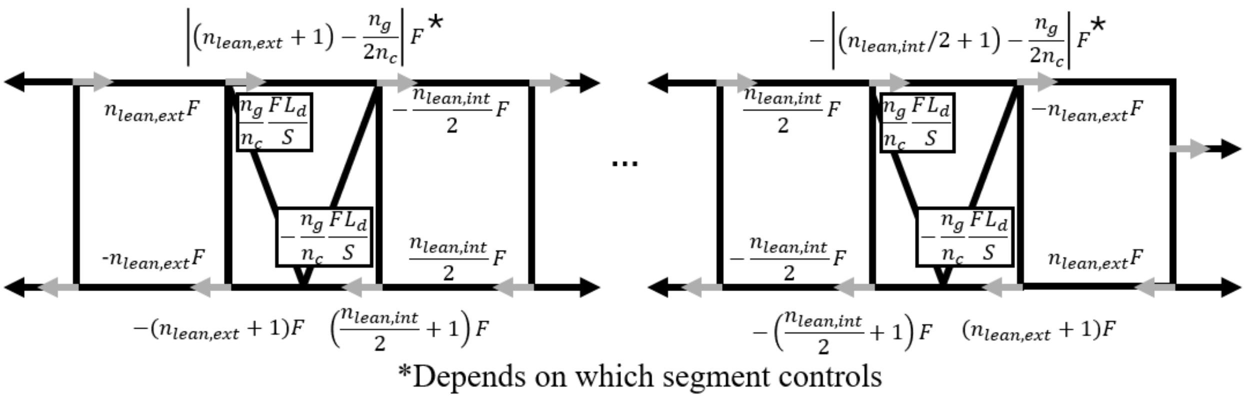

Figure 8-4. K-Frame Bracing Line Force Distribution

The maximum forces for the diagonals and struts in K-frame lines are given by Equations 8.7 and 8.8. Additional equations are given to account for the K-frame top strut forces which tend to only control in conventional cases. These expressions are exact to the 2D derivation for simple cases and provide reasonable approximations for layouts with increased complexity.

$$F_{d,k} = \frac{n_g}{n_c}\frac{FL_d}{S} \tag{8.7}$$

$$F_{s,k} = \max\begin{cases} (n_{lean,ext}+1)F \\ \left(\frac{n_{lean,int}}{2}+1\right)F \\ \left|(n_{lean,ext}+1)-\frac{n_g}{2n_c}\right|F \\ \left|\frac{(n_{lean,int}+1)}{2}-\frac{n_g}{2n_c}\right|F \end{cases} \quad 8.8$$

8.4. Comparison of Brace Forces from 2D FEA, 3D FEA, and Design Expressions

Table 8-1 lists the design expressions for the stability induced forces in the struts and diagonals of the bracing lines. The brace force data for a series of bracing lines with stability induced forces similar to those illustrated in Figure 8-1, are presented in Table 8-2 and Table 8-3. The data was collected from 2D FEA, 3D FEA, and calculations using the design expressions from Table 8-1. Due to the nature of the loading, the results are primarily dependent on the geometry of the braces and the performance of these bracing lines is indicative of the general force behavior observed from the analysis of various bracing lines. In this example, the braces were 96" wide and 60" deep. Overall, the critical brace force of the entire line is used for this comparison as this is what would be referenced in design. The design expressions assume that the forces are uniformly distributed among the diagonal members of the torsional braces. The struts force distribution is also assumed to be uniform in the case of conventional bracing lines, but not in the case of lean-on bracing lines.

Table 8-1. Controlling Brace Forces by Bracing Line and Brace Type

Brace Type	F_d	Brace Line Type	F_s
Z	$\frac{n_g}{n_c}\frac{FL_d}{S}$	Lean-on	$\max\begin{cases}(n_{lean,ext}+1)F \\ \left(\frac{n_{lean,int}}{2}+1\right)F\end{cases}$
		Conventional	F
X	$\frac{n_g}{2n_c}\frac{FL_d}{S}$	Lean-on	$\max\begin{cases}n_{lean,ext}F \\ \frac{n_{lean,int}}{2}F\end{cases}$
		Conventional	$\left|1-\frac{n_g}{2n_c}\right|F$
K	$\frac{n_g}{n_c}\frac{FL_d}{S}$	Lean-on	$\max\begin{cases}(n_{lean,ext}+1)F \\ \left(\frac{n_{lean,int}}{2}+1\right)F\end{cases}$
		Conventional	F

The data in Table 8-2 is from a series of conventional bracing lines with X-frames. In the first column, 1 signifies a bay along the bracing line with an X-frame. Overall, the forces from the expressions are slightly unconservative due to the assumed distribution not matching the actual distribution in the 3D models. This is due to the combination of racking and twist present in the 3D model, discussed in detail in Section 7.4, which alters the force distribution. The critical diagonal members in the 3D models are at X-frame closest to the centroid of the bracing line. In the 2D model, the exterior braces are the most critical. Regarding strut forces, the more braces that are introduced, the more significant the strut forces relative to the diagonals. In the AASHTO 10th Edition (2024), the struts in X-frames are treated as zero-force members due to the single brace assumption.

Table 8-2. Comparison of maximum magnitude of forces given by 2D models, 3D models, and design expressions with X-frames undergoing racking (Conventional Bracing – No Lean-On).

Bracing Line	$\boldsymbol{F_s}$			$\boldsymbol{F_d}$		
	2D FEA (unit load)	**3D FEA (unit load)**	**Eq. 9.8**	**2D FEA (unit load)**	**3D FEA (unit load)**	**Eq. 9.7**
[1]	0	0	0	1.20	1.12	1.18
[1,1]	0.30	0.24	0.25	0.90	0.87	0.88
[1,1,1]	0.30	0.39	0.33	0.90	0.93	0.79
[1,1,1,1]	0.30	0.49	0.38	0.80	0.88	0.73
[1,1,1,1,1]	0.30	0.56	0.40	0.80	0.90	0.71
[1,1,1,1,1,1]	0.30	0.62	0.42	0.80	0.87	0.69

Table 8-3 has data from a series of lean-on bracing lines with X-frames. In the first column, 1 signifies a bay with an X-frame and 0 signifies a bay with only lean-on struts. Overall, the forces from the expressions are conservative as the assumed force distributions are consistent between the 2D and 3D models, and the 3D model does not purely rack.

Table 8-3. Comparison of maximum magnitude of forces given by 2D models, 3D models, and design expressions with X-frames and lean-on undergoing racking.

Bracing Line	$\boldsymbol{F_s}$			$\boldsymbol{F_d}$		
	2D FEA (unit load)	**3D FEA (unit load)**	**Eq. 9.8**	**2D FEA (unit load)**	**3D FEA (unit load)**	**Eq. 9.7**
[1]	0	0	0	1.20	1.12	1.18
[1,0]	1	0.92	1	1.80	1.63	1.77
[1,0,0]	2	1.80	2	2.40	2.12	2.36
[1,0,0,0]	3	2.63	3	2.90	2.59	2.95
[1,0,0,0,0]	4	3.42	4	3.50	3.03	3.54

[1,0,0,0,0,0]	5	4.17	5	4.10	3.45	4.13

After examining the racking case, 2nd order analyses with initial imperfections were conducted with uniform moment loading to further verify the integrity of the design expressions. The geometry and brace member sizes were determined using the stability design expressions, such that the β_T requirement was satisfied. This requirement is based upon an initial twist imperfection of $L_b/500$ and the system having two times the ideal stiffness to control 2nd order amplification effects. A pure sweep imperfection case of a magnitude of L/1000 was also analyzed for comparison purposes. These are illustrated in Figure 8-5 respectively.

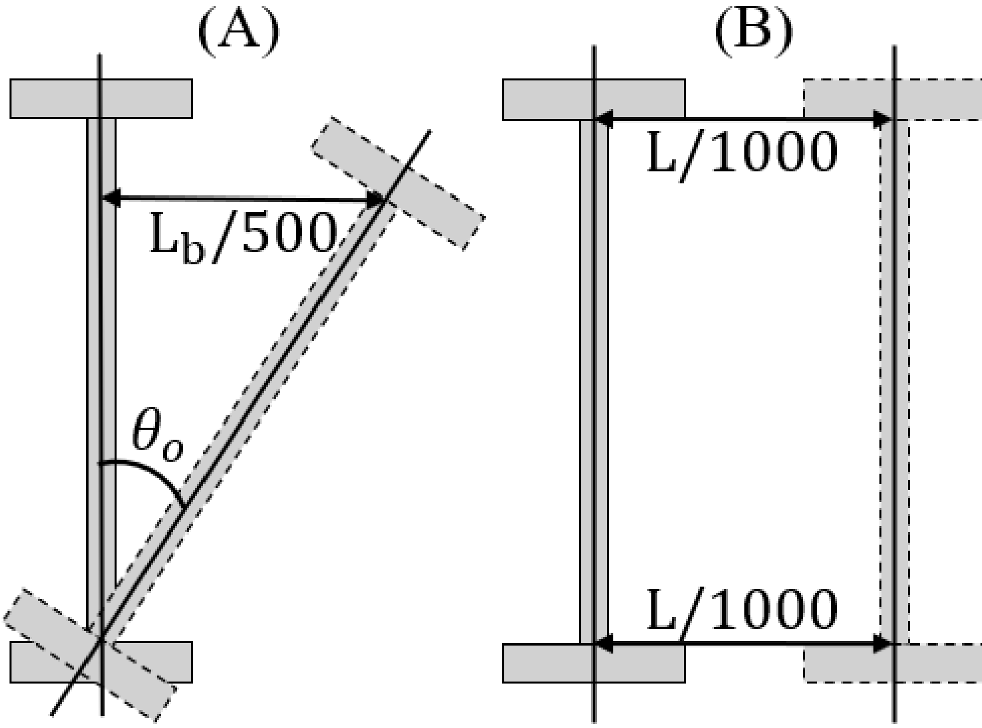

Figure 8-5. Initial Twist (A) and Pure Sweep (B) Imperfections

The results provided in Table 8-4 are indicative of the general behavior of these systems and feature girder systems with a single brace line at midspan. These systems had girder spacings of 10 ft., used girder Section #2 from Figure 6-11, and had girders with a length of 50 ft. Due to the system geometry changing with each additional brace, the brace sizes are adjusted to account for the increase in β_g such that β_T remains consistent. The forces of each bracing member are obtained from the load step prior to the system buckling between the brace points. Less lean-on systems are presented due to the significant loss of β_g ($n_g = 2$ was assumed for the α_x calculation) that occurs when not all bays have a torsional brace along the span due to using a single brace line. This leads to systems that cannot satisfy the stability requirements. Layout behavior regarding brace forces was examined in Section 6.2 and problematic layouts that lead to significant increases, compared to conventional bracing, in brace forces were avoided by the design recommendations.

Table 8-4. Comparison of maximum magnitude of forces given by 3D models and design expressions with X-frames under uniform moment loading.

Bracing Line	A_{br} (in^2)	F_s			F_d		
		3D FEA (pure sweep)	**3D FEA (twist)**	**Eq. 9.8**	**3D FEA (pure sweep)**	**3D FEA (twist)**	**Eq. 9.7**
[1]	5.0	2	3	0	54	68	74
[1,1]	2.5	12	25	17	37	62	56
[1,1,1]	2.0	16	28	22	34	50	50
[1,1,1,1]	1.8	17	29	25	31	44	47
[1,1,1,1,1]	1.7	17	29	27	31	41	45
[1,1,1,1,1,1]	1.6	17	29	28	31	40	43
[1,0]	21.1	29	48	67	49	81	112
[1,0,0]	154.1	53	106	133	61	120	149

Overall, the results in Table 8-4 demonstrate that a twist imperfection is more critical than a pure sweep imperfection as a twist imperfection leads to larger brace forces. This is consistent with the results from Han and Helwig (2020) which examined the impact of various imperfections. Additionally, the design equations achieve reasonable agreement with the FEA results for a twist imperfection. However, as shown by Han and Helwig (2020), the twist imperfection is often more critical than what typically occurs during construction due to fit-up requirements of the torsional braces This means that the expressions will generally be conservative depending on the true imperfection of an actual girder system.

8.5. Summary of Brace Force Equations

A summary of the brace force equations derived from the 2D FEM are provided in Table 8-1. The equations are sorted based on the equations that generally control each brace and bracing line type. Due to these simplifications, Z and K-frames have identical design equations. However, the actual behavior of K-frames is often a combination of Z and X-frames. Additionally, the diagonal terms remain unchanged between lean-on and conventional bracing systems. With the expressions for both stiffness and strength behavior for the lean-on applications established in the last two chapters, the next chapter focuses on the development of design methodologies.

Chapter 9. Refined Design Methodology

The design process for a lean-on bracing system subject to gravity loading during construction is outlined and discussed in this chapter. Two different approaches are developed. The first approach that is covered in Section 9.1 makes use of the stiffness and strength expressions developed in Chapters 7 and 8 and is intended for direct application by design engineers. An alternative approach that makes use of refined FEA modelling is outlined in Section 9.2. The methods employing refined FEA is intended for designers desiring to consider improved accuracy that is tailored for a specific geometry and will likely improve the efficiency compared to the expressions developed for general applications. Numerical design examples for each methodology are included in Chapter 10.

9.1. Equation-Based Lean-On Design Methodology

9.1.1. Determine Girder Layout and Geometry

The design of lean-on bracing systems begin in the same manner as with conventional bracing in that the girders are sized considering in-service conditions as well as the behavior during construction. Girder stability is generally critical during construction. Many bridge applications make use of non-prismatic sections with "stepped flanges" along the unbraced length. The AASHTO 10th edition (2024) Appendix D Article 6.6.3 (Method B) includes an approach that employs effective girder dimensions for considering girder stability that can also be utilized for bracing design. The method of effective section properties was developed and documented in Reichenbach et al. (2020). The fundamental expression is given in Equation 9.1. The equation is given for the effective thickness, the effective flange width can be calculated using the same equation and substituting the plate widths, b, for the thickness, t. Although the flange sizes may have more than two transitions in thickness and width, Reichenbach et al. (2020) showed that basing the behavior on the two smallest plate sizes had good agreement with three-dimensional FEA solutions. Therefore, the effective properties are given as a function of the two smallest dimensions (t_{small} and t_2) and the proportion of the length of the smallest flange size (x_{small}) relative to the total unbraced length.

$$t_{eff} = t_{small}[1 - (1 - x_{small})^2] + t_2(1 - x_{small})^2 \qquad 9.1$$

Where:

t_{eff} is the effective flange thickness;

t_{small} is the smallest flange thickness;

x_{small} is the fraction of the unbraced length with smallest flange thickness; and

t_2 is the second smallest flange thickness.

Each plate in the cross-section is converted to an effective thickness and width. The properties of effective section can then be evaluated for stability calculations (moments of inertia, torsional constants, etc.) by treating the member as an equivalent prismatic section.

9.1.2. Determine Cross-Frame Locations Based on Recommended Layouts

To facilitate good performance of lean-on bracing applications, guidelines were established for the recommended layout as a function of the general bracing application. These recommendations were developed based upon the results primarily outlined in Chapters 6 and 7. The recommended layouts depend on whether the bridge has normal or skewed supports. Lean-on layouts are not generally efficient for systems with less than 4 girders, with the exception of the first CFL (cross-frame line) immediately adjacent to the supports in girder systems with significant support skew when a cross-frame may be omitted to facilitate erection or limit fatigue stresses. However, omitting isolated braces or utilizing isolated cases of top and bottom struts (ie. a lean-on bay) to avoid problematic situations do not generally require modified design procedures compared to traditional systems – but is more likely good design practice. Omitting problematic braces is discussed in more detail in Section 6.4. In general, up to 10% of cross-frames within a span can be replaced with "lean-on bays" without special design approaches compared to traditional systems (no-lean on), provided no more than one lean-on bay is used per bracing line.

The recommended layouts and their appropriate application are shown in Table 9-1 and Table 9-2. Note that a full line of cross-frames is recommended near midspan for all layouts for both systems with normal and skewed supports. The full bracing line near midspan is important to maintain good in-plane girder stiffness, β_g. The bracing line near midspan is the most effective bracing line at improving the in-plane stiffness of the girder system. In addition, the recommended layouts tend to balance the distribution of the "full" cross-frames that have diagonal members to also assist in maintaining good in-plane girder stiffness for the girder system. Further considerations for lean-on layouts are provided in Section 6.4.

While the "X" layout is recommended for bridges with normal supports and systems with more than 5 girders, the Checkerboard layout still provides a reasonable solution for wider girder systems with less than 6 CFLs in a given span. The layouts given in Tables 10-1 and 10-2 only represent general recommendations and a designer may decide to deviate slightly from these recommendations, which will usually maintain a reasonably efficient system and satisfactory behavior. However, in all cases, a full bracing line is recommended near midspan and efforts should be utilized to balance the distribution of the cross-frames to maintain good in-plane stiffness of the girder system.

Table 9-1. Recommended Lean-on Layouts for Bridge Systems with Support Skew ≤ 20°

Layout		# of Girders (# of CFLs)	Notes
ZigZag	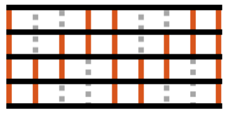	4 or 5 (≥7)	Optional layout for narrow systems
Checkerboard	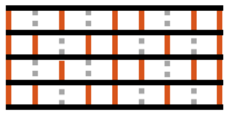	4 or 5 (any number)	Preferred layout for narrow systems
X	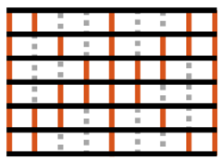	≥6 (≥5)	Preferred layout for wide systems

*CFLs stands for the number of cross-frame lines within the span.

Table 9-2. Recommended Lean-on Layouts for Bridge Systems with Support Skew > 20°

Layout		# of Girders	Notes
Diagonal	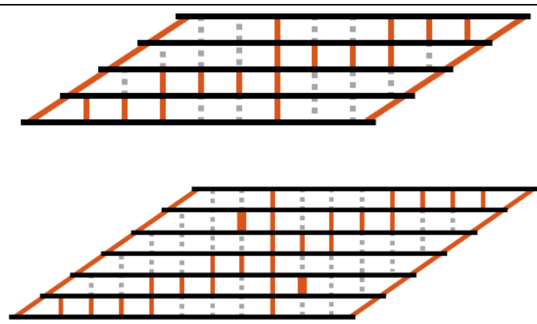	≥4	Preferred layout for skewed systems Additional cross-frames installed as needed to reduce clusters of leaning girders in clear span and also aid in stability during erection
Checker-board	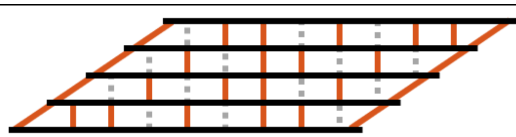	4 or 5	Optional layout for skewed systems

9.1.3. Determine Moment Demands at Each Brace Line

Once the bracing layout has been selected, the moment demand during the critical construction stage for the girders at each brace line should be determined using suitable software or other means of evaluating the design moments. If a simplified approach is preferred, the maximum construction moment of the span can be applied to each bracing line. The maximum construction moment must be checked with the system global buckling capacity as well as the capacity for conventional LTB between the bracing lines, both of which are covered below.

9.1.1.1. Evaluation of System Buckling Resistance

The system buckling mode has been discussed in Sections 2.2.2 and 6.3. The system buckling resistance should be evaluated during erection and construction as appropriate. The mode of buckling often dominates the behavior of narrow girder units and is not significantly impacted by the spacing between cross-frame lines. Therefore, reducing the spacing between the bracing lines will not generally improve the system buckling resistance. Instead, additional bracing or other changes are necessary to improve performance. From the perspective of the system global buckling capacity, the design should begin with assuming no form of warping restraint for which K = 1.0. Sources of warping restraint include top-flange lateral trusses, partial deck pours that allow the concrete to harden, and skewed supports with perpendicular torsional bracing. M_{gs} is given by Equation 9.2 (Fish et al., 2024).

$$M_{gs} = C_{LO} C_{bs} \frac{\pi^2 SE}{(KL)^2} \sqrt{I_y I_x \alpha_x} \qquad 9.2$$

Where:

C_{LO} is 0.95 for bridges with normal supports and 0.85 for bridges with skewed supports;

C_{bs} is 1.1 for simple spans or partially-erected continuous spans, 2.0 for fully erected continuous spans;

S is the girder spacing;

E is the modulus of elasticity of the girders;

K is an effective length factor that accounts for sources of warping restraint;

L is the span length;

I_y is the effective moment of inertia of the girder about the y-axis (minor axis);

I_x is the effective moment of inertia of the girder about the x-axis (major); and

α_x is the system warping stiffness factor given in Equation 9.3, with n_g defined as the number of girders across the bridge width.

$$\alpha_x = \frac{(n_g^2 - 1)}{12} \qquad 9.3$$

AASHTO recommends the maximum factored construction moment, $M_u < 0.7M_{gs}$ to avoid potential issues with 2nd order amplification (Han and Helwig, 2020). The system mode of buckling was discussed previously in Section 2.2.2.

9.1.1.2. Check the Conventional Lateral-Torsional Buckling Moment

The limit state of LTB is defined by the appropriate buckling solution. The AASHTO equations are applicable for singly-symmetric or doubly-symmetric girders. The expression from the main body of the specification neglects the St. Venant term and is intended for sections with slender web. For girders with compact or non-compact webs, the expression from Appendix D should be used, which includes both the St. Venant and Warping terms. Another limit on the maximum moment capacity is the conventional lateral-torsional buckling moment of the braced girder. Therefore, the maximum applied load cannot exceed the M_{cr} capacity given by Equation 9.4 from the AASHTO BDS 10th Edition.

$$M_{cr} = F_{e,eff}S_{xc,eff} = \frac{C_{be}\pi^2 E}{\left(\frac{L_b}{r_{t,eff}}\right)^2}\sqrt{1 + 0.078\frac{J_{eff}}{S_{xc,eff}h_{eff}}\left(\frac{L_b}{r_{teff}}\right)^2}\, S_{xc,eff} \qquad 9.4$$

Where:

$F_{e,eff}$ is the elastic LTB stress for the prismatic unbraced length

C_{be} is the elastic moment-gradient modifier

L_b is the unbraced length of the girder (maximum distance between cross-frame lines)

J_{eff} is the torsional constant of the effective section

$S_{xc,eff}$ is the effective elastic section modulus about the major axis of the section

h_{eff} is the distance between flange centroids of the effective section

I_{cf} is the local strong-axis moment of inertia of the compression flange

r_{teff} is the radius of gyration of the effective section

Check the design moment $M_u < 1.0M_{cr}$

9.1.4. Determine Moment Demands at Each Brace Line

Once the bracing layout with adequate spacing between cross-frame lines is selected to ensure buckling will not control between bracing points, sizing the braces for proper stiffness and strength is necessary. The provisions are based upon the stiffness and strength expressions outlined in the earlier chapters.

9.1.1.3. Determine Required System Stiffness

The required system stiffness is calculated using Equation 9.5.

$$\beta_{T,req} = \frac{2.4L_{b,avg}}{\phi_{sb}EI_{y,eff}}\left(\frac{M_u}{C_b}\right)^2 \qquad 9.5$$

Where:

ϕ_{sb} is the LRFD reduction factor (0.8)

C_b is the moment gradient modifier

$L_{b,avg}$ = average unbraced length within span – L/n_{CFL}

n_{CFL} is the number of bracing lines in the span

$I_{y,eff}$ is the effective moment of inertia about the y-axis

9.1.1.4. Calculate In-Plane Girder Stiffness

Based upon the girder geometry, number of girders, and other factors, the stiffness of the girder system should be evaluated. The stiffness with no top flange truss panels should first be evaluated, for which K = 1.0. Sources of warping restraint include top-flange lateral trusses, partial deck pours that allow the concrete to harden, and skewed supports with perpendicular torsional bracing. The expression for the in-plane girder stiffness is calculated using Equation 9.6 with all variables as defined in Section 9.1.1.1.

$$\beta_g = \frac{C_{LO}^2\pi^4EI_xs^2\alpha_xL_{b,avg}}{(KL)^4} \qquad 9.6$$

9.1.1.5. Evaluation of Cross-Sectional Stiffness

The AASHTO (2024) bracing provisions recommend β_{sec} be taken as infinity for braces deeper than 80% of the web depth, which will often be the case for cross-frame braces. In general, when selecting the cross-frame geometry, the cross-frames should be nearly full depth for maximizing bracing efficiency. In addition, the spacing between the top and bottom lean-on struts should also be nearly full-depth of the girders that are being braced. Cases where more shallow braces are used consist of braces provided by floor beams or other relatively shallow braces. In the event, such braces are used, most designs will not make use of lean-on bracing.

If the braces are shallow compared to the rest of the girder, the stiffness of the cross-section, β_{sec}, may have a significant effect. The provided cross-section stiffness for shallow braces in girders with relatively stocky webs consistent with rolled sections D/t_w < 60 may be calculated using Equation 9.7 (Yura, 2001, Helwig and Yura, 2015).

$$\beta_{sec} = \frac{3.3E}{D}\left(\frac{(1.5D)t_w^3}{12} + \frac{t_s b_s^3}{12}\right) \tag{9.7}$$

Where:

D is the height of the web

t_w is the thickness of the web

t_s is the thickness of the stiffener

b_s is the width of the stiffener

For bridge applications, the webs are generally more slender than rolled sections and the portions above and below the girders contribute to the distortion as a function of the web depth above or below the brace. The portion of the web within the depth of the brace generally does not contribute to the distortion. The corresponding web distortion (β_{sec}) should be evaluated based upon Equations 9.8, 9.9, and 9.10(Yura, 2001):

$$\beta_{sec} = \frac{1}{\frac{1}{\beta_{top}} + \frac{1}{\beta_{bot}}} \tag{9.8}$$

$$\beta_{top} = \frac{3.3E}{h_{top}}\left(\frac{D}{h_{top}}\right)^2 \left(\frac{1.5h_{top}t_w^3}{12} + \frac{t_s b_s^3}{12}\right) \tag{9.9}$$

$$\beta_{bot} = \frac{3.3E}{h_{bot}}\left(\frac{D}{h_{bot}}\right)^2 \left(\frac{1.5h_{bot}t_w^3}{12} + \frac{t_s b_s^3}{12}\right) \tag{9.10}$$

Where:

h_{top} is the height of the web between the top of the brace and the top of the web; and

h_{bot} is the height of the web between the bot of the brace and the bot of the web.

9.1.1.6. Required Brace Stiffness Area

Based upon the required system stiffness given in Equation 9.5 and the other stiffness components, the minimum required stiffness of the brace to ensure a stable system can be determined. The cross-frame stiffness of a given bracing line is represented by Equation 9.11. Note that the term $\beta_{br,line}$, from Chapter 7, has been relabeled $\beta_{br,eff}$ to be consistent with AASHTO. The full solution for C_{strut}, including all terms and permutations, is provided first. This is followed by a simplified approach for calculating C_{strut} that is applicable when the recommended layouts are followed.

$$\beta_{br,eff} = R\frac{ES^2h_b^2}{C_1\frac{L_d^3}{A_d} + [C_{strut} - C_2]\frac{S^3}{A_s}} \qquad 9.11$$

Where:

R is a factor accounting for connection eccentricity (0.65 – during construction when girders are non-composite);

h_b is the height of the brace;

C_{strut} is the strut efficiency term related to the number of girders/braces and leaning girders given in Table 9-3;

C_{ext} is the maximum external leaning girder segment constant given in Equation 9.12;

C_{int} is the maximum internal leaning girder segment constant given in Equation 9.13;

C_1 is a constant term dependent on the bracing type given in Table 9-4;

C_2 is a constant term dependent on the bracing type in Table 9-4;

n_c is the number of cross-frames in the bracing line (or an acceptable idealization);

n_g is the number of girders in the bracing line (or an acceptable idealization);

n_{lean} is the maximum number of grouped leaning girders in the bracing line (or an acceptable idealization) as visualized in Figure 9-1;

A_d is the area of the diagonal braces;

A_s is the area of the top and bottom struts; and,

L_d is the length of a diagonal brace.

Table 9-3. Cases and Values for C_{strut} for $\beta_{br,line}$ Expression

System Type	Case	Condition	C_{strut}
Conventional	-	-	$\frac{n_g + 1.75}{2n_g - 0.25}$
Lean-on	External	$C_{ext} > C_{int}$	$[0.70 - 0.05n_c]C_{ext}$
	Internal	$C_{ext} < C_{int}$	$[0.70 - 0.05n_c]C_{int}$
	Mixed	$C_{ext} = C_{int}$	$[0.85 - 0.05n_c]C_{ext}$

$$C_{ext} = \left(n_{lean,ext} + 1\right)^2 \qquad 9.12$$

$$C_{int} = \left(n_{lean,int}/2 + 1\right)^2 \quad 9.13$$

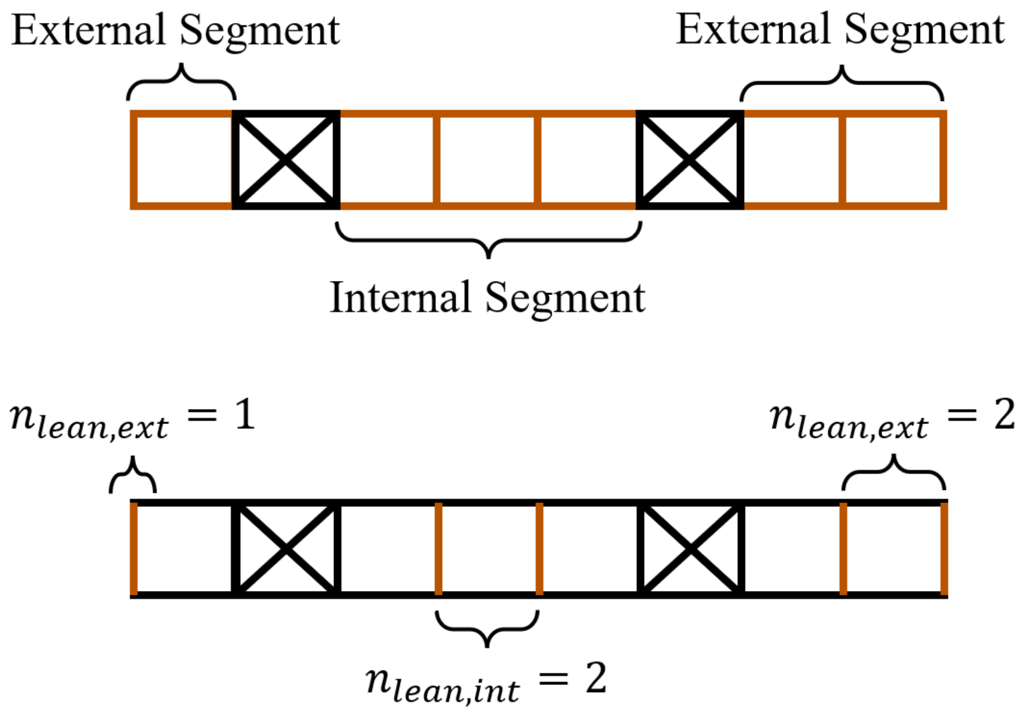

Figure 9-1. Example of Classification of Internal and External Segments and the corresponding n_{lean} Values

Table 9-4. Constants per Brace Type for $\beta_{br,line}$ Expression

Brace Type	C_1	C_2
Z	$\frac{n_g}{n_c}$	0
X	$\frac{n_g}{2n_c}$	$\frac{n_g}{2n_c}$
K	$\frac{2n_g}{n_c}$	$\frac{n_g}{4n_c}$

The total brace stiffness of the system that is provided is given by Equation 9.14.

$$\beta_{T,prov} = \left(\frac{1}{\beta_g} + \frac{1}{\beta_{br,lean}} + \frac{1}{\beta_{sec}}\right)^{-1} \quad 9.14$$

For a given in-plane girder stiffness, a required brace stiffness can be determined with Equation 9.15. A negative value of $\beta_{br,req}$, indicates that one of the stiffness components is less than the required system stiffness ($\beta_{T,req}$) indicating an inadequate system. For example, if β_g is less than $\beta_{T,req}$, the only solution is to focus on improving β_g before the required brace stiffness can be determined. Methods of improving the in-plane brace stiffness can consist of adding top flange lateral bracing panels to improve the K-factor, or the girders must be redesigned with a larger I_x. Alternatively, other solutions such as adding temporary lateral bracing such as guy cables to restrain the girders during construction.

$$\beta_{br,req} = \left(\frac{1}{\beta_{T,req}} - \frac{1}{\beta_g} - \frac{1}{\beta_{sec}}\right)^{-1} \tag{9.15}$$

Once the required brace stiffness is determined, the areas of the struts and diagonals can be selected to provide sufficient stiffness based upon Eq. 10.11. If the same size members are used for the struts and diagonals, the expression can be rearranged to give the minimum required area using the following expression:

$$A_{b,min} = \beta_{br,req} \frac{C_1 L_d^3 + [C_{strut} - C_2] S^3}{E S^2 h^2 R} \tag{9.16}$$

Some simplifications can be made to the recommended layouts so as to ease the design process without compromising accuracy. The zigzag, X, and diagonal layouts are comprised of bracing lines that are unable to be idealized due to their innate asymmetry. Additionally, the mixed and internal cases given in Table 9-3 for C_{strut} will only be relevant to the X layout. Furthermore, the mixed case requires both the internal and external segments to control, which is rare even for the X layout. As such, C_{strut} can be conservatively calculated solely using the external form in Equation 9.12.

When considering the checkerboard layout, configurations can be selected with or without idealization. If the checkerboard system is asymmetric, the previous simplifications apply. If the system is symmetric and does not have a brace in the center, the system must be segmented. However, there are only two possible outcomes: a single brace or a single brace with a single pair of lean-on struts. As summarized in Tables 10-1 and 10-2, the recommended applications for the checkerboard layout are for bracing lines with 4 or 5 bays, which results in relatively few possible permutations.

In essence, the previously discussed procedure simplifies to:

1. Determine n_g, n_{lean}, and n_c from the bracing line (update as needed in step 2).

2. Calculate C_{strut}.

   a. If the bracing line is conventional use $C_{strut} = \frac{n_g+1.75}{2n_g-0.25}$.

   b. If the checkerboard layout is selected, use the values from the following table:

Table 9-5. Checkerboard $\beta_{br,eff}$ reference table.

Bracing Line	n_g	n_c	n_{lean}	C_{strut}
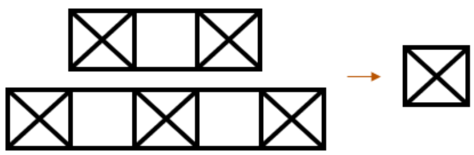	2	1	0	1
	3	1	1	2.6
	4	1	1	2.6
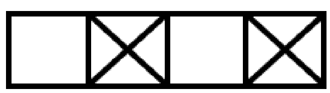	5	2	1	2.4

   c. Otherwise, if the Zigzag or X layouts are used, $C_{strut} = (0.70 - 0.05n_c)(n_{lean} + 1)^2$.

3. Calculate the required brace areas using either Equation 9.11, if the strut and diagonal areas are different, or Equation 9.15. Based upon the required brace areas, actual members sizes can be selected.

9.1.5. Check Strength Requirements

The strength of the brace members in each bracing line must be satisfactory for the force demands.

9.1.1.7. Determine the Total Brace Force Demand in Diagonals and Struts

The moment in the brace, M_{br}, is calculated with Equation 9.17. Note that the constant 2.4 is replaced with 3.6 for shallow braces where the brace depth < 75% of the girder depth.

$$M_{br} = \frac{2.4L_{b,avg}}{EI_{yeff}}\left(\frac{M_u}{C_b}\right)^2\left(\frac{L_b}{500h_o}\right) \qquad 9.17$$

Where:

L is the span length;

L_b unbrace length at the brace under consideration;

$L_{b,avg}$ is the average unbraced length within the span = $L/(n_{CFL}+1)$

n_{CFL} is the number of brace lines;

I_{yeff} is the effective moment of inertia about the y-axis;

E is the modulus of elasticity;

h_0 is the effective depth;

M_u is the applied moment; and,

C_b is the moment gradient factor.

Equation 10.17 provides the brace moment, which for cross-frames is generally idealized as a force couple with a lever arm equal to the height of the bracing, h_b. The magnitude of the force, F is given by the expression:

$$F = \frac{M_{br}}{h_b} \qquad 9.18$$

The forces in the diagonals and the struts are a direction function of the components of the force couple as summarized in Table 9-6 for Z-frames, X-frames, and K-frames.

Table 9-6. Controlling Brace Forces by Brace and Bracing Line Type

Brace Type	$\boldsymbol{F_d}$	**Brace Line Type**	$\boldsymbol{F_s}$
Z	$\frac{n_g}{n_c}\frac{FL_d}{S}$	**Lean-on**	$\max\begin{cases}(n_{lean,ext}+1)F \\ \left(\frac{n_{lean,int}}{2}+1\right)F\end{cases}$
		Conventional	F
X	$\frac{n_g}{2n_c}\frac{FL_d}{S}$	**Lean-on**	$\max\begin{cases}n_{lean,ext}F \\ \frac{n_{lean,int}}{2}F\end{cases}$
		Conventional	$\left\lvert 1-\frac{n_g}{2n_c}\right\rvert F$
K	$\frac{n_g}{n_c}\frac{FL_d}{S}$	**Lean-on**	$\max\begin{cases}(n_{lean,ext}+1)F \\ \left(\frac{n_{lean,int}}{2}+1\right)F\end{cases}$
		Conventional	F

9.1.1.8. Check Strength Capacity

The tensile and compressive capacity of each member should be determined with standard design procedures to ensure adequate behavior.

9.1.1.8.1. Tensile Capacity of Diagonals and Struts

Gross Section Yield

The yield capacity of the bracing members must be greater than the forces calculated using Table 9-6. The yield capacity is given by Equation 9.19.

$$\varphi_y P_{ny} = \varphi_y F_y A_{b,prov} \qquad 9.19$$

Where:

φ_y is the resistance factor for yielding (0.95)

F_y is the yield strength of the brace members

Net Section Fracture

The fracture capacity of the bracing members must be greater than the forces calculated using Table 9-6. The yield capacity is given by Equation 9.20.

$$\varphi\phi_u P_{nu} = \varphi\phi_u F_u A_n R_p U \qquad 9.20$$

Where:

ϕ_u is the resistance factor for fracture (0.8)

R_p is the reduction factor for holes (1.0)

U is the shear lag reduction factor

A_n is the nominal area of the brace member

9.1.1.8.2. Compressive Capacity of Cross-Frame Diagonals and Struts

The compressive resistance of the bracing members must exceed the member forces calculated using Table 9-6. The effective slenderness ratio should be calculated per AASHTO LRFD (2020) Article 6.9.4.4. The factored compressive resistance of a single angle should be calculated using the provisions in AASHTO LRFD Section 6.9.4.1. Alternatively, efficient angle sections can be quickly found in the AISC manual column load tables. For angles, tables are given for concentrically- or eccentrically loaded angles. Eccentric loading is likely a better choice since the angles are generally always loaded through one leg resulting in combined bending and axial stress. The 35% reduction that is applied to the angle stiffness (R= 0.65) in the equations or analysis accounts for impact of the flexibility of the angle as a result of eccentric connection. Using the tables based upon eccentric loading is consistent with the reduction in stiffness. However, arguments can also be made for simply treating the member as an axial loaded member with respect to the buckling capacity since the corresponding angle buckling capacity neglects the end restraint provided by the gusset plates as well as the connection plate.

9.1.1.9. Other Design Requirements

The system must be checked to satisfy all applicable design requirements including but not limited to member and connection designs, varied load conditions, and construction phasing.

9.2. 3D Model-Based Lean-On Bracing Design

The AASHTO Bridge Design Specifications enable designers to use refined analysis techniques to verify design decisions, examine system behavior, and optimize designs. This section is an alternative to the procedures outlined in the last section. Two refined analysis techniques that provide can be used to assess the stability behavior of the system of eigenvalue buckling and nonlinear geometric imperfection analyses. These two analyses are focused on different requirements – both of which are important. Eigenvalue buckling analyses are utilized to determine the controlling buckling mode (local buckling of webs and/or flanges, global lateral torsional buckling, buckling between the brace points, or mixed mode), buckling capacity, and the required brace area for the ideal brace stiffness requirements. Nonlinear geometric imperfection analyses enable designers to evaluate the ability of the bracing system to control excessive deformations and also satisfy the strength requirements. The nonlinear analysis must include a representative imperfection that is consistent with fabrication and erection tolerances.

Stability analyses usually require an iterative procedure of initial sizing, analysis, and potential resizing. From a bracing procedure, a designer conducting a refined analysis will need to begin with an initial configuration for both the girders and bracing. The following sections are based upon the assumption that the initial bridge design has been made using the design methodology outlined in Section 9.1 of this report. The provisions outlined in this section are intended to provide guidance for designers wishing to streamline the layout and design of the bracing systems. The designer should be using analysis software capable of developing refined models of the bridge system that usually consist of shell elements to model the full cross-section of the girders so as to model the flexibility in the cross-section as well as provide a good representation of the connectivity between the braces and the cross-sections. Cross-frames will typically be modelled with line elements; however, the effects of connection eccentricity should be included (Wang, 2013, Battistini et al. 2016, Reichenbach et al. 2021, Park et al. 2022). Designers should use the software to model simple problems and evaluate the behavior with benchmarks to evaluate the capabilities of the software as well as the accuracy of the modelling techniques prior to using the models in design.

9.2.1. General Methodology

Designers should consider the following methodology when verifying or optimizing bridge systems using FEA:

1. Establish a baseline configuration of the bridge components (using equation-based methods outlined in Section 9.1).
2. Create the initial bridge model using guidance in Section 9.2.2. Eigenvalue buckling solutions provide an estimate of the "ideal" brace stiffness, and the equations are often based upon two to three times the ideal stiffness. Therefore, the brace stiffness should be modified accordingly to reflect ideal stiffness conditions. Upon determining the required cross-frame area to achieve ideal conditions – the stiffness should be modified accordingly to satisfy the strength requirements using a non-linear geometrical analysis.
3. Conduct eigenvalue buckling analyses considering the construction conditions and applied loading. The analysis often necessitates an iterative procedure until satisfactory performance is obtained.
    a. Check failure mode (buckled shape) for controlling behavior and eigenvalue for insufficient capacity. The critical stage for most stability and bracing requirements is during casting of the concrete bridge deck; however, some stages during erection may also be critical since the installation of bracing is incomplete at these early stages.
    b. Brace area should be minimized such that the eigenvalues correspond to the required moment demands and the ideal stiffness as noted above. Depending on the cross-frame member geometry, reduction factors (R-factors) may be necessary if members such as angles or WT sections with eccentric connections are utilized. Since most models will make use of line-elements for the cross-frame members, the R-factors account for the reduction in stiffness due to the eccentric connections. Alternatively, "beam" elements can be utilized and the eccentricity can be included in the model (Reichenbach et al. 2021).

c. Once the ideal stiffness has been determined, the stiffness should be increased prior to conducting a non-linear geometrical analysis. A good starting point is to double the cross-frame area which will approximately double the stiffness of the bracing system (Recall that the total system stiffness includes multiple components).

4. Conduct a non-linear geometric analysis on a system with a suitable imperfection using construction conditions until a satisfactory system is obtained. The typical imperfection involves a lateral sweep of the compression flange (Δ_o) equal to L_b /500 with a straight tension flange. Therefore, the resulting imperfection consists of an initial twist, θ_o = $L_b/500D$ (where L_b is the spacing between bracing lines and D is the web depth). This imperfection is illustrated in Figure 9-2. Note that the magnitude of the sweep and twist varies relative to the bracing line being analyzed. A variety of techniques can be used for modelling imperfections. One case is model the imperfection directly by including the imperfect coordinates in the nodes that comprise the girder model. Alternatively, a perfect geometry can be utilized and "notional" or fictitious loads can be used to deform the model in the otherwise "unloaded" state. If notional loads are used, the forces induced in the braces should be accounted for. While there are many possible configurations for the imperfections, the critical cases will usually involve including the imperfection in the unbraced segments in the vicinity of the regions of maximum girder moment. Therefore, these regions can often be predicted based upon a simple knowledge of the moment diagram. Due to the variations in the lean-on bracing configurations, the designer may need to evaluate a few bracing segments near the region of maximum moment.

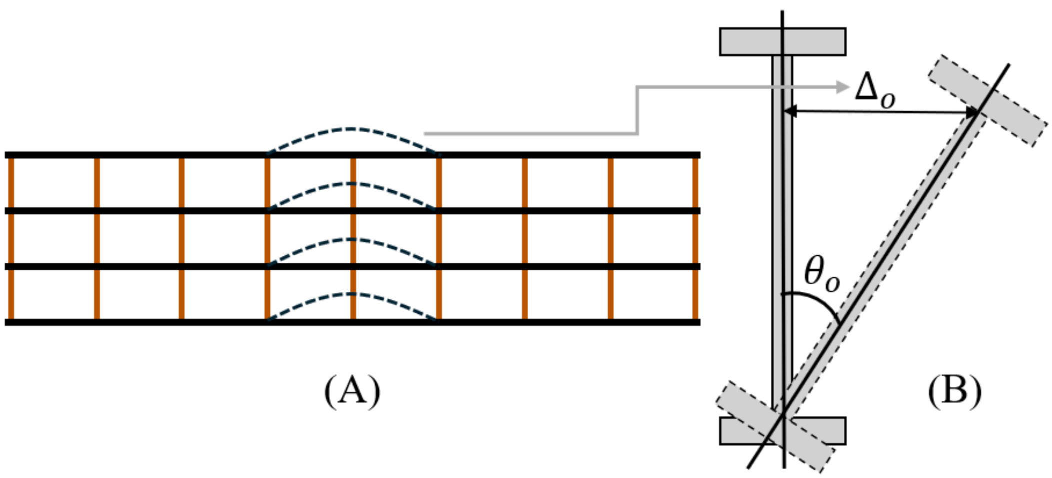

Figure 9-2. Example of the application of a critical brace imperfection in plan (A) and cross-sectional view (B).

a. The design provisions assume that a brace stiffness is provided such that the magnitude of the girder twist, θ, at the maximum load level at the critical construction stage are less than the magnitude of the imperfection, θ_o, (i.e. relative change in girder deformation under load is equal to the initial deformation, considering that $\theta_{tot} = \theta_o + \theta$). In addition, the member stresses/forces should be evaluated relative to the member capacity. The analysis will likely require an iterative procedure until satisfactory proportions are reached. As noted earlier, the critical stage for stability is usually during placement of the concrete bridge deck,

   however, if other construction stages are evaluated – the loads should be consistent with that specific condition.
   b. In some cases, the inclusions of a few panels of a lateral truss may be beneficial to include to improve the efficiency or behaivor of the system. Similar to the discussion of connection eccentric for cross-frames – the same effects impact the behavior of these other bracing members. R-factors can be utilized as noted above, or the braces can be modeled using beam elements that can reflect the eccentricity in the connection (Reichenbach et al. 2021).
   c. If insufficient in any of the requirements, the designer should increase the brace member sizes (to improve brace stiffness) or include lateral trusses (to improve in-plane girder stiffness). The controlling stiffness component can be estimated using the equations relative to the required stiffness.
5. Repeat steps 3 and 4 as necessary with suitable variations in bracing configurations to achieve satisfactory behavior both in terms of deformations and member forces.

The next three sections cover these steps in greater detail.

9.2.2. Preferred 3D Model Settings for Straight Steel I-girder Bridges

The model-based methodology described in subsequent sections can be used for the finite element analysis of straight steel I-girder bridge systems using a finite element model. The modelling that was conducted in the research documented in this report made use of the general purpose FEA program ABAQUS (2022). Elements mentioned below are the designation used in ABAQUS; however, most software will have similar shell or line elements. As noted earlier, the designer should become suitably familiar with the capabilities of the software selected to run such an analysis and evaluate the capabilities using a series of bench marking problems to provide confidence in the accuracy of the software as well as familiarity of the modelling procedures. The focus of the analysis discussed in this section is focused on assessing the stability of the girder system during construction. The model can also be used to evaluate the in-service performance when the girders act composite with the concrete deck and also include a rail/ barrier, however, the focus of this discussion is on the stability during construction. Designers using this methodology should be cognizant of the following settings and modeling assumptions:

1. The deck, barriers, girders, and stiffeners are modeled using shell elements. Linear (S4) or quadratic (S8R) shell elements can be used. The mesh size for shell elements in the discussion presented herein was set to approximately 6 inches. Because the girders were in the elastic range, this mesh provided suitable performance. However, the designer should conduct a mesh sensitivity analysis to ensure proper refinement.
2. Bracing members (cross-frames, diaphragms, or lateral trusses) are modeled using a single linear truss elements (T3D2). Note that the cross-sectional area must be reduced by the appropriate R-factor for truss elements. Alternatively, linear beam elements (B21) can be used with properly offset member properties (accounts for member eccentricity). Bracing models can be fully modeled using shells but require a high degree of modeling skill. As such, shell modeled cross-frames are not recommended due to the complexity of constructing and assembling the modeling components. The complexity does not offer a significant enough advantage in fidelity for most bridge applications.

3. The end nodes on bracing members should be joined to the web-flange juncture nodes for full depth cross-frames. Bracing members not covering a significant proportion (<80%) of the girder depth should be attached solely to the web and flange (if a suitable detail is utilized) at the exact distance.
4. Depending on the stage to be evaluated, components of the concrete deck, rails/parapet or barrier and girder may be coupled via multi-point constraints such as a tie interaction (*for live load performance evaluation*). However, during construction, the steel girder usually supports the entire construction load including the wet concrete. In these cases, multi-point constraints are generally unnecessary. As noted earlier in this report, in some instances a small segment of concrete can be placed and allowed to cure for a few days to provide significant lateral restraint to the top flange, thereby improving the warping resistance. In these cases, the cured concrete can be relied upon to restrain the girders.
5. Mass must be appropriately distributed to all shell elements such that the mass does not overlap and represents the cross-sections. Mass offsets should be used when necessary to ensure proper cross-section representation.
6. During construction, the properties of the steel are limited to the elastic region, which is consistent with the common practice and requirements in the AASHTO BDS (2024).
7. Haunch depth must be considered in the mass distribution (*for live load performance evaluation*). For simplicity, haunch depth can be calculated based upon the thickest top flange.
8. Neglecting rails/parapets/barriers that are often composite with the bridge deck is conservative and recommended (*for live load performance evaluation*). For experimental verification, the barrier should be included and merged with the deck. Any breaks or joints in the bridge curbs and barriers should be modeled by adding gaps in the parts. Many rails/parapets/barriers have a vertically tapered profile. For simplicity, an average thickness can be used for the mass property of barriers. The model can also often approximate the barrier as a rectangular shape from a stiffness perspective with reasonable accuracy if included from a structural perspective.
9. The camber of the girders generally has a negligible impact on the girder behavior and can often be ignored in the model.

9.2.3. Using Eigenvalue Buckling Analysis for Design

To determine the stiffness requirements, the fully-erected bridge girder system should be analyzed using loading that matches the expected load distribution in the appropriate construction condition. The eigenvalue represents an amplifier on the load that is modelled at the stage under consideration. The loading that is applied is often referred to as the “reference load”. Therefore, the designer should be careful in selecting the reference load applied to the model. In most applications, the logical load applied to the model are the expected loads at the stage under consideration, which consists of the self-weight of the girders, concrete deck, screed, and any other suitable loads during the construction condition to be modeled. The eigenvalue therefore represents an amplifier on the applied load. With the applied loading on the bridge elements, some view the eigenvalue as a “factor of safety” against buckling; however, this is not exactly the condition since the true load versus deflection behavior for most stability limit states are nonlinear. However, the eigenvalue does provide an indication of the relative stability of the girder system at the stage under consideration. Questions often arise to the target eigenvalue for a safe condition. If applied loading is the expected load, clearly an eigenvalue below 1.0 represents an unstable condition. However, due to the nonlinear nature of the load-deflection behavior even eigenvalues above 1.0 do not indicate a "safe" condition. If factored loads are utilized, target eigenvalues of 1.5. to 2.0 (or higher) usually indicate safe condition. However, the most clear analysis that defines the stability is a non-linear geometric analysis on an imperfect system since the impact on both girder deformations and brace forces are indicated, which is outlined in Section 9.2.4.

The calculated moment capacity of the system related to the buckling mode can be used to identify insufficiencies with the design. While the eigenvalue represents an amplifier on the applied load leading to an instability, the eigenvector (or buckled shape) that accompanies the eigenvalue represents the mode of buckling that is likely to control the behavior. The analysis may provide several eigenvalues/eigenvectors that represent the different modes of buckling. In general the lowest eigenvalue is of interest in design, since higher eigenvalues will not be reached. However, in many instances, the designer may want to study multiple eigenvalues and the corresponding eigenvector to understand the controlling behavior.

As an example, two possible eigenvalues may exist that are very close to one another. When examining the two eigenvectors (buckled shapes) one may be related to traditional LTB (buckling between the brace points) and the other may be the system or global LTB mode. Understanding these buckled shapes is important for understanding possible methods of improving the behavior. Reducing the spacing between cross-frames can improve traditional LTB, but will have very little impact on the system/global LTB buckling mode.

If the buckling behavior is controlled by the system/global LTB mode of buckling, the dominating stiffness component is likely the in-plane girder stiffness. The reason for this has to do with the relationship of the stiffness components to the ideal stiffness of the bridge girders shown in Figure 9-3.

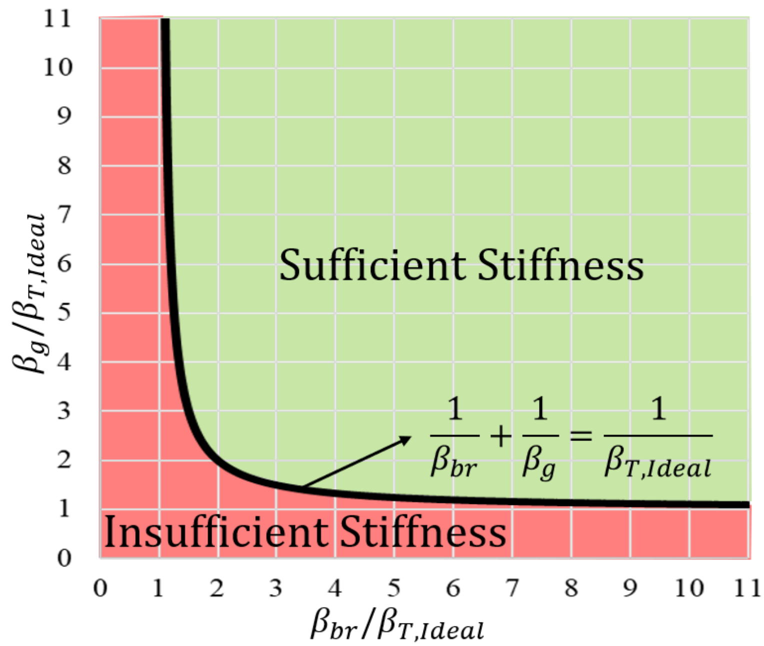

Figure 9-3. Relationship between stiffness components relative to the ideal torsional brace stiffness of the system.

Figure 9-3 highlights how the minimum brace stiffness and in-plane girder stiffness depends on each other relative to the ideal stiffness. If the brace stiffness and in-plane girder stiffness are similar in quantity to each other and the ideal stiffness, the minimum stiffness for both is approximately two times the ideal (~4 times with imperfection). If one component is much greater than the ideal stiffness, for example the in-plane girder stiffness for wide systems or the brace stiffness for conventional systems, the other component requirement reduces to the ideal stiffness. This is relevant for design, since the $2\beta_{ideal}$ design requirement may lead to a design being insufficient due to an individual stiffness component. Since eigenvalue buckling produces results relative to the ideal (β_{ideal}) requirement, eigenvalue buckling alone does not provide a complete picture of the behavior relative to a complete design.

Another example that might occur are local buckling modes. If local buckling of the compression flange or a web controls the behavior, the thickness of the flange or web can be increased or stiffeners may be added. However, even in the case of local buckling controlling – changes in geometry or additional web stiffeners may not be necessary. For example, if the expected loads during construction are utilized in the eigenvalue analysis and flange local buckling is the controlling mode, but the eigenvalue is 5.0 – that local buckling mode is not likely to occur during construction since it will only occur at an approximate (again – linear behavior is assumed) load level 5 times larger than the expected load at that specific stage.

With the previous concepts in mind, designers should find the minimum brace area required to reach the desired moment capacity for the deck pour. As each cross-frame line can be given a brace area based upon the moment loading, a designer should consider the use of an optimization algorithm or methodology to find a minimum brace area. However, utilizing vastly different brace sizes in several regions of the system is highly discouraged since such a system will be costly to fabricate and difficult to erect. In most practical conditions relatively uniform member sizes in the braces should be utilized throughout the bridge. Limiting the number of angle or WT sizes in the bridge will be easier for fabrication.

In addition, designers should note that lean-on layout optimization is nonlinear and changing one cross-frame line may change the stiffness requirement of another. As noted above, in most applications, significant variations in the sizes of bracing members will result in an overly-complicated fabrication and construction procedures. In most applications, the number of different brace areas should be minimized for practicality. Therefore, the term "optimization" should primarily focus on the distribution and layout of braces with a relatively uniform size. A few variations in brace sizes may be acceptable; however, significant variations should be avoided.

Once the system has been optimized, the stiffness equations can be used to check the stiffness values relative to the required stiffness. If the calculated in-plane girder stiffness, using Equation 9.6, tends to dominate the behavior, designers can use lateral trusses or partial deck pours to provide a significant increase to the in-plane girder stiffness. Partial deck pours can conservatively be approximated in eigenvalue buckling by modeling lateral trusses.

For wider systems or skew systems with large in-plane girder stiffnesses relative to the requirement (~10 to 11 times) and full depth cross-frames, doubling the minimum brace area(s) gained from eigenvalue buckling can be used as a rule of thumb.

Designers should also be aware that the skew of supports significantly improves the stability of the system, particularly when bracing lines are oriented perpendicular to the girder lines. The reason for the enhanced stability is that the braces frame between adjacent girders at different points along the length. As a result, the cross-frames provide both torsional and lateral restraint to the system. Using eigenvalue buckling analyses to determine the required cross-frame size in heavily skewed systems can result in impractical members areas indicated from the analysis since the bracing efficiency improves due to the mixture of lateral and torsional bracing from the skewed geometry. Overly-small members sizes will likely result in problems with partially-erected girders. Minimum sizes of cross-frames should be established to avoid impractical systems. For example, in bridges in Texas have historically utilized L4x4x3/8 angle sizes for cross-frames. Angles similar to this size might be a reasonable minimum recommended size.

9.2.4. Using Nonlinear Geometric Imperfection for Design

A nonlinear geometric imperfection analysis is a static analysis that increments loading to determine the stability behavior of structures. For bridge design, a nonlinear geometric imperfection analysis can be used to confirm the moment capacity as well as system stiffness and strength requirements. A common method for conducting these analyses is the Riks Method, which is an arc length method that uses a load proportionality factor to map the bifurcation point and nonlinear response of the structural members. If a designer utilizes a nonlinear geometric analysis for design, a clear understanding of the solution method and load application is important. As noted earlier, for a proper stability assessment, the designer must consider a reasonable imperfection in the model.

The typical critical imperfection that should be used for design of bracing, consists of a lateral sweep of the compression flange of $L_b/500$ as shown in Figure 9-2, while the tension flange remains straight. The imperfections generally consist of a half-sine curve imperfection within the unbraced length (spacing between bracing lines). The imperfection can either be directly modelled by defining the nodal coordinates or make use of "notional loads", which are fictitious loads applied to the structural system in the "unloaded" condition or with zero gravity load. Subsequent load steps with incremental gravity loads are then provided – with the notional loads still applied to the structure. If notional loads are utilized, care should be taken with respect to treatment of the braces. In some instances, the braces can be removed, the notional loads applied to distort the girder, and the braces reinstalled.

If direct modelling of the imperfections is used, designers should manipulate the node coordinates of the mesh with the recommended methods available with the design software that is utilized. Some advanced software that is often used in research applications enable the user to seed the mesh directly with an eigenvalue buckling analysis or direct manipulation of the mesh using a Python macro.

If using the Riks Method, the data extracted from the analysis should be the data at the cross-frame line where the load proportionality factor reaches one (load equal to design load). From here, the designer can use the following to determine if the design is insufficient:

- The analysis diverges or reaches some other limit state before the load proportionality factor reaches one.
- The final displaced shape has an unrealistic magnitude or a magnitude significantly greater than the imperfection applied to the system (i.e. total twist equal to twice initial twist).
- The stresses in the brace members exceed design limits.
- The stresses in the girders exceed design limits.

For straight-girder systems, if the total system displacement ($\theta_{tot} = \theta_o + \theta$) is limited to approximately 2 times the initial imperfection (θ_o) and the stresses are within design limits, the system has sufficient stiffness. For horizontally curved systems – larger girder twists may occur and the designer needs to consider how the twists impact the geometry relative to acceptable tolerances.

If the system is insufficient, the simplest course of action is increasing the areas of the bracing members (maintain proportions if multiple brace sizes are used), especially those in the critical cross-frame lines. If the system stiffness is still insufficient, the designer can either increase the number of cross-frames in a critical cross-frame line or consider adding in lateral trusses near the ends of the spans. Be sure to reference the values calculated using design equations to understand which stiffness component may be controlling to prevent major inefficiencies in the design.

If the system is sufficiently stiff, designers can attempt to reduce the brace member areas to improve system efficiency. Note that designers must check all alterations that reduce the stiffness of the system.

Chapter 10. Design Examples

10.1. Design Example 1

An application of lean-on bracing for a nonskew, single span, five-girder bridge and checkerboard cross-frame layout is illustrated in this example. The girder sections are shown in Figure 10-1.

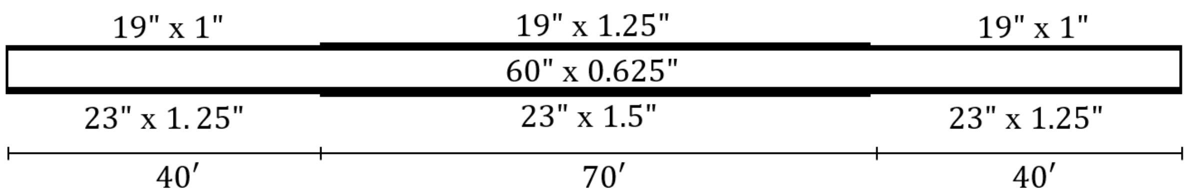

Figure 10-1. Example 1 Girder Section

10.1.1. Determine Girder Layout and Geometry

Span Information

$n_g = 6$	Number of girders
$S = 8\ ft$	Girder spacing
$L = 150\ ft$	Span length
$E = 29{,}000\ ksi$	Modulus of elasticity
$\theta = 0°$	Skew angle

Web Information

$t_w = 0.625\ in$	Thickness of girder web
$D = 60\ in$	Height of girder web

Bottom Flange Information

$b_{bf} = 23\ in$	Width of bottom flange
$t_{bsmall} = 1.25\ in$	Thickness of thinnest section of girder flange
$t_{b2} = 1.5\ in$	Thickness of second thinnest section of girder flange
$x_{bsmall} = \frac{40\ ft + 40ft}{150\ ft} = 0.533$	Fraction of span with t_{bsmall}

Top Flange Information

$b_{tf} = 19\ in$	Width of top flange
$t_{tsmall} = 1\ in$	Thickness of thinnest section of girder flange
$t_{t2} = 1.25\ in$	Thickness of second thinnest section of girder flange
$x_{tsmall} = \frac{40\ ft+40\ ft}{150\ ft} = 0.53$	Fraction of span with t_{bsmall}

Calculated Girder Section Properties, as defined in AASHTO LRFD BDS

$$t_{beff} = t_{bsmall}(1-(1-x_{bsmall})^2) + t_{b2}(1-x_{bsmall})^2 = 1.30\ in$$

$$t_{teff} = t_{tsmall}(1-(1-x_{tsmall})^2) + t_{t2}(1-x_{tsmall})^2 = 1.11\ in$$

Bottom Flange	Top Flange	Web
$y_{bf} = \frac{t_{beff}}{2} = 0.7\ in$	$y_{tf} = \frac{t_{teff}}{2} = 61.7\ in$	$y_w = t_{beff} + \frac{h_w}{2} = 31.3\ in$
$A_{bf} = b_{bf}t_{beff} = 30\ in^2$	$A_{tf} = b_{tf}t_{teff} = 21.1\ in^2$	$A_w = b_w t_w = 37.5\ in^2$
$I_{xbf} = \frac{b_{bf}t_{beff}^3}{12} = 4.3\ in^4$	$I_{xtf} = \frac{b_{tf}t_{teff}^3}{12} = 2.2\ in^4$	$I_{xw} = \frac{b_w t_w^3}{12} = 11250\ in^4$
$I_{ybf} = \frac{t_{beff}b_{bf}^3}{12} = 1323\ in^4$	$I_{ytf} = \frac{t_{teff}b_{tf}^3}{12} = 633.8\ in^4$	$I_{yw} = \frac{t_w b_w^3}{12} = 1.2\ in^4$

$$d_{bot} = \frac{A_{bf}y_{bf}+A_w y_w+A_{tf}y_{tf}}{A_{bf}+A_w+A_{tf}} = 28.1\ in$$

$$d_{top} = t_{beff} + h_w + t_{teff} - d_{bot} = 34.3\ in$$

$$I_x = I_{xbf} + A_{bf}(d_{bot}-y_{bf})^2 + I_{xw} + A_w(d_{bot}-y_w)^2 + I_{xtf} + A_{tf}(d_{bot}-y_{tf})^2 = 57{,}978.5\ in^4$$

$$I_y = I_{ybf} + I_{yw} + I_{ytf} = 1957.6\ in^4$$

$$c = d_{top} - \frac{t_{eff}}{2} = 33.7\ in$$

$$t = d_{bot} - y_{bf} = 27.5\ in$$

$$I_{yeff} = I_{ytf} + \left(\frac{t}{c}\right) I_{ybf} = 1712\ in^4$$

$$J = \frac{b_{bf}t_{beff}^3}{3} + \frac{b_{tf}t_{teff}^3}{3} + \frac{h_w t_w^3}{3} = 31\ in^4$$

10.1.2. Determine Cross-Frame Locations Based on Recommended Layouts

As a starting point for configuring the bracing layout, Tables 9-1 and 9-2 provide guidance in the recommended lean-on layout. Because the bridge is a relatively short (<6 cross-frame lines) nonskewed system with five girders, the checkerboard is an acceptable cross-frame layout. In Figure 10-2 and following calculations, CFL represents "cross-frame line," open rectangles represent lean-on struts, and shaded rectangles represent cross-frames. A cross-section view of each bracing line is shown in Figure 10-3.

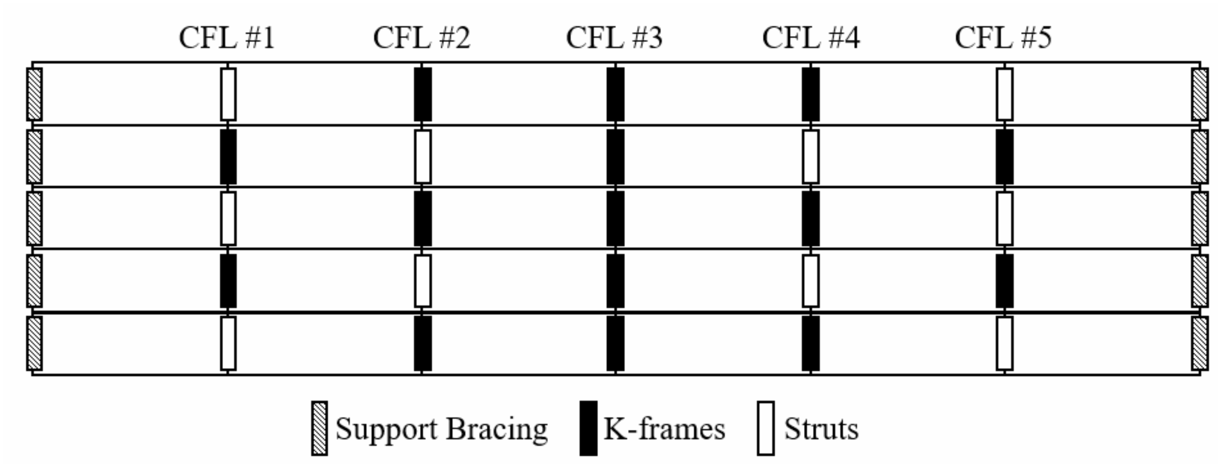

Figure 10-2. Example 1 Cross-Frame Layout

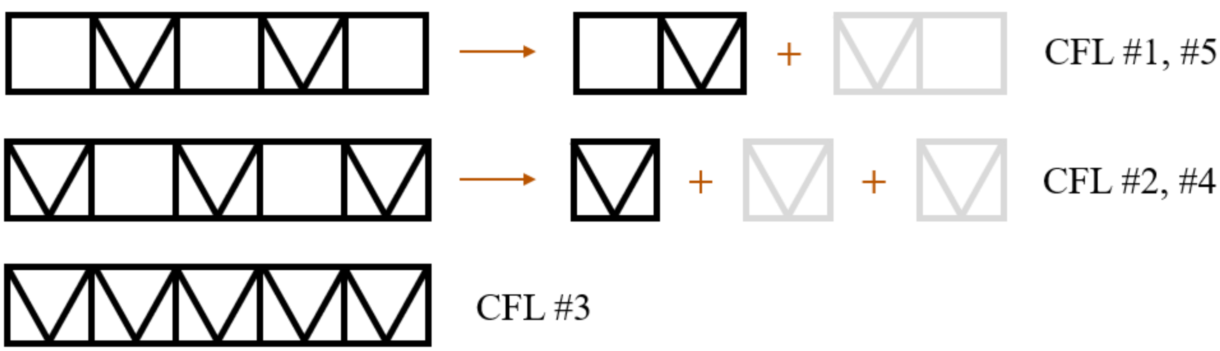

Figure 10-3. Example 1 Bracing Line Cross-sectional View

Connection Plate Information

$b_s = 9\ in$	Width of connection plate
$h_i = 5\ in$	Distance from top of cross-frame to bottom of top flange
$t_s = 0.5\ in$	Thickness of connection plate
Min Lap = 5 in	Minimum overlap of brace member and connection plate

Brace Information

$n_{CFL} = 5$	Number of intermediate cross-frame lines in the span
$L_b = \frac{L}{n_{CFL}+1} = 25\ ft$	Unbraced length (cross-frame spacing)
$h_b = h_w - 2h_i = 50\ in$	Height of cross-frame
$L_s = S - 2(b_s - \text{Min Lap}) = 88\ in$	Length of top and bottom struts
$L_d = \sqrt{\left(\frac{L_s}{2}\right)^2 + h_b^2} = 66.6\ in$	Length of diagonal braces

10.1.3. Check Moment Demands

10.1.3.1. Calculate the Moment Loading at Each Cross-Frame Line

Loading Information

$\rho_{concrete} = 150\frac{lb}{ft^3}$	Density of concrete
$t_{deck} = 8.5\ in$	Thickness of deck
$\rho_{steel} = 490\frac{lb}{ft^3}$	Density of steel
$DL_{form} = 5\frac{lb}{ft^2}$	Load of formwork
$w_{deck} = \rho_{concrete} * t_{deck} * S = 850\frac{lb}{ft}$	Self-weight of wet concrete
$w_{girder} = (A_{bf} + A_{tf} + A_w) * \rho_{steel} = 301\frac{lb}{ft}$	Self-weight of girder
$w_{form} = DL_{form} * S = 40\frac{lb}{ft}$	Self-weight of formwork
$w_{CLL} = 150\frac{lb}{ft}$	Construction live load
$w_{total} = 1.25(w_{deck} + w_{girder} + w_{form}) + 1.5w_{CLL} = 1714\frac{lb}{ft}$	Total line load (factored)
$w_{total} = 1.4(w_{deck} + w_{girder} + w_{form} + w_{CLL}) = 1878\frac{lb}{ft}$	Total line load (factored)

The maximum moment for a single span with uniformly distributed load is:

$$M_u = \frac{w_{total}L^2}{8} = 5{,}282\ kip - ft$$

The moment at each cross-frame line for a uniformly distributed load is:

$$M = \frac{w_{total}x(L-x)}{2}\ [kip - ft]$$

Bracing Line	$\boldsymbol{x}$	$\boldsymbol{M_u}$
#1/5	$25\ ft$	$2{,}934\ kip - ft$
#2/4	$50\ ft$	$4{,}695\ kip - ft$
#3	$75\ ft$	$5{,}282\ kip - ft$

10.1.3.2. Check System Global Buckling Moment

$C_{LO} = 0.95$	Lean-On Factor - 0.95 for bridges with less than 30° skew and 0.85 greater than or equal to 30° skew
$C_{bs} = 1.1$	1.1 for single span, 2.0 for continuous span
$\alpha_x = \frac{(n_g^2-1)}{12} = 2.917$	System warping stiffness factor
$K = 1.0$	1.0 since there are no forms of end warping restraint

$$0.7M_{gs} = 0.7C_{LO}C_{BS}\frac{\pi^2 SE}{(KL)^2}\sqrt{I_y I_x \alpha_x} = 9{,}406\ kip - ft$$

$M_u < 0.7M_{gs}$ OK

NOTE: In the event $M_u > 0.7M_{gs}$, no amount of cross-frames will be satisfactory. The girders must be resized or spacing increased to resist system mode of buckling.

10.1.3.3. Check Conventional Lateral-Torsional Buckling Moment

$C_b = 1$	LTB moment gradient factor
$C_w = \frac{I_{y,eff}}{2} \cdot \frac{h_w^2}{2} = 570{,}440\ in^6$	Torsional warping constant
$G = 11{,}600\ ksi$	Shear modulus

$$M_0 = C_b\frac{\pi}{L_b}\sqrt{EI_{yeff}GJ + \frac{\pi^2E^2I_{yeff}C_w}{L_b^2}} = 9{,}055\ kip - ft$$

$M_u < M_0$ OK

10.1.4. Determine Minimum Brace Area for Each Bracing Line

10.1.4.1. Determine Required System Stiffness at Each Bracing Line

$\phi_{sb} = 0.8$ Resistance factor for stability bracing

The required stiffness at each bracing line is given by:

$$\beta_{T,req} = \frac{2.4 L_{b,avg}}{\phi_{sb} E I_{y,eff}} \left(\frac{M_u}{C_b}\right)^2$$

Bracing Line	$\boldsymbol{\beta_{T,req}}$
#1/5	$22{,}472 \frac{kip\text{–}in}{rad}$
#2/4	$57{,}529 \frac{kip\text{–}in}{rad}$
#3	$72{,}811 \frac{kip\text{–}in}{rad}$

10.1.4.2. Calculate In-Plane girder Stiffness (Constant)

$$\beta_g = \frac{C_{LO}^2 \pi^4 E I_x s^2 \alpha_x L_{b,avg}}{(KL)^4} = 113{,}546 \frac{kip - in}{rad}$$

$\beta_g > \beta_{Treq}$ OK

10.1.4.3. Calculate Cross-Sectional Stiffness (Constant)

The cross-frames are greater than 80% of the web depth, so the cross-sectional stiffness may be taken as infinite.

$$\beta_{sec} = \infty \frac{kip - in}{rad}$$

$\beta_g > \beta_{sec}$ OK

10.1.4.4. Use the Brace Stiffness Equation to Determine the Minimum Brace Area for Each Line

$R = 0.65$ Connection eccentricity factor

Use the following equations to determine the minimum area requirement for each bracing line with K-frames:

$$\beta_{br,req} = \left(\frac{1}{\beta_{T,req}} - \frac{1}{\beta_g} - \frac{1}{\beta_{sec}}\right)$$

$$A_{br,req} = \beta_{br,req} \frac{\frac{2n_g}{n_c} L_d^3 + \left(C_{strut} - \frac{n_g}{4n_c}\right) S^3}{ES^2 h_b^2 R}$$

For conventional lines:

$$C_{strut} = \frac{n_g + 1.75}{2n_g - 0.25}$$

For lean-on bracing lines:

$$C_{strut} = (0.7 - 0.05n_c)(n_{lean} + 1)^2$$

NOTE: You must idealize the bracing line when possible! The expression fit for C_{strut} does not apply to bracings lines that are able to be idealized.

Bracing Line	**Idealize?**	**Conventional?**	n_g	n_c	n_{lean}	C_{strut}	$\beta_{br,req}$	$A_{br,req}$
#1/5	Yes	No	3	1	1	2.6	$28{,}018 \frac{kip-in}{rad}$	$0.22\ in^2$
#2/4	Yes	Yes	2	1	0	1	$116{,}613 \frac{kip-in}{rad}$	$0.44\ in^2$
#3	No	Yes	6	5	0	0.66	$202{,}953 \frac{kip-in}{rad}$	$0.48\ in^2$

The minimum brace area is dictated by CFL3. $A_{br,req} = 0.48\ in^2$.

10.1.4.5. Select Brace Member Size

A L4x4x3/8 angle (minimum TxDOT standard size) is selected for all brace lines, resulting in $A_{br,prov} = 2.86\ in^2$.

10.1.5. Check Strength Requirements for Each Bracing Line

10.1.5.1. Determine the Force Demand in Diagonals and Struts for Each Cross-Frame Line

The maximum brace moment and corresponding brace force of each bracing line is calculated using the following expressions:

$$M_{br} = \frac{2.4L_{b,avg}}{EI_{yeff}} \left(\frac{M_u}{C_b}\right)^2 \left(\frac{L_b}{500h_o}\right)$$

$$F_{br,max} = \frac{M_{br}}{h_b}$$

The force in the struts and diagonals is dependent on n_c, n_g, and n_{lean}, so the force will need to be calculated for each bracing line. The force equations for K-frames are:

Brace Type	$\boldsymbol{F_d}$	Brace Line Type	$\boldsymbol{F_s}$
K	$\frac{n_g}{n_c}\frac{FL_d}{S}$	**Lean-on**	$\max\begin{cases}(n_{lean,ext}+1)F \\ \left(\frac{n_{lean,int}}{2}+1\right)F\end{cases}$
		Conventional	F

Bracing Line	Idealize?	Conventional?	$\boldsymbol{n_g}$	$\boldsymbol{n_c}$	$\boldsymbol{n_{lean}}$	$\boldsymbol{F_{br,max}}$	$\boldsymbol{F_d}$	$\boldsymbol{F_s}$
#1/5	Yes	No	3	1	1	3.5 kip	7.3 kip	7.0 kip
#2/4	Yes	Yes	2	1	0	9.0 kip	12.5 kip	9.0 kip
#3	No	Yes	6	5	0	11.4 kip	9.5 kip	11.4 kip

The maximum force in the diagonals is $F_d = 12.5\ kip$ and the maximum force in the struts is $F_s = 11.4\ kip$.

10.1.5.2. Check Strength Capacity

Brace Angle Information

$F_u = 70\ ksi$	Tensile strength
$F_y = 50\ ksi$	Yield strength
$\bar{x} = 1.23\ in$	Centroid of angle
$r_x = 1.23\ in$	Radius of gyration
$t_{leg} = 0.375\ in$	Thickness of leg

Brace Connection Information

$d_b = 1\ in$	Bolt diameter
$F_{ub} = 120\ ksi$	Tensile strength of bolt
$F_{yb} = 70\ ksi$	Yield strength of bolt
$L_{bolt} = 2\ in$	Bolt spacing
$A_b = \frac{\pi}{4}d_b^2 = 0.785\ in$	Area of bolt

10.1.5.2.1. Tensile Capacity of Diagonals and Struts

Gross Section Yield

$\phi_y = 0.95$ Resistance factor for yielding

$\phi_y P_{ny} = \varphi_y F_y A_{b,prov} = 135.9\ kip$

$\phi_y P_{ny} > F_d$ OK, $\phi_y P_{ny} > F_s$ OK

Net Section Fracture

$\phi_u = 0.8$ Resistance factor for fracture

$R_p = 1.0$ Reduction factor for holes

$U = 1 - \frac{\bar{x}}{L_{bolt}} = 0.4$ Shear lag reduction factor

$A_n = A_{b,prov} - 1\left(d_b + \frac{1}{8}\ in\right) t_{leg} = 2.4\ in^2$ Nominal area of brace member

$\phi_u P_{nu} = \varphi_u F_u A_n R_p U = 59.4\ kip$

$\phi_u P_{nu} > F_d$ OK, $\phi_u P_{nu} > F_s$ OK

10.1.5.2.2. Compressive Capacity of Cross-Frame Diagonals

As per AASHTO LRFD Article 6.9.4.4:

$$\frac{L_d}{r_x} = 54.1$$

Hence, effective slenderness ratio is calculated as:

AASHTO LRFD Eqn. 6.9.4.4-1:

$$\left(\frac{KL_d}{r_x}\right)_{eff} = 72 + 0.75\frac{L_d}{r_x} = 112.6$$

Elastic critical buckling resistance of single angle is calculated as:

AASHTO LRFD Eqn. 6.9.4.1.2-1:

$$P_e = \frac{\pi^2 E}{\left(\frac{KL_d}{r_x}\right)_{eff}} A_g = 64.5\ kip$$

Nominal yield resistance:

AASHTO LRFD Article 6.9.4.1

$$P_0 = F_y A_{b,prov} = 143\ kip$$

As per AASHTO LRFD Article 6.9.4.1:

$$\frac{P_o}{P_e} = 2.2 \leq 2.25$$

Hence, nominal compressive resistance of a single angle is:

AASHTO LRFD Eqn. 6.9.4.1-2

$$P_n = \left[0.658^{\frac{P_0}{P_e}}\right] P_o = 56.6\ kip$$

Factored compressive resistance of a single angle is:

$\phi_c = 0.95$ Resistance factor for compression

$$\phi_c P_n = 53.7\ kip > F_d\ OK$$

10.1.5.2.3. Compressive Capacity of Top and Bottom Struts

As per AASHTO LRFD Article 6.9.4.4:

$$\frac{L_s}{r_x} = 71.5$$

Hence, effective slenderness ratio is calculated as:

AASHTO LRFD Eqn. 6.9.4.4-1:

$$\left(\frac{KL_s}{r_x}\right)_{eff} = 72 + 0.75\frac{L_s}{r_x} = 125.7$$

Elastic critical buckling resistance of single angle is calculated as:

AASHTO LRFD Eqn. 6.9.4.1.2-1:

$$P_e = \frac{\pi^2 E}{\left(\frac{KL_s}{r_x}\right)_{eff}} A_g = 51.8\ kip$$

Nominal yield resistance:

AASHTO LRFD Article 6.9.4.1

$$P_0 = F_y A_{b,prov} = 143.0\ kip$$

As per AASHTO LRFD Article 6.9.4.1:

$$\frac{P_o}{P_e} = 2.8 > 2.25$$

Hence, nominal compressive resistance of a single angle is:

AASHTO LRFD Eqn. 6.9.4.1-2

$$P_n = 0.877 P_e = 45.5\ kip$$

Factored compressive resistance of a single angle is:

$$\phi_c P_n = 43.2\ kip > F_s\ OK$$

10.1.5.2.4. Limiting Slenderness Ratio Check

$$\frac{KL_s}{r_x} = 125.7 < 140\ OK$$

10.1.6. FEA Check of Moment Capacity and Stiffness (Optional)

10.1.6.1. Conduct Eigenvalue Buckling Analysis of Bridge FEA Model and Examine Results

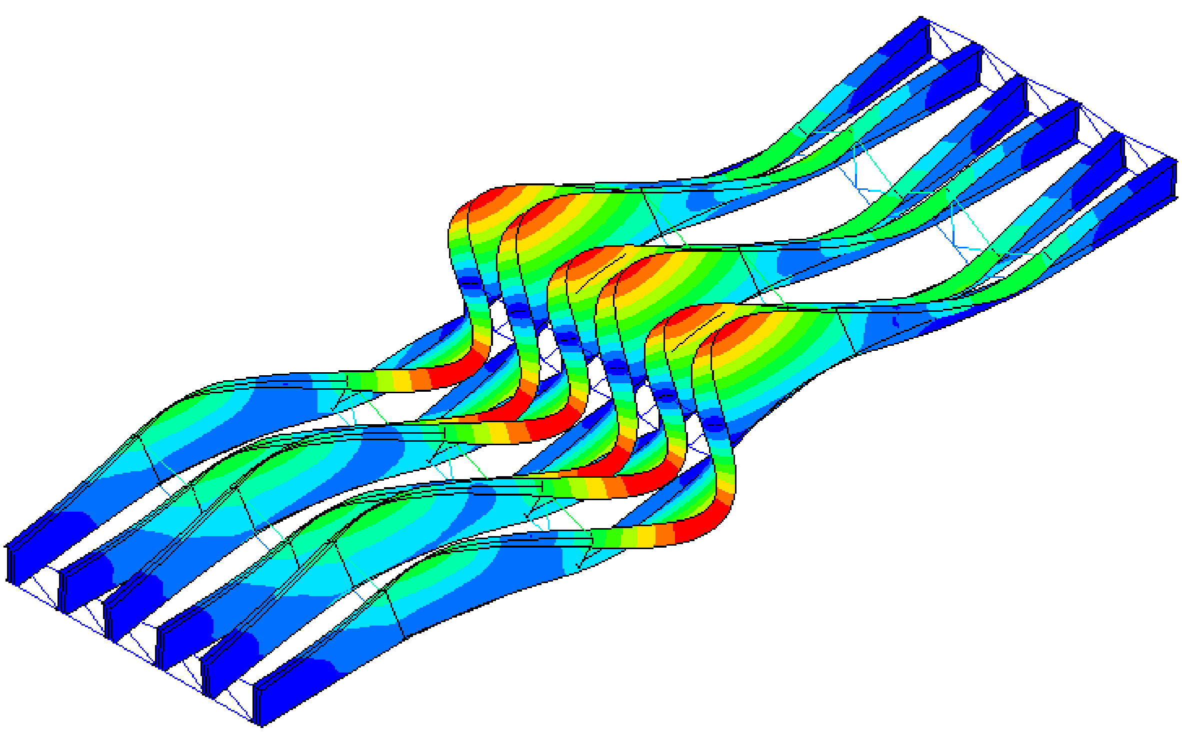

Figure 10-4. Buckled shape of Design Example #1 Obtained from Eigenvalue Buckling Analysis

The loading applied to the model is a factored gravity (self-weight) load and a factored lump sum pressure of the deck self-weight, formwork self-weight, and construction live load on the top flanges of the girders. The buckled shape can be seen in Figure 10-4 and the eigenvalue result is as follows:

$$\lambda = 2.31 M_u > 1.0 M_u \ OK$$

The eigenvalue appears reasonable based upon the ratio between the calculated M_u and M_o (1.71) and the conservative nature of the averaged section values.

For K-frames, beam elements must be used for the bottom struts to prevent a rigid buckling mode at the bottom strut diagonal juncture. Generalized beam sections with reduced areas can be used to account for moment eccentricity or the section offset from the element.

10.1.6.2. Conduct Nonlinear Geometric Imperfection analysis of Bridge FEA Model and Examine Results

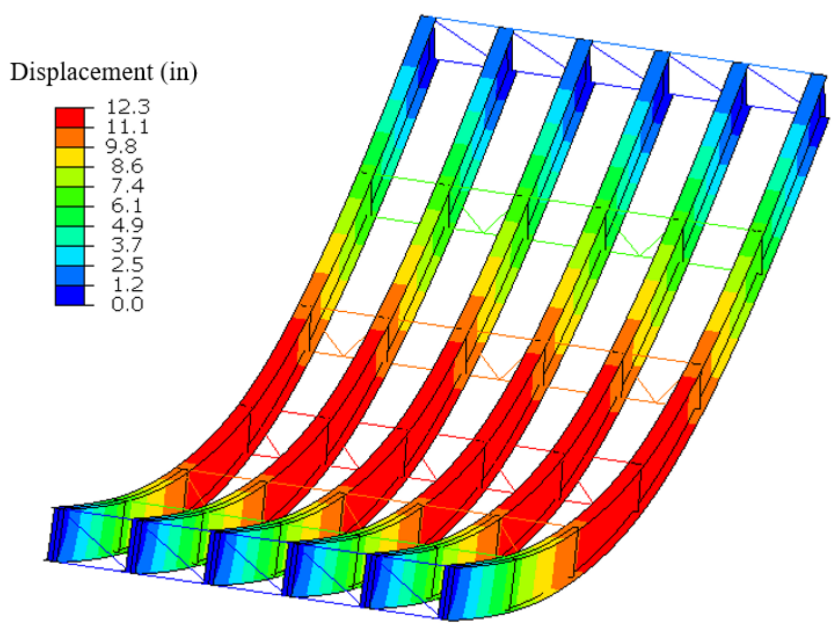

Figure 10-5. Displaced Shape of Design Example #1 using Nonlinear Geometric Imperfection Analysis

The final displaced shape of the system is displayed in Figure 10-5. The maximum horizontal displacement without lateral trusses is 0.97 in, which is beneath the L/500 requirement (3.6 in). The system has sufficient stiffness.

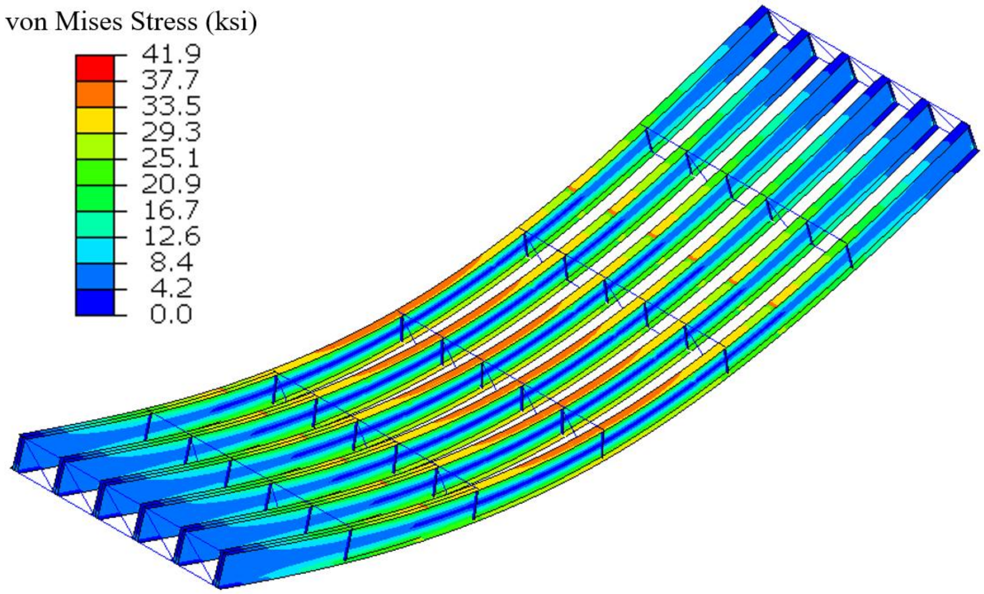

Figure 10-6. von Mises Stress Distribution of Design Example #1 using Nonlinear Geometric Imperfection Analysis

The von Mises stress distribution is given in Figure 10-6. The maximum von Mises stress of 41.9 ksi is less than the yield limit of 50 ksi for Grade 50 steel. The system remains elastic and meets the material assumptions of the model. All bracing member stress are within 1 to 2 ksi. The hand calculation estimate, based on the highest force and reduced section, is conservatively at approximately 6.7 ksi.

10.2. Design Example 2

An application of lean-on bracing for a 56° skew, single span, seven-girder bridge with a cross-frame layout resembling an X is illustrated in this example. The girder sections are shown in Figure 10-7.

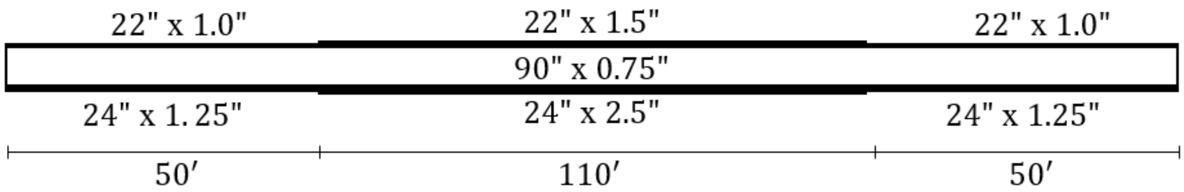

Figure 10-7. Example 2 Girder Section

10.2.1. Determine Girder Layout and Geometry

Span Information

$n_g = 7$	Number of girders
$S = 8\ ft$	Girder spacing
$L = 210\ ft$	Span length
$E = 29{,}000\ ksi$	Modulus of elasticity
$\theta = 60°$	Skew angle

Web Information

$t_w = 0.75\ in$	Thickness of girder web
$D = 90\ in$	Height of girder web

Bottom Flange Information

$b_{bf} = 24\ in$	Width of bottom flange
$t_{bsmall} = 1.25\ in$	Thickness of thinnest section of girder flange
$t_{b2} = 2.5\ in$	Thickness of second thinnest section of girder flange
$x_{bsmall} = \frac{50\ ft + 50\ ft}{110\ ft} = 0.48$	Fraction of span with t_{bsmall}

Top Flange Information

$b_{tf} = 22\ in$	Width of top flange
$t_{tsmall} = 1.0\ in$	Thickness of thinnest section of girder flange
$t_{t2} = 1.5\ in$	Thickness of second thinnest section of girder flange
$x_{tsmall} = \frac{50\ ft + 50\ ft}{110\ ft} = 0.48$	Fraction of span with t_{bsmall}

Calculated Girder Section Properties, as defined in AASHTO LRFD BDS

$$t_{beff} = t_{bsmall}(1 - 1 - x_{bsmall})^2) + t_{b2}(1 - x_{bsmall})^2 = 1.59\ in$$

$$t_{teff} = t_{tsmall}(1 - 1 - x_{tsmall})^2) + t_{t2}(1 - x_{tsmall})^2 = 1.41\ in$$

Bottom Flange	Top Flange	Web
$y_{bf} = \frac{t_{beff}}{2} = 0.8\ in$	$y_{tf} = \frac{t_{teff}}{2} = 92.1\ in$	$y_w = t_{beff} + \frac{h_w}{2} = 46.6\ in$
$A_{bf} = b_{bf}t_{beff} = 38.2\ in^2$	$A_{tf} = b_{tf}t_{teff} = 31.1\ in^2$	$A_w = b_w t_w = 67.5\ in^2$
$I_{xbf} = \frac{b_{bf}t_{beff}^3}{12} = 8.1\ in^4$	$I_{xtf} = \frac{b_{tf}t_{teff}^3}{12} = 5.2\ in^4$	$I_{xw} = \frac{b_w t_w^3}{12} = 45562.5\ in^4$
$I_{ybf} = \frac{t_{beff}b_{bf}^3}{12} = 1835.0\ in^4$	$I_{ytf} = \frac{t_{teff}b_{tf}^3}{12} = 1252.5\ in^4$	$I_{yw} = \frac{t_w b_w^3}{12} = 3.2\ in^4$

$$d_{bot} = \frac{A_{bf}y_{bf} + A_w y_w + A_{tf}y_{tf}}{A_{bf} + A_w + A_{tf}} = 44.1\ in$$

$$d_{top} = t_{beff} + h_w + t_{teff} - d_{bot} = 48.9\ in$$

$$I_x = I_{xbf} + A_{bf}\left(d_{bot} - y_{bf}\right)^2 + I_{xw} + A_w(d_{bot} - y_w)^2 + I_{xtf} + A_{tf}\left(d_{bot} - y_{tf}\right)^2 = 189{,}287\ in^4$$

$$I_y = I_{ybf} + I_{yw} + I_{ytf} = 3090.8\ in^4$$

$$c = d_{top} - \frac{t_{eff}}{2} = 48.2\ in$$

$$t = d_{bot} - y_{bf} = 43.3\ in$$

$$I_{yeff} = I_{ytf} + \left(\frac{t}{c}\right) I_{ybf} = 2903\ in^4$$

$$J = \frac{b_{bf}t_{beff}^3}{3} + \frac{b_{tf}t_{teff}^3}{3} + \frac{h_w t_w^3}{3} = 66.0\ in^4$$

10.2.2. Determine Cross-Frame Locations Based on Recommended Layouts

Because the bridge is skewed with seven girders, the diagonal layout is recommended. X-frames are used because the web depth is greater than 75% of the girder spacing. Eleven cross-frame lines are used to keep the maximum spacing to approximately 25 feet. In Figure 10-8 and following calculations, CFL represents "cross-frame line," dashed lines represent lean-on struts, and thick lines represent cross-frames. A cross-section view of CFL 4 is shown in Figure 10-9.

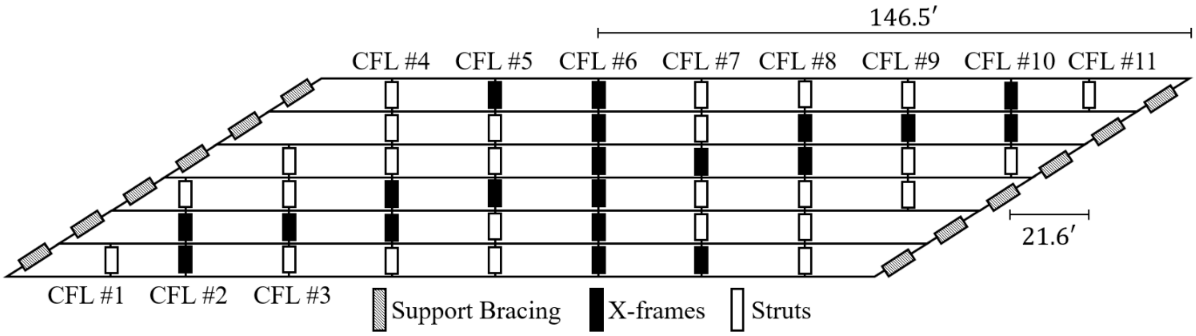

Figure 10-8. Example 2 Cross-Frame Layout

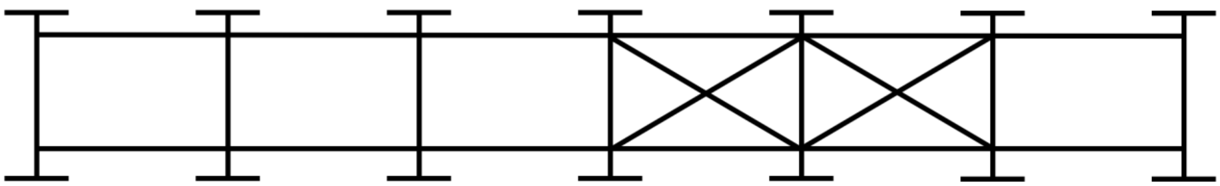

Figure 10-9. Example 2 CFL 4 Section View

Connection Plate Information

$b_s = 9\ in$	Width of connection plate
$h_i = 5\ in$	Distance from top of cross-frame to bottom of top flange
$t_s = 0.5\ in$	Thickness of connection plate
Min Lap = 5 in	Minimum overlap of brace member and connection plate

Brace Information

$n_{CFL} = 11$	Number of intermediate cross-frame lines in the span
$L_b = 25\ ft$	Unbraced length (maximum cross-frame spacing)
$h_b = h_w - 2h_i = 80\ in$	Height of cross-frame
$L_d = \sqrt{L_s^2 + h_b^2} = 88\ in$	Length of diagonal braces
$L_s = S - 2(b_s - \text{Min Lap}) = 118.9\ in$	Length of top and bottom struts

10.2.3. Check Moment Demands

10.2.3.1. Calculate the Moment Loading at Each Cross-Frame Line

Loading Information

$\rho_{concrete} = 150 \frac{lb}{ft^3}$	Density of concrete
$t_{deck} = 10\ in$	Thickness of deck
$\rho_{steel} = 490 \frac{lb}{ft^3}$	Density of steel
$DL_{form} = 5 \frac{lb}{ft^2}$	Load of formwork
$w_{deck} = \rho_{concrete} + t_{deck} * S = 1500 \frac{lb}{ft}$	Self-weight of wet concrete
$w_{girder} = \left(A_{bf} + A_{tf} + A_w\right) * \rho_{steel} = 751 \frac{lb}{ft}$	Self-weight of girder
$w_{form} = DL_{form} * S = 60 \frac{lb}{ft}$	Self-weight of formwork
$w_{CLL} = 150 \frac{lb}{ft}$	Construction live load
$w_{total} = 1.25\left(w_{deck} + w_{girder} + w_{form}\right) + 1.5w_{CLL} = 1919 \frac{lb}{ft}$	Total line load (factored)
$w_{total} = 1.4\left(w_{deck} + w_{girder} + w_{form} + w_{CLL}\right) = 2108 \frac{lb}{ft}$	Total line load (factored)

The demand in each bracing line depends on the moment at each bracing line. For a single simple span girder, the moment can be calculated at any point using the following equation:

$$M = \frac{w_{total}x(L - x)}{2}\ [kip - ft]$$

However, due to the skew, the moment along each girder is not as easily calculated due to changing tributary areas at the end regions of the deck. For simplicity, the governing moment M_u can be used for all bracing lines. The maximum moment for a single girder with uniformly distributed load is:

$$M_u = \frac{w_{total}L^2}{8} = 11{,}618\ kip - ft$$

10.2.3.2. Check System Global Buckling Moment

$C_{LO} = 0.85$	Lean-On Factor - 0.95 for bridges with less than 30° skew and 0.85 greater than or equal to 30° skew
$C_{BS} = 1.1$	1.1 for single span, 2.0 for continuous span
$\alpha_x = \frac{(n_g^2-1)}{12} = 4$	System warping stiffness factor
$K = 0.7$	For skew ≥ 30°

$$0.7M_{gs} = 0.7C_{LO}C_{BS}\frac{\pi^2 SE}{(KL)^2}\sqrt{I_y I_x \alpha_x} = 23{,}298\ kip - ft$$

$M_u < 0.7M_{gs}$ OK

NOTE: there is no additional stiffness benefit of adding lateral trusses to this bridge, since K is equal to 0.7 for bridges with ≥ 30° skew.

10.2.3.3. Check Conventional Lateral-Torsional Buckling Moment

$C_b = 1$	LTB modification factor
$C_w = \frac{I_{ytf}}{2} \cdot \frac{h_w^2}{2} = 5{,}879{,}184\ in^6$	Torsional warping constant
$G = 11600\ ksi$	Shear modulus

$$M_0 = C_b \frac{\pi}{L_b}\sqrt{EI_{yeff}GJ + \frac{\pi^2 E^2 I_{yeff} C_w}{L_b^2}} = 35{,}322\ kip - ft$$

$M_u < M_0$ OK

10.2.4. Determine Minimum Brace Area for Each Bracing Line

10.2.4.1. Determine Required System Stiffness at Each Bracing Line

$\phi_{sb} = 0.8$	Resistance factor for stability bracing

The required stiffness at each bracing line is given by ($L_{b,avg}$ is conservatively taken as 25 ft. for simplicity):

$$\beta_{T,req} = \frac{2.4L_{b,avg}}{\phi_{sb}EI_{y,eff}}\left(\frac{M_u}{C_b}\right)^2 = 207{,}779\frac{kip - in}{rad}$$

10.2.4.2. Calculate In-Plane girder Stiffness (Constant)

$$\beta_g = \frac{C_{LO}^2 \pi^4 E I_x s^2 \alpha_x L_{b,avg}}{(KL)^4} = 441{,}252 \frac{kip - in}{rad}$$

10.2.4.3. Calculate Cross-Sectional Stiffness (Constant)

The cross-frames are greater than 80% of the web depth, so the cross-sectional stiffness may be taken as infinite.

$$\beta_{sec} = \infty \frac{kip - in}{rad}$$

10.2.4.4. Use the Brace Stiffness Equation to Determine the Minimum Brace Area for Each Line

$R = 0.65$ Connection eccentricity factor

Use the following equations to determine the minimum area requirement for each bracing line with X-frames:

$$\beta_{br,req} = \left(\frac{1}{\beta_{T,req}} - \frac{1}{\beta_g} - \frac{1}{\beta_{sec}}\right)$$

$$A_{br,req} = \beta_{br,req} \frac{\frac{n_g}{2n_c} L_d^3 + \left(C_{strut} - \frac{n_g}{2n_c}\right) S^3}{E S^2 h_b^2 R}$$

For conventional lines:

$$C_{strut} = C_{ng} = \frac{n_g + 1.75}{2n_g - 0.25}$$

For lean-on bracing lines:

$$C_{strut} = (0.7 - 0.05 n_c)(n_{lean} + 1)^2$$

NOTE: You must idealize the bracing line when possible! The expression fit for C_{strut} does not apply to bracings lines that are able to be idealized.

Bracing Line	Idealize?	Conventional?	n_g	n_c	n_{lean}	C_{strut}	$\beta_{br,req}$	$A_{br,req}$
#1/11	No	No	2	0	1	N/A	N/A	N/A
#2/10	No	No	4	2	1	2.4	$392{,}692 \dfrac{kip-in}{rad}$	$1.03\ in^2$
#3/9	No	No	5	1	2	5.85	$392{,}692 \dfrac{kip-in}{rad}$	$1.45\ in^2$
#4/8	No	No	7	2	3	9.6	$392{,}692 \dfrac{kip-in}{rad}$	$2.32\ in^2$
#5/7	No	No	7	2	2	5.4	$392{,}692 \dfrac{kip-in}{rad}$	$3.49\ in^2$
#6	No	Yes	7	6	0	0.636	$392{,}692 \dfrac{kip-in}{rad}$	$0.36\ in^2$

CFL #1/#11 experience minimal moments and are restrained by the nearby support. To reduce fatigue stresses in these members, only lateral struts are used. The minimum brace area is dictated by bracing line #5/7. $A_{br,req} = 3.49\ in^2$.

10.2.4.5. Select Brace Member Size

A L5x5x3/8 angle is selected for all brace lines, resulting in $A_{br,prov} = 3.65\ in^2$.

10.2.5. Check Strength Requirements for Each Bracing Line

10.2.5.1. Determine the Force Demand in Diagonals and Struts for Each Cross-Frame Line

It is simplest to use the maximum moment in the span to check all brace lines.

$$M_{br} = \frac{2.4L_{b,avg}}{EI_{yeff}}\left(\frac{M_u}{C_b}\right)^2\left(\frac{L_b}{500h_o}\right) = 1090\ kip-in$$

$$F_{br} = \frac{M_{br}}{h_b} = 13.6\ kip$$

The force in the struts and diagonals is dependent on n_c, n_g, and n_{lean}, so the force will need to be calculated for each bracing line. The force equations for X-frames are:

Brace Type	F_d	Brace Line Type	F_s
X	$\frac{n_g}{2n_c}\frac{FL_d}{S}$	Lean-on	$\max\begin{cases} n_{lean,ext}F \\ \frac{n_{lean,int}}{2}F \end{cases}$
		Conventional	$\left\lvert 1-\frac{n_g}{2n_c}\right\rvert F$

Bracing Line	Idealize?	Conventional?	n_g	n_c	n_{lean}	$F_{br,max}$	F_d	F_s
#1/11	No	No	2	0	1	$10.4\ kip$	$0\ kip$	$13.6\ kip$
#2/10	No	No	4	2	1	$10.4\ kip$	$16.9\ kip$	$13.6\ kip$
#3/9	No	No	5	1	2	$10.4\ kip$	$42.2\ kip$	$27.2\ kip$
#4/8	No	No	7	2	3	$10.4\ kip$	$29.5\ kip$	$40.9\ kip$
#5/7	No	No	7	2	2	$10.4\ kip$	$29.5\ kip$	$27.2\ kip$
#6	No	Yes	7	6	0	$10.4\ kip$	$9.8\ kip$	$5.7\ kip$

The maximum brace forced is used to calculate the maximum diagonal and strut forces for simplicity. The maximum force in the diagonals is $F_d = 42.2\ kip$ and the maximum force in the struts is $F_s = 40.9\ kip$.

10.2.5.2. Check Strength Capacity

Brace Angle Information

$F_u = 70\ ksi$	Tensile strength
$F_y = 50\ ksi$	Yield strength
$\bar{x} = 1.37\ in$	Centroid of angle
$r_x = 1.55\ in$	Radius of gyration
$t_{leg} = 0.375\ in$	Thickness of leg

Brace Connection Information

$d_b = 1\ in$	Bolt diameter
$F_{ub} = 120\ ksi$	Tensile strength of bolt
$F_{yb} = 70\ ksi$	Yield strength of bolt
$L_{bolt} = 2\ in$	Bolt spacing
$A_b = \frac{\pi}{4} d_b^2 = 0.785\ in$	Area of bolt

10.2.5.2.1. Tensile Capacity of Diagonals and Struts

Gross Section Yield

$\phi_y\ = 0.95$	Resistance factor for yielding

$\phi_y P_{ny} = \varphi_y F_y A_{b,prov} = 173.4\ kip$

$\phi_y P_{ny} > F_d$ OK, $\phi_y P_{ny} > F_s$ OK

Net Section Fracture

$\phi_u\ = 0.8$	Resistance factor for fracture
$R_p = 1.0$	Reduction factor for holes
$U = 1 - \frac{\bar{x}}{L_{bolt}} = 0.3$	Shear lag reduction factor
$A_n = A_{b,prov} - 1\left(d_b + \frac{1}{8}\ in\right) t_{leg} = 3.2\ in^2$	Nominal area of brace member

$\phi_u P_{nu} = \phi_u F_u A_n R_p U = 56.9\ kip$

$\phi_u P_{nu} > F_d$ OK, $\phi_u P_{nu} > F_s$ OK

10.2.5.2.2. Compressive Capacity of Cross-Frame Diagonals

As per AASHTO LRFD Article 6.9.4.4:

$$\frac{L_d}{r_x} = 76.7$$

Hence, effective slenderness ratio is calculated as:

AASHTO LRFD Eqn. 6.9.4.4-1:

$$\left(\frac{KL_d}{r_x}\right)_{eff} = 72 + 0.75\frac{L_d}{r_x} = 129.5$$

Elastic critical buckling resistance of single angle is calculated as:

AASHTO LRFD Eqn. 6.9.4.1.2-1:

$$P_e = \frac{\pi^2 E}{\left(\frac{KL_d}{r_x}\right)_{eff}} A_g = 62.3\ kip$$

Nominal yield resistance:

AASHTO LRFD Article 6.9.4.1

$$P_0 = F_y A_{b,prov} = 182.5\ kip$$

As per AASHTO LRFD Article 6.9.4.1:

$$\frac{P_o}{P_e} = 2.9 > 2.25$$

Hence, nominal compressive resistance of a single angle is:

AASHTO LRFD Eqn. 6.9.4.1-2

$$P_n = 0.877 P_e = 54.6\ kip$$

Factored compressive resistance of a single angle is:

$\phi_c = 0.95$ Resistance factor for compression

$$\phi_c P_n = 51.9\ kip > F_d\ OK$$

10.2.5.2.3. Compressive Capacity of Top and Bottom Struts

As per AASHTO LRFD Article 6.9.4.4:

$$\frac{L_s}{r_x} = 56.8$$

Hence, effective slenderness ratio is calculated as:

AASHTO LRFD Eqn. 6.9.4.4-1:

$$\left(\frac{KL_s}{r_x}\right)_{eff} = 72 + 0.75\frac{L_s}{r_x} = 114.6$$

Elastic critical buckling resistance of single angle is calculated as:

AASHTO LRFD Eqn. 6.9.4.1.2-1:

$$P_e = \frac{\pi^2 E}{\left(\frac{KL_d}{r_x}\right)_{eff}} A_g = 79.6\ kip$$

Nominal yield resistance:

AASHTO LRFD Article 6.9.4.1

$$P_0 = F_y A_{b,prov} = 182.5\ kip$$

As per AASHTO LRFD Article 6.9.4.1:

$$\frac{P_o}{P_e} = 2.3 > 2.25$$

Hence, nominal compressive resistance of a single angle is:

AASHTO LRFD Eqn. 6.9.4.1-2

$$P_n = 0.877 P_e = 69.8\ kip$$

Factored compressive resistance of a single angle is:

$$\phi_c P_n = 66.3\ kip > F_s\ OK$$

10.2.5.2.4. Limiting Slenderness Ratio Check

$$\frac{KL_s}{r_x} = 129.5 < 140\ OK$$

10.2.6. FEA Check of Moment Capacity and Stiffness (Optional)

10.2.6.1. Conduct Eigenvalue Buckling Analysis of Bridge FEA Model and Examine Results

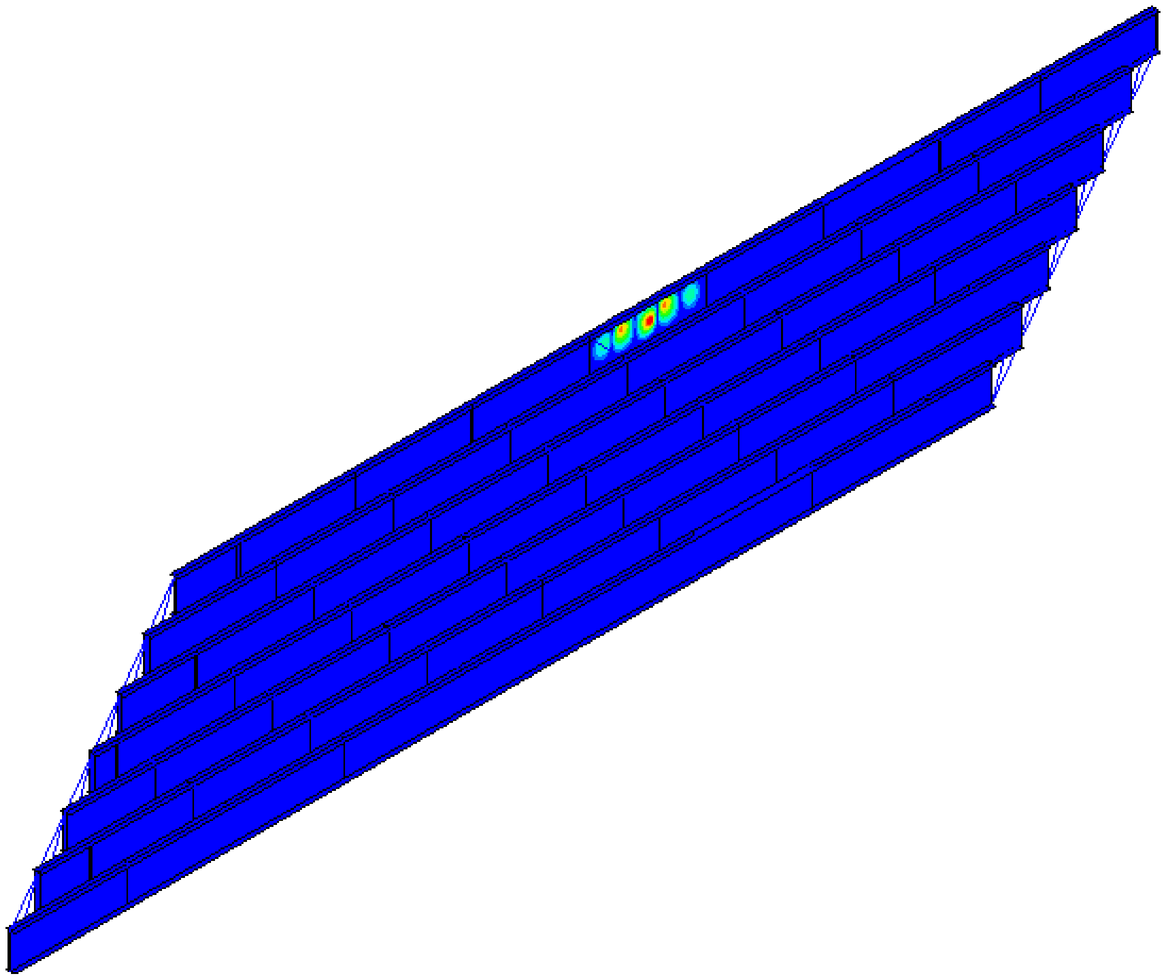

Figure 10-10. Buckled shape of Design Example #2 obtained from eigenvalue buckling analysis.

The loading applied to the model is a factored gravity (self-weight) load and a factored lump sum pressure of the deck self-weight, formwork self-weight, and construction live load on the top flanges of the girders. The eigenvalue result is as follows:

$$\lambda = 1.21M_u > 1.0M_u\ OK$$

The model is controlled by local web buckling as illustrated by Figure 10-10.

10.2.6.2. Conduct Nonlinear Geometric Imperfection analysis of Bridge FEA Model and Examine Results

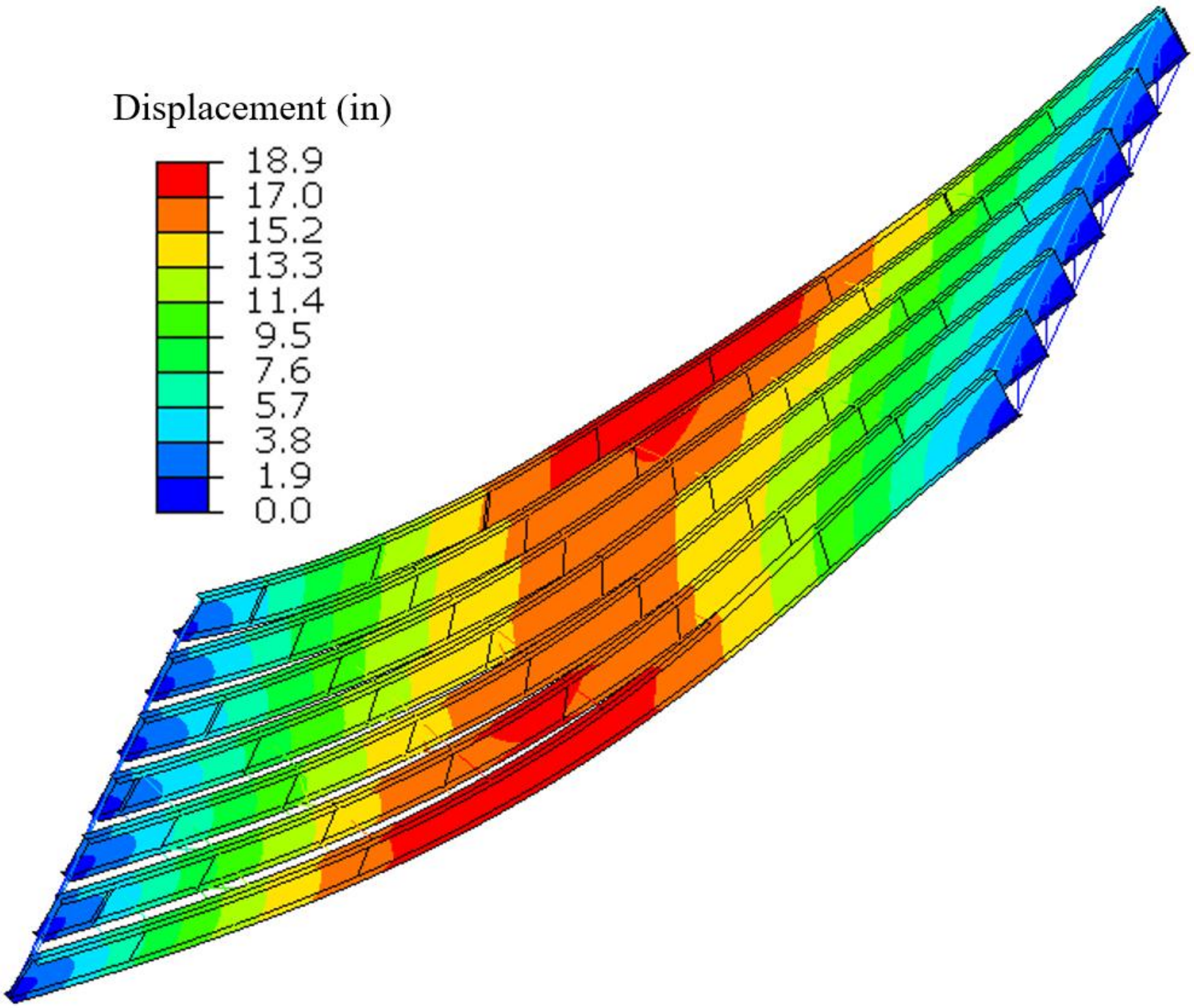

Figure 10-11. Displaced shape of Design Example #2 obtained from nonlinear geometric imperfection analysis.

The final displaced shape of the second design example can be seen in Figure 10-11. When restricting the top-flange, the maximum horizontal displacement at midspan is 1.29 in, which is beneath the L/500 requirement (5 in). Thus, the system has sufficient stiffness.

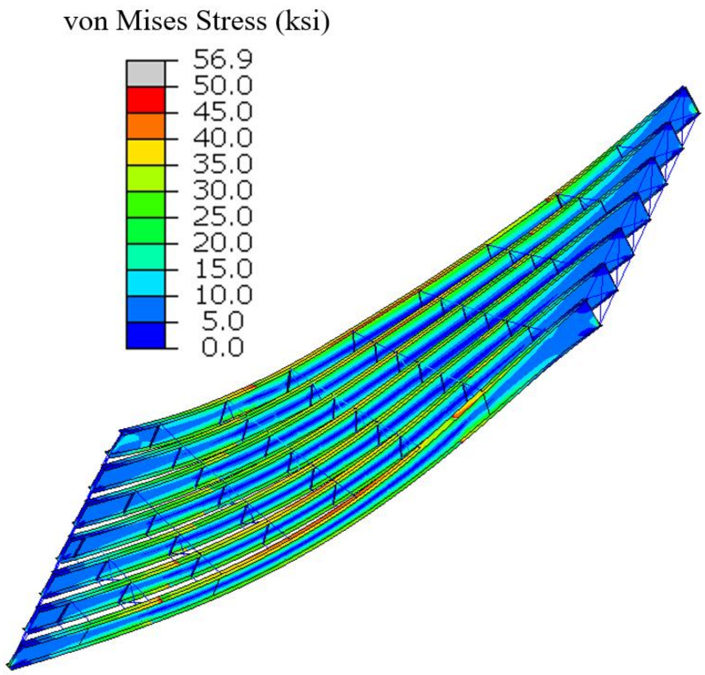

Figure 10-12. von Mises Stress Distribution of Design Example #2 using Nonlinear Geometric Imperfection Analysis

The von Mises stress distribution can be viewed in Figure 10-12. A maximum von Mises stress of 56.9 ksi occurs along the top flange at the spliced region near the support. This stress concentration is localized, and additional plates would be used to transition between splices in the real bridge system. Overall, the girders have lower stresses than the yield limit of 50 ksi for Grade 50 steel and thus the system is generally elastic.

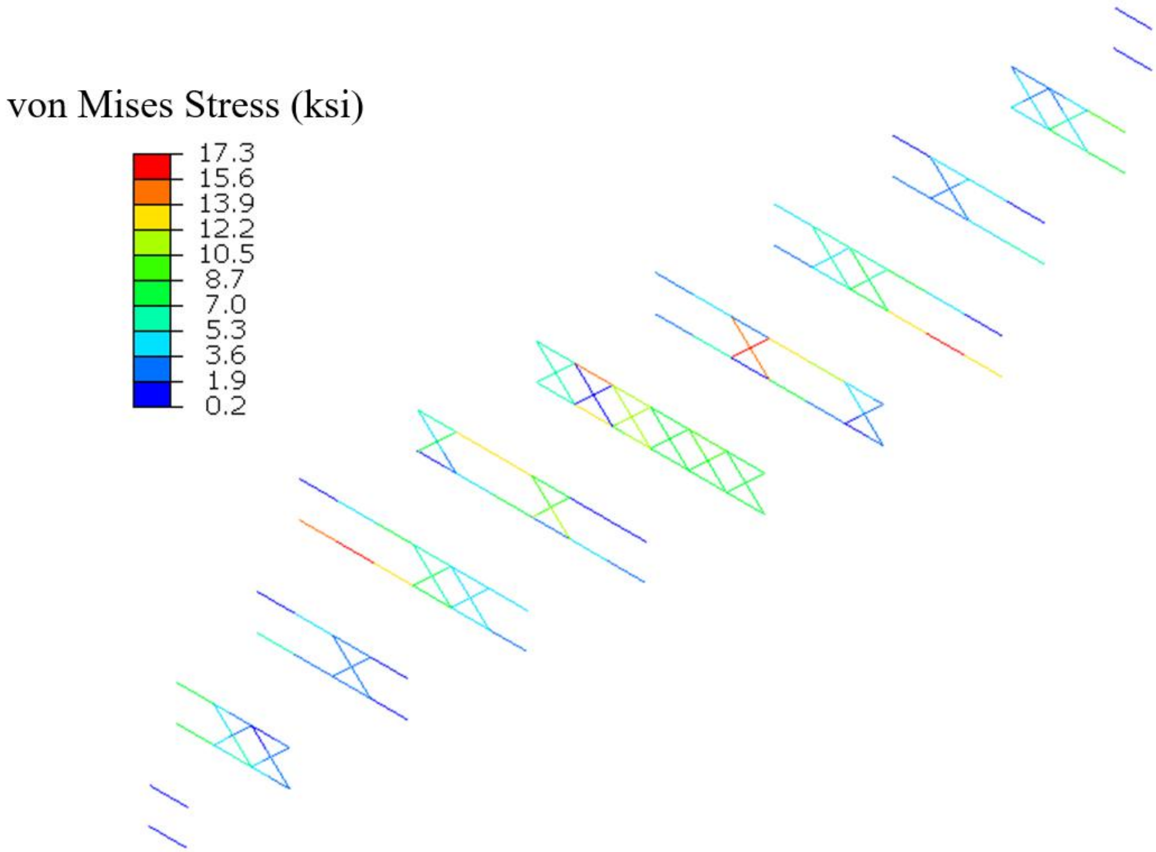

Figure 10-13. Stress Distribution of Brace Members in Design Example #2 using Nonlinear Geometric Imperfection Analysis

As seen in Figure 10-13, the bracing member stresses typically vary between 0.2 to 17.3 ksi, with higher brace stresses occurring in the bracing lines in the nonskewed section of the bridge. Note that stress distributions are nonsymmetric due to the imperfection on the system and that stress depends on the reduced section properties (R-factor applied). Considering the maximum stability induced stresses in the hand calculations would be estimated at 17.8 ksi, the results are reasonable.

Chapter 11. Conclusions

11.1. Research Contributions

The project successfully addressed many of the previous limitations of design methods for lean-on bracing. At the outset of the study, a comprehensive literature review was performed to capture the current state of knowledge. Then, field instrumentation and live-load testing of two Texas bridges with lean-on bracing were conducted, and corresponding finite element analysis models were developed and validated based on the recorded data. These models were used in a substantial parametric study to provide an understanding of the behavior of lean-on bracing systems and layout effects. The primary research contributions were in four areas, which are summarized below.

1. Cross-frame layouts: Before the research, the optimum cross-frame layouts for nonskew and skewed systems were undefined. As a result of this study, designers now have clear guidance and rules for the strategic placement of cross-frames in lean-on systems based on skew angle, number of girders, and span length.

2. In-plane girder stiffness equation (β_g): Due to uncertainty regarding the in-plane girder stiffness in lean-on systems, research by Helwig and Wang (2003) recommended a 50% reduction in the in-plane girder stiffness. Using the studies in this report and an updated version of the in-plane girder stiffness expression, the uncertainty with lean-on systems was heavily reduced (through the introduction of new terms), minimizing the reduction to 5% in nonskew systems and 15% in skewed systems in comparison to conventional bracing. Additionally, the warping restraint provided by skewed supports was quantified.

3. Brace stiffness equation ($\beta_{br,line}$): Prior lean-on stiffness equations were limited to a single exterior cross-frame in every bracing line. These equations also assumed only one diagonal was active (tension-only model) and ignored the contribution of a second diagonal (X frames). As part of this study, a revised equation was derived for the brace stiffness, which now can account for any number, position, or shape of cross-frames.

4. Strength equations: The original strength equations for lean-on systems had similar limitations to the brace stiffness equations, as previously mentioned. Revised brace diagonal (F_d) and strut (F_s) strength design equations were developed to correspond with the brace stiffness expression. These strength equations were updated for varied cross-frame geometry, number, and position along the cross-frame line.

The research team also provided several practical contributions. This includes detailed methodologies for equation-based and 3D model-based design. In addition, two design examples were developed to convey a conventional nonskew and skew lean-on bracing design using the equation-based methodology.

11.2. Future Work

The project resulted in several significant contributions to lean-on bracing design. The resulting design equations and procedures are applicable to straight bridges with any skew angle. In order to expand the application of lean-on bracing and remove some built-in conservativism of the approach, there are several avenues that should be pursued as part of future research:

- The scope of this research did not include curved bridges. Lean-on bracing is a viable concept for curved bridges, but additional study is recommended to quantify additional considerations induced by the curvature of bridge girders.

- The parametric study was exclusive to lean-on braces with full-depth cross-frames, resulting in the cross-sectional stiffness term becoming inconsequential. If lean-on layouts with cross-frames less than 80% of the web depth are to be used, additional study is recommended to develop detailed recommendations.

- Connection eccentricity factors (R-factors) were studied in detail for conventional bracing systems (Reichenbach *et al.*, 2021). These recommendations were applied directly for lean-on bracing. Additional study is recommended to refine connection eccentricity factors for lean-on bracing.

- Simply supported spans were the focus of the studies. Further study may be beneficial in order to better quantify layout effects as well as determine layout factors for continuous systems.

- A component of K_{skew} for skew systems may be impacted by the span length of the system, making it more effective for shorter spans, and less effective for longer systems. This effect may be worthwhile to better quantify.

- It is recommended that it is inconsequential to remove approximately 10% or less of the cross-frames in a conventional bracing system. Further study in quantifying a maximum value of cross-frames that may be removed without application of lean-on equations is worthwhile.

- Finally, the girder erection process may be streamlined with additional study of construction phasing for the recommended lean-on layouts.

Acknowledgements

The research team would like to express immense appreciation for the contributions of the following groups and organizations, without whom this project would not have been possible:

- TxDOT panel that helped guide the study – Martin Dassi, Jamie Farris, Michelle Romage-Chambers, Greg Turco, David Fish
- TxDOT personnel who helped coordinate SH105 Bridge for field instrumentation and testing - Brandon Montgomery
- Greg Kochersperger for his feedback on lean-on bracing design for the Chisholm Trail Bridge
- Personnel that helped coordinate Chisholm Trail Bridge for field instrumentation and testing – Yang You (NTTA), Roger Doddy (NTTA), Mark Bouma (NTTA), and Janet Crawford (Johnson County TxDOT)
- The original designers of IH35E overpass for their feedback on the design process – Elaine Jin (HDR) and John Van Heukelem (HDR)
- Jeremiah Fasl (WJE) for providing the instrumentation data for the Lubbock Bridge (TxDOT Project 5-1772)
- Matthew Reichenbach for his mentorship and guidance on computing, data acquisition, and data processing
- Students who assisted with field work –Xiaoyi Chen, Sheyenne Davis, Xiaomeng Ge, Shengyi Shi, Ryan Stevens, and Eric Stoddard
- High performance computing centers – University of Texas at Austin High Performance Computing, Texas A&M High Performance Research Computing, Auburn High Performance Computing

References

AASHTO (2020) *LRFD Bridge Design Specifications*. 9th ed. Washington, DC: American Association of State Highway and Transportation Officials.

ABAQUS Documentation (2022). Version 2022. Dassault Systems, USA.

AISC (2017) *Manual of Steel Construction*. 15th ed. Chicago.

AISC (2022) *Specification for Structural Steel Buildings*. Chicago: American Institute of Steel Construction.

American Concrete Institute (ACI) (2019) *Building Code Requirements for Structural Concrete (ACI 318-19)*. Farmington Hills, Michigan: American Concrete Institute.

Battistini, A., Wang, W., Donahue, S., Helwig, T., Engelhardt, M., and Frank, K. (2013) *Improved Cross Frame Details*. Research Report 0–6564.

Battistini, A., Wang, W., Helwig, T., Engelhardt, M., and Frank, K. (2016) "Stiffness Behavior of Cross Frames in Steel Bridge Systems," *ASCE Journal of Bridge Engineering*, 21(6), pp. 04016024-1–11.

Belivanis, K., Han, L., Sun, C., Helwig, T., Engelhardt, M., Tassoulas, J., and Williamson, E. (2016) "Extending Use of Steel-Laminated Elastomeric Bearings to Higher Demand Applications," *TxDOT Project 0-6785* [Preprint], (Publication No. FHWA/Tx-16/0-6785-1).

Fish, D. (2021) *Refined Design Expressions for In-Plane Girder Stiffness and System Buckling Capacity*. MS Thesis, University of Texas at Austin.

Fish, D., Bjelland A., Park, S., Helwig, T., and Engelhardt M., (2025) "Improved Design Expressions For The Global Buckling Capacity And In-Plane Girder Stiffness Of Torsionally Braced I-Girder Systems.", https://doi.org/10.1061/JSENDH.STENG-14925.

Gasser, C.E., Bjelland, A., Park, S., Yarnold, M., Helwig, T., Engelhardt, M., Hebdon, M., and Hurlebaus, S. (2024) "Identification of Critical Bracing Lines in Lean-on Bracing Systems and Corresponding Stiffness/Strength Expressions," *Structural Stability Research Council Conference Proceedings* [Preprint].

Greenlee, R. (2010) "Finite Element Truss." University of New Mexico. Available at: https://www.unm.edu/~bgreen/ME360/Finite%20Element%20Truss.pdf.

Han, L. (2016) *Elastomeric bearings in high demand applications : numerical study and experimental validation*. PhD Dissertation, The University of Texas at Austin.

Han, L. and Helwig, T. (2016) "Effect of Girder Continuity and Imperfections on System Buckling of Narrow I-girder Systems," in. *Annual Stability Conference Structural Stability Research Council*, Orlando, FL.

Han, L. and Helwig, T. (2020) "Elastic Global Lateral-Torsional Buckling of Straight I-Shaped Girder Systems," *ASCE Journal of Structural Engineering*, 146(No .4), p. (10 pages).

Helwig, T. and Yura, J. (2015) "Bracing System Design," in *Steel Bridge Design Handbook*. US DOT, Federal Highway Administration (Publication No. FHWA-HIF-16- 002).

Helwig, T., Yura, J. and Frank, K. (1993) "Bracing Forces in Diaphragms and Cross Frames," in *Structural Stability Research Council Conference "Is Your Structure Suitably Braced?,"* pp. 129–140.

Helwig, T.A. and Fan, Z. (2000) *Field and Computational Studies of Steel Trapezoidal Box Girder Bridges*. Texas Department of Transportation.

Helwig, T.A., Frank, K.H. and Yura, J.A. (1997) "Lateral-Torsional Buckling of Singly Symmetric I-Beams," *Journal of Structural Engineering*, 123(9), pp. 1172–1179. Available at: https://doi.org/10.1061/(ASCE)0733-9445(1997)123:9(1172).

Helwig, T.A. and Wang, L. (2003) *Cross-Frame and Diaphragm Behavior for Steel Bridges with Skewed Supports*. Research Report 1772–1. Report for Texas Department of Transportation.

Holt, J.M., Romage-Chambers, M., Clancy, C., Panchal, D., and Wasserman, E. (2022) "Lean-on Bracing Reference Guide," *National Steel Bridge Alliance*.

Liu, Y. and Helwig, T. (2020a) "Torsional Brace Strength Requirements for Steel I-Girder Systems," *Journal of Structural Engineering*, 146(1), p. 04019185. Available at: https://doi.org/10.1061/(ASCE)ST.1943-541X.0002482.

Liu, Y. and Helwig, T. (2020b) "Torsional Bracing Stiffness Requirements for Steel I-Girder Systems," *Journal of Structural Engineering*, 146(1).

Park, S., Reichenbach, M., Helwig, T., Engelhardt, M., Connor, R., and Grubb, M. (2022) "Proposed Modifications to AASHTO Cross-Frame Analysis and Design: Stage 2 - Cross-Frames with WT Members," *Final Report NCHRP 1045 (project 12-113)*.

Prado, E.P. and White, D.W. (2015) *Assessment of Basic Steel I-Section Beam Bracing Requirements by Test Simulation*. Master's Thesis. Georgia Institute of Technology.

Reichenbach, M., Liu, Y., Helwig, T., and Engelhardt, M., (2020) "Lateral-Torsional Buckling of Singly Symmetric I-Girders with Stepped Flanges," *ASCE Journal of Structural Engineering*, https://doi-org.ezproxy.lib.utexas.edu/10.1061/(ASCE)ST.1943-541X.0002780146(10), pp. 04020203-1–15.

Reichenbach, M., White, J., Park, S., Zecchin, E., Moore, M., Liu, Y., Liang, C., Kovesdi, B., Helwig, T., Engelhardt, M., Connor, R., and Grubb, M. (2021) *Proposed Modification to AASHTO Cross-Frame Analysis and Design*. Washington, D.C.: Transportation Research Board, p. 26074. Available at: https://doi.org/10.17226/26074.

Romage, M.L. (2008) *Field Measurements on Lean-On-Bracing for Steel Girder Bridges with Skewed Supports*. M.S. Thesis. University of Texas at Austin.

Sanchez, T.A. and White, D.W. (2012) "Stability of Curved Steel I-Girder Bridges during Construction," *Transportation Research Record: Journal of the Transportation Research Board*, 2268(1), pp. 122–129. Available at: https://doi.org/10.3141/2268-14.

Taylor, A.C. and Ojalvo, M. (1966) "Torsional Restraint of Lateral Buckling," *Journal of the Structural Division, ASCE, ST2*, pp. 115–129.

Timoshenko, S. and Gere, J. (1961) *Theory of Elastic Stability*. New York: McGraw-Hill.

Topkaya, C., Yura, J.A. and Williamson, E.B. (2004) "Composite Shear Stud Strength at Early Concrete Ages," *Journal of Structural Engineering*, 130(6), pp. 952–960. Available at: https://doi.org/10.1061/(ASCE)0733-9445(2004)130:6(952).

Trahair, N.S. and Nethercot, D.A. (1984) "Bracing requirements in thin-walled structures," in J.R. Rhodes and A.C. Walker (eds.) *Developments in Thin-Walled Structures*. Elsevier New York, pp. 93–130.

Tran, D.Q. (2009) *Toward Improved Flange Bracing Requirements for Metal Building Frame Systems*. Georgia Institute of Technolovy.

Wang, L. and Helwig, T.A. (2005) "Critical Imperfections for Beam Bracing Systems," *Journal of Structural Engineering*, 131(6), pp. 933–940. Available at: https://doi.org/10.1061/(ASCE)0733-9445(2005)131:6(933).

Wang, W. (2013) "A Study of Stiffness of Steel Bridge Cross Frames," p. 250., PhD Dissertation, The University of Texas at Austin.

Winter, G. (1960) "Lateral Bracing of Columns and Beams," *ASCE Transactions*, 125, pp. 809–825.

Yura, J., Helwig, T.A., Herman, R., and Zhou, C., (2008) "Global Lateral Buckling of I-Shaped Girder Systems," *Journal of Structural Engineering*, 134(9), pp. 1487–1494. Available at: https://doi.org/10.1061/(ASCE)0733-9445(2008)134:9(1487).

Yura, J.A. (1992) *Bracing of Steel Beams in Bridges*. 1239–4F. Texas Department of Transportation, p. 96.

Yura, J.A. (2001) "Fundamentals of Beam Bracing," *Engineering Journal*, Vol. 38, p. 11-26.

Appendix A. SH 105 Bridge Sensor List Conventions

Sensor List Conventions		
Bay/ Girder #	G#	girder #
	B#	bay #
Member Type	GR	girder
	ST	strut, top
	SB	strut, bottom
	XT	cross-frame, top
	XB	cross-frame, bottom
Location on Member: Girders	N1	north bottom
	S1	south bottom
	N2	north middle
	S2	south middle
Location on Member: Angle	OH	outer horizontal
	IH	inner horizontal
	OV	outer vertical
	IV	inner vertical

Appendix B. SH 105 Bridge Sensor List

Strain Gauge Count	Datalogger	Multiplexer	Channel	Cross-frame Line	Bay/ Girder Number	Member Type	Location on Member	Label
1	D1	M1	C01	L5	G1	GR	N1	D1M1C01-L5G1-GR-N1
2	D1	M1	C03	L5	G1	GR	S1	D1M1C03-L5G1-GR-S1
3	D1	M1	C05	L5	B1	ST	OH	D1M1C05-L5B1-ST-OH
4	D1	M1	C07	L5	B1	ST	IH	D1M1C07-L5B1-ST-IH
5	D1	M1	C09	L5	B1	ST	OV	D1M1C09-L5B1-ST-OV
6	D1	M1	C11	L5	B1	ST	IV	D1M1C11-L5B1-ST-IV
7	D1	M1	C13	L5	B1	SB	OH	D1M1C13-L5B1-SB-OH
8	D1	M1	C15	L5	B1	SB	IH	D1M1C15-L5B1-SB-IH
9	D1	M1	C17	L5	B1	SB	OV	D1M1C17-L5B1-SB-OV
10	D1	M1	C19	L5	B1	SB	IV	D1M1C19-L5B1-SB-IV
11	D1	M1	C21	L5	G2	GR	N1	D1M1C21-L5G2-GR-N1
12	D1	M1	C23	L5	G2	GR	S1	D1M1C23-L5G2-GR-S1
13	D1	M1	C25	L5	G3	GR	N1	D1M1C25-L5G3-GR-N1
14	D1	M1	C27	L5	G3	GR	S1	D1M1C27-L5G3-GR-S1
15	D1	M1	C29	L5	G3	GR	N2	D1M1C29-L5G3-GR-N2
16	D1	M1	C31	L5	G3	GR	S2	D1M1C31-L5G3-GR-S2
1	D1	M2	C01	L5	B2	ST	OH	D1M2C01-L5B2-ST-OH

2	D1	M2	C03	L5	B2	ST	IH	D1M2C03-L5B2-ST-IH
3	D1	M2	C05	L5	B2	ST	OV	D1M2C05-L5B2-ST-OV
4	D1	M2	C07	L5	B2	ST	IV	D1M2C07-L5B2-ST-IV
5	D1	M2	C09	L5	B2	SB	OH	D1M2C09-L5B2-SB-OH
6	D1	M2	C11	L5	B2	SB	IH	D1M2C11-L5B2-SB-IH
7	D1	M2	C13	L5	B2	SB	OV	D1M2C13-L5B2-SB-OV
8	D1	M2	C15	L5	B2	SB	IV	D1M2C15-L5B2-SB-IV
9	D1	M2	C17	L5	B2	XT	OH	D1M2C17-L5B2-XT-OH
10	D1	M2	C19	L5	B2	XT	IH	D1M2C19-L5B2-XT-IH
11	D1	M2	C21	L5	B2	XT	OV	D1M2C21-L5B2-XT-OV
12	D1	M2	C23	L5	B2	XT	IV	D1M2C23-L5B2-XT-IV
13	D1	M2	C25	L5	B2	XB	OH	D1M2C25-L5B2-XB-OH
14	D1	M2	C27	L5	B2	XB	IH	D1M2C27-L5B2-XB-IH
15	D1	M2	C29	L5	B2	XB	OV	D1M2C29-L5B2-XB-OV
16	D1	M2	C31	L5	B2	XB	IV	D1M2C31-L5B2-XB-IV
1	D1	M3	C01	L5	B3	ST	OH	D2M3C01-L5B3-ST-OH
2	D1	M3	C03	L5	B3	ST	IH	D2M3C03-L5B3-ST-IH
3	D1	M3	C05	L5	B3	ST	OV	D2M3C05-L5B3-ST-OV
4	D1	M3	C07	L5	B3	ST	IV	D2M3C07-L5B3-ST-IV
5	D1	M3	C09	L5	B3	SB	OH	D2M3C09-L5B3-SB-OH
6	D1	M3	C11	L5	B3	SB	IH	D2M3C11-L5B3-SB-IH
7	D1	M3	C13	L5	B3	SB	OV	D2M3C13-L5B3-SB-OV
8	D1	M3	C15	L5	B3	SB	IV	D2M3C15-L5B3-SB-IV

9	D1	M3	C17	L5	B3	XT	OH	D2M3C17-L5B3-XT-OH
10	D1	M3	C19	L5	B3	XT	IH	D2M3C19-L5B3-XT-IH
11	D1	M3	C21	L5	B3	XT	OV	D2M3C21-L5B3-XT-OV
12	D1	M3	C23	L5	B3	XT	IV	D2M3C23-L5B3-XT-IV
13	D1	M3	C25	L5	B3	XB	OH	D2M3C25-L5B3-XB-OH
14	D1	M3	C27	L5	B3	XB	IH	D2M3C27-L5B3-XB-IH
15	D1	M3	C29	L5	B3	XB	OV	D2M3C29-L5B3-XB-OV
16	D1	M3	C31	L5	B3	XB	IV	D2M3C31-L5B3-XB-IV
1	D1	M4	C01	L5	G4	GR	N1	D2M4C01-L5G4-GR-N1
2	D1	M4	C03	L5	G4	GR	S1	D2M4C03-L5G4-GR-S1
3	D1	M4	C05	L5	B4	ST	OH	D2M4C05-L5B4-ST-OH
4	D1	M4	C07	L5	B4	ST	IH	D2M4C07-L5B4-ST-IH
5	D1	M4	C09	L5	B4	ST	OV	D2M4C09-L5B4-ST-OV
6	D1	M4	C11	L5	B4	ST	IV	D2M4C11-L5B4-ST-IV
7	D1	M4	C13	L5	B4	SB	OH	D2M4C13-L5B4-SB-OH
8	D1	M4	C15	L5	B4	SB	IH	D2M4C15-L5B4-SB-IH
9	D1	M4	C17	L5	B4	SB	OV	D2M4C17-L5B4-SB-OV
10	D1	M4	C19	L5	B4	SB	IV	D2M4C19-L5B4-SB-IV
11	D1	M4	C21	L5	G5	GR	N1	D2M4C21-L5G5-GR-N1
12	D1	M4	C23	L5	G5	GR	S1	D2M4C23-L5G5-GR-S1
1	D2	M5	C01	L3	B1	ST	OH	D3M5C01-L3B1-ST-OH
2	D2	M5	C03	L3	B1	ST	IH	D3M5C03-L3B1-ST-IH
3	D2	M5	C05	L3	B1	ST	OV	D3M5C05-L3B1-ST-OV

4	D2	M5	C07	L3	B1	ST	IV	D3M5C07-L3B1-ST-IV
5	D2	M5	C09	L3	B1	SB	OH	D3M5C09-L3B1-SB-OH
6	D2	M5	C11	L3	B1	SB	IH	D3M5C11-L3B1-SB-IH
7	D2	M5	C13	L3	B1	SB	OV	D3M5C13-L3B1-SB-OV
8	D2	M5	C15	L3	B1	SB	IV	D3M5C15-L3B1-SB-IV
9	D2	M5	C17	L3	B1	XT	OH	D3M5C17-L3B1-XT-OH
10	D2	M5	C19	L3	B1	XT	IH	D3M5C19-L3B1-XT-IH
11	D2	M5	C21	L3	B1	XT	OV	D3M5C21-L3B1-XT-OV
12	D2	M5	C23	L3	B1	XT	IV	D3M5C23-L3B1-XT-IV
13	D2	M5	C25	L3	B1	XB	OH	D3M5C25-L3B1-XB-OH
14	D2	M5	C27	L3	B1	XB	IH	D3M5C27-L3B1-XB-IH
15	D2	M5	C29	L3	B1	XB	OV	D3M5C29-L3B1-XB-OV
16	D2	M5	C31	L3	B1	XB	IV	D3M5C31-L3B1-XB-IV
1	D2	M6	C01	L3	B2	ST	OH	D3M6C01-L3B2-ST-OH
2	D2	M6	C03	L3	B2	ST	IH	D3M6C03-L3B2-ST-IH
3	D2	M6	C05	L3	B2	ST	OV	D3M6C05-L3B2-ST-OV
4	D2	M6	C07	L3	B2	ST	IV	D3M6C07-L3B2-ST-IV
5	D2	M6	C09	L3	B2	SB	OH	D3M6C09-L3B2-SB-OH
6	D2	M6	C11	L3	B2	SB	IH	D3M6C11-L3B2-SB-IH
7	D2	M6	C13	L3	B2	SB	OV	D3M6C13-L3B2-SB-OV
8	D2	M6	C15	L3	B2	SB	IV	D3M6C15-L3B2-SB-IV
9	D2	M6	C17	L3	B2	XT	OH	D3M6C17-L3B2-XT-OH
10	D2	M6	C19	L3	B2	XT	IH	D3M6C19-L3B2-XT-IH

11	D2	M6	C21	L3	B2	XT	OV	D3M6C21-L3B2-XT-OV
12	D2	M6	C23	L3	B2	XT	IV	D3M6C23-L3B2-XT-IV
13	D2	M6	C25	L3	B2	XB	OH	D3M6C25-L3B2-XB-OH
14	D2	M6	C27	L3	B2	XB	IH	D3M6C27-L3B2-XB-IH
15	D2	M6	C29	L3	B2	XB	OV	D3M6C29-L3B2-XB-OV
16	D2	M6	C31	L3	B2	XB	IV	D3M6C31-L3B2-XB-IV
1	D2	M7	C01	L3	B3	ST	OH	D4M7C01-L3B3-ST-OH
2	D2	M7	C03	L3	B3	ST	IH	D4M7C03-L3B3-ST-IH
3	D2	M7	C05	L3	B3	ST	OV	D4M7C05-L3B3-ST-OV
4	D2	M7	C07	L3	B3	ST	IV	D4M7C07-L3B3-ST-IV
5	D2	M7	C09	L3	B3	SB	OH	D4M7C09-L3B3-SB-OH
6	D2	M7	C11	L3	B3	SB	IH	D4M7C11-L3B3-SB-IH
7	D2	M7	C13	L3	B3	SB	OV	D4M7C13-L3B3-SB-OV
8	D2	M7	C15	L3	B3	SB	IV	D4M7C15-L3B3-SB-IV
9	D2	M7	C17	L3	B4	ST	OH	D4M7C17-L3B4-ST-OH
10	D2	M7	C19	L3	B4	ST	IH	D4M7C19-L3B4-ST-IH
11	D2	M7	C21	L3	B4	ST	OV	D4M7C21-L3B4-ST-OV
12	D2	M7	C23	L3	B4	ST	IV	D4M7C23-L3B4-ST-IV
13	D2	M7	C25	L3	B4	SB	OH	D4M7C25-L3B4-SB-OH
14	D2	M7	C27	L3	B4	SB	IH	D4M7C27-L3B4-SB-IH
15	D2	M7	C29	L3	B4	SB	OV	D4M7C29-L3B4-SB-OV
16	D2	M7	C31	L3	B4	SB	IV	D4M7C31-L3B4-SB-IV

Appendix C. SH 105 Bridge Live Load Testing Layout

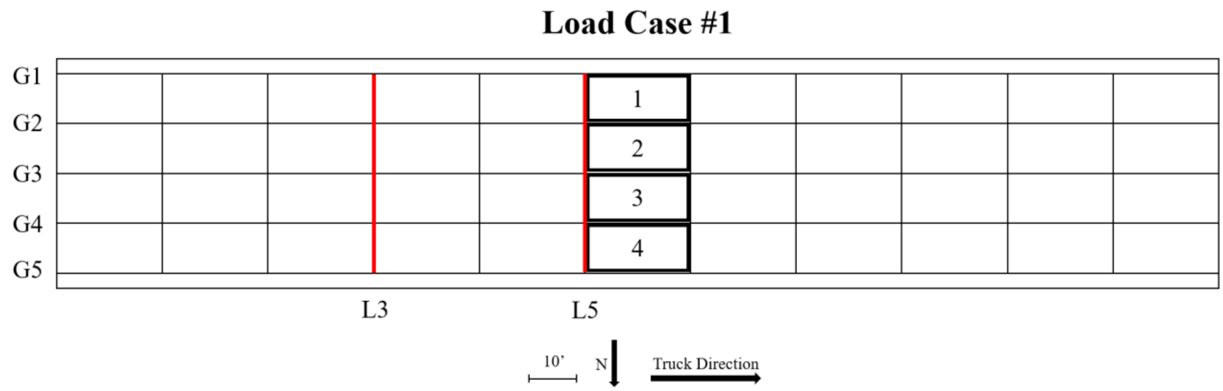

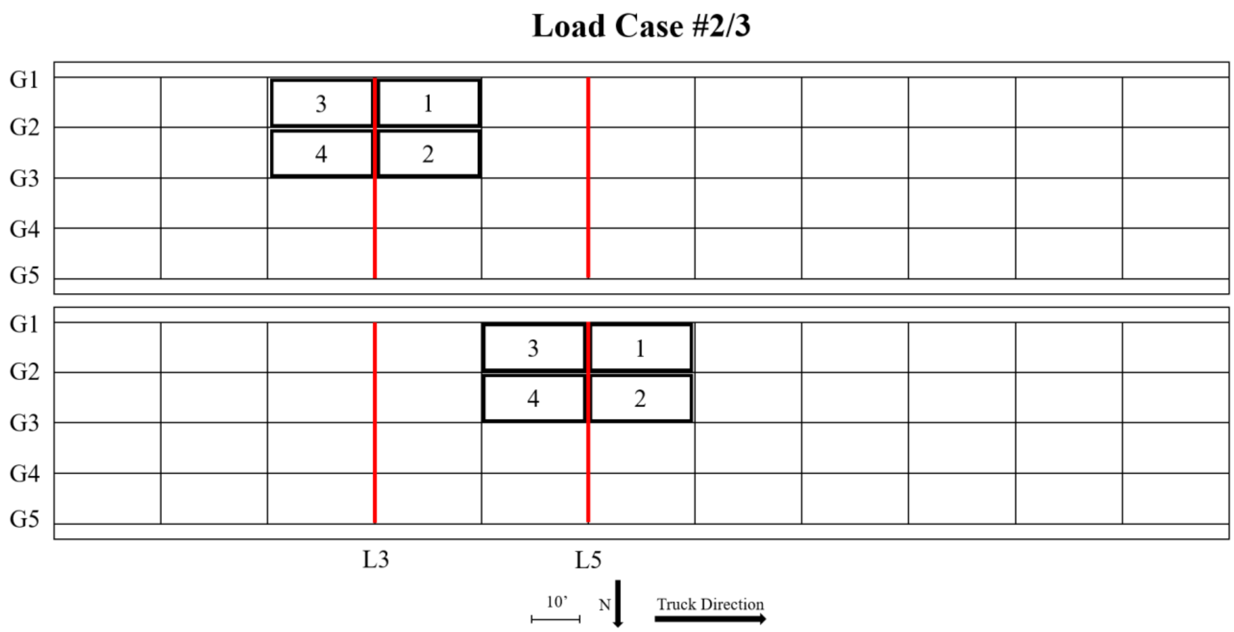

Load Case #4/5

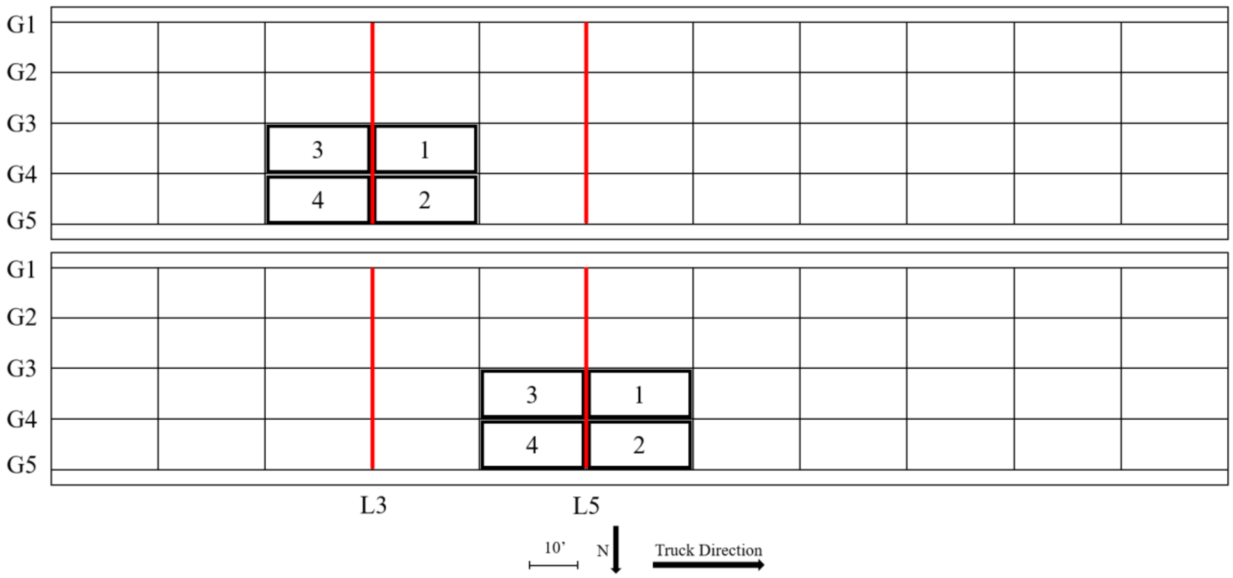

Load Case #6/7

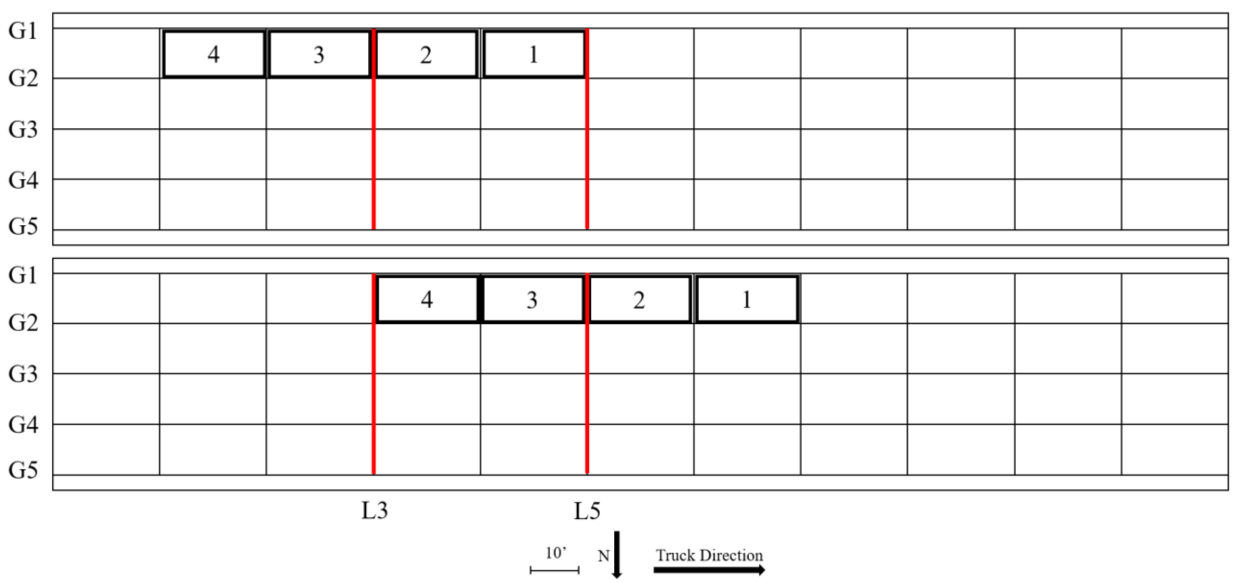

Load Case #8/9

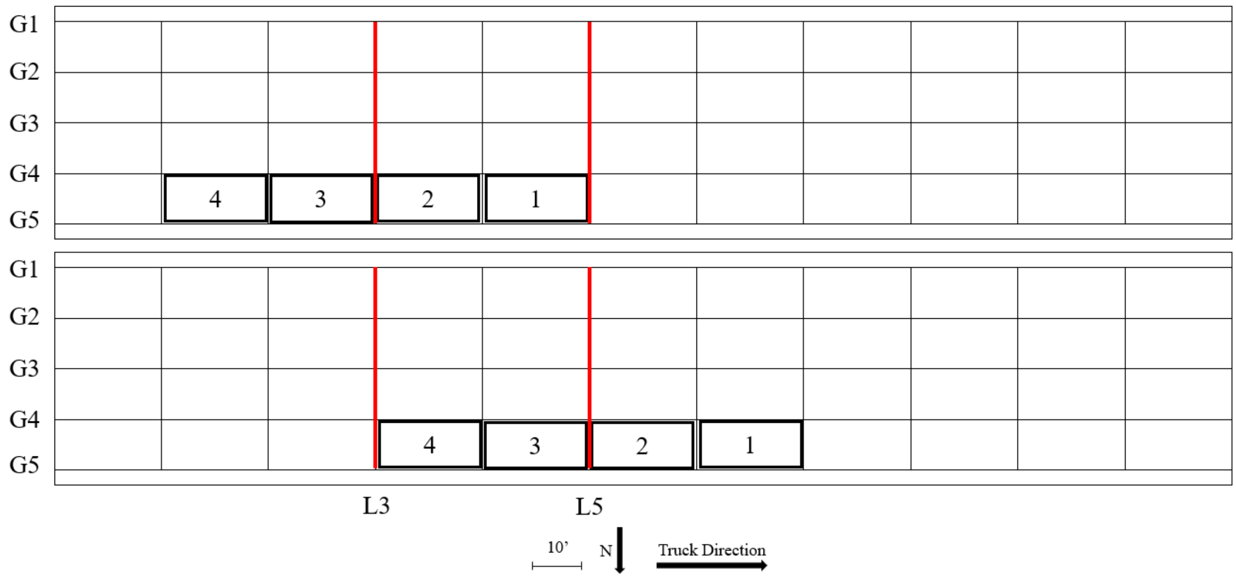

Appendix D. Chisholm Trail Bridge Sensor List Conventions

Sensor List Conventions		
Bay/ Girder #	G#	girder #
	B#	bay #
Member Type	GR	girder
	ST	strut top
	SB	strut bottom
	SBE	strut bottom east
	SBW	strut bottom west
	KE	k-frame east
	KW	k-frame west
Location on Member: Girders	N1	north bottom
	S1	south bottom
	N2	north middle
	S2	south middle
Location on Member: Single Angle	OH	outer horizontal
	IH	inner horizontal
	OV	outer vertical
	IV	inner vertical
Location on Member: Double Angle	OHN/S	outer horizontal north/south
	IHN/S	inner horizontal north/south
	IVN/S	inner vertical north/south

Appendix E. Chisholm Trail Bridge Sensor List

Strain Gauge Count	Multiplexer	Channel	Cross-frame Line	Bay/Girder Number	Member Type	Location on Member	Label
1	M1	C01	L8	B1	ST	OH	M1C01-L8B1-ST-OH
2	M1	C02	L8	B1	ST	IH	M1C02-L8B1-ST-IH
3	M1	C03	L8	B1	ST	OV	M1C03-L8B1-ST-OV
4	M1	C04	L8	B1	ST	IV	M1C04-L8B1-ST-IV
5	M1	C05	L8	B1	SB	OH	M1C05-L8B1-SB-OH
6	M1	C06	L8	B1	SB	IH	M1C06-L8B1-SB-IH
7	M1	C07	L8	B1	SB	OV	M1C07-L8B1-SB-OV
8	M1	C08	L8	B1	SB	IV	M1C08-L8B1-SB-IV
9	M1	C09	L8	B2	ST	OH	M1C09-L8B2-ST-OH
10	M1	C10	L8	B2	ST	IH	M1C10-L8B2-ST-IH
11	M1	C11	L8	B2	ST	OV	M1C11-L8B2-ST-OV
12	M1	C12	L8	B2	ST	IV	M1C12-L8B2-ST-IV
13	M1	C13	L8	B2	SB	OH	M1C13-L8B2-SB-OH
14	M1	C14	L8	B2	SB	IH	M1C14-L8B2-SB-IH
15	M1	C15	L8	B2	SB	OV	M1C15-L8B2-SB-OV
16	M1	C16	L8	B2	SB	IV	M1C16-L8B2-SB-IV
1	M2	C01	L8	G3	GR	N1	M2C01-L8G3-GR-N1
2	M2	C02	L8	G3	GR	S1	M2C02-L8G3-GR-S1

3	M2	C03	L8	G3	GR	N2	M2C03-L8G3-GR-N2
4	M2	C04	L8	G3	GR	S2	M2C04-L8G3-GR-S2
5	M2	C05	L8	B3	ST	OH	M2C05-L8B3-ST-OH
6	M2	C06	L8	B3	ST	IH	M2C06-L8B3-ST-IH
7	M2	C07	L8	B3	ST	OV	M2C07-L8B3-ST-OV
8	M2	C08	L8	B3	ST	IV	M2C08-L8B3-ST-IV
9	M2	C09	L8	B3	SBE	OH	M2C09-L8B3-SBE-OH
10	M2	C10	L8	B3	SBE	IH	M2C10-L8B3-SBE-IH
11	M2	C11	L8	B3	SBE	OV	M2C11-L8B3-SBE-OV
12	M2	C12	L8	B3	SBE	IV	M2C12-L8B3-SBE-IV
13	M2	C13	L8	B3	SBW	OH	M2C13-L8B3-SBW-OH
14	M2	C14	L8	B3	SBW	IH	M2C14-L8B3-SBW-IH
15	M2	C15	L8	B3	SBW	OV	M2C15-L8B3-SBW-OV
16	M2	C16	L8	B3	SBW	IV	M2C16-L8B3-SBW-IV
1	M3	C01	L8	G4	GR	N1	M3C01-L8G4-GR-N1
2	M3	C02	L8	G4	GR	S1	M3C02-L8G4-GR-S1
3	M3	C03	L8	G4	GR	N2	M3C03-L8G4-GR-N2
4	M3	C04	L8	G4	GR	S2	M3C04-L8G4-GR-S2
5	M3	C05	L8	B3	KE	OH	M3C05-L8B3-KE-OH
6	M3	C06	L8	B3	KE	IH	M3C06-L8B3-KE-IH
7	M3	C07	L8	B3	KE	OV	M3C07-L8B3-KE-OV
8	M3	C08	L8	B3	KE	IV	M3C08-L8B3-KE-IV
9	M3	C09	L8	B3	KW	OH	M3C09-L8B3-KW-OH

10	M3	C10	L8	B3	KW	IH	M3C10-L8B3-KW-IH
11	M3	C11	L8	B3	KW	OV	M3C11-L8B3-KW-OV
12	M3	C12	L8	B3	KW	IV	M3C12-L8B3-KW-IV
13	M3	C13	L8	B4	ST	OH	M3C13-L8B4-ST-OH
14	M3	C14	L8	B4	ST	IH	M3C14-L8B4-ST-IH
15	M3	C15	L8	B4	ST	OV	M3C15-L8B4-ST-OV
16	M3	C16	L8	B4	ST	IV	M3C16-L8B4-ST-IV
1	M4	C01	L8	B4	SB	OH	M4C01-L8B4-SB-OH
2	M4	C02	L8	B4	SB	IH	M4C02-L8B4-SB-IH
3	M4	C03	L8	B4	SB	OV	M4C03-L8B4-SB-OV
4	M4	C04	L8	B4	SB	IV	M4C04-L8B4-SB-IV
5	M4	C05	L8	G5	GR	N1	M4C05-L8G5-GR-N1
6	M4	C06	L8	G5	GR	S1	M4C06-L8G5-GR-S1
7	M4	C07	L8	B5	ST	OH	M4C07-L8B5-ST-OH
8	M4	C08	L8	B5	ST	IH	M4C08-L8B5-ST-IH
9	M4	C09	L8	B5	ST	OV	M4C09-L8B5-ST-OV
10	M4	C10	L8	B5	ST	IV	M4C10-L8B5-ST-IV
11	M4	C11	L8	B5	SB	OH	M4C11-L8B5-SB-OH
12	M4	C12	L8	B5	SB	IH	M4C12-L8B5-SB-IH
13	M4	C13	L8	B5	SB	OV	M4C13-L8B5-SB-OV
14	M4	C14	L8	B5	SB	IV	M4C14-L8B5-SB-IV
15	M4	C15	L8	G6	GR	N1	M4C15-L8G6-GR-N1
16	M4	C16	L8	G6	GR	S1	M4C16-L8G6-GR-S1

1	M5	C01	L8	G1	GR	N1	M5C01-L8G1-GR-N1
2	M5	C02	L8	G1	GR	S1	M5C02-L8G1-GR-S1
3	M5	C03	L8	G2	GR	N1	M5C03-L8G2-GR-N1
4	M5	C04	L8	G2	GR	S1	M5C04-L8G2-GR-S1
5	M5	C05	L13	B1	ST	OH	M5C05-L13B1-ST-OH
6	M5	C06	L13	B1	ST	IH	M5C06-L13B1-ST-IH
7	M5	C07	L13	B1	ST	OV	M5C07-L13B1-ST-OV
8	M5	C08	L13	B1	ST	IV	M5C08-L13B1-ST-IV
9	M5	C09	L15	B1	SBE	OH	M5C09-L15B1-SBE-OH
10	M5	C10	L15	B1	SBE	IH	M5C10-L15B1-SBE-IH
11	M5	C11	L15	B1	SBE	OV	M5C11-L15B1-SBE-OV
12	M5	C12	L15	B1	SBE	IV	M5C12-L15B1-SBE-IV
13	M5	C13	L15	B1	SBW	OH	M5C13-L15B1-SBW-OH
14	M5	C14	L15	B1	SBW	IH	M5C14-L15B1-SBW-IH
15	M5	C15	L15	B1	SBW	OV	M5C15-L15B1-SBW-OV
16	M5	C16	L15	B1	SBW	IV	M5C16-L15B1-SBW-IV
1	M6	C01	L13	B1	SBE	OH	M6C01-L13B1-SBE-OH
2	M6	C02	L13	B1	SBE	IH	M6C02-L13B1-SBE-IH
3	M6	C03	L13	B1	SBE	OV	M6C03-L13B1-SBE-OV
4	M6	C04	L13	B1	SBE	IV	M6C04-L13B1-SBE-IV
5	M6	C05	L13	B1	SBW	OH	M6C05-L13B1-SBW-OH
6	M6	C06	L13	B1	SBW	IH	M6C06-L13B1-SBW-IH
7	M6	C07	L13	B1	SBW	OV	M6C07-L13B1-SBW-OV

8	M6	C08	L13	B1	SBW	IV	M6C08-L13B1-SBW-IV
9	M6	C09	L13	B1	KE	OH	M6C09-L13B1-KE-OH
10	M6	C10	L13	B1	KE	IH	M6C10-L13B1-KE-IH
11	M6	C11	L13	B1	KE	OV	M6C11-L13B1-KE-OV
12	M6	C12	L13	B1	KE	IV	M6C12-L13B1-KE-IV
13	M6	C13	L13	B1	KW	OH	M6C13-L13B1-KW-OH
14	M6	C14	L13	B1	KW	IH	M6C14-L13B1-KW-IH
15	M6	C15	L13	B1	KW	OV	M6C15-L13B1-KW-OV
16	M6	C16	L13	B1	KW	IV	M6C16-L13B1-KW-IV
1	M7	C01	L13	B2	ST	IHE	M7C01-L13B2-ST-IHE
2	M7	C02	L13	B2	ST	IVE	M7C02-L13B2-ST-IVE
3	M7	C03	L13	B2	ST	IHW	M7C03-L13B2-ST-IHW
4	M7	C04	L13	B2	ST	IVW	M7C04-L13B2-ST-IVW
5	M7	C05	L13	B2	SB	IHE	M7C05-L13B2-SB-IHE
6	M7	C06	L13	B2	SB	IVE	M7C06-L13B2-SB-IVE
7	M7	C07	L13	B2	SB	IHW	M7C07-L13B2-SB-IHW
8	M7	C08	L13	B2	SB	IVW	M7C08-L13B2-SB-IVW
9	M7	C09	L13	B3	ST	IHN	M7C09-L13B3-ST-IHN
10	M7	C10	L13	B3	ST	IVN	M7C10-L13B3-ST-IVN
11	M7	C11	L13	B3	ST	HIS	M7C11-L13B3-ST-HIS
12	M7	C12	L13	B3	ST	IVS	M7C12-L13B3-ST-IVS
13	M7	C13	L13	B3	SB	OHN	M7C13-L13B3-SB-OHN
14	M7	C14	L13	B3	SB	IVN	M7C14-L13B3-SB-IVN

15	M7	C15	L13	B3	SB	OHS	M7C15-L13B3-SB-OHS
16	M7	C16	L13	B3	SB	IVS	M7C16-L13B3-SB-IVS
1	M8	C01	L15	B1	KE	OH	M8C01-L15B1-KE-OH
2	M8	C02	L15	B1	KE	IH	M8C02-L15B1-KE-IH
3	M8	C03	L15	B1	KE	OV	M8C03-L15B1-KE-OV
4	M8	C04	L15	B1	KE	IV	M8C04-L15B1-KE-IV
5	M8	C05	L15	B1	KW	OH	M8C05-L15B1-KW-OH
6	M8	C06	L15	B1	KW	IH	M8C06-L15B1-KW-IH
7	M8	C07	L15	B1	KW	OV	M8C07-L15B1-KW-OV
8	M8	C08	L15	B1	KW	IV	M8C08-L15B1-KW-IV
9	M8	C09	L15	B2	ST	IHE	M8C09-L15B2-ST-IHE
10	M8	C10	L15	B2	ST	IVE	M8C10-L15B2-ST-IVE
11	M8	C11	L15	B2	ST	IHW	M8C11-L15B2-ST-IHW
12	M8	C12	L15	B2	ST	IVW	M8C12-L15B2-ST-IVW
13	M8	C13	L15	B2	SB	OHN	M8C13-L15B2-SB-OHN
14	M8	C14	L15	B2	SB	IVN	M8C14-L15B2-SB-IVN
15	M8	C15	L15	B2	SB	OHS	M8C15-L15B2-SB-OHS
16	M8	C16	L15	B2	SB	IVS	M8C16-L15B2-SB-IVS

Appendix F. Chisholm Trail Bridge Live Load Testing Layouts

Load Case #1

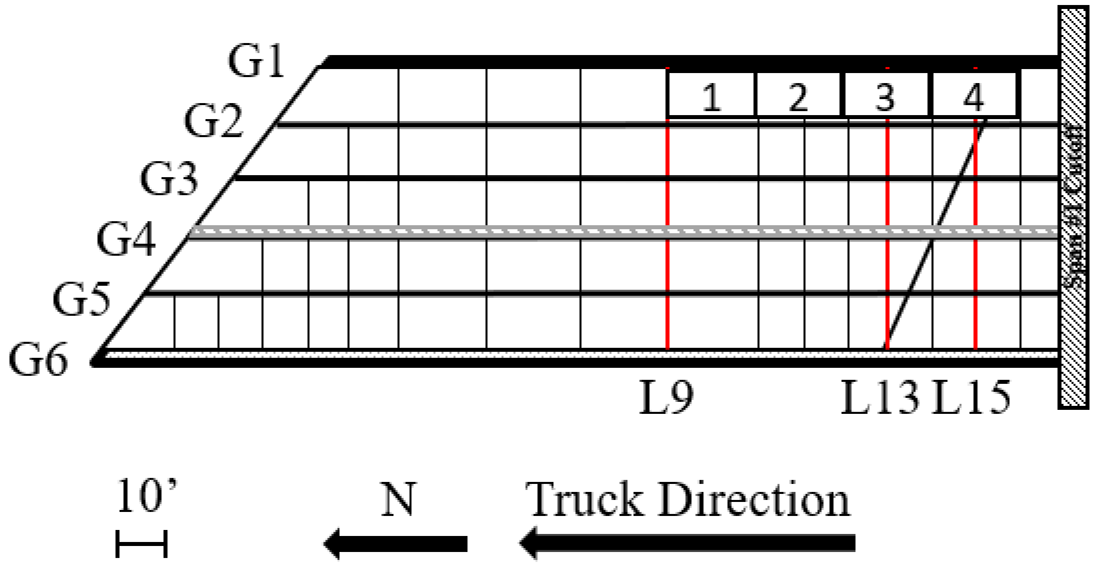

Load Case #2

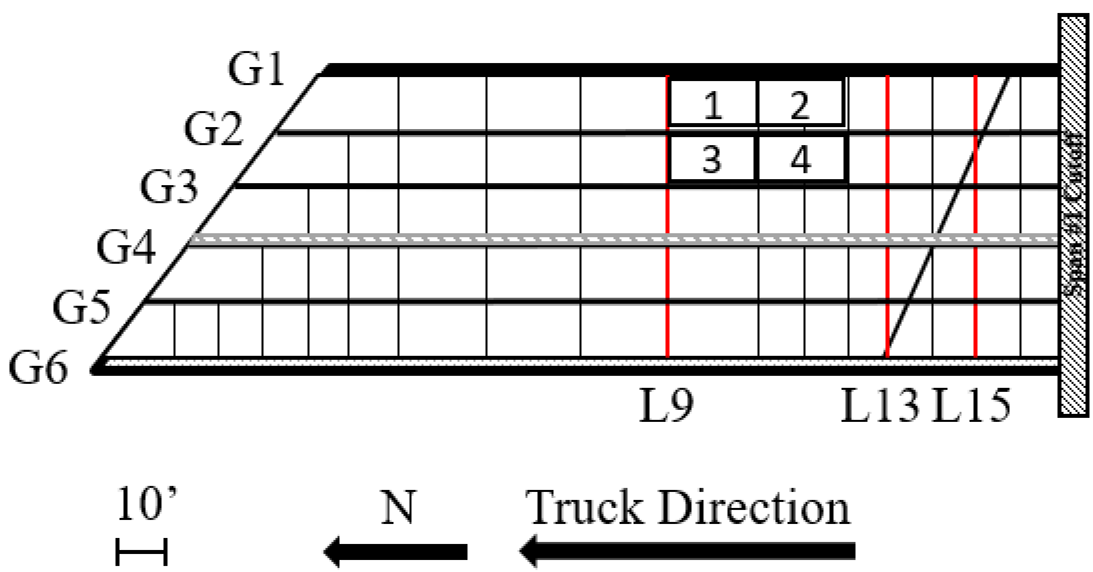

Load Case #3

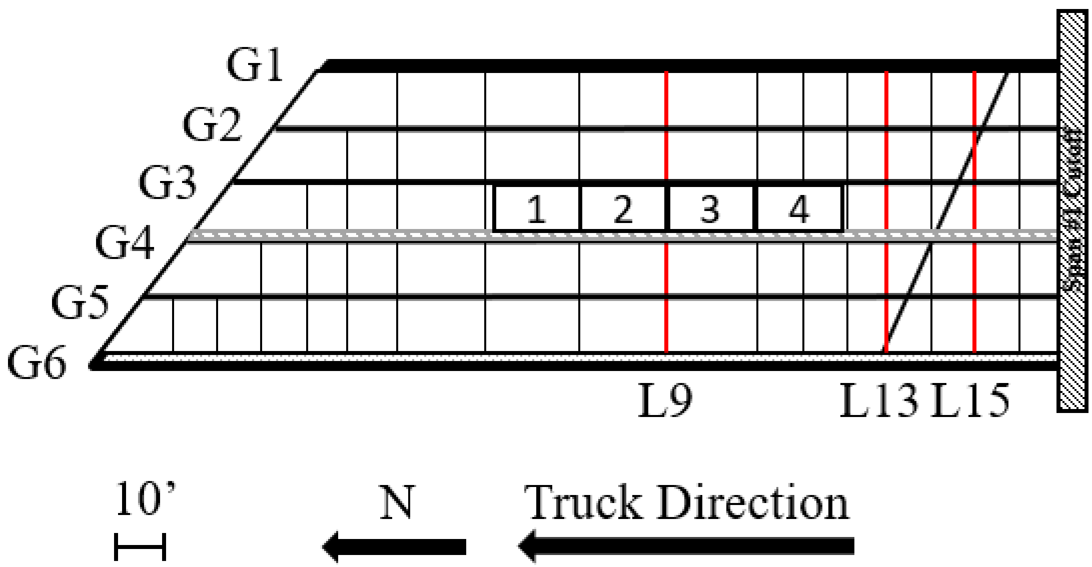

Load Case #4

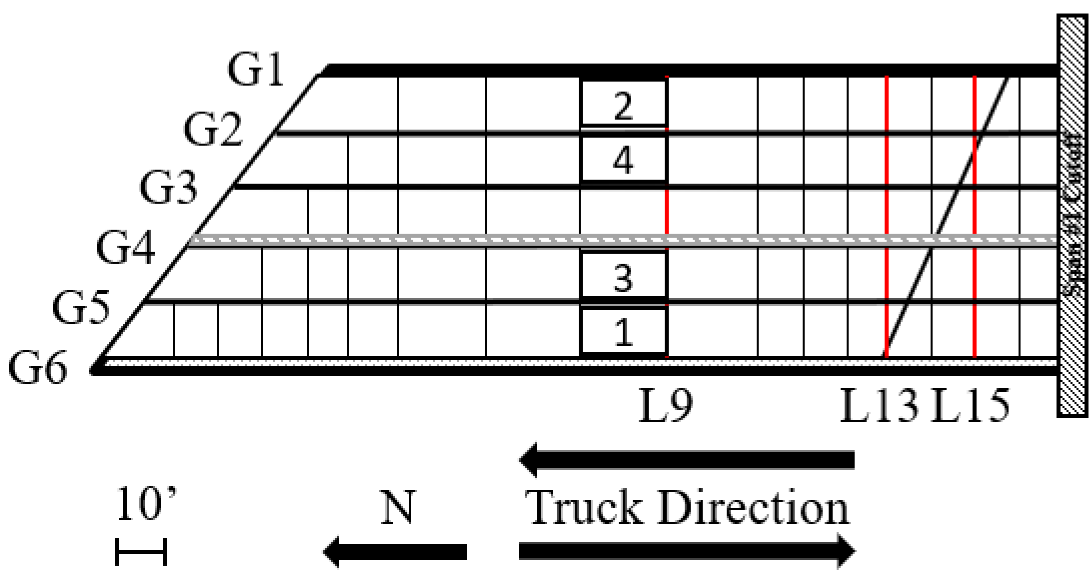

Load Case #5

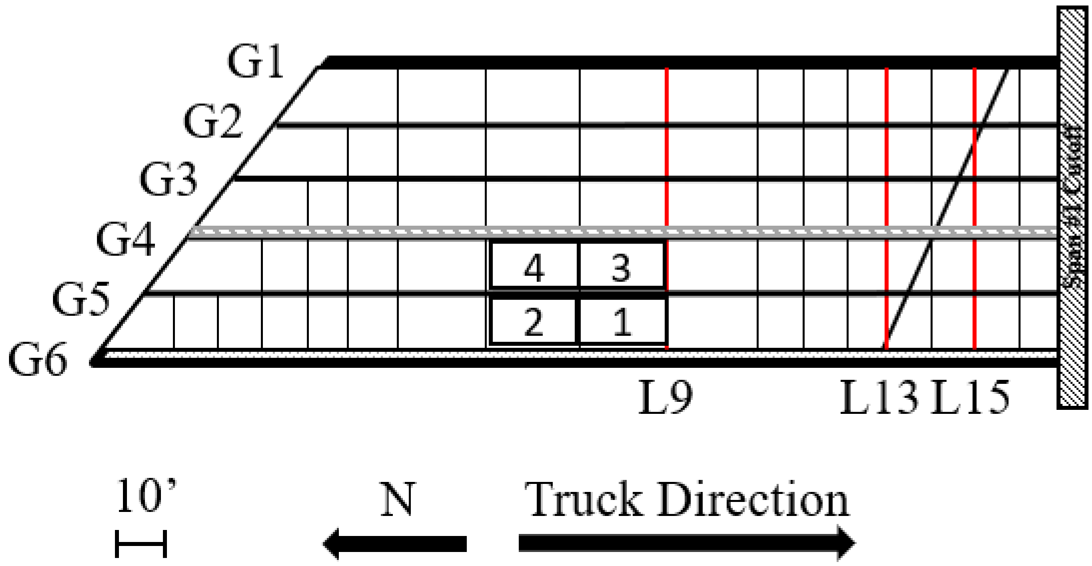

Load Case #6

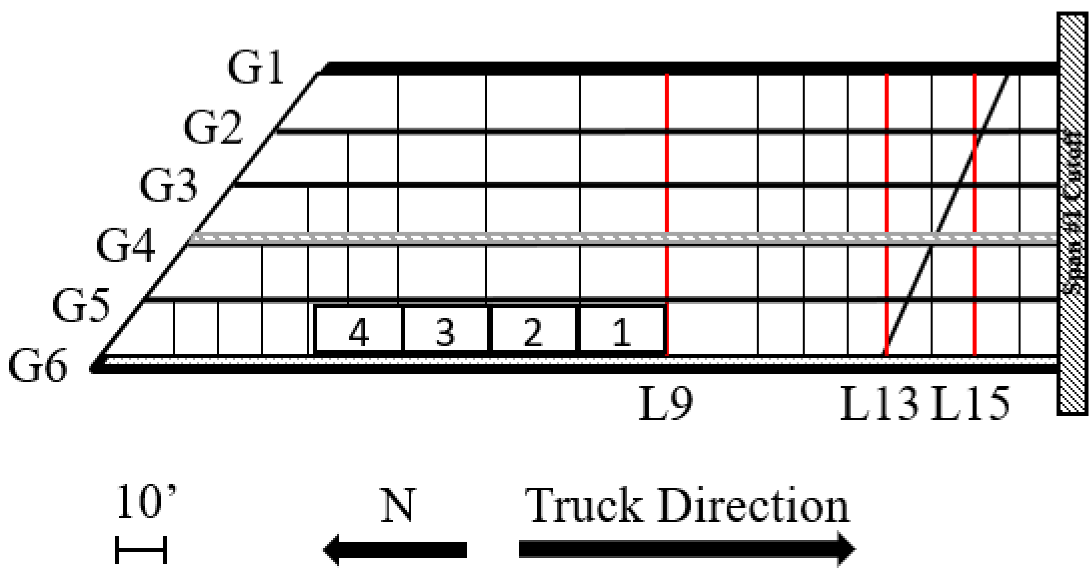

Appendix G. Lubbock Bridge Live Load Testing Layouts

Load Case Staggered Ahead Station

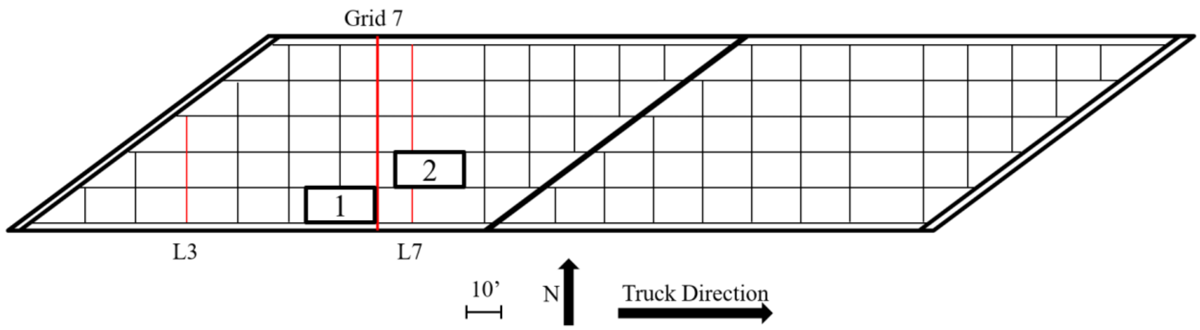

Load Case Staggered Behind Station

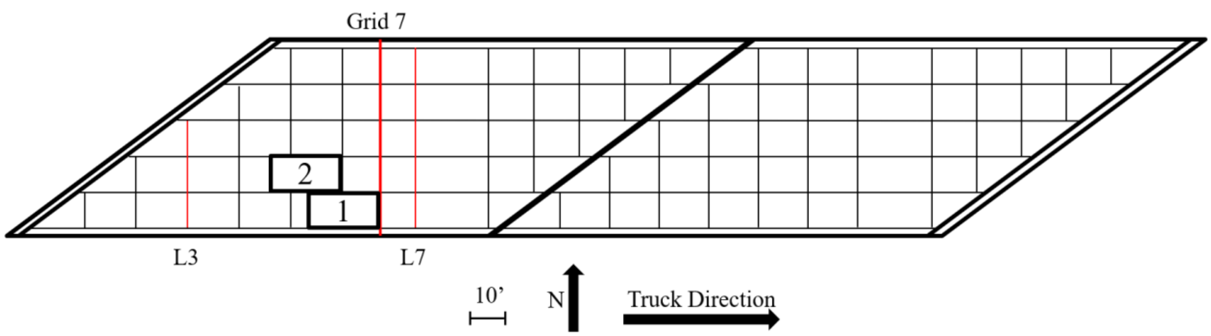

Load Case Side-by-Side South

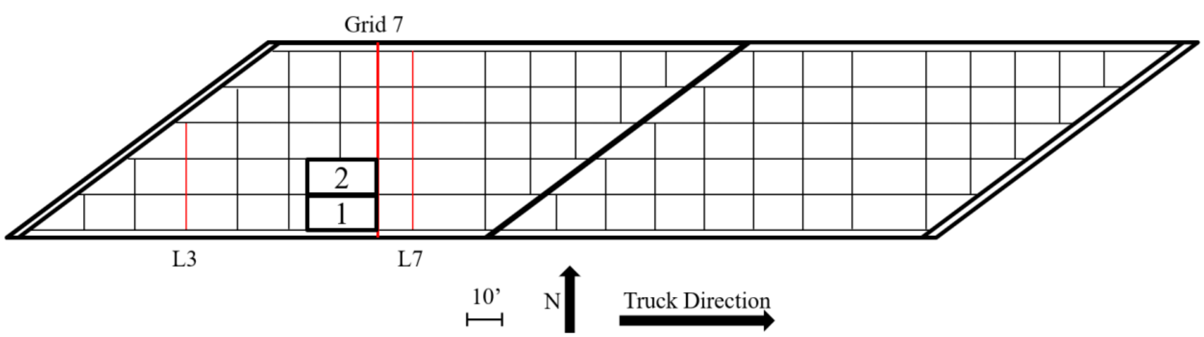

Load Case Side-by-Side North

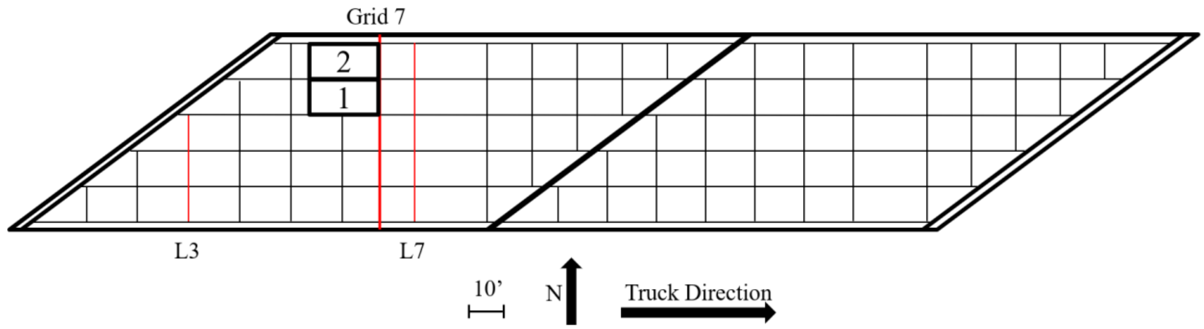

Load Case End-to-End South

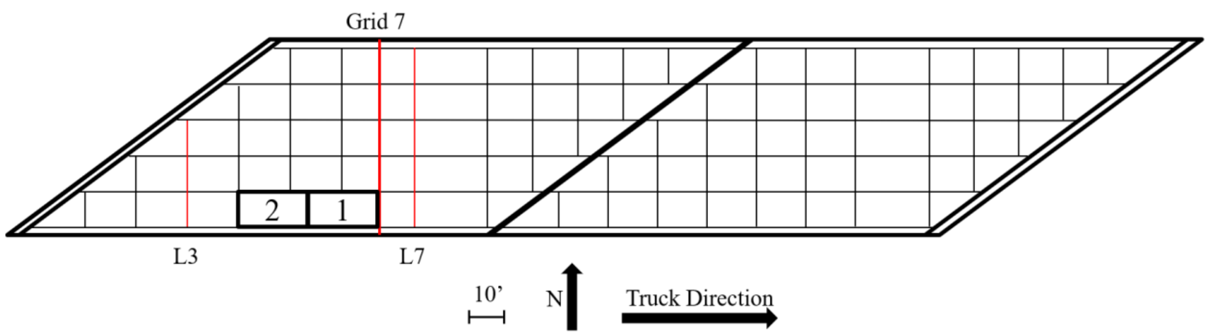

Load Case End-to-End Central

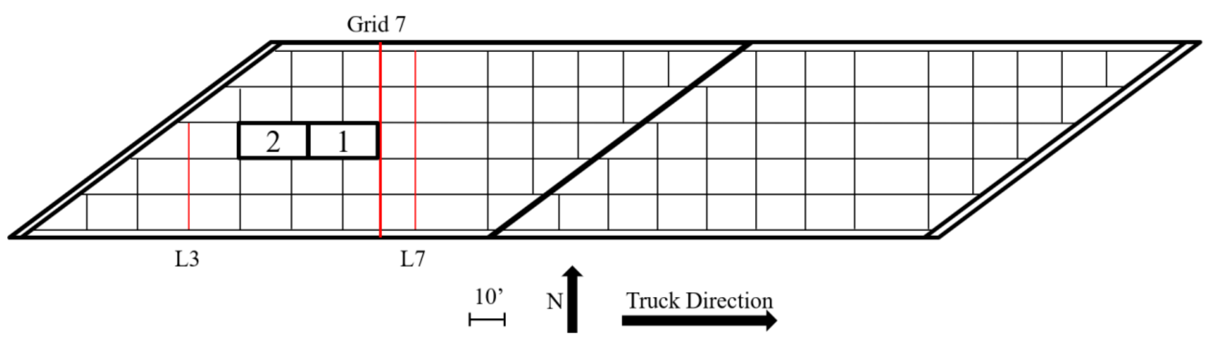

Appendix H. Axial Force Sample Calculations

Sample Problem - 20 kip Pure Axial Load

Measured Strains and Locations

Area of member $A := 6.45\ in^2$

centroid i.e. origin of member: $x0 := 0$ in $y0 := 0$ in

strain 1 - OH	$\varepsilon 1 := 107$	microstrain	$x1 := 3.3\ in$	$y1 := 1.7\ in$
strain 2 - IH	$\varepsilon 2 := 107$	microstrain	$x2 := 3.3\ in$	$y2 := 1.14\ in$
strain 3 - OV	$\varepsilon 3 := 107$	microstrain	$x3 := -1.7\ in$	$y3 := -3.3\ in$
strain 4 - IV	$\varepsilon 4 := 107$	microstrain	$x4 := -1.14\ in$	$y4 := -3.3\ in$

Calculations

$$\varepsilon b := \frac{\varepsilon 1 + \varepsilon 2 + \varepsilon 3 + \varepsilon 4}{4} = 107$$

$$xb := \frac{x1 + x2 + x3 + x4}{4} = 0.94\ in$$ [ε_bar, x_bar, y_bar]

$$yb := \frac{y1 + y2 + y3 + y4}{4} = -0.94\ in$$

$$I_{11} := (x1 - xb)^2 + (x2 - xb)^2 + (x3 - xb)^2 + (x4 - xb)^2 = 22.435\ in^2$$

$$I_{22} := (y1 - yb)^2 + (y2 - yb)^2 + (y3 - yb)^2 + (y4 - yb)^2 = 22.435\ in^2$$

$$I_{12} := (x1 - xb)(y1 - yb) + (x2 - xb)(y2 - yb) + (x3 - xb)(y3 - yb) + (x4 - xb)(y4 - yb)$$

$$I_{21} := I_{12} = 22.278\ in^2$$

$$I_{10} := (x1 - xb)(\varepsilon 1 - \varepsilon b) + (x2 - xb)(\varepsilon 2 - \varepsilon b) + (x3 - xb)(\varepsilon 3 - \varepsilon b) + (x4 - xb)(\varepsilon 4 - \varepsilon b)$$

$$I_{10} = 0\ in$$

$$I_{20} := (y1 - yb)(\varepsilon 1 - \varepsilon b) + (y2 - yb)(\varepsilon 2 - \varepsilon b) + (y3 - yb)(\varepsilon 3 - \varepsilon b) + (y4 - yb)(\varepsilon 4 - \varepsilon b)$$

$$I_{20} = 0\ in$$

Solve for b and c using   I11*b + I12*c = I10   and   I21*b + I22*c = I20

$$I_{11} \cdot b + I_{12} \cdot c = I_{10}$$
$$I_{21} \cdot b + I_{22} \cdot c = I_{20}$$

$$M := \begin{bmatrix} I_{11} & I_{12} \\ I_{21} & I_{22} \end{bmatrix}$$

$$v := \begin{bmatrix} I_{10} \\ I_{20} \end{bmatrix}$$

$$\begin{bmatrix} b \\ c \end{bmatrix} := M^{-1} \cdot v = \begin{bmatrix} 0 \\ 0 \end{bmatrix} \frac{1}{m}$$

$a := \varepsilon b - b \cdot xb - c \cdot yb = 107$ microstrain

Axial Stress

Axial Stress

$E := 29000\ ksi$

$\sigma := E \cdot \dfrac{a}{10^6} = 3.103\ ksi$ 10^6 for microstrain

Axial Force

$F := A \cdot \sigma = 20\ kip$

Sample Problem - 20 kip Axial and 0.01 k/ft Transverse Loading

***orientation change for Strand7 validation

Measured Strains and Locations

Area of member $A := 6.45\ in^2$

centroid i.e. origin of member: $x0 := 0$ in $y0 := 0$ in

strain 1 - OH	$\varepsilon 1 := 155$	microstrain	$x1 := 3.3\ in$	$y1 := -1.7\ in$
strain 2 - IH	$\varepsilon 2 := 131$	microstrain	$x2 := 3.3\ in$	$y2 := -1.14\ in$
strain 3 - OV	$\varepsilon 3 := -8.6$	microstrain	$x3 := -1.7\ in$	$y3 := 3.3\ in$
strain 4 - IV	$\varepsilon 4 := -14.5$	microstrain	$x4 := -1.14\ in$	$y4 := 3.3\ in$

Calculations

$$\varepsilon b := \frac{\varepsilon 1 + \varepsilon 2 + \varepsilon 3 + \varepsilon 4}{4} = 65.725$$

$$xb := \frac{x1 + x2 + x3 + x4}{4} = 0.94\ in$$ [ε _bar, x_bar, y_bar]

$$yb := \frac{y1 + y2 + y3 + y4}{4} = 0.94\ in$$

$$I_{11} := (x1 - xb)^2 + (x2 - xb)^2 + (x3 - xb)^2 + (x4 - xb)^2 = 22.435\ in^2$$

$$I_{22} := (y1 - yb)^2 + (y2 - yb)^2 + (y3 - yb)^2 + (y4 - yb)^2 = 22.435\ in^2$$

$$I_{12} := (x1 - xb)\ (y1 - yb) + (x2 - xb)\ (y2 - yb) + (x3 - xb)\ (y3 - yb) + (x4 - xb)\ (y4 - yb)$$

$$I_{21} := I_{12} = -22.278\ in^2$$

$$I_{10} := (x1 - xb)\ (\varepsilon 1 - \varepsilon b) + (x2 - xb)\ (\varepsilon 2 - \varepsilon b) + (x3 - xb)\ (\varepsilon 3 - \varepsilon b) + (x4 - xb)\ (\varepsilon 4 - \varepsilon b)$$

$$I_{10} = 727.824\ in$$

$$I_{20} := (y1 - yb)\ (\varepsilon 1 - \varepsilon b) + (y2 - yb)\ (\varepsilon 2 - \varepsilon b) + (y3 - yb)\ (\varepsilon 3 - \varepsilon b) + (y4 - yb)\ (\varepsilon 4 - \varepsilon b)$$

$$I_{20} = -736.196\ in$$

Solve for b and c using I11*b + I12*c = I10 and I21*b + I22*c = I20

$$I_{11} \cdot b + I_{12} \cdot c = I_{10}$$
$$I_{21} \cdot b + I_{22} \cdot c = I_{20}$$

$$M := \begin{bmatrix} I_{11} & I_{12} \\ I_{21} & I_{22} \end{bmatrix}$$

$$v := \begin{bmatrix} I_{10} \\ I_{20} \end{bmatrix}$$

$$\begin{bmatrix} b \\ c \end{bmatrix} := M^{-1} \cdot v = \begin{bmatrix} -406.5097 \\ -1.6956 \cdot 10^{3} \end{bmatrix} \frac{1}{m}$$

$$a := \varepsilon b - b \cdot xb - c \cdot yb = 115.914$$ microstrain

Axial Stress

Axial Stress

$$E := 29000\ ksi$$

$$\sigma := E \cdot \frac{a}{10^{6}} = 3.362\ ksi$$ 10^6 for microstrain

Axial Force

$$F := A \cdot \sigma = 22\ kip$$

Appendix I. SH-105 Bridge Axial Forces and Deflections

CFL #3 [SA] - Load Case #1 - Axial Force [kip]

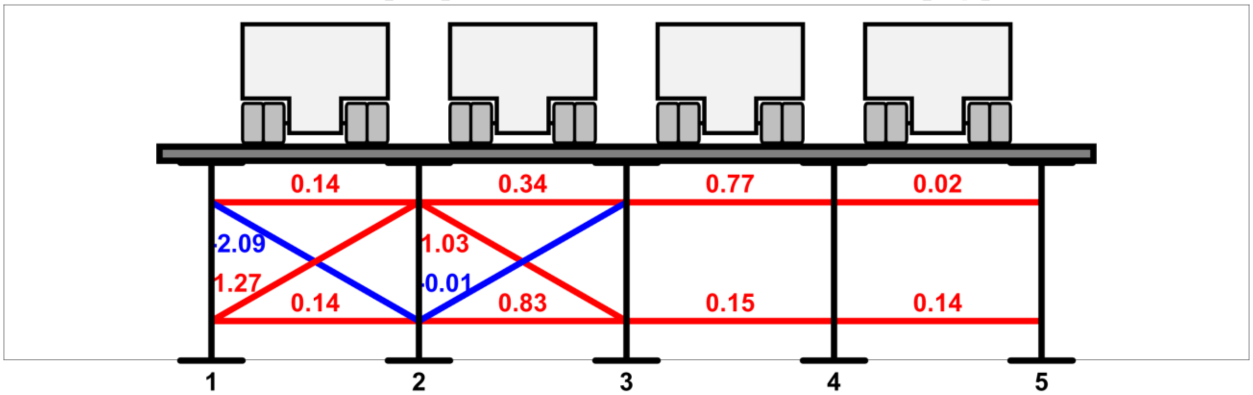

CFL #5 [SA] - Load Case #1 - Axial Force [kip]

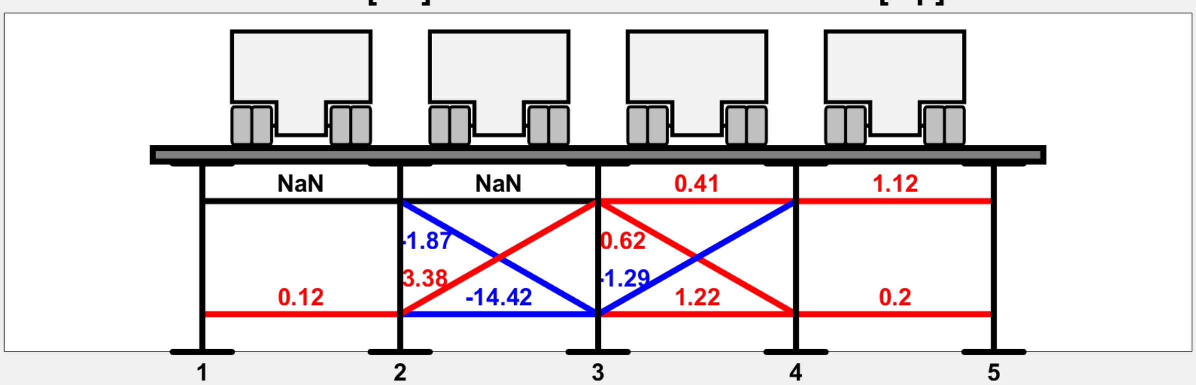

Measured Deflections [in]

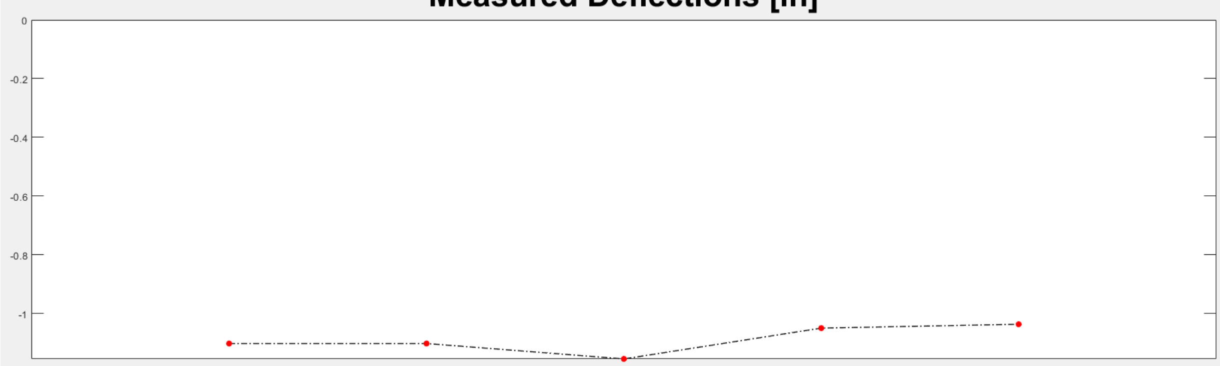

CFL #3 [SA] - Load Case #2 - Axial Force [kip]

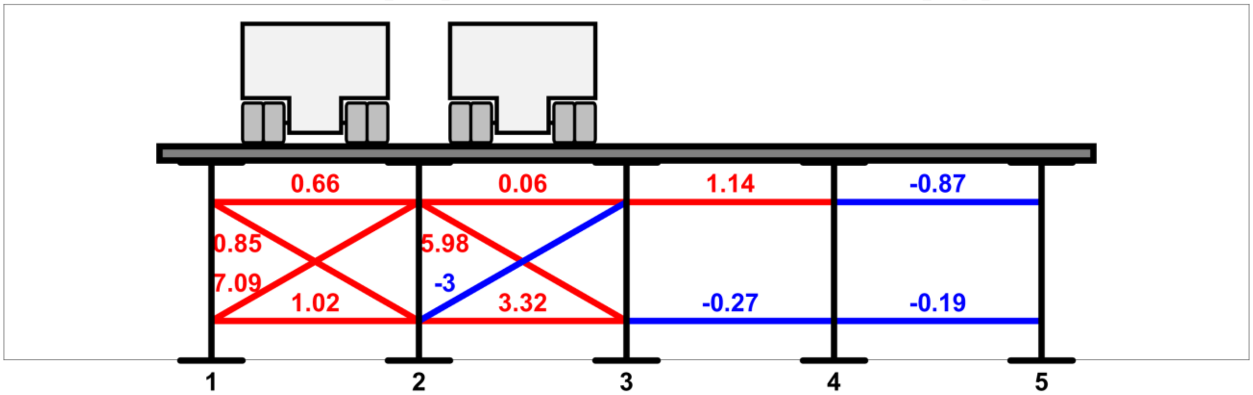

CFL #5 [SA] - Load Case #2 - Axial Force [kip]

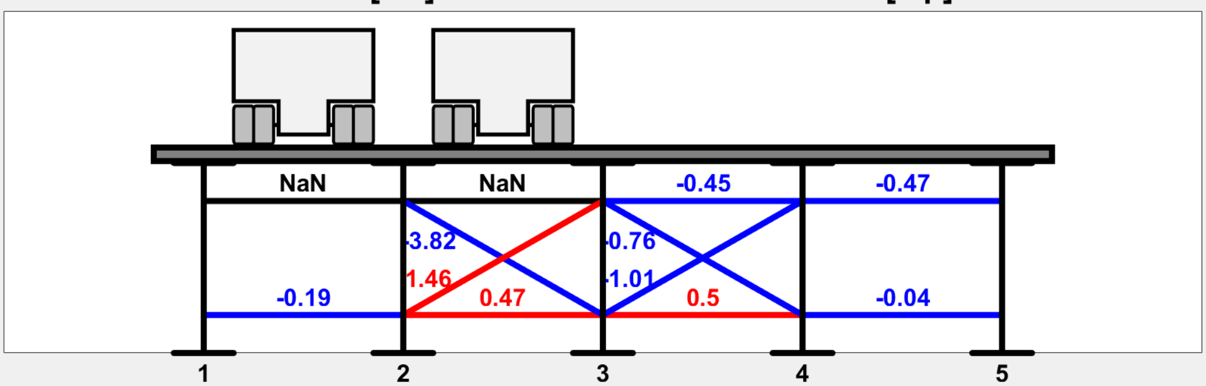

Measured Deflections [in]

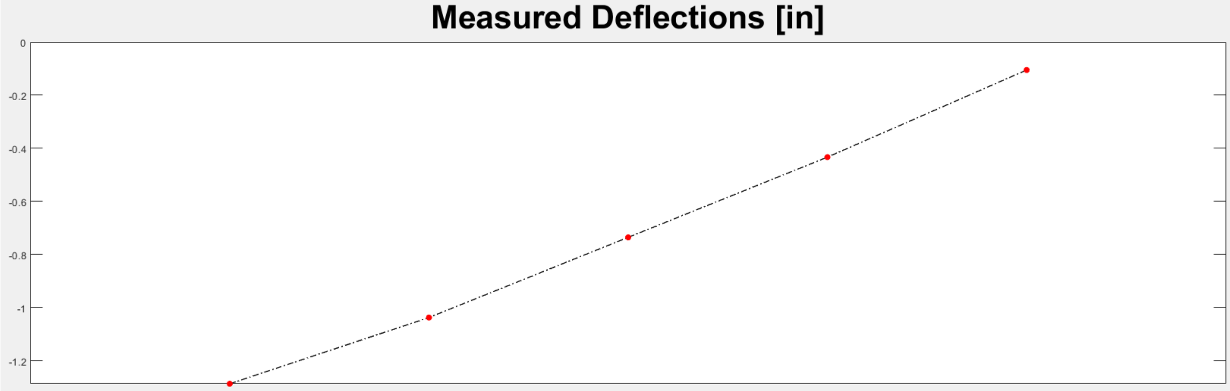

CFL #3 [SA] - Load Case #3 - Axial Force [kip]

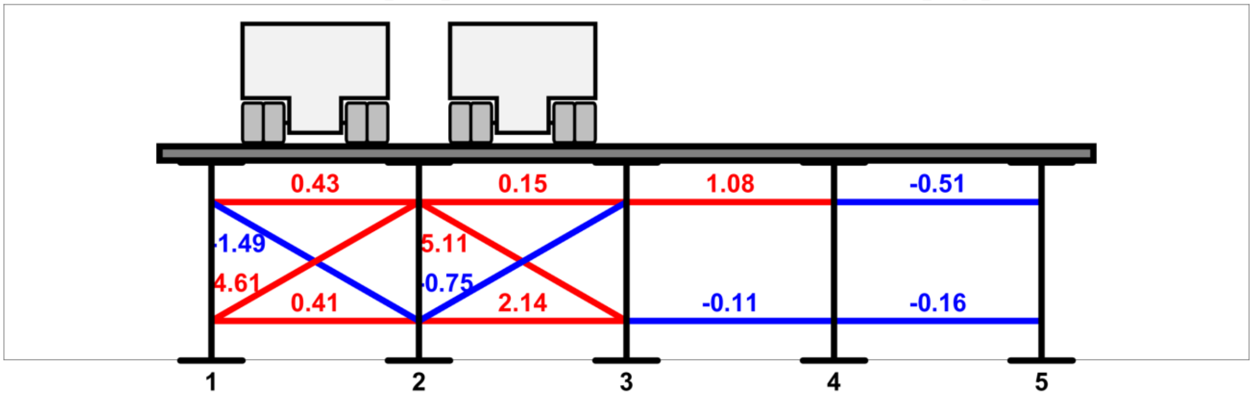

CFL #5 [SA] - Load Case #3 - Axial Force [kip]

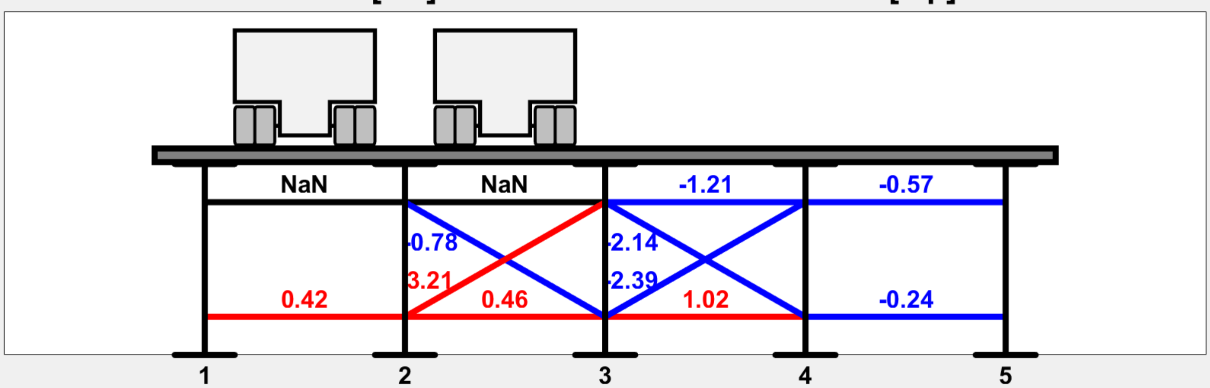

Measured Deflections [in]

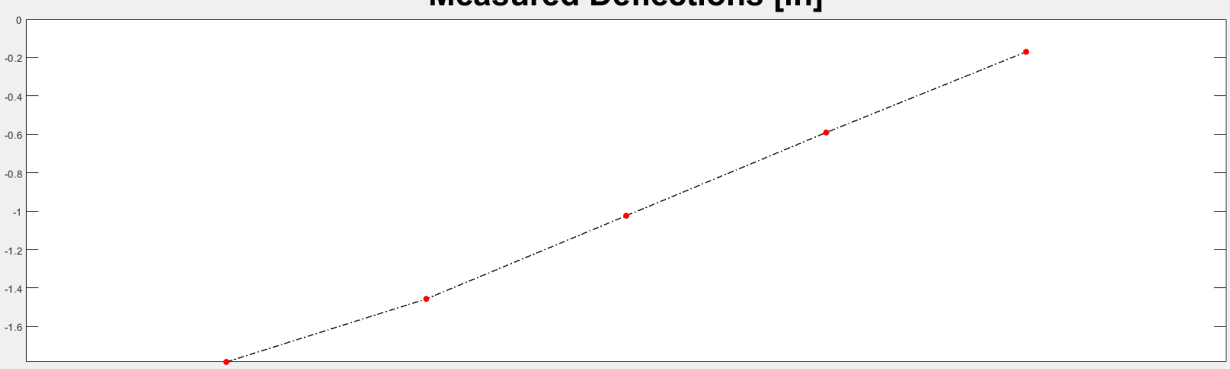

CFL #3 [SA] - Load Case #4 - Axial Force [kip]

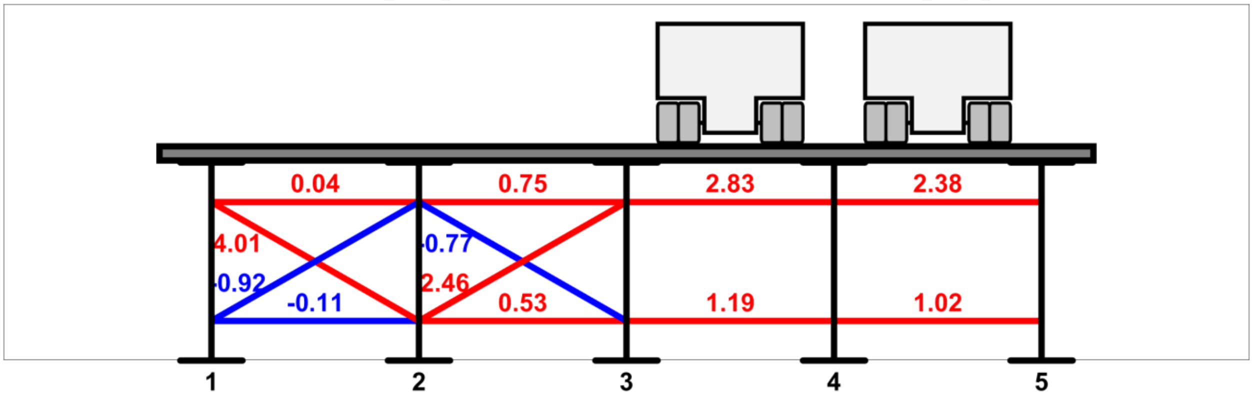

CFL #5 [SA] - Load Case #4 - Axial Force [kip]

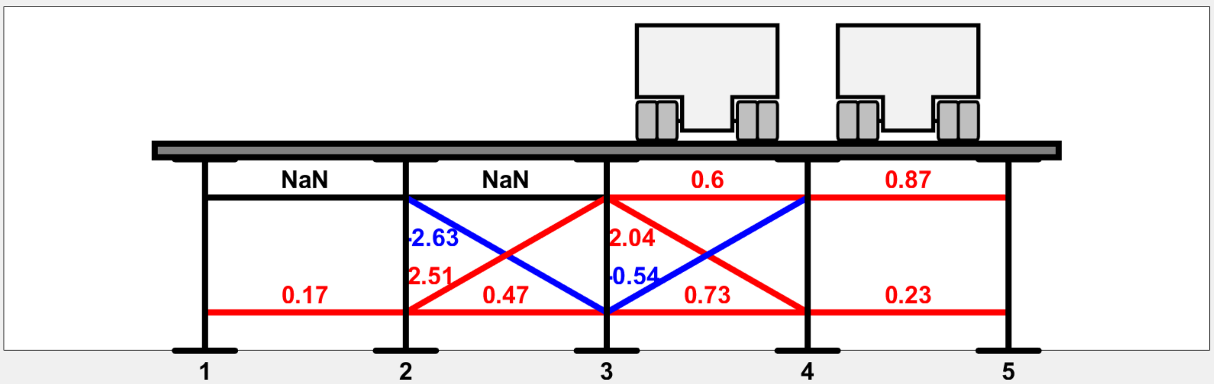

Measured Deflections [in]

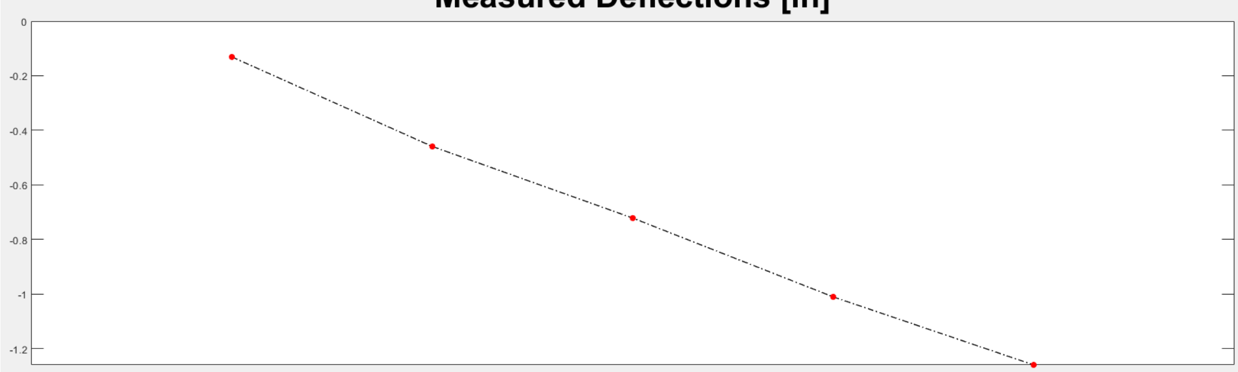

CFL #3 [SA] - Load Case #5 - Axial Force [kip]

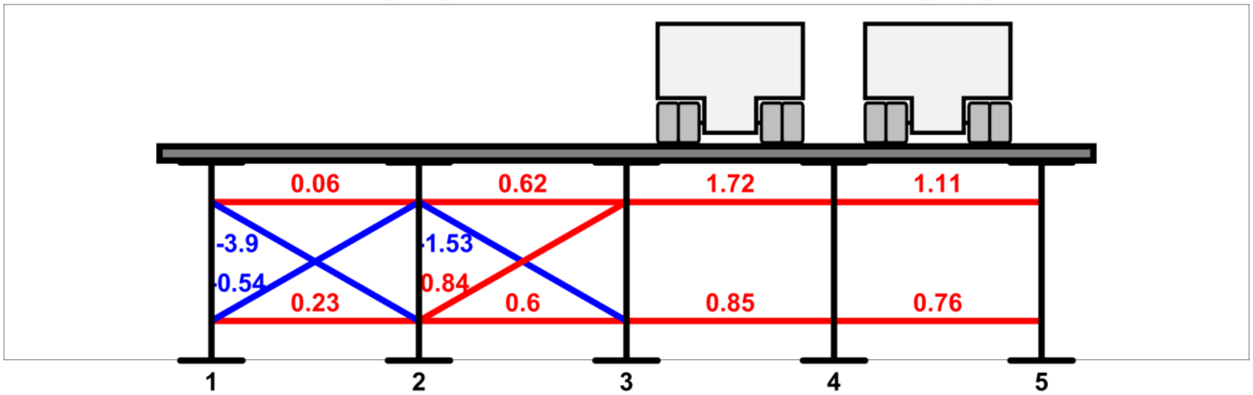

CFL #5 [SA] - Load Case #5 - Axial Force [kip]

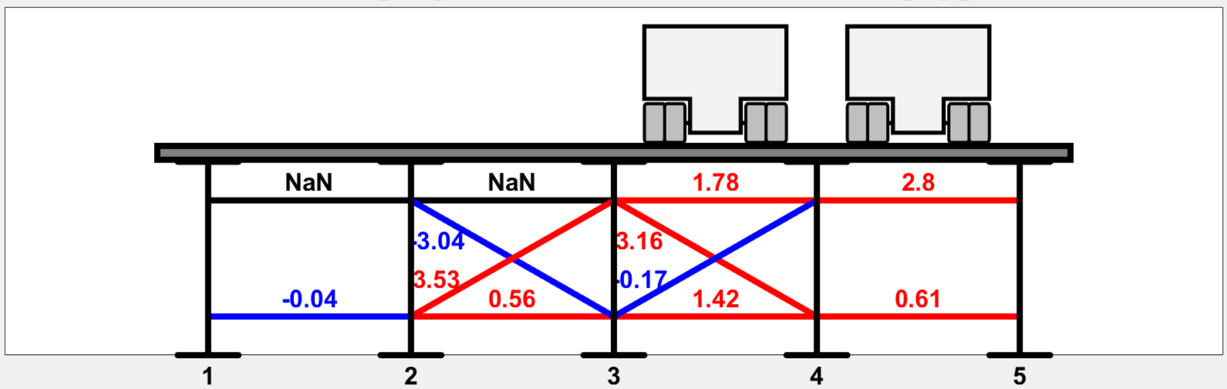

Measured Deflections [in]

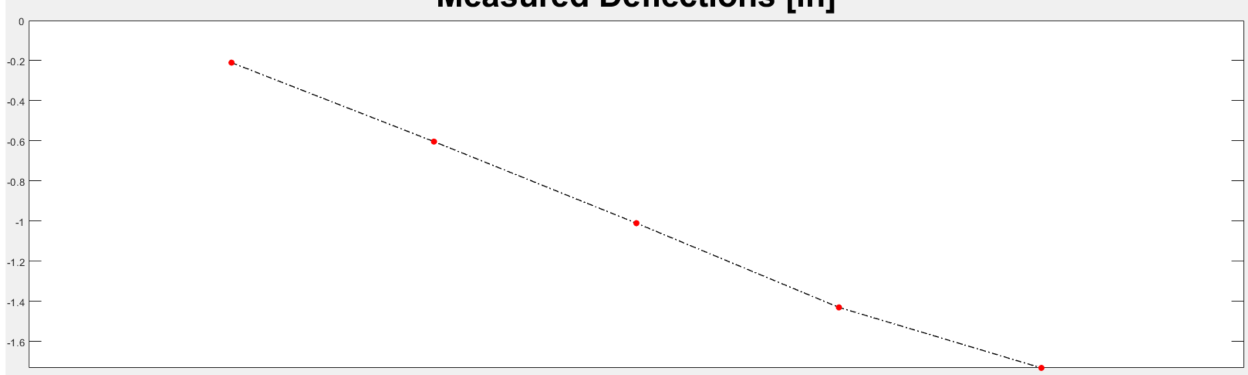

CFL #3 [SA] - Load Case #6 - Axial Force [kip]

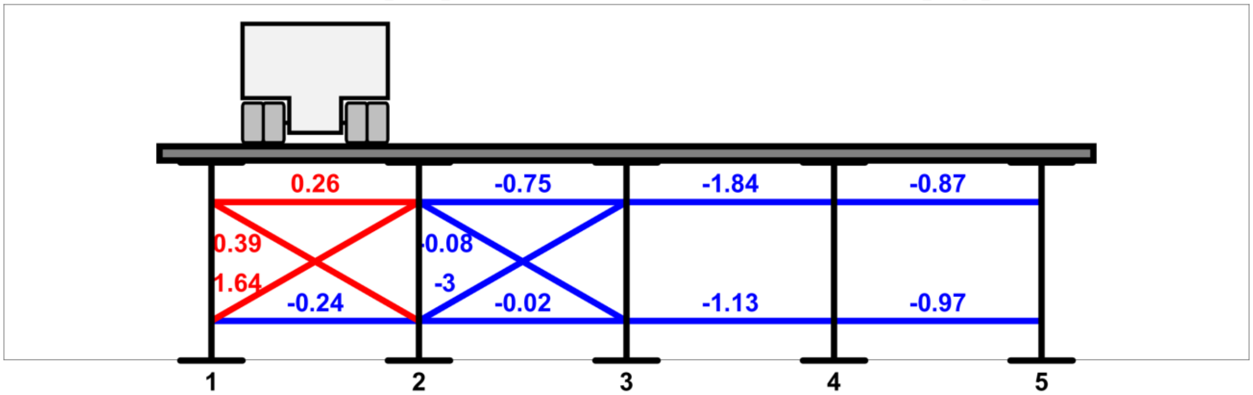

CFL #5 [SA] - Load Case #6 - Axial Force [kip]

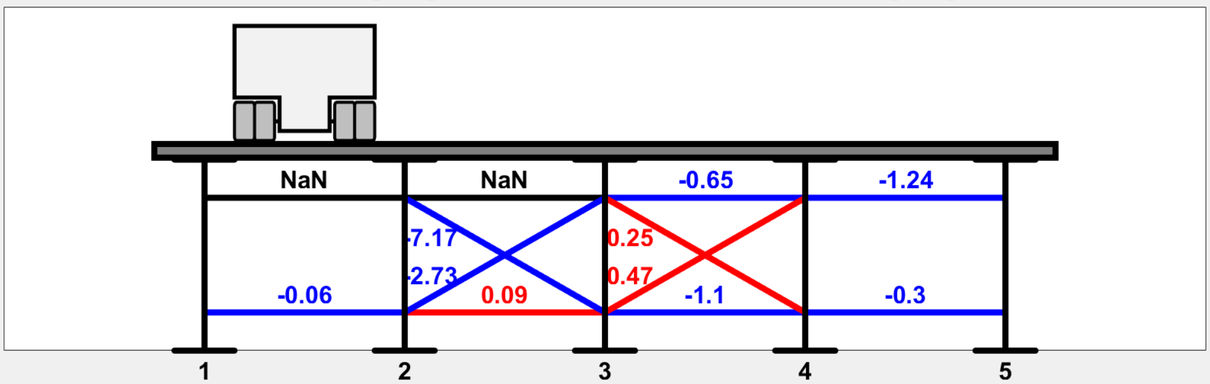

Measured Deflections [in]

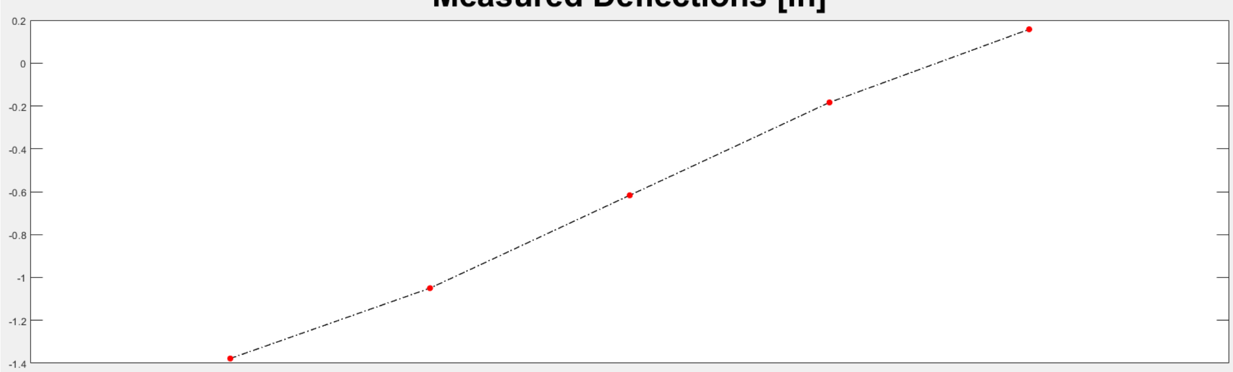

CFL #3 [SA] - Load Case #7 - Axial Force [kip]

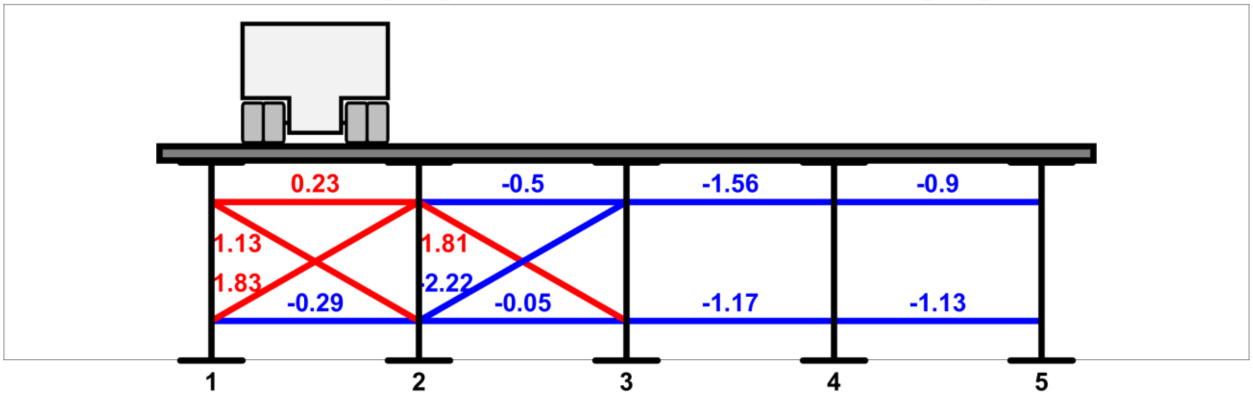

CFL #5 [SA] - Load Case #7 - Axial Force [kip]

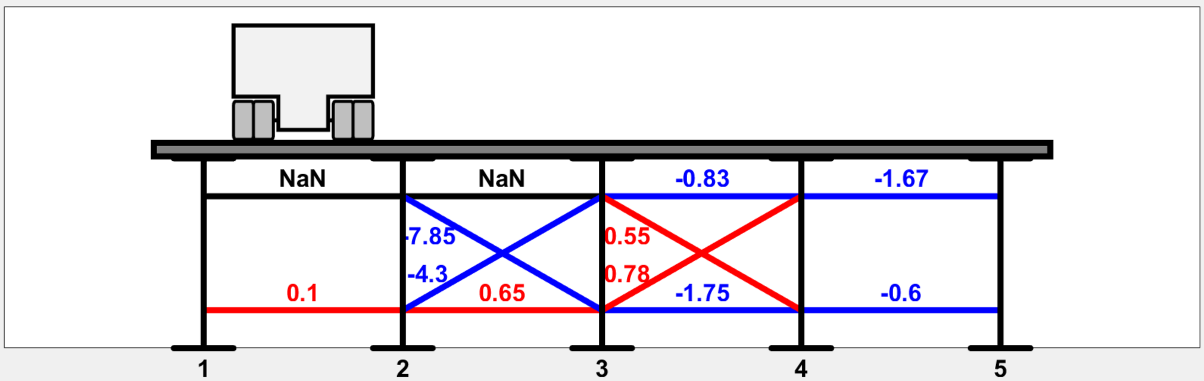

Measured Deflections [in]

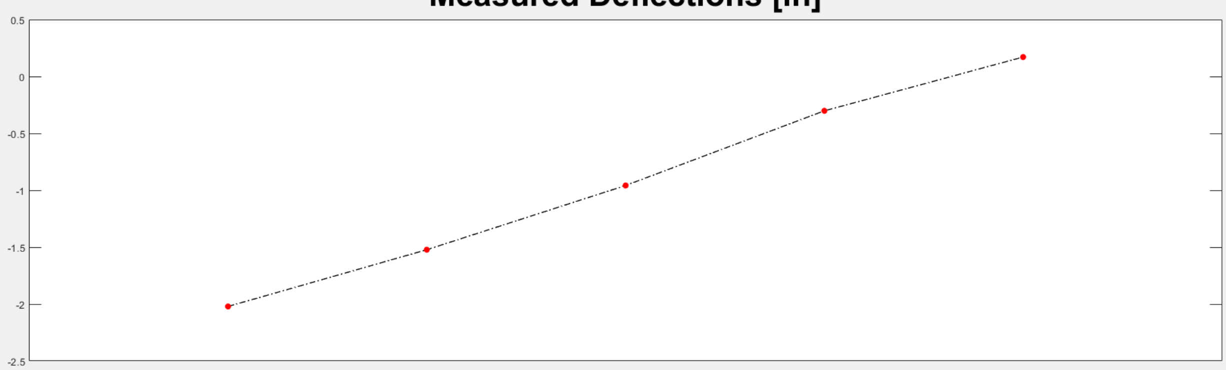

CFL #3 [SA] - Load Case #8 - Axial Force [kip]

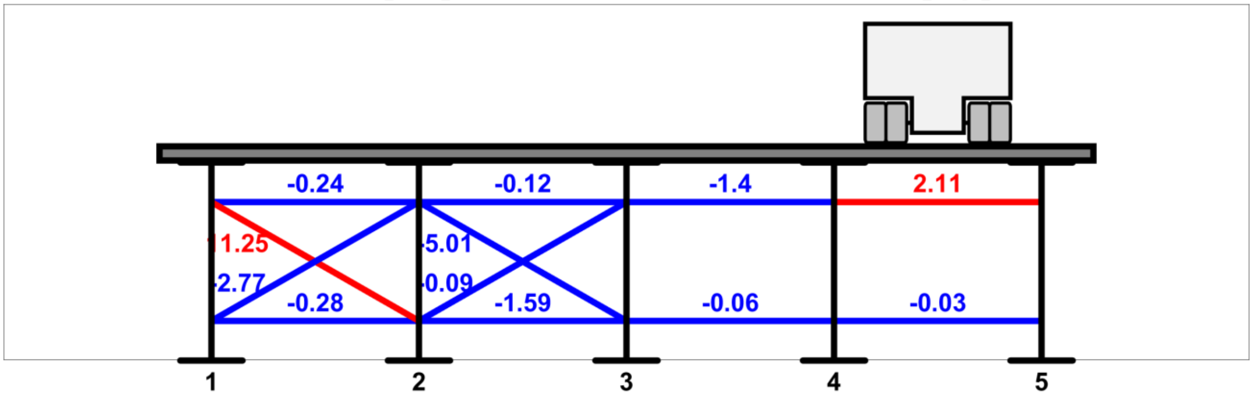

CFL #5 [SA] - Load Case #8 - Axial Force [kip]

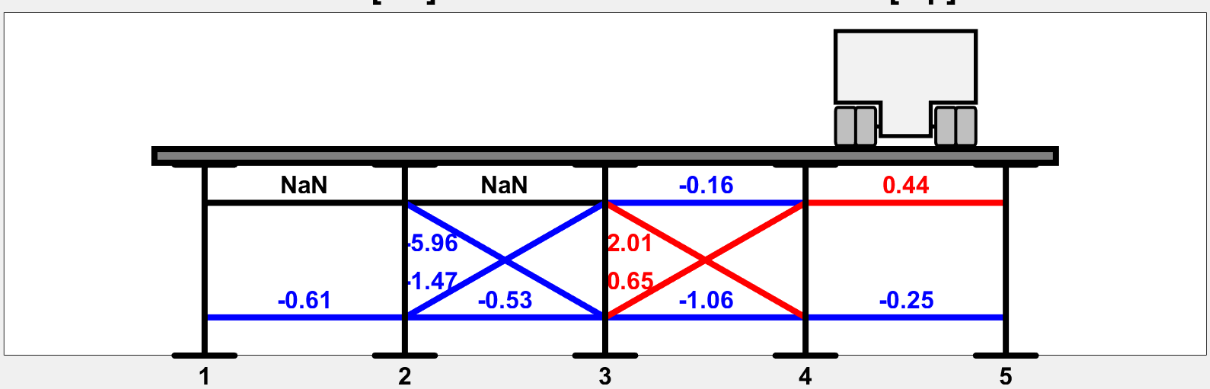

Measured Deflections [in]

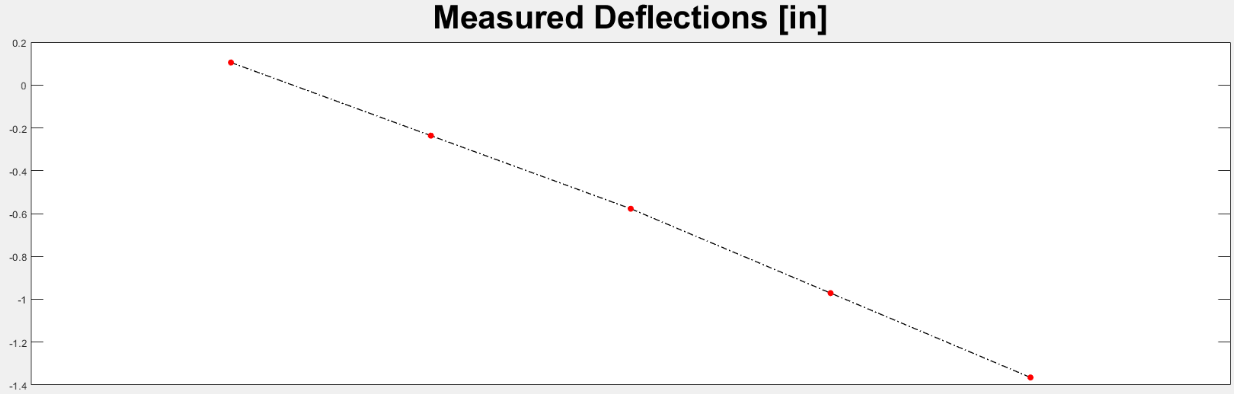

CFL #3 [SA] - Load Case #9 - Axial Force [kip]

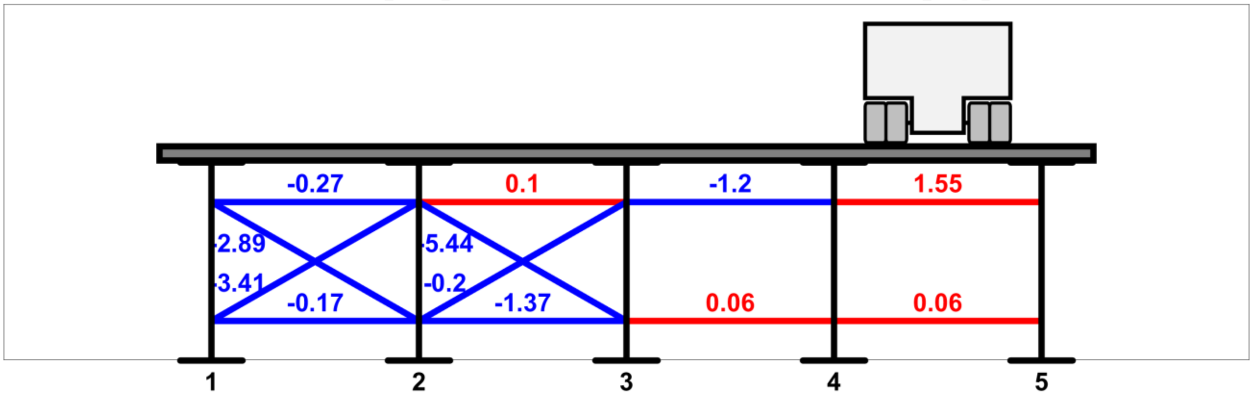

CFL #5 [SA] - Load Case #9 - Axial Force [kip]

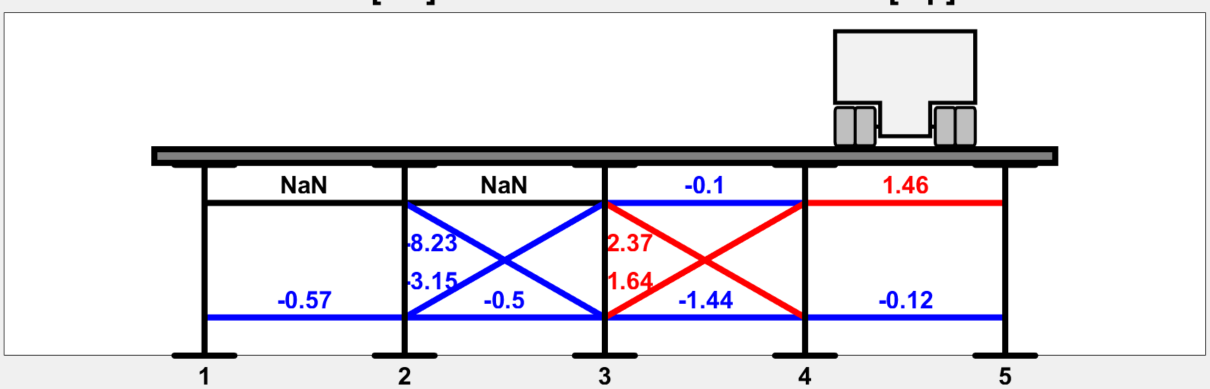

Measured Deflections [in]

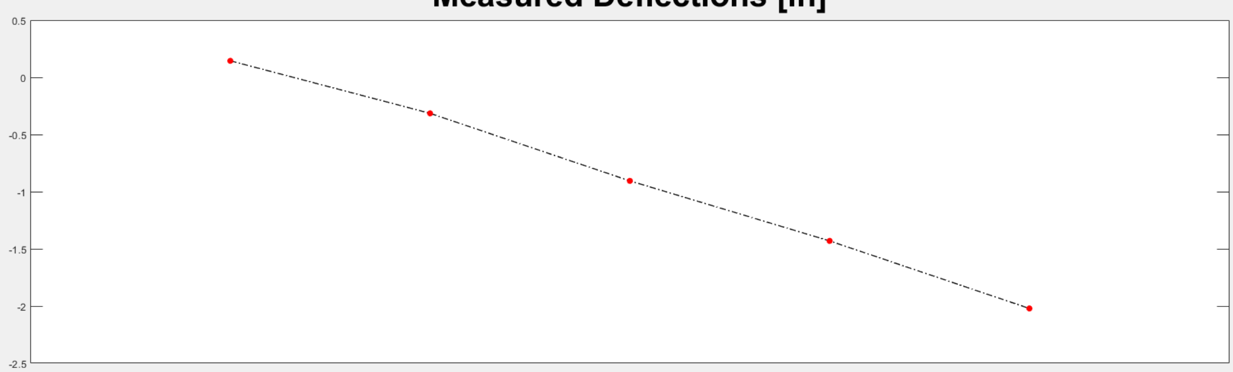

Appendix J. Chisholm Trail Bridge Axial Forces and Deflections

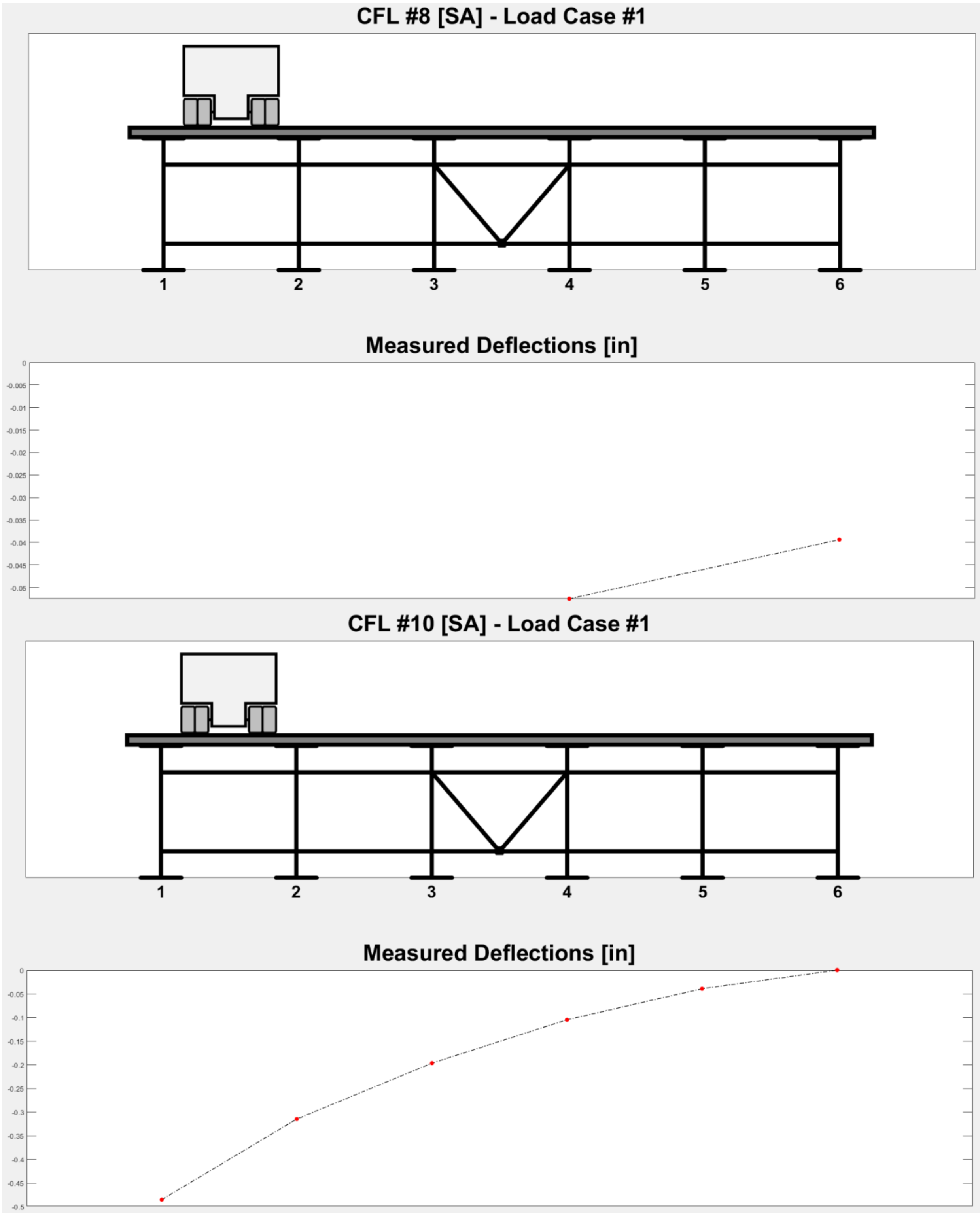

CFL #9 [SA] - Load Case #1 - Axial Force [kip]

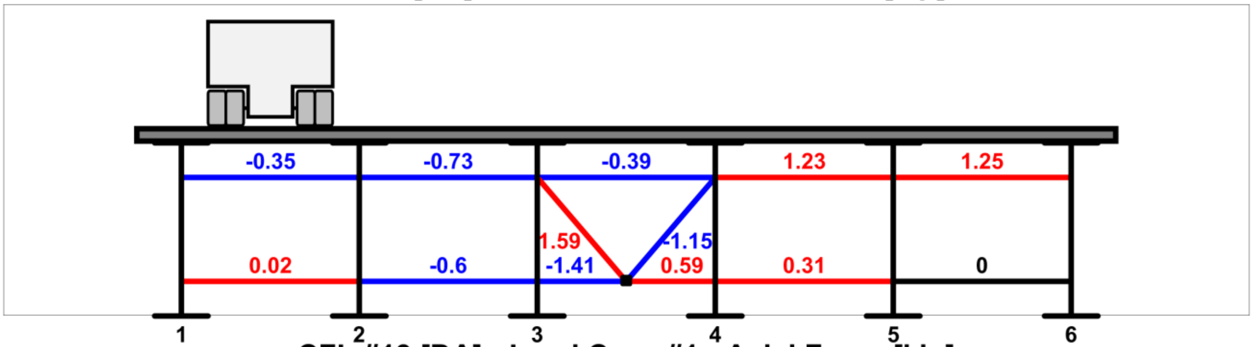

CFL #13 [DA] - Load Case #1 - Axial Force [kip]

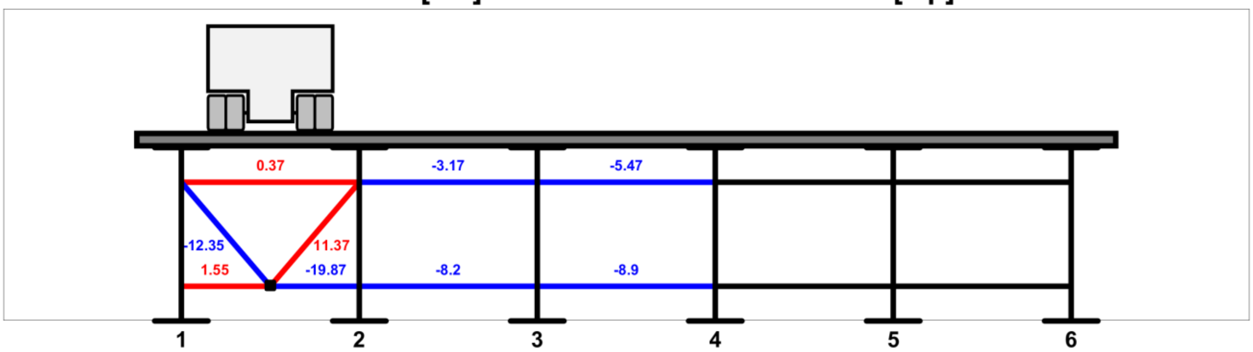

CFL #15 [DA] - Load Case #1 - Axial Force [kip]

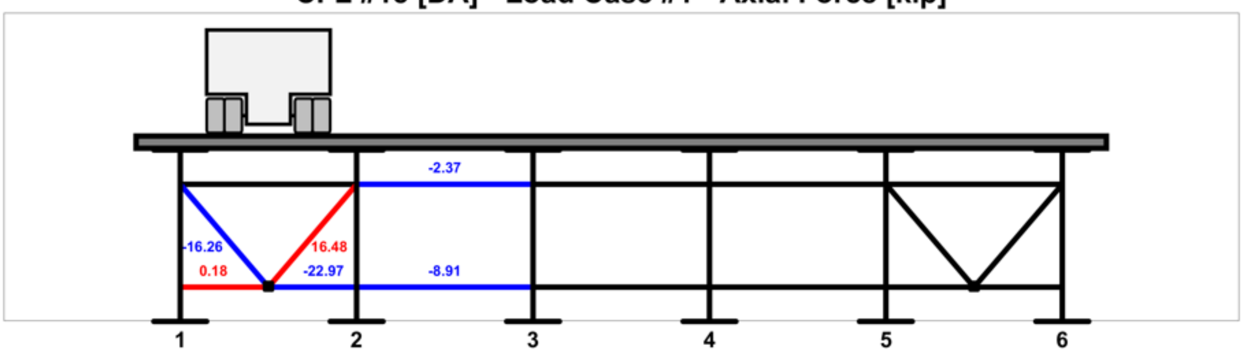

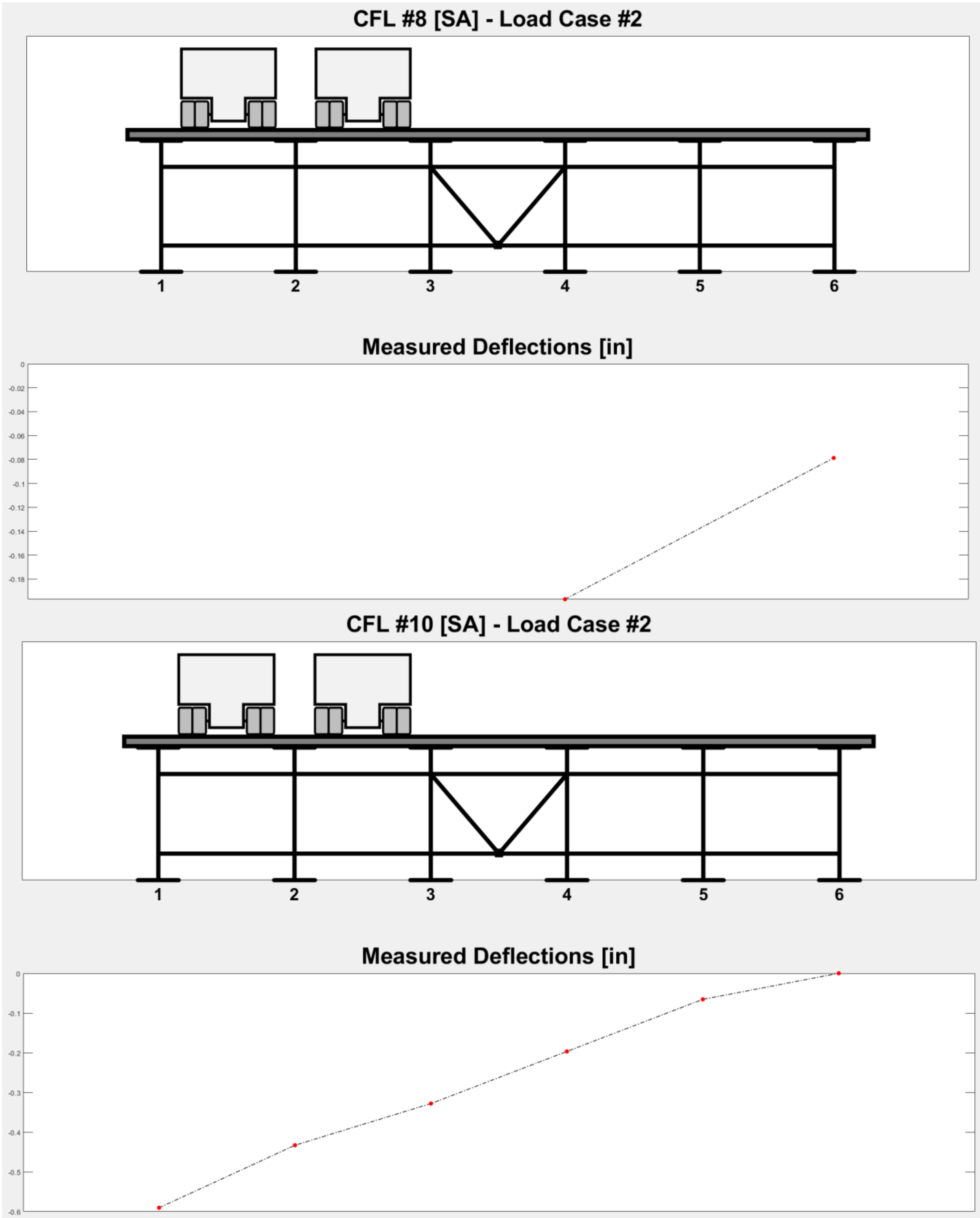
CFL #8 [SA] - Load Case #2
1
2
3
4
5
6
Measured Deflections [in]
0
-0.02
-0.04
-0.06
-0.08
-0.1
-0.12
-0.14
-0.16
-0.18
CFL #10 [SA] - Load Case #2
1
2
3
4
5
6
Measured Deflections [in]
0
-0.1
-0.2
-0.3
-0.4
-0.5
-0.6

CFL #9 [SA] - Load Case #2 - Axial Force [kip]

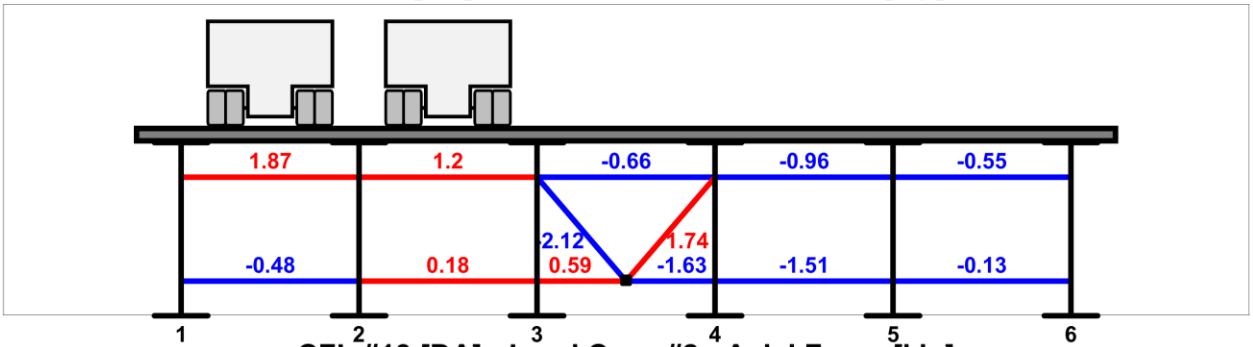

CFL #13 [DA] - Load Case #2 - Axial Force [kip]

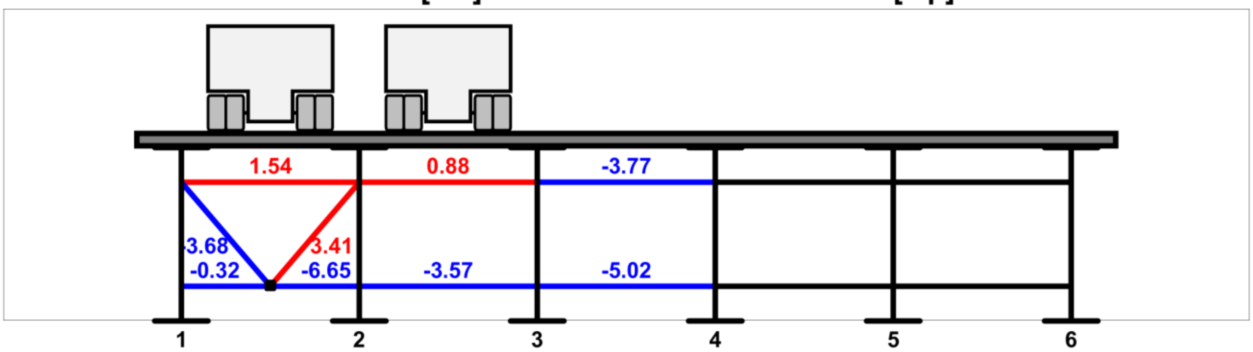

CFL #15 [DA] - Load Case #2 - Axial Force [kip]

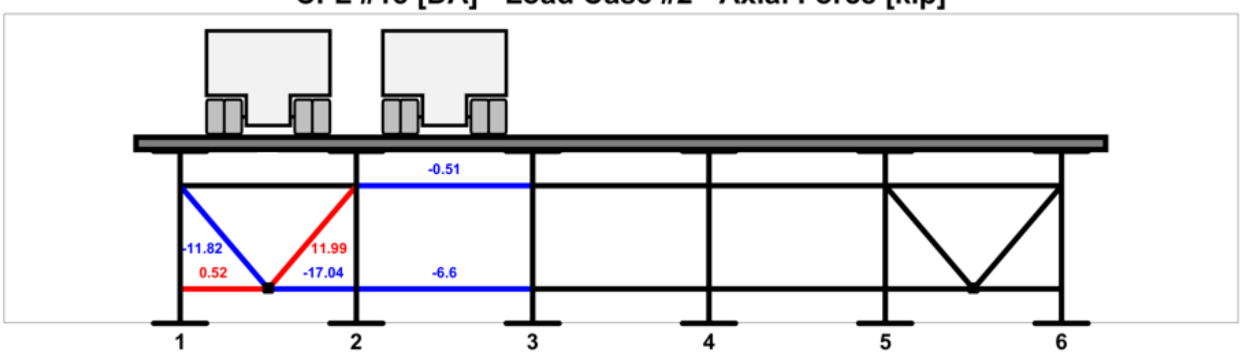

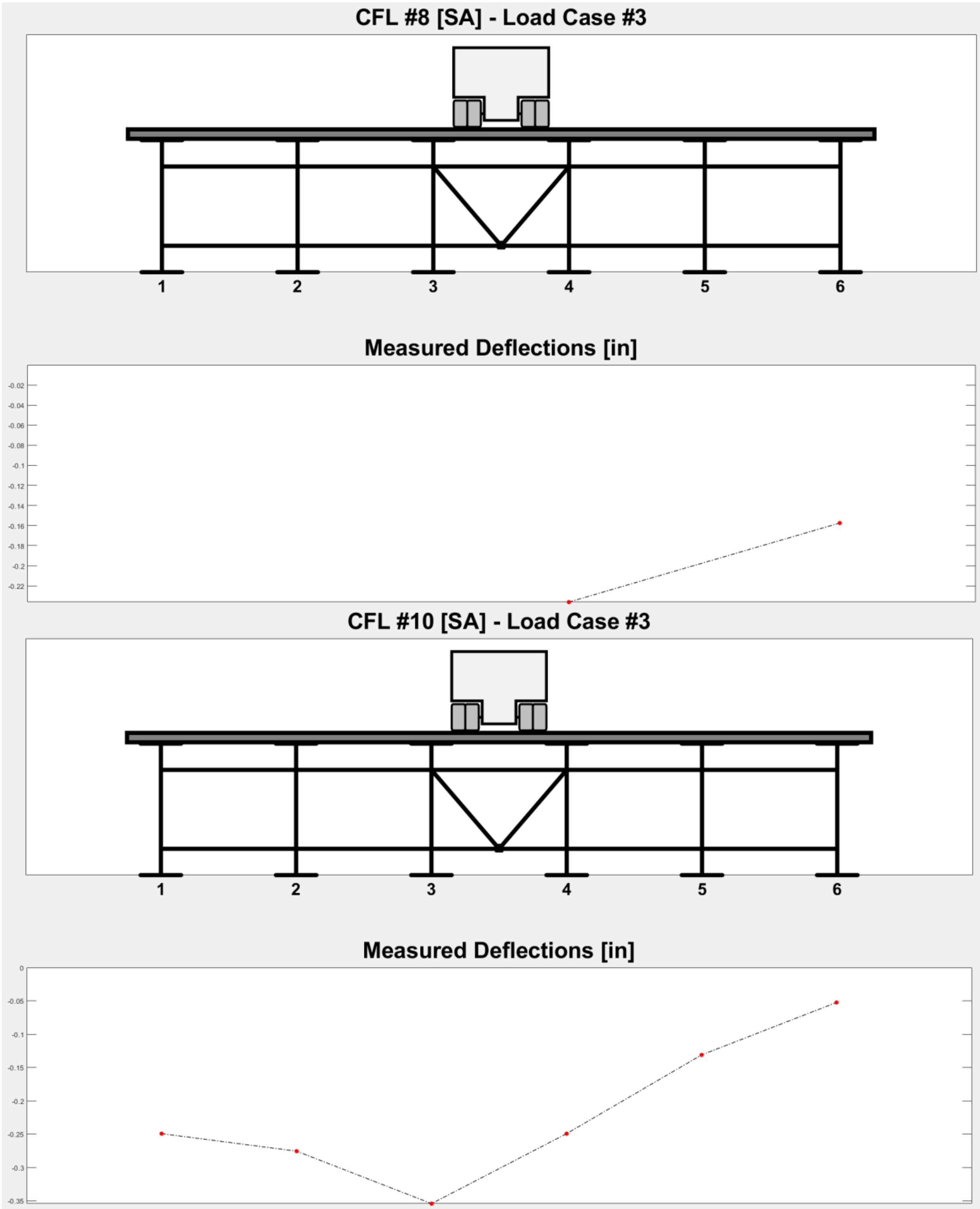
CFL #8 [SA] - Load Case #3
1
2
3
4
5
6
Measured Deflections [in]
-0.02
-0.04
-0.06
-0.08
-0.1
-0.12
-0.14
-0.16
-0.18
-0.2
-0.22
CFL #10 [SA] - Load Case #3
1
2
3
4
5
6
Measured Deflections [in]
0
-0.05
-0.1
-0.15
-0.2
-0.25
-0.3
-0.35

CFL #9 [SA] - Load Case #3 - Axial Force [kip]

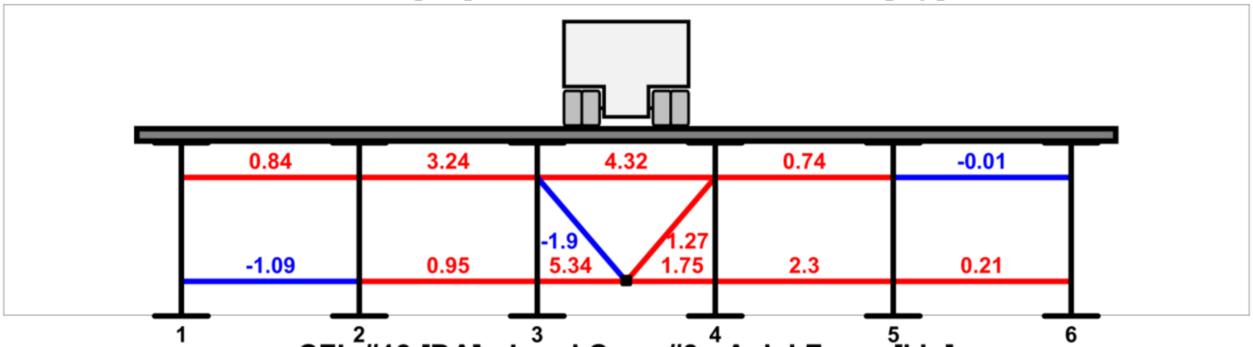

CFL #13 [DA] - Load Case #3 - Axial Force [kip]

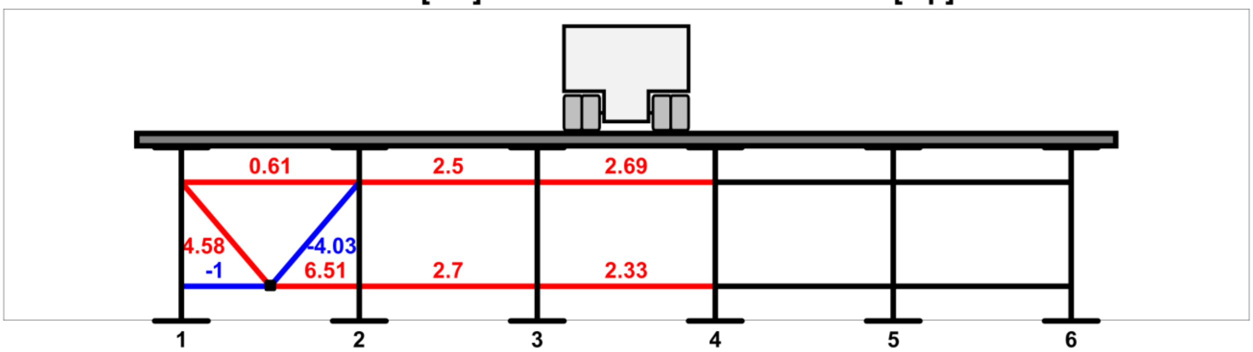

CFL #15 [DA] - Load Case #3 - Axial Force [kip]

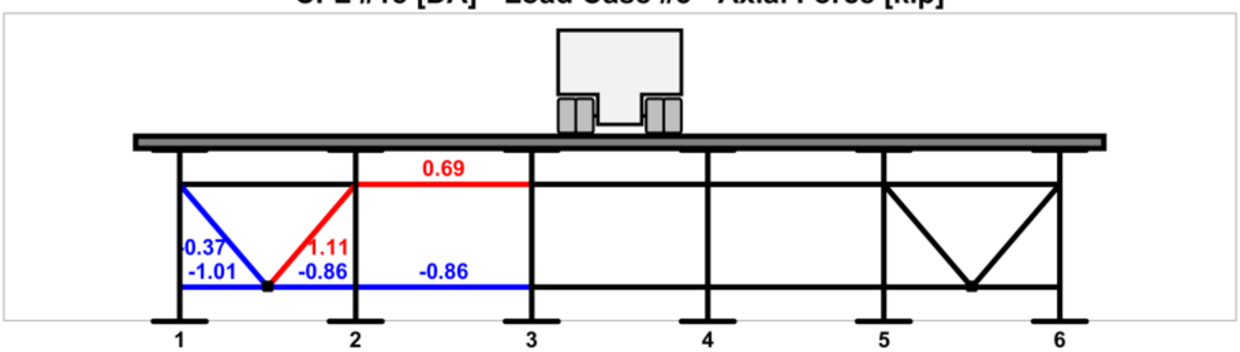

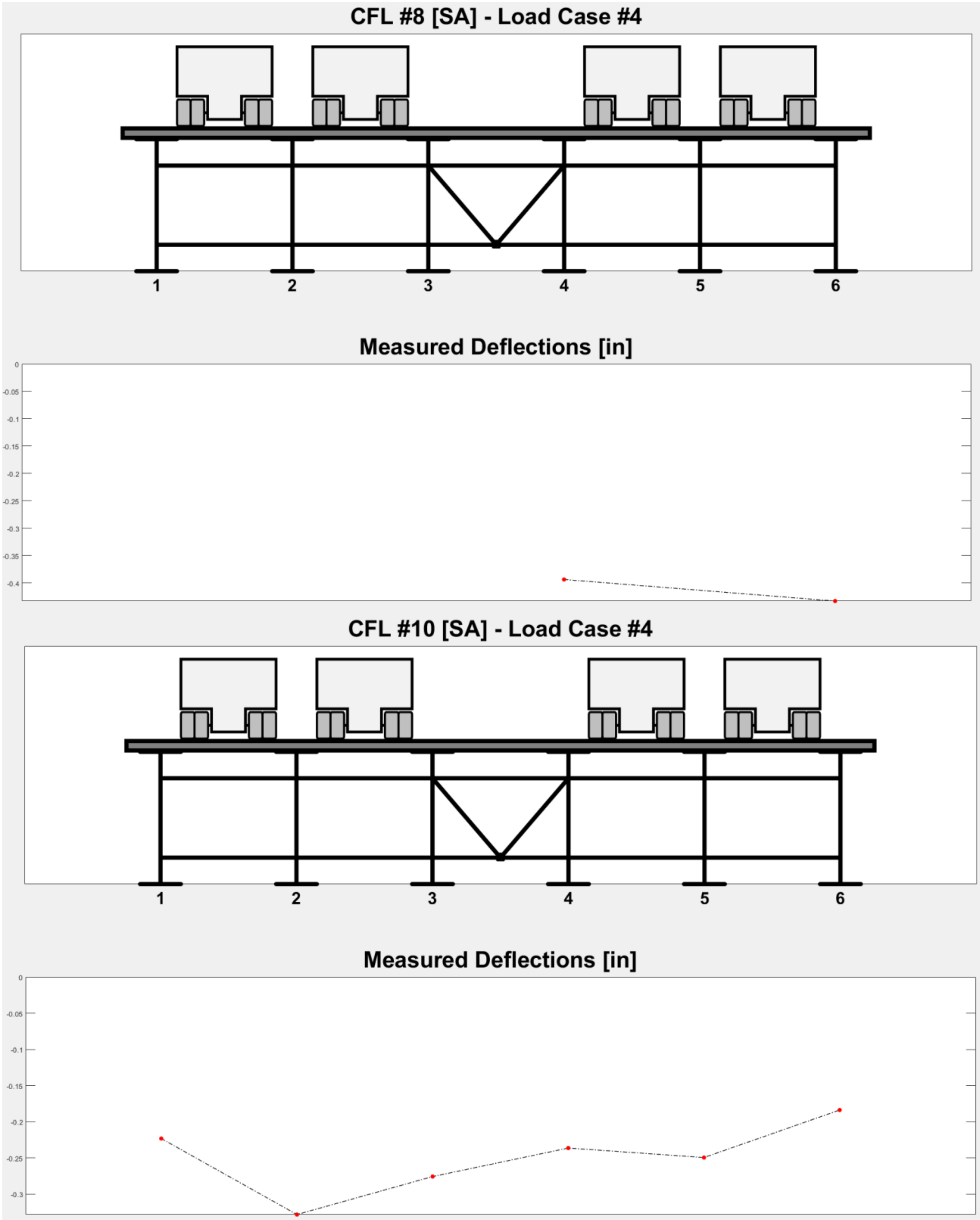
CFL #8 [SA] - Load Case #4
1
2
3
4
5
6
Measured Deflections [in]
0
-0.05
-0.1
-0.15
-0.2
-0.25
-0.3
-0.35
-0.4
CFL #10 [SA] - Load Case #4
1
2
3
4
5
6
Measured Deflections [in]
0
-0.05
-0.1
-0.15
-0.2
-0.25
-0.3

CFL #9 [SA] - Load Case #4 - Axial Force [kip]

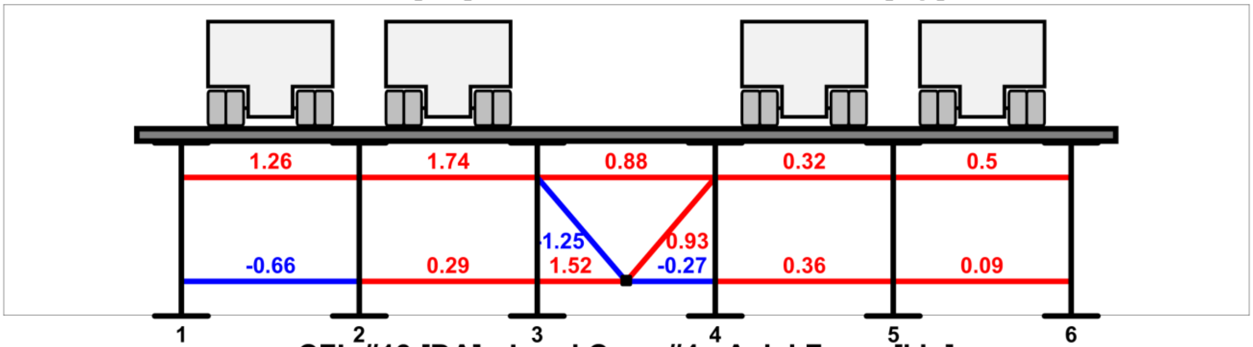

CFL #13 [DA] - Load Case #4 - Axial Force [kip]

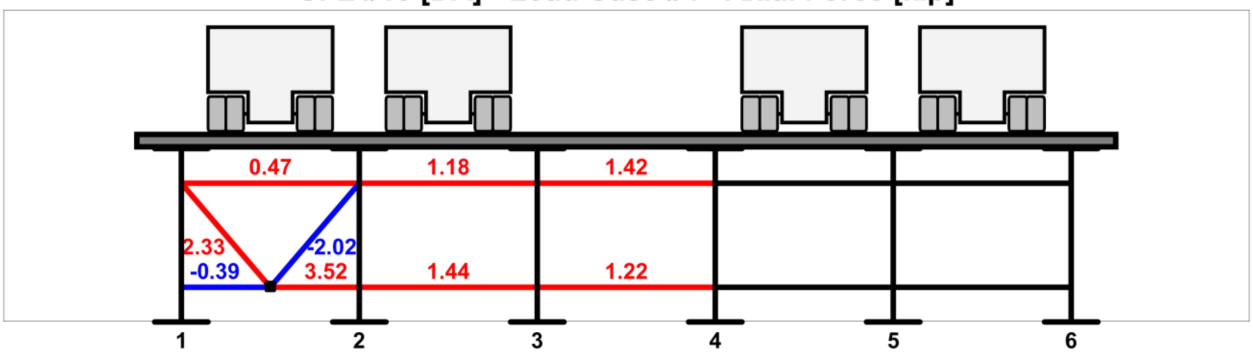

CFL #15 [DA] - Load Case #4 - Axial Force [kip]

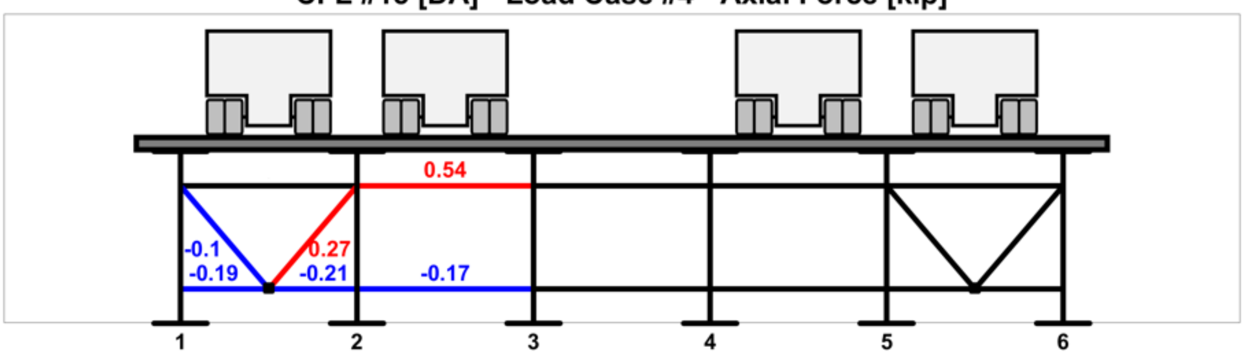

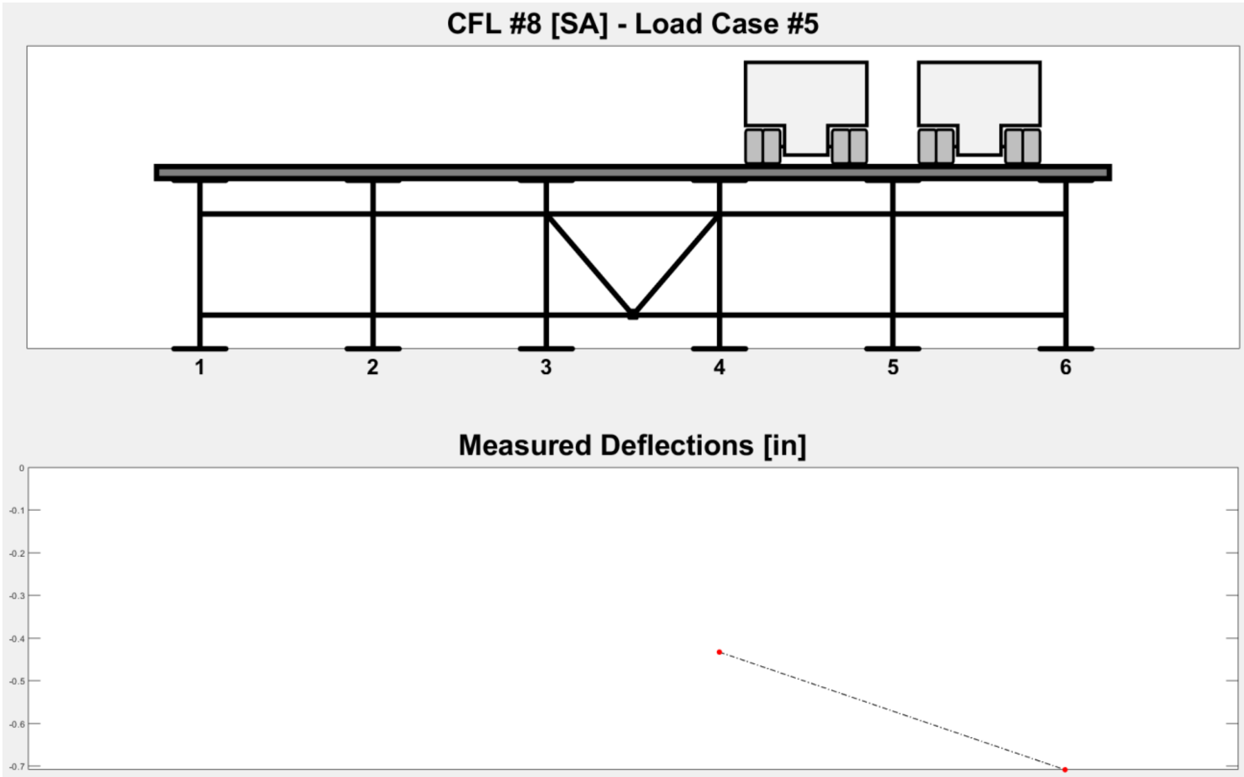
CFL #8 [SA] - Load Case #5
1
2
3
4
5
6
Measured Deflections [in]
0
-0.1
-0.2
-0.3
-0.4
-0.5
-0.6
-0.7

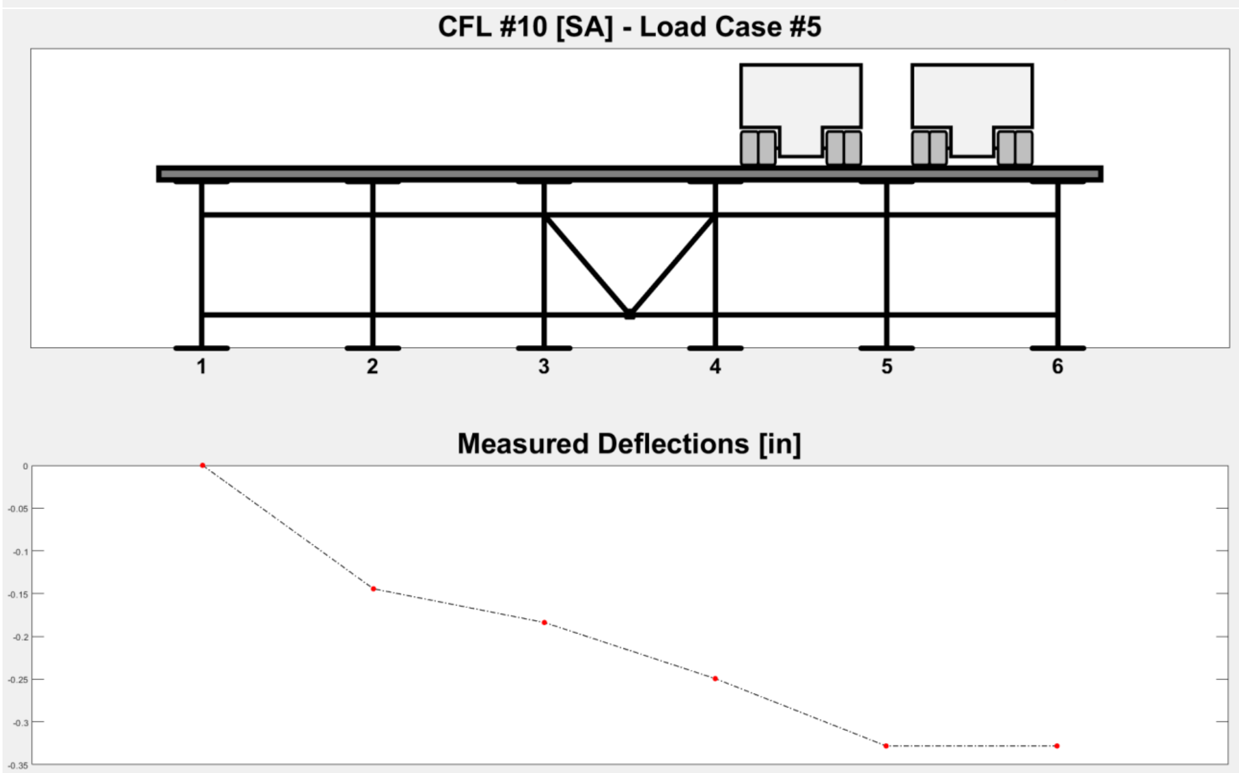
CFL #10 [SA] - Load Case #5
1
2
3
4
5
6
Measured Deflections [in]
0
-0.05
-0.1
-0.15
-0.2
-0.25
-0.3
-0.35

CFL #9 [SA] - Load Case #5 - Axial Force [kip]

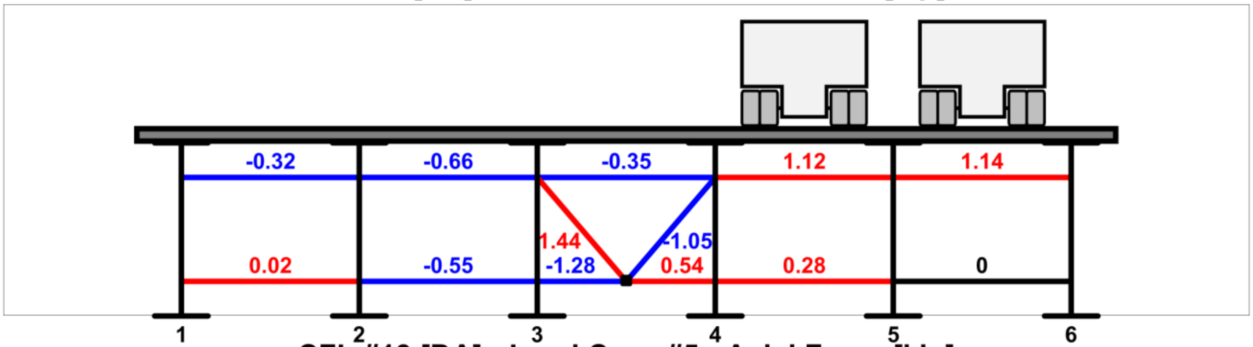

CFL #13 [DA] - Load Case #5 - Axial Force [kip]

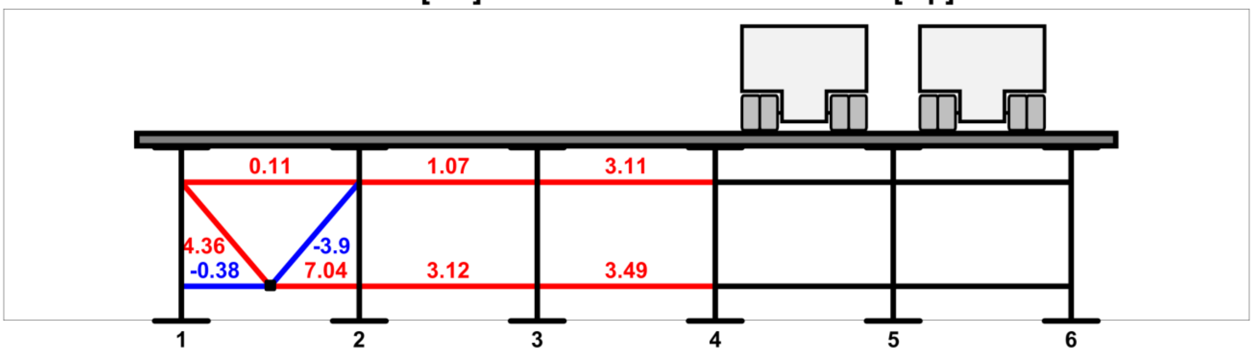

CFL #15 [DA] - Load Case #5 - Axial Force [kip]

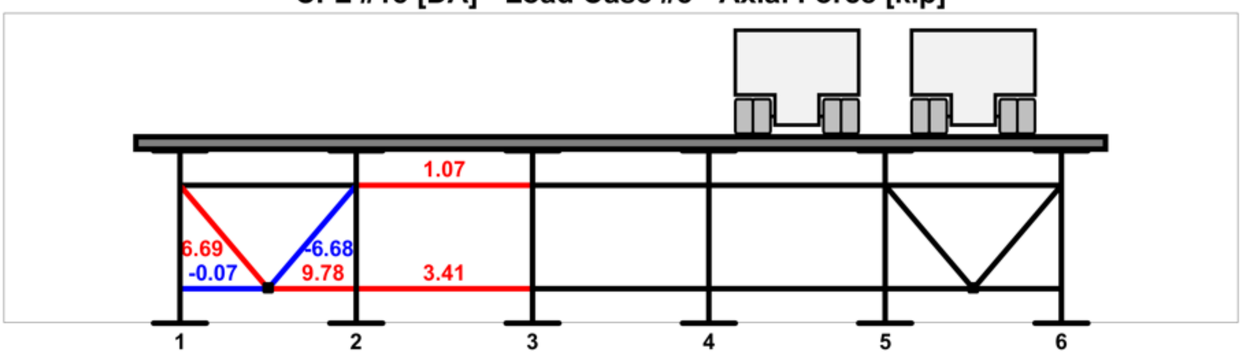

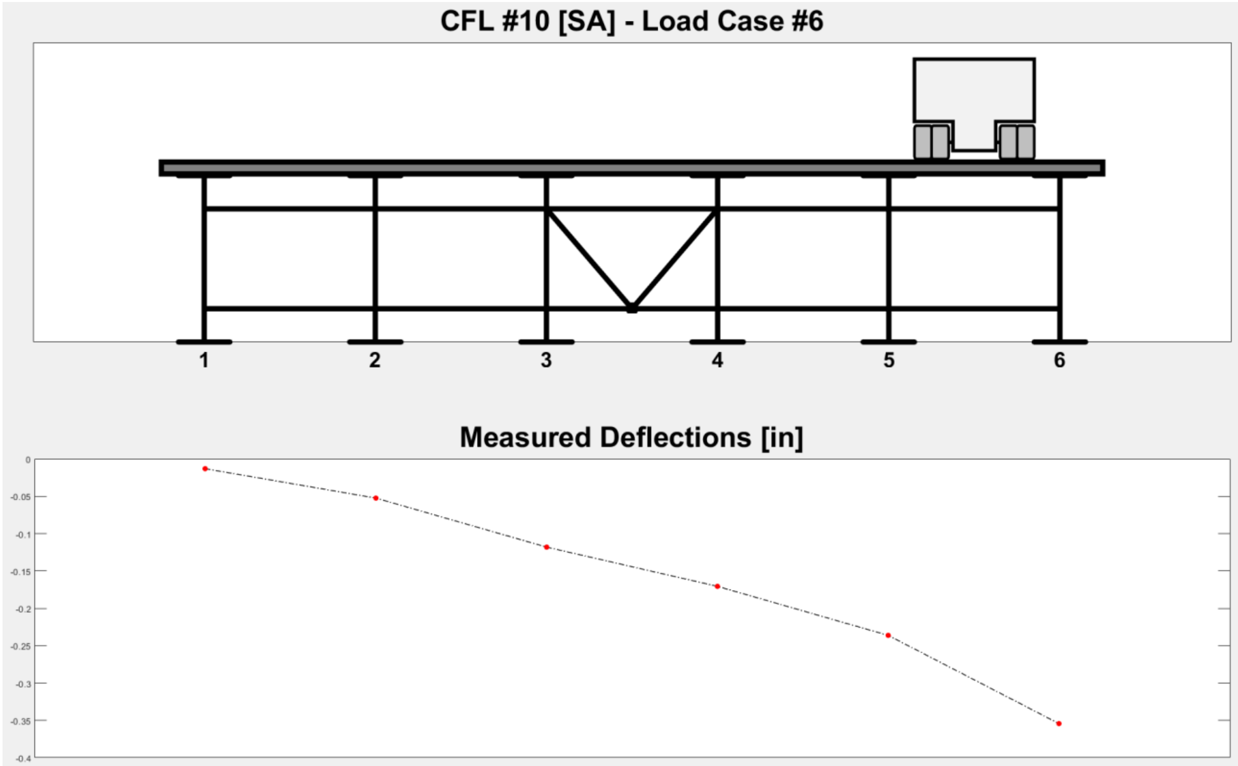
CFL #10 [SA] - Load Case #6
1
2
3
4
5
6
Measured Deflections [in]
0
-0.05
-0.1
-0.15
-0.2
-0.25
-0.3
-0.35
-0.4

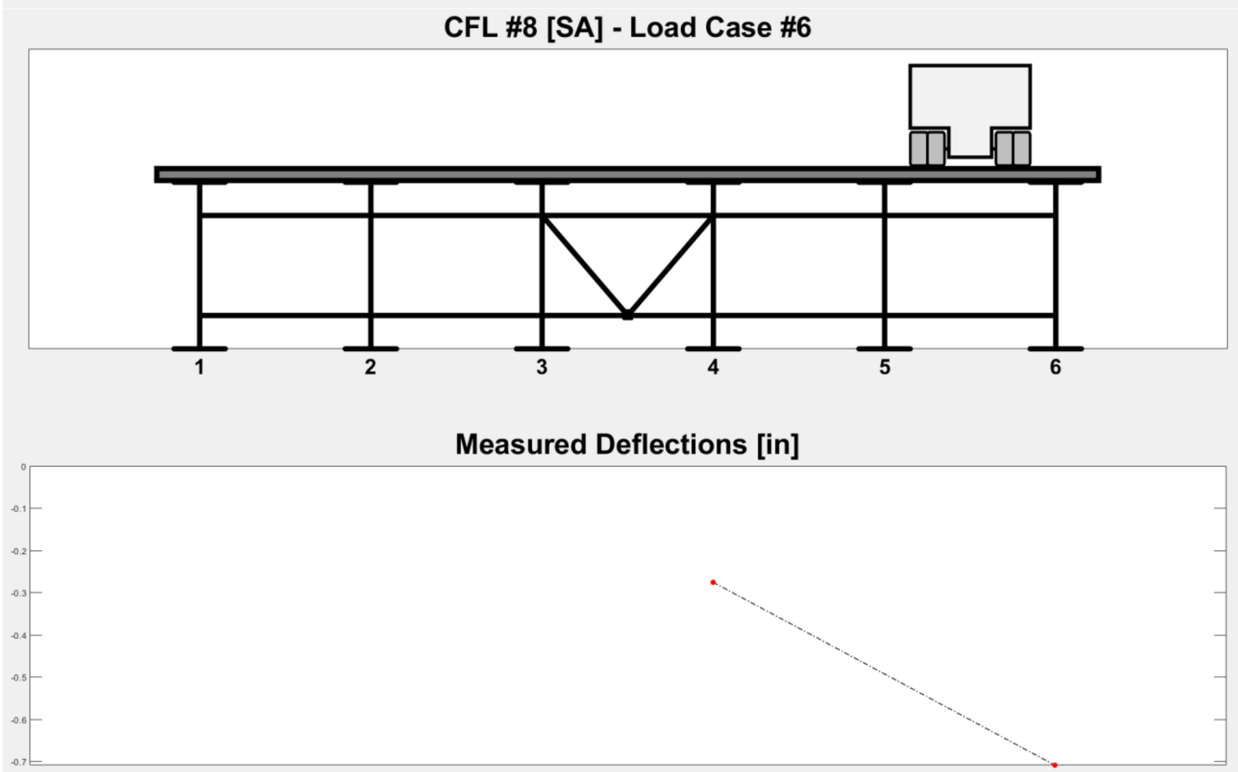
CFL #8 [SA] - Load Case #6
1
2
3
4
5
6
Measured Deflections [in]
0
-0.1
-0.2
-0.3
-0.4
-0.5
-0.6
-0.7

CFL #9 [SA] - Load Case #6 - Axial Force [kip]

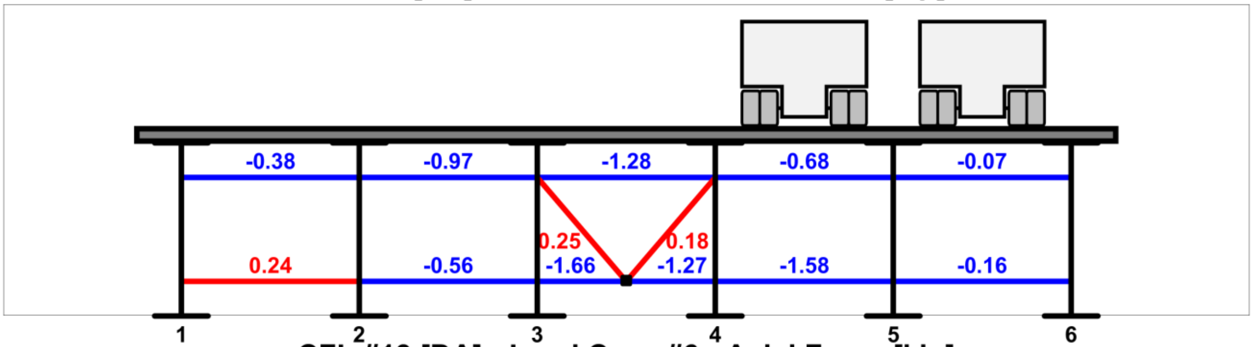

CFL #13 [DA] - Load Case #6 - Axial Force [kip]

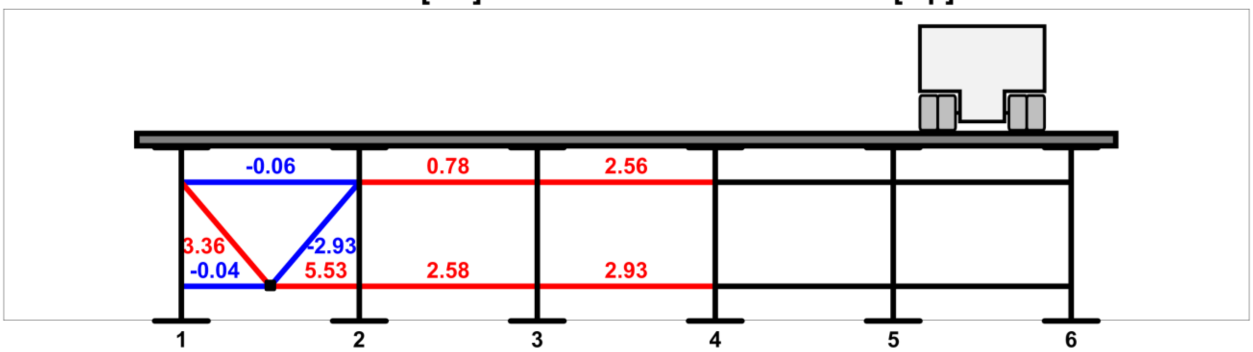

CFL #15 [DA] - Load Case #6 - Axial Force [kip]

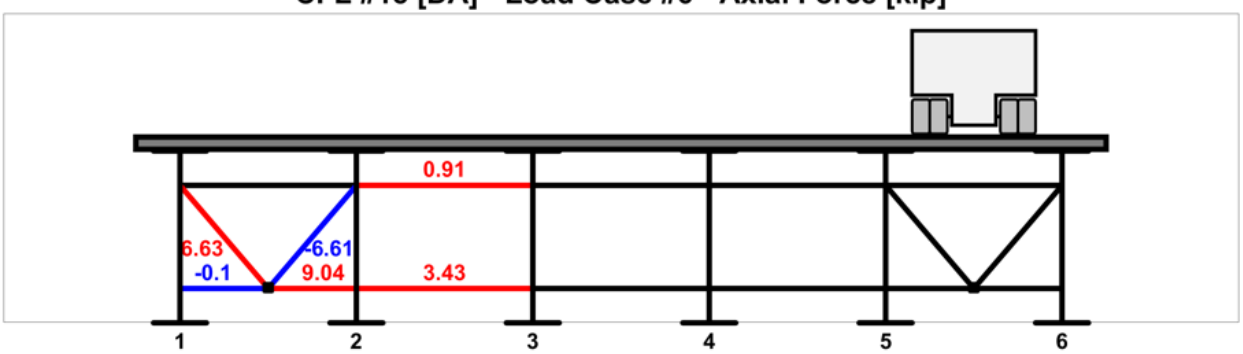

Appendix K. Lubbock Bridge Axial Forces (No Deflections Included)

CFL #7 [SA] - Load Case Grid #7 SAS - Axial Force [kip]

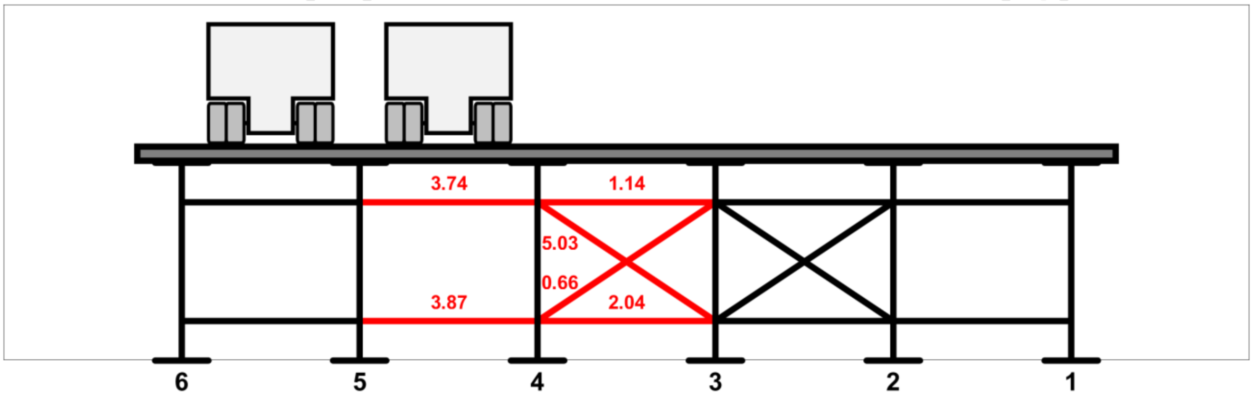

CFL #3 [SA] - Load Case Grid #7 SAS - Axial Force [kip]

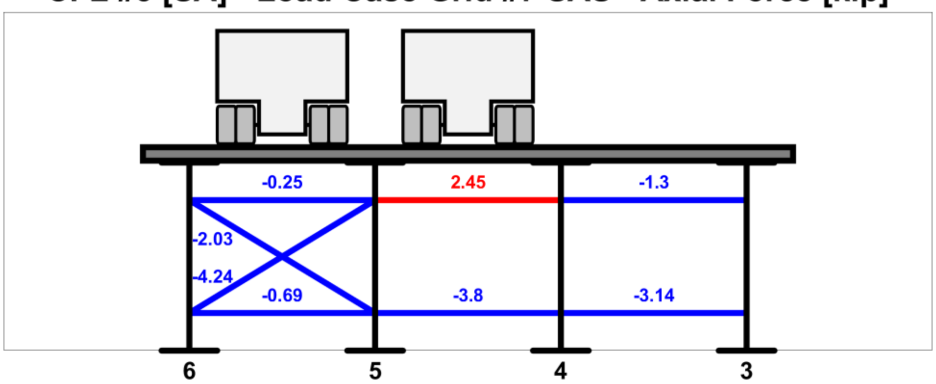

CFL #7 [SA] - Load Case Grid #7 SBS - Axial Force [kip]

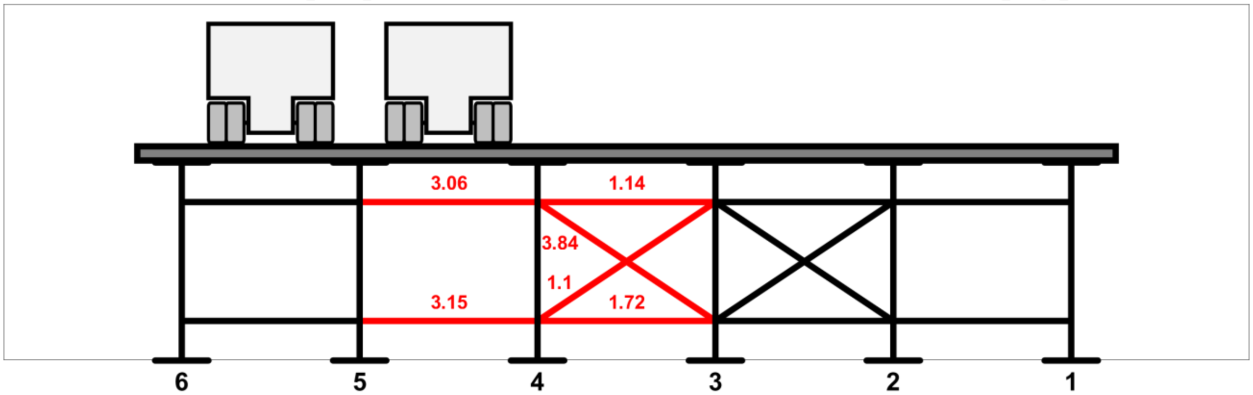

CFL #3 [SA] - Load Case Grid #7 SBS - Axial Force [kip]

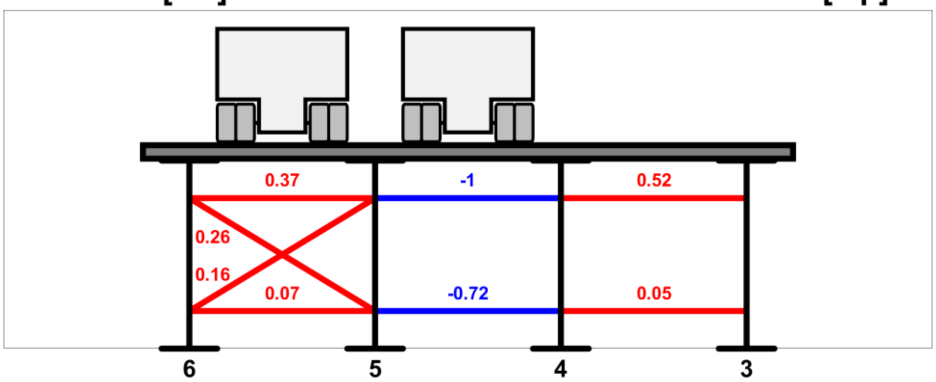

CFL #7 [SA] - Load Case Grid #7 SSS - Axial Force [kip]

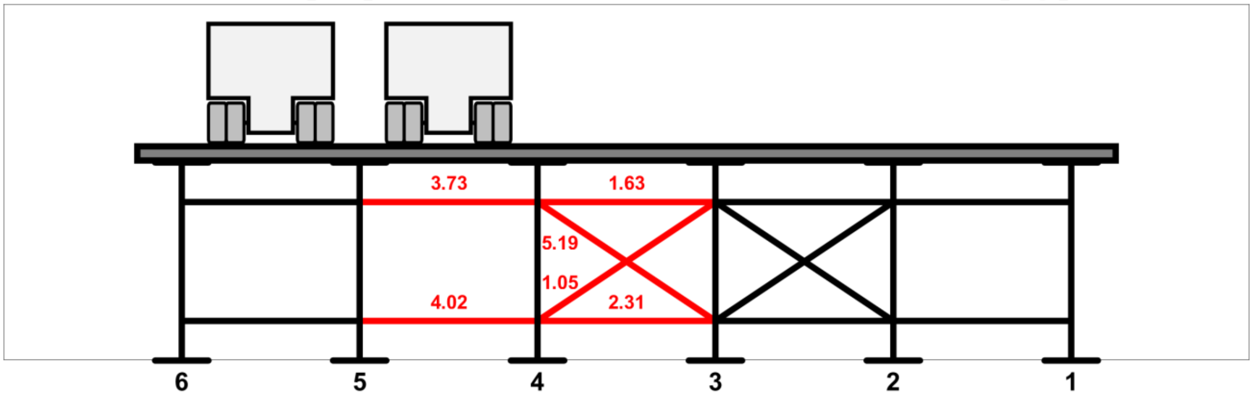

CFL #3 [SA] - Load Case Grid #7 SSS - Axial Force [kip]

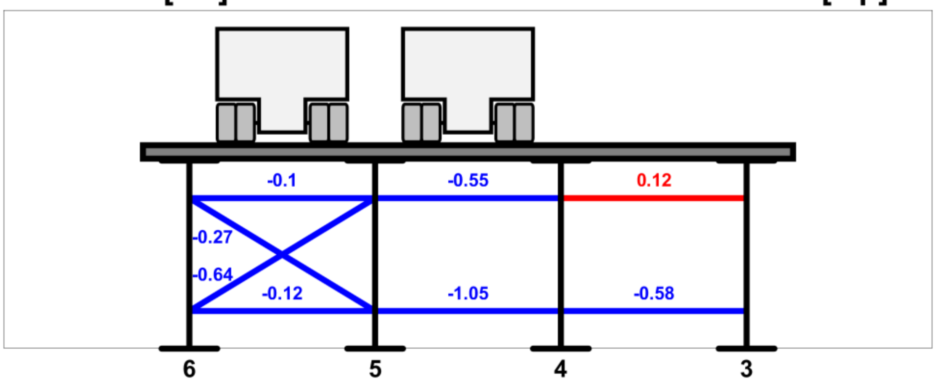

CFL #7 [SA] - Load Case Grid #7 SSN - Axial Force [kip]

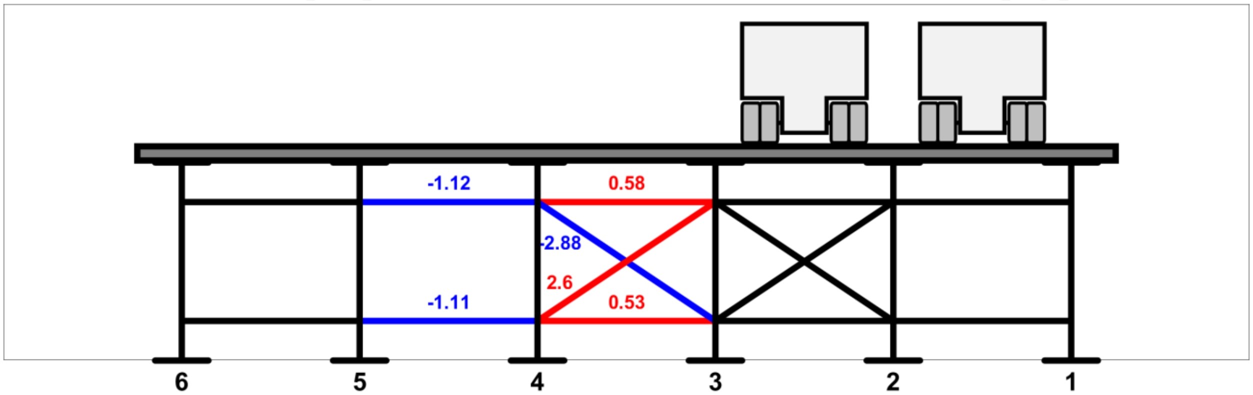

CFL #3 [SA] - Load Case Grid #7 SSN - Axial Force [kip]

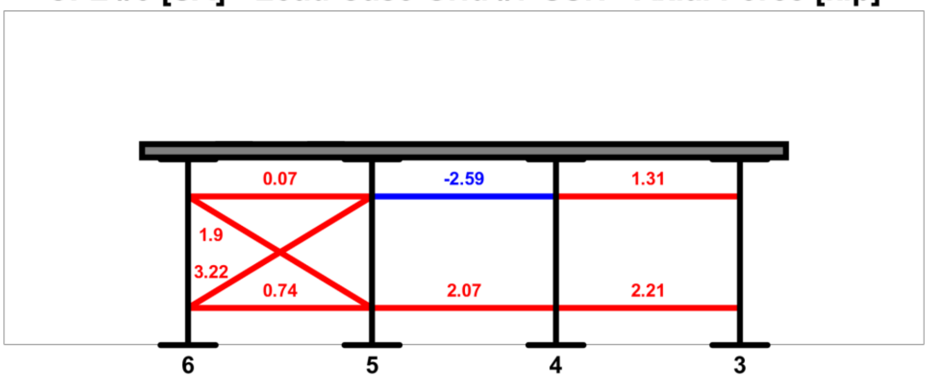

CFL #7 [SA] - Load Case Grid #7 EES - Axial Force [kip]

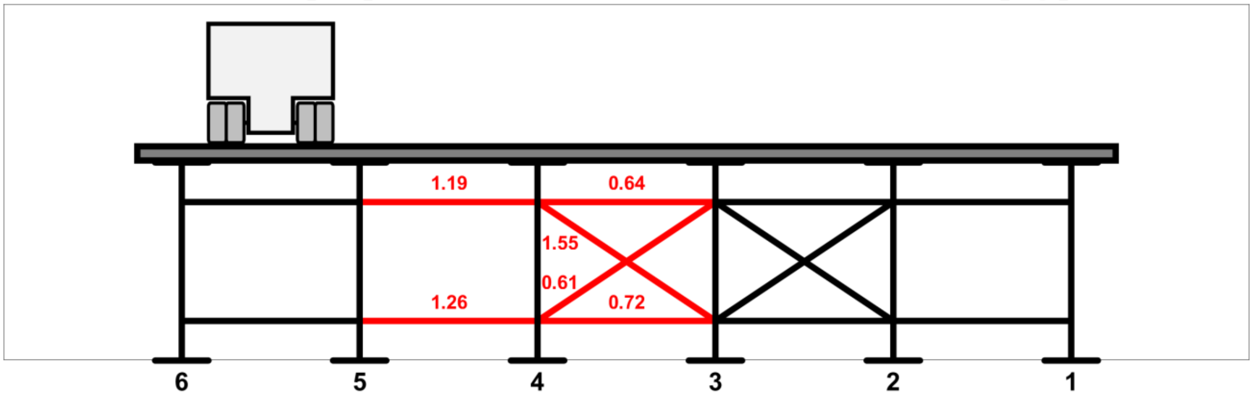

CFL #3 [SA] - Load Case Grid #7 EES - Axial Force [kip]

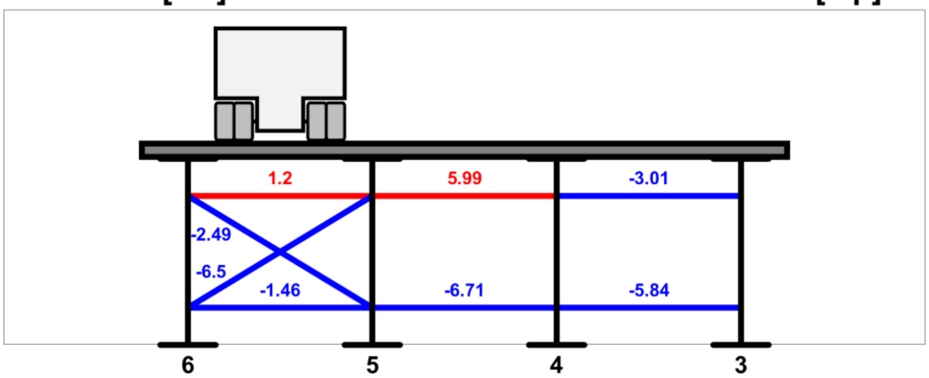

CFL #7 [SA] - Load Case Grid #7 EEC - Axial Force [kip]

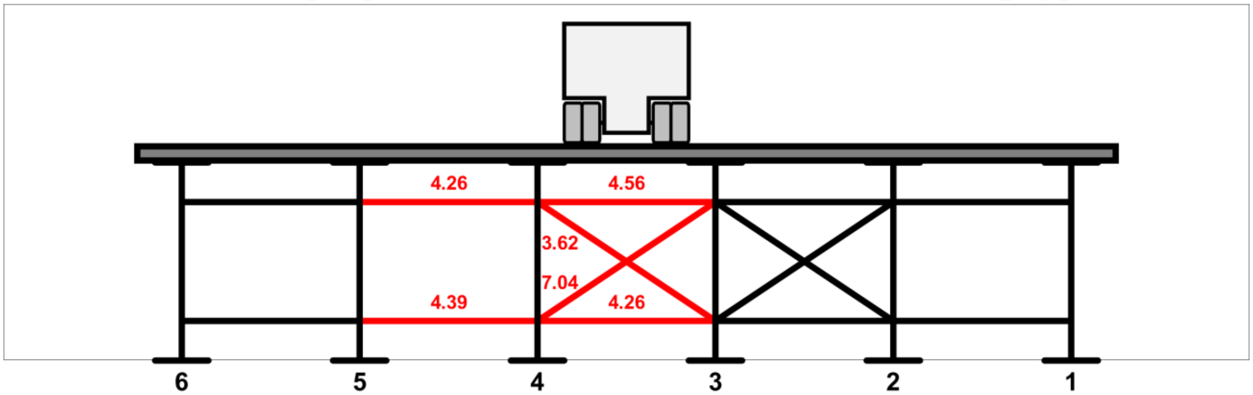

CFL #3 [SA] - Load Case Grid #7 EEC - Axial Force [kip]

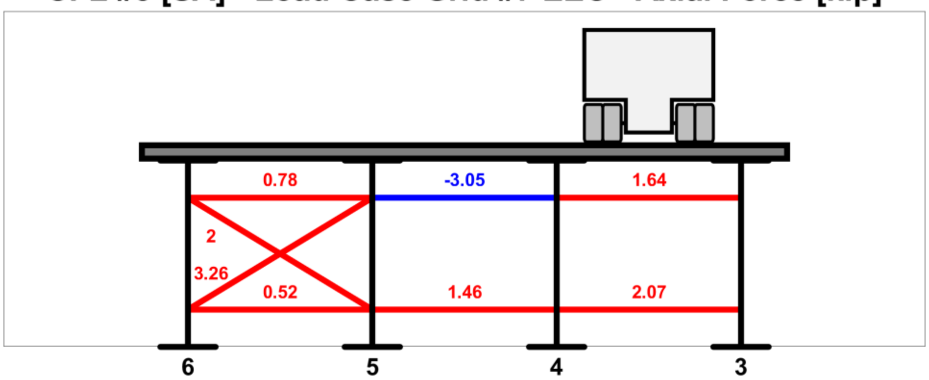

Appendix L. Phase 1 Lateral Truss Results

As outlined in Chapter 2, the bracing provisions in AASHTO allow the use of lateral trusses near the ends of the section to reduce the required stiffness for cross-frame systems. The lateral trusses tend to improve the in-plane stiffness of the girders and therefore improve the effectiveness of the cross-frame bracing. Therefore, the systems summarized in Table 5.1 were also analyzed with lateral trusses near the ends of the span to determine the impact of lateral trusses on the in-plane girder stiffness and thus the brace stiffness required to reach the ideal stiffness. The lateral struts and diagonals of the lateral trusses were sized at 3 in^2 and 5 in^2 respectively. The moment capacity gained by implementing lateral trusses into the tested bridge systems is shown in Figure L-0-1. The data in the figure was sorted based on number of girders (G) and whether the data was for single (SSp) or continuous spans (CSp).

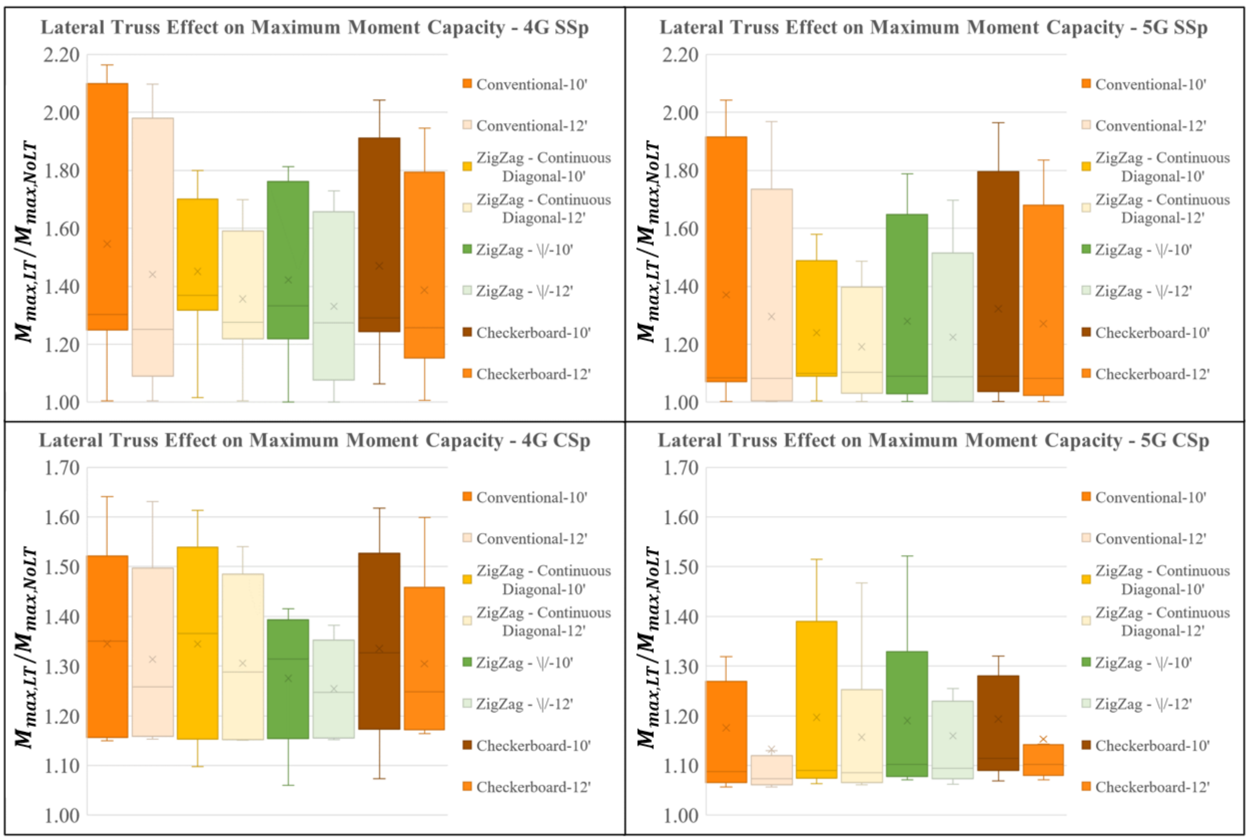

Figure L-0-1. Comparison of Capacity Gained with Lateral Trusses for Each Layout at Various Bridge Widths

Overall, the results in Figure L-0-1 demonstrate lateral trusses increased the buckling moment capacity relative to the width of the system. Wider systems had diminishing returns as the in-plane girder stiffness had less control on the overall resulting behavior. Additionally, continuous span systems benefited less from the lateral trusses than their single-span counterparts which is likely caused by the change in moment distribution.

When compared to Table 6-1, the data in Table L.0-1 shows a significant decrease in the required brace area, further highlighting the increase to the in-plane girder stiffness.

Table L.0-1. Minimum Average Brace Area of Layouts Compared to Conventional Bracing for Systems with Lateral Trusses

Layout	**Single Span – No LT**		**Continuous Span – No LT**	
	$\bar{A}_{br}$	$\frac{\bar{A}_{br,lean}}{\bar{A}_{br,conventional}}$	$\bar{A}_{br}$	$\frac{\bar{A}_{br,lean}}{\bar{A}_{br,conventional}}$
Conventional	1.76	1.00	1.03	1.00
ZigZag – Continuous Diagonal	2.67	1.51	1.51	1.47
ZigZag – ψ	2.22	1.26	1.33	1.29
Checkerboard	2.94	1.67	1.12	1.09

Appendix M. Approaches Considered for Brace Stiffness with Greater than One Cross-Frame

Helwig and Wang (2003) derived a generalized equation for the brace stiffness contribution in a lean-on bracing system based on the tension model idealization developed by Yura (2001). In this expression, the number of cross-frames per bracing line is implicitly assumed to be one, so n_{gc} is effectively the number of girders. As an example, the idealization of a four-girder system is shown in Figure M-0-1. The corresponding value of n_{gc} is four.

Figure M-0-1 Four Girder, One Z Frame Lean-On Bracing Stiffness Idealization

Some designs that have made use of Equation 7.5 have included more than one brace in a given line (Holt et al., 2022), which results in an erroneous estimate of the stiffness demand since the resulting value of n_{gc} in those cases is not representative of the force distribution across the cross-frame line. In these cases, n_{gc} is calculated as the ratio of girders cross-frames. For example, as shown in Figure M-0-2, a bracing line with four girders and two Z-frames would be reduced to the same stiffness as a system with two girders and one Z-frame since both have a girder to cross-frame ratio of 2:1.

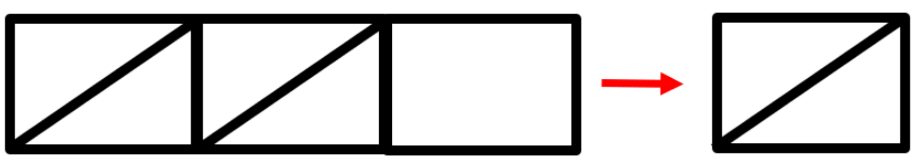

Figure M-0-2 Four Girder, Two Z Frame Lean-On Bracing Stiffness Idealization

Currently, designers that have utilized lean-on bracing concepts often make use of more than one cross-frame in each line in their application of lean-on bracing. Using more than one brace per line is done in an attempt to reduce the demand on the cross-frame. However, the resulting n_{gc} that is used is not representative of the stiffness derivation for Equation 7.5. It is therefore necessary to develop an expression for the brace stiffness that accounts for the additional cross-frame relative to the Helwig and Wang expression in Equation 7.5. Four potential alternative approaches are described in the following sections in the context of a four-girder system with two Z-frames. All four approaches were compared preliminarily, and the most promising approach was generalized to account for varying numbers of girders and cross-frames configurations. A detailed parametric study was conducted to finalize the best approach and was validated for K and X-frames as well.

M.1. Cross-Section Slice Approach

The first method is entitled a "Cross-Section Slice Approach," where a redundant cross-frame is essentially ignored. This is shown for a four-girder system with two cross-frames in Figure M-0-3, where the left cross-frame is not considered in determining the brace stiffness. This results in Δ_{crit} equal to the sum of $\Delta_{T3}, \Delta_{T4}, \Delta_{B3}, and\ \Delta_{B4}$. The brace stiffness of the configuration is then calculated using Equation 7.5 or virtual work for a three-girder system, resulting in Equation 0.1.

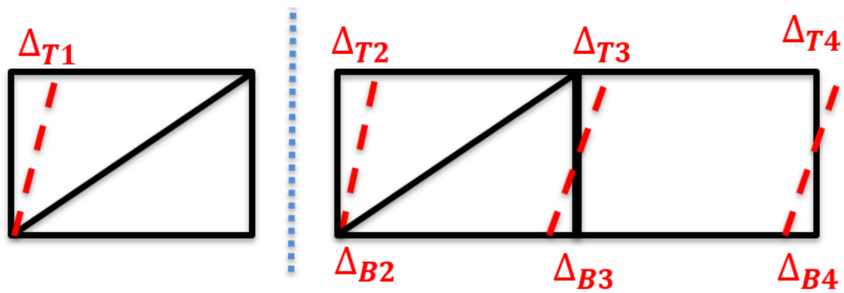

Figure M-0-3. Cross-Section Slice

$$\beta_b = \frac{Fh^2}{\Delta_{crit}} = \frac{Fh^2}{\frac{3FL_d^3}{S^2 A_d E} + \frac{4FS}{A_S E}} \qquad 0.1$$

M.2. Displacement Combination Approach

A second method has been entitled the "Displacement Combination Approach", which is similar to the "Cross-Section Slice Approach," but the displacement of the second girder is accounted for differently. In the "Cross-Section Slice Approach," the displacement is ignored, whereas in "Displacement Combination Approach" the displacement is accounted for by adding the second girder from the first cross-frame to the result obtained in the "Cross-Section Slice Approach." This is shown in Figure M-0-4, and the resulting stiffness is Equation 0.2. In this approach, Δ_{crit} is equal to the sum of $\Delta_{T2}, \Delta_{T3}, \Delta_{T4}, \Delta_{B2}, \Delta_{B3}, and\ \Delta_{B4}$.

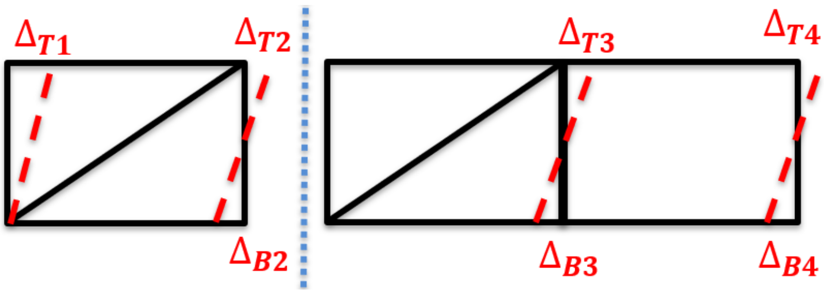

Figure M-0-4. Displacement Combination

$$\beta_b = \frac{Fh^2}{\Delta_{crit}} = \frac{Fh^2}{\frac{5FL_d^3}{S^2 A_d E} + \frac{5FS}{A_S E}} \qquad 0.2$$

M.3. Stiffness Superposition Approach

The third method is entitled the "Stiffness Superposition Approach" and is the least conservative of the three approaches. In this idealization, the cross-frame line is essentially broken into two single-cross-frame systems, and the respective stiffness values of each system are added together. This is shown for the four-girder, two-cross-frame system in Figure M-0-5, with the resulting brace stiffness equation shown in Equation 0.3.

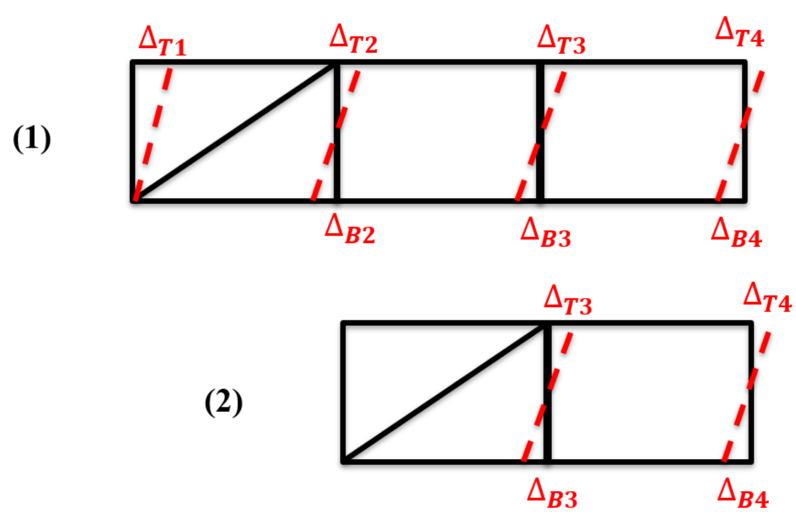

Figure M-0-5. Stiffness Superposition

$$\beta_b = \beta_{b1} + \beta_{b2} = \frac{Fh^2}{\frac{4FL_d^3}{S^2 A_d E} + \frac{9FS}{A_S E}} + \frac{Fh^2}{\frac{3FL_d^3}{S^2 A_d E} + \frac{4FS}{A_S E}} \qquad 0.3$$

M.4. Comparison of Results

Given that the equation variability from the model is insensitive to the geometry of the system, the same representative dimensions were used to run additional preliminary models in order to narrow down the approaches to include in the parametric study. In addition to the four girder system with two cross-frames, stiffnesses of six-girder systems with two and three cross-frames were calculated based on the four approaches and compared against the respective full cross-frame model. Results are shown in Table M-0-1. The Cross-Section Slice (CSS) approach was shown to be conservative in all cases without being excessively conservative, and thus was selected for further study.

Table M-0-1. Preliminary Comparison of Approaches: $\frac{\beta_{br,approach}}{\beta_{br,SAP\ model}}$

	4G 2 CF	**6G 2CF**	**6G 3CF**
SAP Model - Tension System	1.0	1.0	1.0
Helwig and Wang (1 CF)	0.5	0.6	0.4
Lean-On Guide Interpretation	1.6	2.3	2.8
Cross-Section Slice	0.8	0.9	0.8
Displacement Combination	0.6	0.7	0.4
Stiffness Superposition	1.3	1.5	1.5
Cross-Frame Coefficient	1.0	1.2	1.2

M.5. Generalized CSS Approach

Several methods for expanding the application of the lean-on bracing brace stiffness equations to cross-frame lines with multiple cross-frames were considered and are included in Appendix M. The method selected for the design approach is entitled a "Cross-Section Slice Approach. When a given cross-frame line has multiple cross-frames in a line, the cross-frame with the most lean-on girders is assumed to be the critical cross-frame and the other cross-frame is conservatively ignored. For example, considering a four-girder system with two cross-frames on the left of the cross-frame line in Figure 0-6, the cross-frame in the center bay will be critical since the cross-frame is the first in the load path to receive the lean-on forces. Therefore, the left cross-frame in the line is conservative neglected in determining the brace stiffness. This results in value of Δ that represents the relative deformation between the top and the bottom of the cross-frame equal to the sum of $\Delta_{T3}, \Delta_{T4}, \Delta_{B3}, and\ \Delta_{B4.}$ For the purpose of developing the generalized design approach, the brace stiffness of the configuration is then calculated using Equation 7.5 or virtual work for a three-girder system, resulting in Equation 0.4.

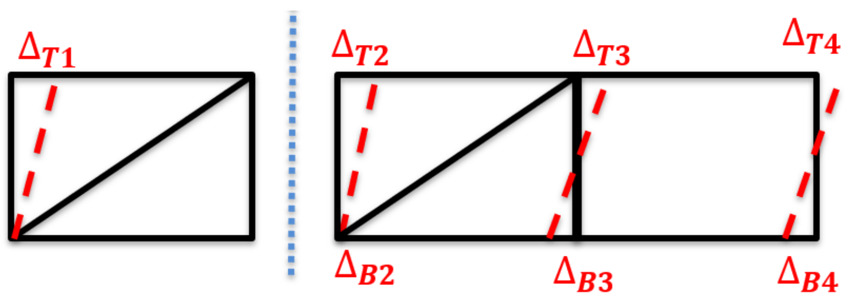

Figure 0-6. Cross-Section Slice Representation

$$\beta_{brZ}(n_g = 4, n_c = 2) = \frac{Fh_b^2}{\Delta} = \frac{Fh_b^2}{\frac{3FL_d^3}{S^2 A_d E} + \frac{4FS}{A_S E}} \qquad 0.4$$

M.5.1 Generalization of Cross-Section Slice Approach

With the goal of developing a simplified design approach for cases with multiple cross-frames in a line and the cross-section slice approach, the originally expression developed in Helwig and Wang (2003) and shown in Equation 7.5 was utilized and was based upon n_{gc} = number of girders per cross-frame. That expression assumed that there was a single cross-frame in a line and the cross-frame was located in an exterior bay. The cross-section slice approach essentially neglects cross-frames that are not "critical", which can be done by replacing n_{gc} with the difference between the number of girders (n_g) and the number of cross-frames in the line (n_c) and adding 1. This results in the following expression:

$$\beta_{brZ} = \frac{ES^2 h_b^2}{\frac{(n_g - n_c + 1)L_d^3}{A_d} + \frac{(n_g - n_c)^2 S^3}{A_S}} \quad 0.5$$

Where:

n_g is the number of girders

n_c is the number of cross-frames in the bracing line

M.5.2 Detailed Validation of CSS Approach

A parametric study was conducted utilizing the representative cross-frame geometry discussed above. As discussed previously, the accuracy of the approach was found to be insensitive to the girder spacing, cross-frame height, and area of the cross-frame members. The remaining variable was the positioning of the cross-frame and lean-on struts along a cross-frame line. Various cross-frame positions in girder systems ranging from two to sixteen girders were investigated. Model results were compared with the Cross-Section Slice (CSS) approach. A detailed discussion of the CSS validation is included in Gasser et al. (2024).

The CSS approach results in the same stiffness value regardless of cross-frame placement within the cross-frame line, as it is only dependent on the number of cross-frames and girders. The limiting cross-frame placement was found to be "cross-frames biased to one of the exterior girders," which is where all of the lean-on girders in a bracing line are on one side of the cross-frame(s) in that line. Such a case results in the largest possible number of adjacent lean-on bays. Examples of this configuration for five girders is shown in Figure 0-7. In Case (a), there are no lean-on girders and the system shown essentially represents a conventional bracing layout. In Case (b) the girder on the right leans on the cross-frame lines. In case (c), the two girders on the right lean on the cross-frames. In Case (d), the three girders on the right lean on the single cross-frame in the line. Intuitively, the demand on the cross-frame in Case (d) would obviously be the largest of the 4 cases shown.

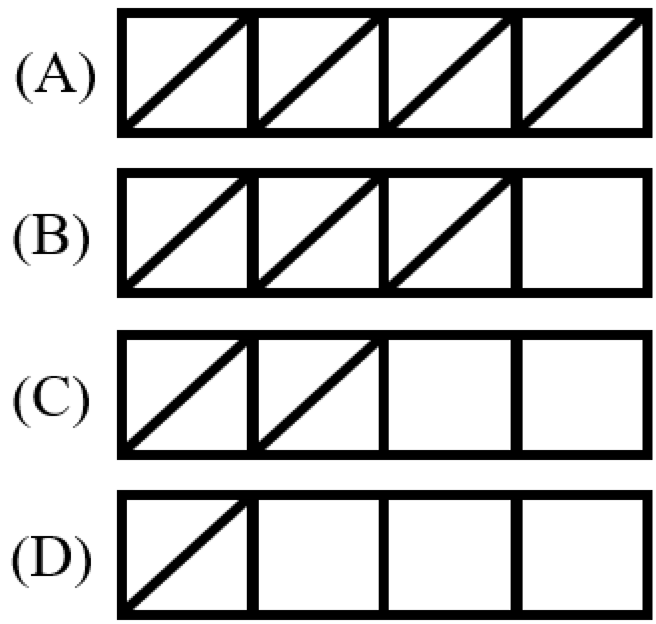

Figure 0-7. Cross-Frames Exterior Aligned Configurations for Five Girders

For the purpose of evaluating the performance of the CSS approach and the relative conservatism, the stiffness obtained from the CSS equation was divided by the stiffness obtained from the SAP model to obtain a ratio where a value greater than one indicates the CSS equation was unconservative. These results are shown in Figure 0-8, where all values are less than or equal to one, indicating an accurate or conservative expression. The vertical axis represents the number of girders ranging from 1 to 16. The horizontal axis represents the number of cross-frames provided in the line, with a maximum possible equal to 1 less than the number of girders. The contour shades in the graph provide an indication of the level of conservatism with yellow representing perfect agreement and darker shades trending to orange and green indicating higher levels of conservatism. The equation results in perfect agreement with the SAP model for the Case (D) situation with only one cross-frame, since that matches the case Eq. 7.5 and therefore Eq. 7.19 were developed for. The approach is conservative for all of the other cases with more cross-frames and is the most conservative for the case with conventional bracing depicted in Case (A). The minimum value in the plot is 0.75, indicating that the CSS approach results in at least 75% of the brace stiffness result from the SAP model. Therefore, the maximum error associated with this case where the lean on girders are all located to one side of the cross-frame is approximately 25% conservatism with most case with significant lean-on in a bracing line being significantly less.

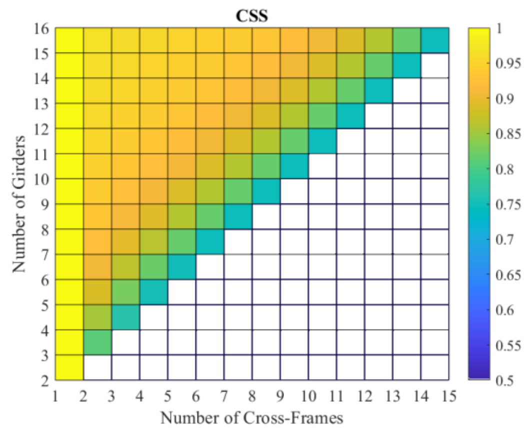

Figure 0-8. $\frac{\beta_{br,CSS}}{\beta_{br,SAP\ model}}$ for Z-Frames Cross-Frames Aligned Exterior

In other configurations, the model predicted greater stiffness values, making the CSS equation even more conservative for cross-frames positioned near the interior or spaced out along the cross-frame line. Quantification of these increased stiffness values is discussed in Sections 0 and 0.

M.5.3 Validation of CSS Approach for Other Cross-Frame Shapes

The CSS approach was validated for X-frames and K-frames in addition to the Z-frame shape. The equations derived in the previous section were modified and generalized to account for the CSS approach, and the procedure comparing SAP models with the equations used for Z-frames was applied similar to the graphical approach shown in Figure 7-16.

M.5.4 Lean-On K- Frames

In the K-frame lean-on derivation, the generalized displacement of the critical girder is given by Equation 0.6.

$$\Delta = 2n_g\left(\frac{FL^3}{S^2A_dE}\right) + \left[\frac{1}{4}(n_g-2) + \frac{n_g-1}{2} + (n_g-1)(n_g-2)\right]\left(\frac{FS}{A_sE}\right) \qquad 0.6$$

In order to apply the CSS approach and remove the implicit assumption of one cross-frame at an exterior bay, the expression may be rewritten as Equation 0.7

$$\Delta = 2(n_g-n_c+1)\left(\frac{FL^3}{S^2A_dE}\right) + \left[\frac{1}{4}(n_g-n_c-1) + \frac{n_g-n_c}{2} + (n_g-n_c)(n_g-n_c-1)\right]\left(\frac{FS}{A_sE}\right) \qquad 0.7$$

Which can be reduced to the form of Equation 0.8.

$$\Delta = 2n_g\left(\frac{FL^3}{S^2A_dE}\right) + \left[n_g^2 + n_c^2 - 2n_gn_c - \frac{n_g}{4} + \frac{n_c}{4} - \frac{1}{4}\right]\left(\frac{FS}{A_sE}\right) \qquad 0.8$$

This form can be used to determine the stiffness as Equation 0.9.

$$\beta_{br,X} = \frac{ES^2h_b^2}{2(n_g-n_c+1)\frac{L_d^3}{A_d}+\left(n_g^2+n_c^2-2n_gn_c-\frac{n_g}{4}+\frac{n_c}{4}-\frac{1}{4}\right)\frac{S^3}{A_S}} \qquad 0.9$$

The result for when the stiffness given by Equation 0.9 is divided by the stiffnesses from a K-frame SAP model with the same cross-frames aligned in the exterior configuration is shown in Figure 0-9. The agreement between the equation and SAP model is better than shown in the last section with Z-frames, likely due to the ability of K-frame members to carry compression as well as tension to better distribute the forces across the adjacent cross-frames. There is perfect agreement in systems with just one cross-frame, and the minimum value in the plot is 0.83.

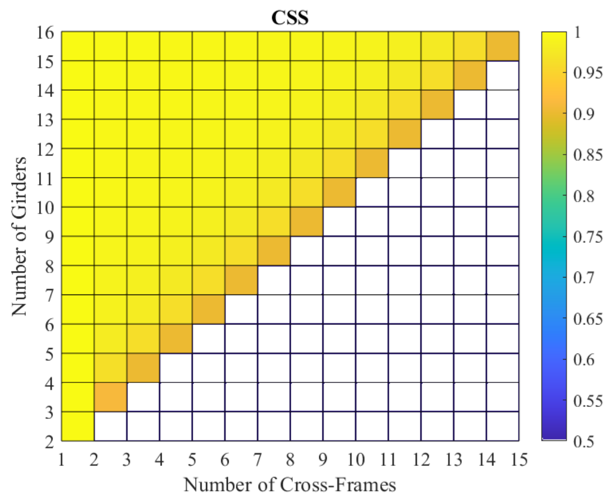

Figure 0-9. $\frac{\beta_{br,CSS}}{\beta_{br,SAP\ model}}$ for K-Frames Cross-Frames Aligned Exterior

The expression in Equation 0.9 contains several terms, which can be complicated for design applications. To the simplify the expression for design applications, the last three terms in the in the second term of the denominator were neglected yielding the following expression:

$$\beta_b = \frac{ES^2h_b^2}{2(n_g-n_c+1)\frac{L_d^3}{A_d}+(n_g-n_c)^2\frac{S^3}{A_S}} \qquad 0.10$$

A comparison of the accuracy of Equation 0.10 relative to the stiffness from the K-frame SAP model is shown in Figure 0-10. Similar trends are observed as for Equation 0.9, but the equation is more conservative. The maximum value in the plot is 0.98 and the minimum is 0.68. The conservatism increases with fewer lean-on girders in a bracing line and becomes the most conservative for a conventional bracing system which occurs along the diagonal of the graph ($n_c = n_g-1$).

While the expression is more conservative, the relative simplicity of the stiffness equation lends itself better to design compared to Eq. 7.23.

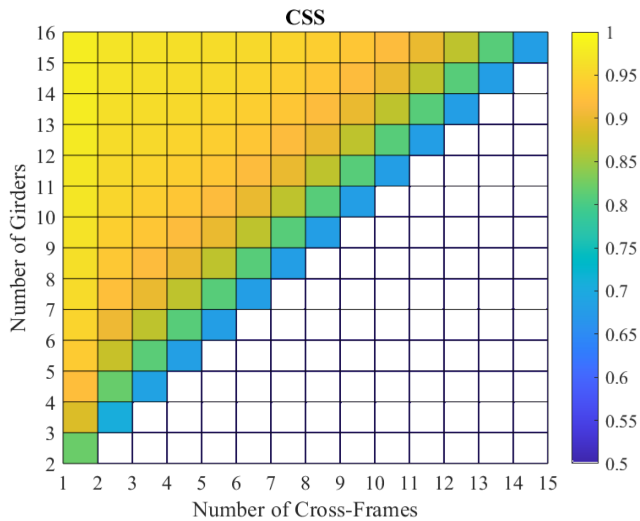

Figure 0-10. $\frac{\beta_{br,CSS}}{\beta_{br,SAP\ model}}$ for Simplified K-Frame Equation Cross-Frames Aligned Exterior

M.5.5 Lean-On X-Frames

In similar fashion to the K-frame equation, in the X-frame lean-on derivation, the generalized displacement of the critical girder is given by Equation 0.11

$$\Delta = \frac{1}{2} n_g \left(\frac{FL^3}{S^2 A_d E}\right) + \left[\frac{1}{2}\left(n_g - 2\right) + \frac{n_g - 1}{2} + \left(n_g - 1\right)\left(n_g - 2\right)\right]\left(\frac{FS}{A_s E}\right) \qquad 0.11$$

In order to apply the CSS approach and remove the implicit assumption of one cross-frame, the expression may be rewritten as Equation 0.12.

$$\Delta = \frac{1}{2}\left(n_g - n_c + 1\right)\left(\frac{FL^3}{S^2 A_d E}\right) + \left[\frac{1}{2}\left(n_g - n_c - 1\right) + \left(n_g - n_c\right)\left(n_g - n_c - 1\right)\right]\left(\frac{FS}{A_s E}\right) \qquad 0.12$$

Which can be reduced to the form of Equation 0.13.

$$\Delta = \frac{1}{2}\left(n_g - n_c + 1\right)\left(\frac{FL^3}{S^2 A_d E}\right) + \left[n_g^2 + n_c^2 - 2n_g n_c - \frac{n_g}{2} + \frac{n_c}{2} - \frac{1}{2}\right]\left(\frac{FS}{A_s E}\right) \qquad 0.13$$

This form can be used to determine the stiffness as Equation 0.14.

$$\beta_{brX} = \frac{ES^2 h_b^2}{\frac{1}{2}\left(n_g - n_c + 1\right)\frac{L_d^3}{A_d} + \left(n_g^2 + n_c^2 - 2n_g n_c - \frac{n_g}{2} + \frac{n_c}{2} - \frac{1}{2}\right)\frac{S^3}{A_s}} \qquad 0.14$$

The result for when the stiffness given by Equation 0.14 is divided by the stiffness determined from the X-frame SAP model with the same cross-frames aligned with full braces in the exterior bays is shown in Figure 0-11. The agreement between the equation and SAP model is again better than with the Z-frames, likely due to the X-frame members ability to carry compression as well as tension to better distribute the forces across the adjacent cross-frames. There is perfect agreement in systems with just one cross-frame in the exterior bay, and the minimum value in the plot is 0.85.

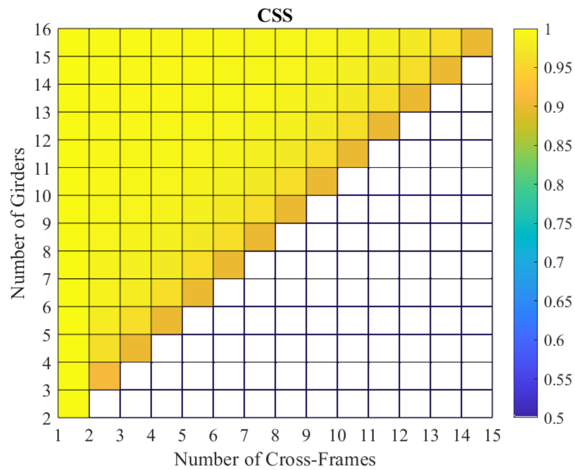

Figure 0-11. $\frac{\beta_{br,CSS}}{\beta_{br,SAP\ model}}$ for X-Frames Cross-Frames Aligned Exterior

The expression in Equation 0.14 contains several terms, which can complicate the use in design. Therefore, to simplify the expression the last three values in the second term of the denominator were neglected producing the following expression:

$$\beta_{brX} = \frac{ES^2 h_b^2}{\frac{1}{2}(n_g - n_c + 1)\frac{L_d^3}{A_d} + (n_g - n_c)^2 \frac{S^3}{A_s}} \qquad 0.15$$

A comparison of the accuracy of Equation 0.15 compared to the stiffness provided from a comparable X-frame SAP model is shown in Figure 0-12. The equation is more conservative with the maximum value in the plot at 0.97 and the minimum at 0.57. As with the Z-frame and K-frame models, the conservatism increases with fewer lean-on girders in a bracing line and becomes the most conservative for a conventional bracing system which occurs along the diagonal of the graph ($n_c = n_g-1$).

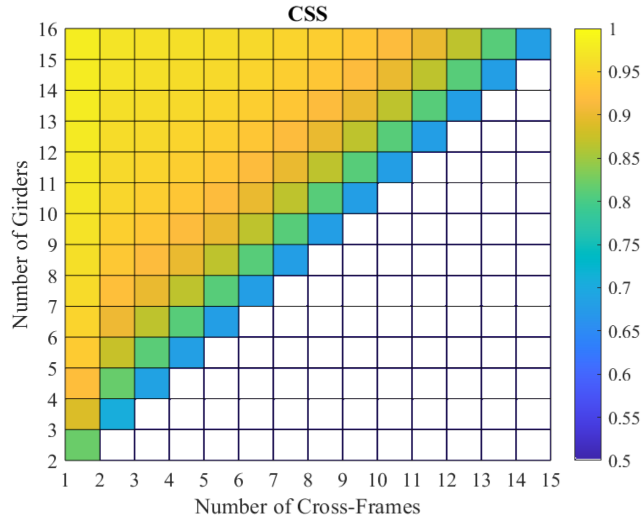

Figure 0-12. $\frac{\beta_{br,CSS}}{\beta_{br,SAP\ model}}$ for Simplified X-Frame Equation Cross-Frames Aligned Exterior

M.6. CCS Adjustments for Interior Bay Cross-Frames

The last section focused on the critical stiffness of a bracing line in which the full cross-frames within the line begin in an exterior bay. To control the in-plane stiffness of the overall system, cross-frames need to be spread out along the width of the bridge. As a result, in many instances, cross-frames may not be located in the exterior bays and will instead by located only in interior bays. This subsection focuses on the appropriate stiffness for the Cross Section Slice (CSS) approach when the cross-frames are on the interior and lean on girders are located on either side.

M.6.1 Performance of Cross-Section Slice with Interior Cross-Frame Placement

When a single cross-frame is placed near the middle of the cross-frame line, as opposed to in an exterior bay, the maximum force in the lean-on struts are reduced compared to cases where the cross-frames are pushed to the exterior bay. This reduction in the strut force distribution results in an increased stiffness of the system. However, the equations derived in Sections 7.1 and 7.2 and with the CSS approach do not take this into account. A comparison of stiffness results from SAP models with the equation for constant cross-frame dimensions is shown in Figure 0-13 for one, two, and three Z, X, or K-frames positioned in the middle of the bracing line. The vertical axis is the ratio of the stiffness of the given bracing line as determined from the computational model divided by the stiffness predicted by the equations developed in the last section. A value of 1.0 means perfect agreement, while values greater than one show the equation is conservative relative to the SAP prediction. As shown, depending on the location of the cross-frame within the bracing line, the conservatism changes significantly. in some cases the model may indicate almost three times the stiffness as predicted by the equation, which assumes the cross-frames are pushed to the exterior bay. The different cross-frame shapes are shown to behave similarly, but the equation is consistently most conservative for X-Frames and least conservative for Z-frames.

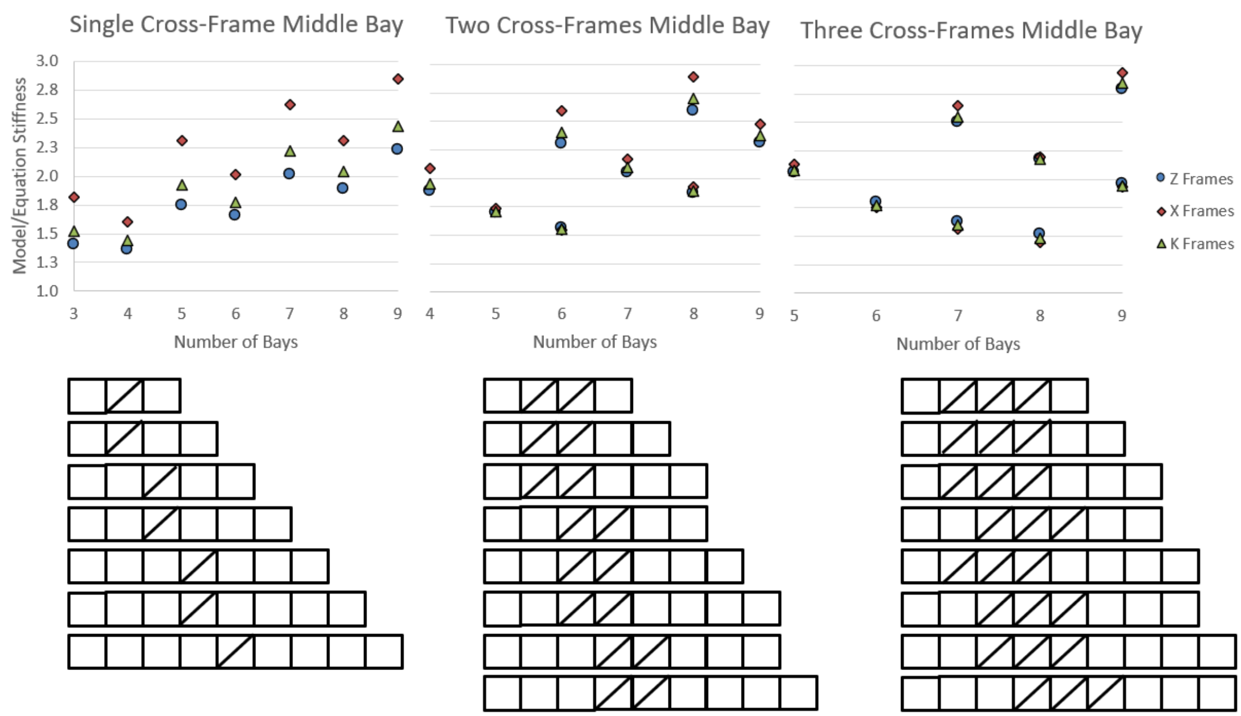

Figure 0-13. Stiffness Increase of Interior Cross-Frame Placement

The stiffness of the bracing lines in Figure 0-13 are superimposed in Figure 0-14 to compare the significance of the number of cross-frames on the stiffness of the system. The results vary depending on the number of bays in the system. For systems with an even number of bays, systems with two cross-frames have highest stiffness relative to the equation, while systems with an odd number of bays have highest stiffness relative to the equation for one or three cross-frames. These are configurations where the cross-frames are perfectly centered in the bracing line.

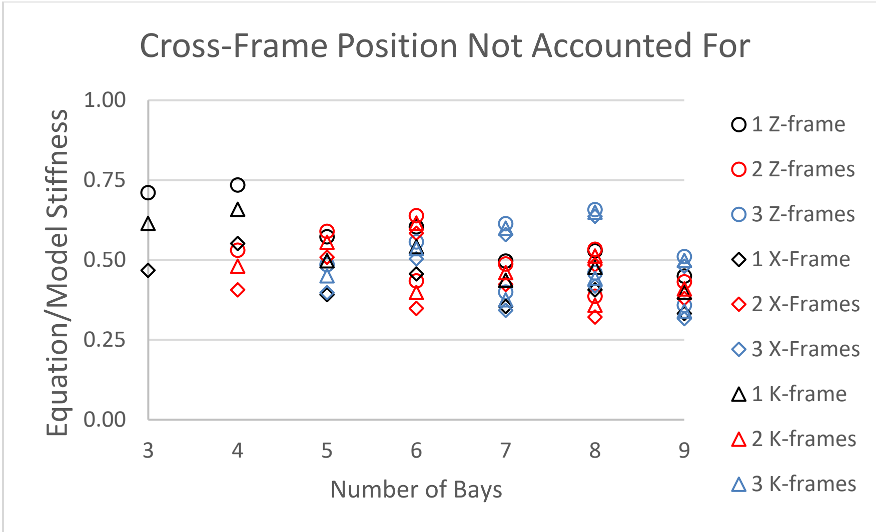

Figure 0-14. Brace Stiffness of Interior Cross-Frame Placement

11.5.1.1. Revised Idealizations and Equation

In an effort to minimize the conservatism for cases with interior cross-frames, a term "n_{lean}" was introduced that reflects the number of leaning girders in the bracing line and further accounts for the location of the cross-frame within the bracing line. Examples are shown in Table M-0-2. A revised equation reflecting these changes is given by Equation 0.16. In order to avoid multiple equations for Z-, X-, or K-frames, the variable C_{CF}, was also introduced into Eq. 7.30 to reflect the type of cross-frame that is utilized. The table idealizes the cross-frame layout to fit the Cross Section Slice layout with parts of the section "grayed" out to represent portions that are conservatively neglected in the calculations of the effective stiffness. Although "X-type" cross-frames are shown in the table, the results also apply to Z-frames and K-frames. The table shows five cases for an 8-girder system and highlights the value of the variables that are to be used in the equation. The variables n_g and n_c are intuitive and simply account for the respective number of girders in the bracing line and the number of cross frames. The value of n_{lean} in the table accounts for the position of the cross-frame in a line. If the cross frames are pushed out to an exterior bay, the number of leaning girders are intuitive and just summed as shown in Case 2 in Table 7-6 where the two cross-frames are pushed to the left side of the bracing line leaving 5 leaning girders that are idealized to all lean on the cross-frame located in the 2nd bay from the left. For the cases with cross-frames located on the interior of the bracing line, the value of n_{lean} is the "critical case" and considers the largest number of leaning bays on either side of the interior cross-frame.

Table M-0-2. Revised CSS Idealization

Real System	n_g	n_c	CSS Equation Idealization	n_{lean}	Revised CSS Idealization
	8	7		0	
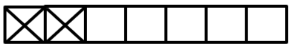	8	2	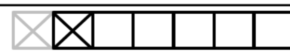	5	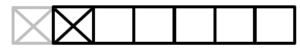
	8	1	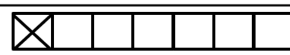	3	
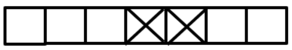	8	2	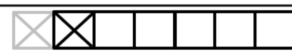	3	
	8	3	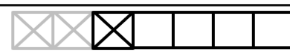	2	

$$\beta_{br,leanAdjCF} = \frac{ES^2 h_b^2}{C_{CF}(n_g - n_c + 1)\frac{L_d^3}{A_d} + (n_{lean}+1)^2 \frac{S^3}{A_s}} \qquad 0.16$$

Where:

C_{CF} is 1.0 for Z-Frames, 0.5 for X-Frames, 2.0 for K-Frames

n_{lean} is the maximum number of adjacent lean-on bays (or leaning girders)

M.6.2 Modified Equation Performance

The comparison of the predicted cross-frame stiffness using Eq. 7.30 versus the SAP model stiffness is shown in Figure 7-23. The cross-frames were positioned in an interior bay. The horizontal axis shows the number of bracing bays available in the specific problem. Therefore, for the case with 3 bays – the system would have 4 total girders. The revised expression substantially reduces the error relative to the model for Z, X, and K-frames, while still maintaining a conservative representation of the stiffness. Layouts that have perfectly centered cross-frames on the bracing line are the most conservative, while layouts with off-center cross-frames approach the same value as the model.

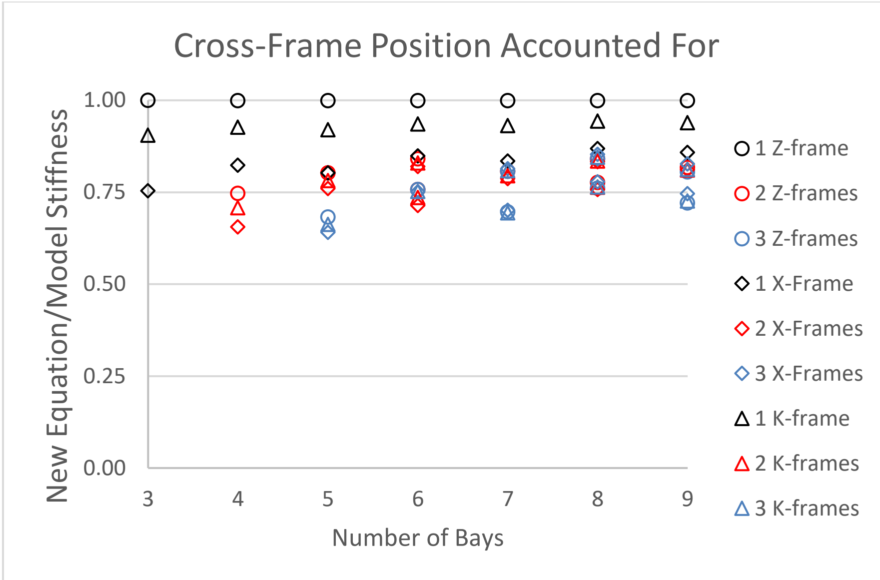

Figure 0-15. Modified Brace Stiffness Equation with Interior Cross-Frames

M.7. CCS Adjustments for Nonadjacent Cross-Frames

The cross-section slice approach was observed to be excessively conservative for cross-frame lines with nonadjacent cross-frames, such as in the checkerboard and X layouts. The equation was studied and adjusted to increase precision without compromising the simplicity of equation application.

M.7.1 Checkerboard Layouts

Cross-frame patterns that would be included in a Checkerboard layout using Z-, X-, or K-frames were modeled in SAP2000. The respective stiffness values were calculated using the displacement of the critical girder, consistent with the method used previously. These values are shown in Figure 0-16.

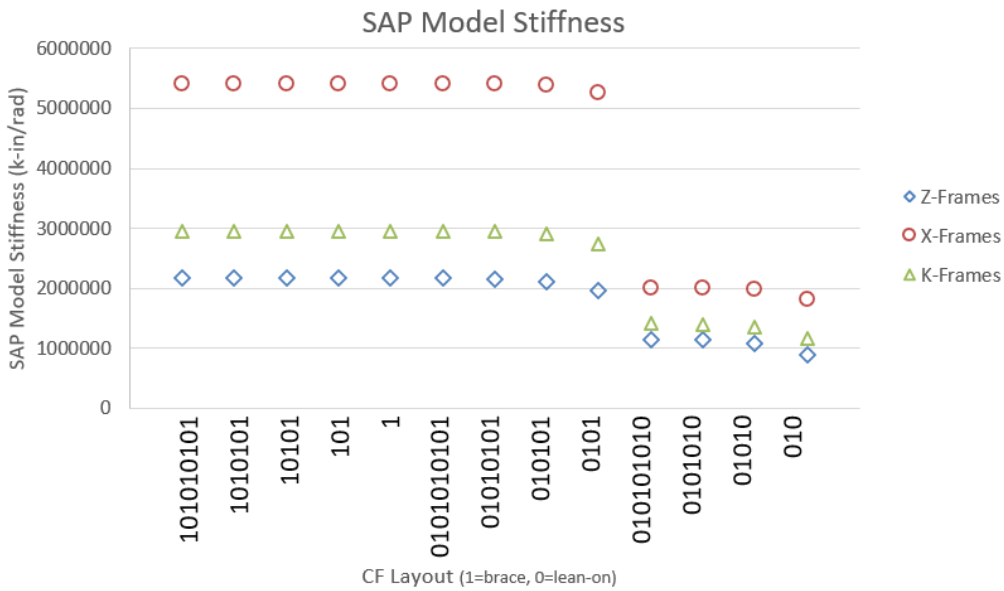

Figure 0-16. Model Stiffness of Checkerboard Bracing Lines

A significant reduction in stiffness can be observed for cross-frame lines with lean-on bays on both exterior bays. With this distinction, checkerboard cross-frame lines can be split into two groups: (1) lines with cross-frames in one or both of the exterior bays, or (2) lines with lean-on struts in both of the exterior bays. The cross-frame lines in the first group may be idealized as a single cross-frame, while the lines in the second group may be idealized as a single cross-frame with a lean-on bay on each side. To confirm this, the SAP model stiffnesses were divided by the idealized stiffness and plotted, as shown in Figure 0-17. Values in the plot that are less than or equal to 1.0 indicate the equation is predicting a lower stiffness than the model, and the two values greater than 1.0 are within 10%.

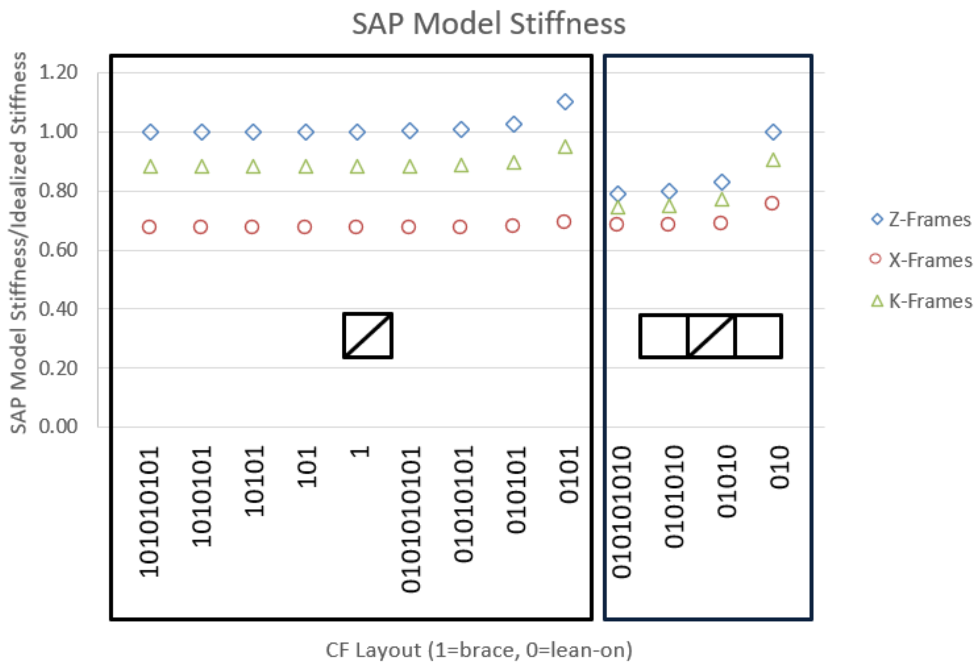

Figure 0-17. Checkerboard Model Stiffness/Idealized Stiffness

As a result, it is appropriate to use "effective" values of $n_{g,eff} = 2, n_{c,eff} = 1$, and $n_{lean,eff} = 0$ for checkerboard cross-frame lines with at least one exterior bay with a cross frame. For lines with two lean-on exterior bays, $n_{g,eff} = 4, n_{c,eff} = 1$, and $n_{lean,eff} = 1$. These findings are summarized in Table M-0-3.

Table M-0-3. Effective Values for Checkerboard Patterns

Number of Bays	Exterior Bay Cross-Frames	Example Patterns	Idealization	Equation Values
Odd	2 Cross-Frames	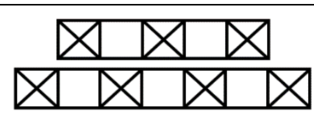	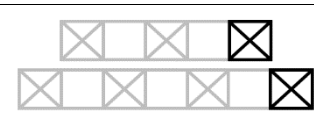	$n_{g,eff} = 2$ $n_{c,eff} = 1$ $n_{lean,eff} = 0$
Even	1 Cross-Frame, 1 Lean-On	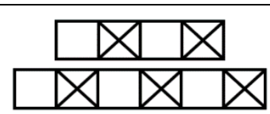	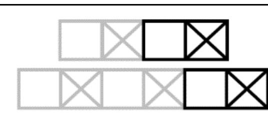	$n_{g,eff} = 3$ $n_{c,eff} = 1$ $n_{lean,eff} = 1$
Odd	2 Lean-On	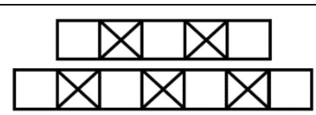	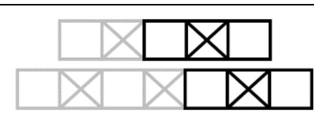	$n_{g,eff} = 4$ $n_{c,eff} = 1$ $n_{lean,eff} = 1$

M.7.2. Other Nonadjacent Cross-Frame Patterns

Similar analysis was conducted for other nonadjacent cross-frame patterns. These remaining instances are grouped into cross-frame lines where greater than 50% of bays contain cross-frames and both exterior cross-frames contain cross-frames, cross-frame lines where less than 50% of bays contain cross-frames and both exterior cross-frames contain cross-frames, and instances where one or both exterior bays are lean-on. For cross-frame lines where greater than 50% of bays and both exterior bays contain cross-frames, the twin girder idealization may be used. When less than 50% of bays contain cross-frames and both exterior bays contain cross-frames, the number of leaning girders may be system may be reduced to reflect the governing section; meaning that the maximum number of adjacent lean-on bays may be divided by two and rounded up to the nearest whole number. Examples of these three cases are shown in Table M-0-4.

Table M-0-4. Example Idealizations for Non-Checkerboard Nonadjacent Cross-Frame Patterns

Number of Bays	**Exterior Bay Cross-Frames**	**Example Patterns**	**Idealization**	**Equation Values**
> 50%	2 Cross-Frames (Bounded)	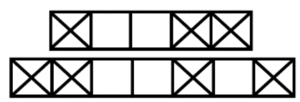	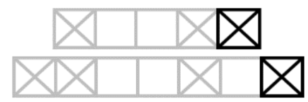	$n_{g,eff} = 2$ $n_{c,eff} = 1$ $n_{lean,eff} = 0$
≤ 50%	2 Cross-Frames (Bounded)	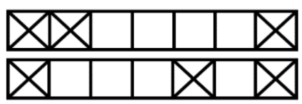	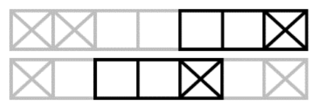	$n_{g,eff} = 4$ $n_{c,eff} = 1$ $n_{lean,eff} = 2$
Any	1 or 2 Lean-On (Unbounded)	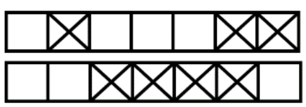	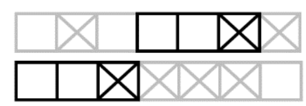	$n_{g,eff} = 4$ $n_{c,eff} = 1$ $n_{lean,eff} = 2$

M.7. Summary of CSS Brace Stiffness Equation

Because the simplified expressions for all three cross-frame types are similar, it is possible to write the generalized brace stiffness equation given by Equation 0.17.

$$\beta_{br,lean} = R\frac{ES^2h_b^2}{C_{CF}(n_{g,eff} - n_{c,eff} + 1)\frac{L_d^3}{A_d} + (n_{lean,eff} + 1)^2\frac{S^3}{A_s}} \quad 0.17$$

Where:

R is the stiffness reduction factor for connection eccentricity, 0.65

C_{CF} is 1.0 for Z-Frames, 0.5 for X-Frames, and 2.0 for K-Frames

$n_{g,eff}$ is the effective number of girders

$n_{c,eff}$ is the effective number of cross-frames in a given bracing line

$n_{lean,eff}$ is the effective number lean-on bays

It is important to note that in lean-on systems, even when a full cross-frame line is present, the C_{nc} factor for conventional bracing cannot be used.

Examples of correct $n_{g,eff}$, $n_{c,eff}$, and $n_{lean,eff}$ values for given bracing lines are shown in Table M-0-5.

Table M-0-5. Correct Values for Brace Stiffness Equation

Cross-Frame Line Pattern Category	**Example Cross-Frame Line**	$n_{g,eff}$	$n_{c,eff}$	$n_{lean,eff}$
Adjacent: Exterior Bay Cross-Frame	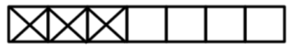	8	3	4
Adjacent: Interior Bay Cross-Frame		8	2	**3**
Checkerboard: ≥ 1 Exterior Cross-Frame		**2**	**1**	**0**
Checkerboard: No Exterior Cross-Frame		**4**	**1**	**1**
Nonadjacent: 2 Exterior Cross-Frames and > 50% Cross-Frames	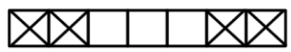	8	4	**2**
Nonadjacent: 2 Exterior Cross-Frames and ≤ 50% Cross-Frames	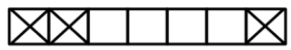	8	3	**4**
Nonadjacent: ≥ 1 Exterior Lean-On	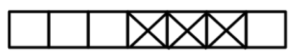	8	3	**3**

M.8. FEM Solution Reference

The following tables provide the constants obtained from the 2D FEM solution that were utilized to derive the brace stiffness and strength expressions.

Table M-0-6. Z-frame 2D FEM Stiffness Results

Bracing Line	$C_1 \frac{FL_d^3}{A_d E S^2}$	$C_2 \frac{FS}{A_s E}$	n_g	$n_{lean,ext}$	$n_{lean,int}$	n_c
Z	2	1	2	0	0	1
Z-L	3	4	3	1	0	1
Z-L-L	4	9	4	2	0	1
Z-L-L-L	5	16	5	3	0	1
Z-L-L-L-L	6	25	6	4	0	1
L-Z-L	4	4	4	1	0	1
L-L-Z-L-L	6	9	6	2	0	1
L-L-L-Z-L-L-L	8	16	8	3	0	1
L-L-L-L-Z-L-L-L-L	10	25	10	4	0	1
L-Z-L-L	5	9	5	2	0	1
L-Z-L-L-L	6	16	6	3	0	1
L-Z-L-L-L-L	7	25	7	4	0	1
L-Z-L-L-L-L-L	8	36	8	5	0	1
L-L-Z-L-L-L	7	16	7	3	0	1
L-L-Z-L-L-L-L	8	25	8	4	0	1
L-L-Z-L-L-L-L-L	9	36	9	5	0	1

L-L-L-Z-L-L-L-L	9	25	9	4	0	1
L-L-L-Z-L-L-L-L-L	10	36	10	5	0	1
L-Z-Z-L	5/2	4	5	1	0	2
L-L-Z-Z-L-L	7/2	9	7	2	0	2
L-L-L-Z-Z-L-L-L	9/2	16	9	3	0	2
L-L-L-L-Z-Z-L-L-L-L	11/2	25	11	4	0	2
Z-Z	3/2	1	3	0	0	2
Z-L-Z	4/2	1	4	0	0	2
Z-L-L-Z	5/2	5/2	5	0	1	2
Z-L-L-L-Z	6/2	4	6	0	2	2
Z-L-L-L-L-Z	7/2	13/2	7	0	3	2
Z-L-L-L-L-L-Z	8/2	9	8	0	4	2
Z-L-L-L-L-L-L-Z	9/2	25/2	9	0	5	2
Z-L-L-L-L-L-L-L-Z	10/2	16	10	0	6	2
Z-L-L-L-L-L-L-L-L-Z	11/2	41/2	11	0	7	2
L-Z-L-Z-L	6/2	4	6	1	0	2
L-Z-L-L-Z-L	7/2	4	7	1	1	2
L-Z-L-L-L-Z-L	8/2	4	8	1	2	2
L-Z-L-L-L-L-Z-L	9/2	13/2	9	1	3	2
L-Z-L-L-L-L-L-Z-L	10/2	9	10	1	4	2
L-Z-L-L-L-L-L-L-Z-L	11/2	25/2	11	1	5	2
L-L-Z-L-Z-L-L	8/2	9	8	2	0	2
L-L-Z-L-L-Z-L-L	9/2	9	9	2	1	2
L-L-Z-L-L-L-Z-L-L	10/2	9	10	2	2	2
L-L-Z-L-L-L-L-Z-L-L	11/2	9	11	2	3	2
L-L-Z-L-L-L-L-L-Z-L-L	12/2	9	12	2	4	2
L-L-Z-L-L-L-L-L-L-Z-L-L	13/2	25/2	13	2	5	2
L-L-L-Z-L-Z-L-L-L	10/2	16	10	3	0	2
L-L-L-Z-L-L-Z-L-L-L	11/2	16	11	3	1	2
L-L-L-Z-L-L-L-Z-L-L-L	12/2	16	12	3	2	2
L-L-L-Z-L-L-L-L-Z-L-L-L	13/2	16	13	3	3	2
L-L-L-Z-L-L-L-L-L-Z-L-L-L	14/2	16	14	3	4	2
L-L-L-Z-L-L-L-L-L-L-Z-L-L-L	15/2	16	15	3	5	2

Table M-0-7. X-frame 2D FEM Stiffness Results

Bracing Line	$C_1 \frac{FL_d^3}{A_d E S^2}$	$C_2 \frac{FS}{A_s E}$	n_g	$n_{lean,ext}$	$n_{lean,int}$	n_c
X	2/2	0	2	0	0	1
X-L	3/2	10/4	3	1	0	1
X-L-L	4/2	28/4	4	2	0	1
X-L-L-L	5/2	54/4	5	3	0	1
X-L-L-L-L	6/2	88/4	6	4	0	1
L-X-L	4/2	8/4	4	1	0	1
L-L-X-L-L	6/2	24/4	6	2	0	1

L-L-L-X-L-L-L	8/2	48/4	8	3	0	1
L-L-L-L-X-L-L-L-L	10/2	80/4	10	4	0	1
L-X-X-L	5/4	11/4	5	1	0	2
L-L-X-X-L-L	7/4	29/4	7	2	0	2
L-L-L-X-X-L-L-L	9/4	55/4	9	3	0	2
L-L-L-L-X-X-L-L-L-L	11/4	89/4	11	4	0	2
X-X	3/4	1/4	3	0	0	2
X-L-X	4/4	0	4	0	0	2
X-L-L-X	5/4	5/4	5	0	1	2
X-L-L-L-X	6/4	10/4	6	0	2	2
X-L-L-L-L-X	7/4	19/4	7	0	3	2
X-L-L-L-L-L-X	8/4	28/4	8	0	4	2
X-L-L-L-L-L-L-X	9/4	41/4	9	0	5	2
X-L-L-L-L-L-L-L-X	10/4	54/4	10	0	6	2
X-L-L-L-L-L-L-L-L-X	11/4	71/4	11	0	7	2
L-X-L-X-L	6/4	10/4	6	1	0	2
L-X-L-L-X-L	7/4	9/4	7	1	1	2
L-X-L-L-L-X-L	8/4	8/4	8	1	2	2
L-X-L-L-L-L-X-L	9/4	17/4	9	1	3	2
L-X-L-L-L-L-L-X-L	10/4	26/4	10	1	4	2
L-X-L-L-L-L-L-L-X-L	11/4	39/4	11	1	5	2
L-L-X-L-X-L-L	8/4	28/4	8	2	0	2
L-L-X-L-L-X-L-L	9/4	27/4	9	2	1	2
L-L-X-L-L-L-X-L-L	10/4	26/4	10	2	2	2
L-L-X-L-L-L-L-X-L-L	11/4	25/4	11	2	3	2
L-L-X-L-L-L-L-L-X-L-L	12/4	24/4	12	2	4	2
L-L-X-L-L-L-L-L-L-X-L-L	13/4	37/4	13	2	5	2
L-L-L-X-L-X-L-L-L	10/4	54/4	10	3	0	2
L-L-L-X-L-L-X-L-L-L	11/4	53/4	11	3	1	2
L-L-L-X-L-L-L-X-L-L-L	12/4	52/4	12	3	2	2
L-L-L-X-L-L-L-L-X-L-L-L	13/4	51/4	13	3	3	2
L-L-L-X-L-L-L-L-L-X-L-L-L	14/4	50/4	14	3	4	2
L-L-L-X-L-L-L-L-L-L-X-L-L-L	15/4	49/4	15	3	5	2

Table M-0-8. K-frame 2D FEM Stiffness Results

Bracing Line	$C_1 \frac{FL_d^3}{A_d E S^2}$	$C_2 \frac{FS}{A_s E}$	n_g	$n_{lean,ext}$	$n_{lean,int}$	n_c
K	4	2/4	2	0	0	1
K-L	6	13/4	3	1	0	1
K-L-L	8	32/4	4	2	0	1
K-L-L-L	10	59/4	5	3	0	1
K-L-L-L-L	12	94/4	6	4	0	1

L-K-L	8	12/4	4	1	0	1
L-L-K-L-L	12	30/4	6	2	0	1
L-L-L-K-L-L-L	16	56/4	8	3	0	1
L-L-L-L-K-L-L-L-L	20	90/4	10	4	0	1
L-K-K-L	5	27/8	5	1	0	2
L-L-K-K-L-L	7	65/8	7	2	0	2
L-L-L-K-K-L-L-L	9	119/8	9	3	0	2
L-L-L-L-K-K-L-L-L-L	11	189/8	11	4	0	2
K-K	3	5/8	3	0	0	2
K-L-K	4	4/8	4	0	1	2
K-L-L-K	5	3/8	5	0	2	2
K-L-L-L-K	6	2/8	6	0	3	2
K-L-L-L-L-K	7	1/8	7	0	4	2
K-L-L-L-L-L-K	8	0	8	0	5	2
L-K-L-K-L	6	26/8	6	1	1	2
L-K-L-L-K-L	7	25/8	7	1	2	2
L-K-L-L-L-K-L	8	24/8	8	1	3	2
L-K-L-L-L-L-K-L	9	23/8	9	1	4	2
L-L-K-L-K-L-L	8	64/8	8	2	1	2
L-L-K-L-L-K-L-L	9	63/8	9	2	2	2
L-L-K-L-L-L-K-L-L	10	62/8	10	2	3	2
L-L-K-L-L-L-L-K-L-L	11	61/8	11	2	4	2
L-L-L-K-L-K-L-L-L	10	118/8	10	3	1	2
L-L-L-K-L-L-K-L-L-L	11	117/8	11	3	2	2
L-L-L-K-L-L-L-K-L-L-L	12	116/8	12	3	3	2
L-L-L-K-L-L-L-L-K-L-L-L	13	115/8	13	3	4	2

Table M-0-9. Z-frame 2D FEM Strength Results

Bracing Line	$C_{diag}\frac{FL_d}{S}$	$C_{slean}F$	$C_{st,sb}F$	n_g	$n_{lean,ext}$	$n_{lean,int}$	n_c
Z	2	0	1	2	0	0	1
Z-L	3	1	2	3	1	0	1
Z-L-L	4	2	3	4	2	0	1
Z-L-L-L	5	3	4	5	3	0	1
Z-L-L-L-L	6	4	5	6	4	0	1
L-Z-L	4	1	2	4	1	0	1
L-L-Z-L-L	6	2	3	6	2	0	1
L-L-L-Z-L-L-L	8	3	4	8	3	0	1
L-L-L-L-Z-L-L-L-L	10	4	5	10	4	0	1
L-Z-Z-L	5/2	1	2	5	1	0	2
L-L-Z-Z-L-L	7/2	2	3	7	2	0	2

L-L-L-Z-Z-L-L-L	9/2	3	4	9	3	0	2
L-L-L-L-Z-Z-L-L-L-L	11/2	4	5	11	4	0	2
Z-Z	3/2	0	1	3	0	0	2
Z-L-Z	2	0	1	4	0	0	2
Z-L-L-Z	5/2	1/2	3/2	5	0	1	2
Z-L-L-L-Z	3	1	2	6	0	2	2
Z-L-L-L-L-Z	7/2	3/2	5/2	7	0	3	2
Z-L-L-L-L-L-Z	4	2	3	8	0	4	2
Z-L-L-L-L-L-L-Z	9/2	5/2	7/2	9	0	5	2
Z-L-L-L-L-L-L-L-Z	5	3	4	10	0	6	2
Z-L-L-L-L-L-L-L-L-Z	11/2	7/2	9/2	11	0	7	2
L-Z-L-Z-L	3	1	2	6	1	0	2
L-Z-L-L-Z-L	7/2	1	2	7	1	1	2
L-Z-L-L-L-Z-L	4	1	2	8	1	2	2
L-Z-L-L-L-L-Z-L	9/2	3/2	5/2	9	1	3	2
L-Z-L-L-L-L-L-Z-L	5	2	3	10	1	4	2
L-Z-L-L-L-L-L-L-Z-L	11/2	5/2	7/2	11	1	5	2
L-L-Z-L-Z-L-L	4	2	3	8	2	0	2
L-L-Z-L-L-Z-L-L	9/2	2	3	9	2	1	2
L-L-Z-L-L-L-Z-L-L	5	2	3	10	2	2	2
L-L-Z-L-L-L-L-Z-L-L	11/2	2	3	11	2	3	2
L-L-Z-L-L-L-L-L-Z-L-L	6	2	3	12	2	4	2
L-L-Z-L-L-L-L-L-L-Z-L-L	13/2	5/2	7/2	13	2	5	2
L-L-L-Z-L-Z-L-L-L	5	3	4	10	3	0	2
L-L-L-Z-L-L-Z-L-L-L	11/2	3	4	11	3	1	2
L-L-L-Z-L-L-L-Z-L-L-L	6	3	4	12	3	2	2
L-L-L-Z-L-L-L-L-Z-L-L-L	13/2	3	4	13	3	3	2
L-L-L-Z-L-L-L-L-L-Z-L-L-L	7	3	4	14	3	4	2
L-L-L-Z-L-L-L-L-L-L-Z-L-L-L	15/2	3	4	15	3	5	2

Table M-0-10. X-frame 2D FEM Strength Results

Bracing Line	$C_{diag}\frac{FL_d}{S}$	$C_{slean}F$	$C_{st,sb}F$	n_g	$n_{lean,ext}$	$n_{lean,int}$	n_c
X	1	0	0	2	0	0	1
X-L	3/2	1	-1/2	3	1	0	1
X-L-L	2	2	-2/2	4	2	0	1
X-L-L-L	5/2	3	-3/2	5	3	0	1
X-L-L-L-L	3	4	-4/2	6	4	0	1
L-X-L	2	1	0	4	1	0	1
L-L-X-L-L	3	2	0	6	2	0	1
L-L-L-X-L-L-L	4	3	0	8	3	0	1

L-L-L-L-X-L-L-L-L	5	4	0	10	4	0	1
L-X-X-L	5/4	1	3/4	5	1	0	2
L-L-X-X-L-L	7/4	2	5/4	7	2	0	2
L-L-L-X-X-L-L-L	9/4	3	7/4	9	3	0	2
L-L-L-L-X-X-L-L-L-L	11/4	4	9/4	11	4	0	2
X-X	3/4	0	1/4	3	0	0	2
X-L-X	4/4	0	0	4	0	0	2
X-L-L-X	5/4	1/2	-1/4	5	0	1	2
X-L-L-L-X	6/4	1	-2/4	6	0	2	2
X-L-L-L-L-X	7/4	3/2	-3/4	7	0	3	2
X-L-L-L-L-L-X	8/4	2	-4/4	8	0	4	2
X-L-L-L-L-L-L-X	9/4	5/2	-5/4	9	0	5	2
X-L-L-L-L-L-L-L-X	10/4	3	-6/4	10	0	6	2
X-L-L-L-L-L-L-L-L-X	11/4	7/2	-7/4	11	0	7	2
L-X-L-X-L	6/4	1	2/4	6	1	0	2
L-X-L-L-X-L	7/4	1	1/4	7	1	1	2
L-X-L-L-L-X-L	8/4	1	0	8	1	2	2
L-X-L-L-L-L-X-L	9/4	3/2	-1/4	9	1	3	2
L-X-L-L-L-L-L-X-L	10/4	2	-2/4	10	1	4	2
L-X-L-L-L-L-L-L-X-L	11/4	5/2	-3/4	11	1	5	2
L-L-X-L-X-L-L	8/4	2	4/4	8	2	0	2
L-L-X-L-L-X-L-L	9/4	2	3/4	9	2	1	2
L-L-X-L-L-L-X-L-L	10/4	2	2/4	10	2	2	2
L-L-X-L-L-L-L-X-L-L	11/4	2	1/4	11	2	3	2
L-L-X-L-L-L-L-L-X-L-L	12/4	2	0	12	2	4	2
L-L-X-L-L-L-L-L-L-X-L-L	13/4	5/2	-1/4	13	2	5	2
L-L-L-X-L-X-L-L-L	10/4	3	6/4	10	3	0	2
L-L-L-X-L-L-X-L-L-L	11/4	3	5/4	11	3	1	2
L-L-L-X-L-L-L-X-L-L-L	12/4	3	4/4	12	3	2	2
L-L-L-X-L-L-L-L-X-L-L-L	13/4	3	3/4	13	3	3	2
L-L-L-X-L-L-L-L-L-X-L-L-L	14/4	3	2/4	14	3	4	2
L-L-L-X-L-L-L-L-L-L-X-L-L-L	15/4	3	1/4	15	3	5	2

Table M-0-11. K-frame 2D FEM Strength Results

Bracing Line	$C_{diag}\frac{FL_d}{S}$	$C_{slean}F$	$C_{sb}F$	$C_{st}F$	n_g	$n_{lean,ext}$	$n_{lean,int}$	n_c
K	2	0	1	0	2	0	0	1
K-L	3	1	2	1/2	3	1	0	1
K-L-L	4	2	3	2/2	4	2	0	1
K-L-L-L	5	3	4	3/2	5	3	0	1
K-L-L-L-L	6	4	5	4/2	6	4	0	1

L-K-L	4	1	2	0	4	1	0	1
L-L-K-L-L	6	2	3	0	6	2	0	1
L-L-L-K-L-L-L	8	3	4	0	8	3	0	1
L-L-L-L-K-L-L-L-L	10	4	5	0	10	4	0	1
L-K-K-L	5/2	1	2	3/4	5	1	0	2
L-L-K-K-L-L	7/2	2	3	5/4	7	2	0	2
L-L-L-K-K-L-L-L	9/2	3	4	7/4	9	3	0	2
L-L-L-L-K-K-L-L-L-L	11/2	4	5	9/4	11	4	0	2
K-K	3/2	0	1	1/4	3	0	0	2
K-L-K	4/2	0	1	0	4	0	0	2
K-L-L-K	5/2	1/2	3/2	-1/4	5	0	1	2
K-L-L-L-K	6/2	2/2	4/2	-2/4	6	0	2	2
K-L-L-L-L-K	7/2	3/2	5/2	-3/4	7	0	3	2
K-L-L-L-L-L-K	8/2	4/2	6/2	-4/4	8	0	4	2
K-L-L-L-L-L-L-K	9/2	5/2	7/2	-5/4	9	0	5	2
K-L-L-L-L-L-L-L-K	10/2	6/2	8/2	-6/4	10	0	6	2
K-L-L-L-L-L-L-L-L-K	11/2	7/2	9/2	-7/4	11	0	7	2
L-K-L-K-L	6/2	1	2	2/4	6	1	0	2
L-K-L-L-K-L	7/2	1	2	1/4	7	1	1	2
L-K-L-L-L-K-L	8/2	1	2	0	8	1	2	2
L-K-L-L-L-L-K-L	9/2	3/2	5/2	-1/4	9	1	3	2
L-K-L-L-L-L-L-K-L	10/2	4/2	6/2	-2/4	10	1	4	2
L-K-L-L-L-L-L-L-K-L	11/2	5/2	7/2	-3/4	11	1	5	2
L-L-K-L-K-L-L	8/2	2	3	4/4	8	2	0	2
L-L-K-L-L-K-L-L	9/2	2	3	3/4	9	2	1	2
L-L-K-L-L-L-K-L-L	10/2	2	3	2/4	10	2	2	2
L-L-K-L-L-L-L-K-L-L	11/2	2	3	1/4	11	2	3	2
L-L-K-L-L-L-L-L-K-L-L	12/2	2	3	0	12	2	4	2
L-L-K-L-L-L-L-L-L-K-L-L	13/2	5/2	7/2	-1/4	13	2	5	2
L-L-L-K-L-K-L-L-L	10/2	3	4	6/4	10	3	0	2
L-L-L-K-L-L-K-L-L-L	11/2	3	4	5/4	11	3	1	2
L-L-L-K-L-L-L-K-L-L-L	13/2	3	4	4/4	12	3	2	2
L-L-L-K-L-L-L-L-K-L-L-L	14/2	3	4	3/4	13	3	3	2
L-L-L-K-L-L-L-L-L-K-L-L-L	15/2	3	4	2/4	14	3	4	2
L-L-L-K-L-L-L-L-L-L-K-L-L-L	16/2	3	4	1/4	15	3	5	2

Appendix N. Value of Research

N.1. Motivation and Significance

I-shaped girders are often utilized in steel bridge systems as an efficient and economical solution in a wide range of bridge applications. During construction stages, the steel section alone generally supports the full load. Construction stages are often critical for lateral-torsional buckling (LTB), which is a limit state that involves lateral movement of the compression flange and twist of the section. Conventional practice in steel bridges is to provide cross frames in each bay between adjacent girders along the width of the bridge to improve the LTB capacity of the section during construction. However, this leads to high construction costs, as well as significant handling and fabrication requirements. Therefore, refining the design and detailing of cross frame systems such that they can be placed at strategically identified locations along the width and length of the bridge is advantageous.

This research project has demonstrated that if properly detailed and distributed along the length and width of the bridge, lean-on bracing systems can reduce the number of full cross frames required while potentially improving the long-term behavior of bridge. A well-designed and detailed lean-on bracing system potentially offers significant savings in fabrication costs, simplifies the erection process, and alleviates in-service cross-frame force demands in heavily skewed bridges.

The research approach includes the following tasks: (1) conducting background studies and literature review; (2) reviewing recent bridge designs utilizing lean-on bracing; (3) preparing field instrumentation plans; (4) performing field instrumentation and monitoring; (5) conducting live load testing on completed bridges; (6) conducting parametric FEA analysis of lean-on bracing in steel bridges; and (7) developing enhancements of design methodology and detailed design examples.

The research team conducted field studies on bridge designs that currently utilize lean-on bracing in an effort to identify problems faced by engineers during the design process with the application of limited existing expressions. The research team studied the system performance of different locations of cross-frames in combination with lean-on struts and developed modifications to the in-plane girder stiffness equation to account for the lean-on bracing. The research team performed derivations to develop expressions for the provided brace stiffness of different cross frame shapes (Z-, X-, or K) and their placement in lean-on system. Based on the results obtained by parametric FEA analysis, different layouts are recommended for different types of bridges, for example, ZigZag layout for normal bridges with 4-5 girders, X layout for normal bridges with more than 5 girders, Diagonal layout for skew bridges, and Checkerboard layout for skew bridges as well as normal bridges with 4-5 girders.

N.2. Qualitative Values

Qualitative values are non-monetary intangible subjective benefits. Qualitative values are something that cannot be measured numerically or in terms of quantity. These values are subjective and often described in terms of qualities, properties, or characteristics rather than being measured in numerical terms.

N.2.1. Level of Knowledge

The Texas Department of Transportation has over 6779 steel girder bridges in the bridge inventory. As steel I-girders are prone to LTB, all of these bridges require torsional bracing. The conventional approach is to place the cross-frames in each bay along the bridge length and width. This project delivers methods to reduce the number of cross-frames in a bridge. The research in this project involved field monitoring and inspection along with detailed parametric finite element analysis. The behavior of various cross-frame layouts and types were investigated.

This research project will benefit all stakeholders. At the end of this project, TxDOT will receive design methodology with clear set of instructions that will aid the designers and engineers to strategically place cross-frames in a bridge along with potential cross-frame layout recommendations for various types of bridges. Increasing the level of knowledge is important for TxDOT so that the bridge engineers and inspectors have a better understanding of the behavior and can assure the safety of these bridges while reducing costs.

N.2.2. Environmental Sustainability

Steel production has a number of impacts on the environment, including air emissions, wastewater contaminants, hazardous wastes, and solid wastes. Virtually all the greenhouse emissions associated with steel production are from the carbon dioxide emissions related to energy consumption. Gaseous emissions and metal dust are the most prominent sources of waste from electric arc furnaces, a process used in the production of steel.

This research will reduce the number of cross-frames, thereby reducing the quantity of steel utilized in bridges. Consequently, this decrease in steel usage will lessen the demand for steel production, subsequently mitigating its environmental impact. Moreover, the reduced need for steel transportation will contribute to decline in pollution related with transportation.

N.3. Economic Values

This research project aimed to deliver economic benefits to the Texas Department of Transportation by suggesting Refined Design Methods for Lean-On Bracing that can be implemented on Texas bridges. This will result in a lesser number of cross-frames being used along the length and width of the bridge. The potential economic value of this research is to reduce construction, operations, and maintenance cost of steel bridge structures based on developed design guidelines.

N.3.1. Increased Service Life

Findings from this research allow for a reduced number of cross-frames to be utilized to brace girders as compared to a conventional bracing approach. In skew scenarios, cross-frames may be replaced with lean-on struts near the support, thereby eliminating some of the fatigue prone cross-frames. This will improve the fatigue performance of lean-on system as compared to the conventional system.

N.3.2. Expedited Project Delivery

The time required to build a bridge using refined design methods for lean-on bracing will be significantly less than that required to build a bridge using conventional cross-frame layout. This is due to the fact that fewer cross-frames will need to be bolted or welded between the girders. The utilization of fewer cross-frames will further reduce the time taken to build the bridge. Therefore, as the application of lean-on bracing developed in this project will allow the bridge to open faster than conventional bracing, the results have a direct positive effect on public transportation by increasing the availability of new roadway.

N.3.3. Reduced Construction, Operations, and Maintenance Cost

As the number of cross-frames that need to be provided will be reduced, the construction cost will also be reduced significantly. According to US Bureau of Labor Statistics, the hourly mean wage of construction laborers in the Highway, Street, and Bridge Construction industry is $26.52. The mean hourly wage for Construction Managers is $57.69 and for Civil Engineers, its $41.97. Moreover, the costs associated to the equipment present on-site are substantial. These costs can add up to large amounts even if the construction takes a few more days. By utilizing the refined design methods for lean-on bracing, these costs can be directly reduced because the project can be built in relatively less amount of time.

At the time this report was being prepared, 57520 bridges had been constructed in Texas according to TxDOT (2023). Most of these structures (about 35693 bridges) are concrete and steel bridges, which is about 62% of all bridges in the state. Among these, 492 are weathering steel, and 6,287 are painted steel bridges. Therefore, the total number of steel bridges in the state is 6779. In addition, according to Texas bridge database (TxDOT, 2023), on an average 6000 new bridges will be built in every 10 years, including 708 steel bridges (12 % of total). Therefore, it can be forecasted that there will be 71 new steel bridges being constructed per year for the next 10 years.

Consider a 5-girder bridge with 250 ft span length and 25 ft of unbraced lengths. The number of cross-frames required according to the traditional design approach will be 44. The recommended cross-frame layout from the research for a 5-girder bridge with or without skew is checkerboard. This layout will have a total of 28 cross-frames. Assuming girder spacing to be 10 ft, height of cross-frame to be 74 in, length of top and bottom struts to be 102 in, the length of diagonal comes out to be 126 in. Steel length required for one cross-frame will be equal to 604 in. For 44 and 28 cross-frames this come out to be 2215 ft and 1409 ft respectively. Assuming L6x6x$\frac{5}{8}$ angle is used for the diagonal and the top and bottom struts; the total volume of steel will be the product of the steel length and the area of the angle. Therefore, the volume of steel required for 44 and 28 cross-frames will be 110 ft^3 and 70 ft^3 respectively. Density of steel is 490 $\frac{lb}{ft^3}$. Hence, the total weight of steel required for 44 and 28 cross-frames will be 53900 lb and 34300 lb respectively. There will be 32 more top and bottom struts in the lean-on layout, this will add 6600 lb to the lean-on weight. Assuming steel and fabrication costs to be \$2/lb, the total cost for cross-frames in conventional and lean-on layout will be \$107,800 and \$81,800 respectively for one bridge. For 6779 bridges, this equals to \$730,776,200 and \$554,522,200. Therefore, the cost saving will be \$176,254,000.

Table N-0-1: Cost of one cross-frame for conventional vs. lean-on layout

	Conventional layout	Lean-on layout
Number of cross-frames required	44	28
Quantity of steel required	110 ft^3	70 ft^3
Weight of steel required	54,000 lb	34,000 lb
Total cost for cross-frames per bridge	\$108,000	\$82,000

Steel bridges need repair and maintenance over the bridge service life. As a result of the lower number of cross-frames that need to be inspected, there will be a reduction in the amount of time the lanes will be closed to the traffic for inspection. The results of the current project have a direct positive effect on public transportation by reducing the time spent on the roads. Indirect costs include wasted time for drivers stuck in congestion, excess fuel consumption, and environmental impact of traffic jams. Additionally, steel must be painted and touched up regularly to avoid corrosion. According to NCHRP Synthesis 354, lane closures incur an economic loss of \$11,000 per hour per lane (Connor et al., 2005). In addition, longer duration for the resulting inspections and maintenance provides increased safety risks to the inspection personnel and travelling public. While some traffic control may still be necessary (as with any bridge inspection), the length of time will be significantly less.

A major difficulty for TxDOT is managing and maintaining sufficient maintenance staff for inspection and repair of the bridge inventory. Refined methods for lean-on bracing reduce the inspection and maintenance demands, thereby reducing administrative demands on the TxDOT Maintenance Division.

The cost savings as seen in Table N-0-1 per bridge is \$26,000. As 71 new steel bridges will be constructed in the state per year for the next 10 years, the cost savings per year will be \$1,846,000.

The expected total saving after 10 years is calculated to be \$15,634,000. Another relevant number is the payback period which indicates the length of time it requires to recover the budget of the project. The payback period for this project is 0.53 years, thus after approximately 7 months of termination of this research project, the project will reach the break-even point and start to generate profits.

The net present value (NPV) determines the current value of future cash flow by accounting for the time value of money. It provides a dynamic approach for evaluating project costs and benefits over time. The NPV formula used by TxDOT (2015) is:

$$NPV = \sum_{t=1}^{T} \frac{C_t}{(1+r)^t} - C_0 \tag{1}$$

where C_t represents net cash inflow during the period, C_0 is the initial investment, r is the discount rate, and t stands for the number of time periods. The discount rate is typically 5% (TxDOT, 2015), and the cost analysis is estimated for a 10-year period. Figure N-0-1 shows the progression of NPV over the next 10 years. Finally, the benefit-cost ratio (BCR) can be determined by:

$$BCR = \frac{NPV}{Project\ Budget} \tag{2}$$

The benefit-cost ratio was calculated to be 13, which indicates that the Texas Department of Transportation can expect a benefit of \$13 with each dollar invested in this research project.

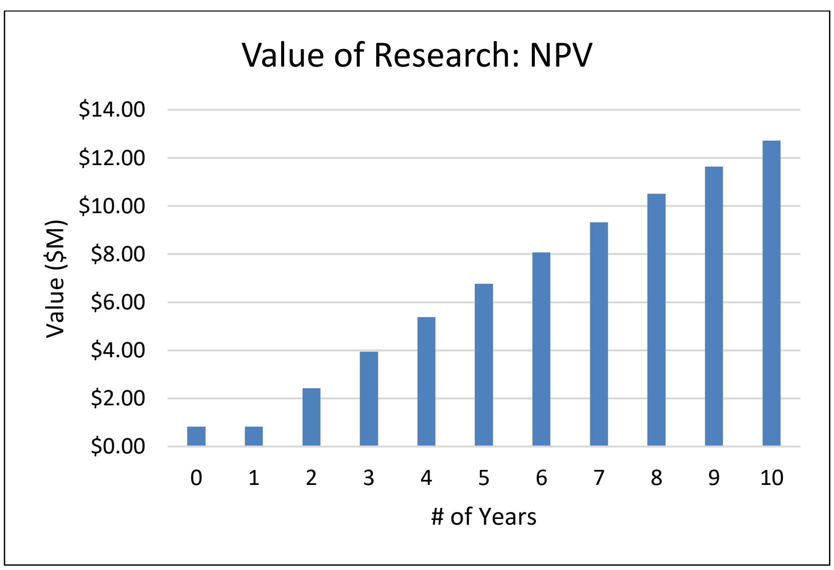

Figure N-0-1: Progression of Net Present Value over 10 years

Figure N-0-2 shows a snipped image of value of research calculation. The image also shows the cost saving in terms of net present value for next 10 years in the form of bar chart along with data presented in tabular form.

Project #	0-7093				
Project Name:	Refined Design Methods for Lean-On Bracing				
Agency:	CTR/TTI	Project Budget	$	9,80,000	
Project Duration (Yrs)	3.5	Exp. Value (per Yr)	$	18,46,000	
Expected Value Duration (Yrs)	10	Discount Rate		5%	
Economic Value					
Total Savings:	$ 1,56,34,000	Net Present Value (NPV):	$	1,27,25,931	
Payback Period (Yrs):	0.530878	Cost Benefit Ratio (CBR, $1 : $___):	$	13	

Years	Expected Value
0	$8,66,000
1	$0
2	$18,46,000
3	$18,46,000
4	$18,46,000
5	$18,46,000
6	$18,46,000
7	$18,46,000
8	$18,46,000
9	$18,46,000
10	$18,46,000

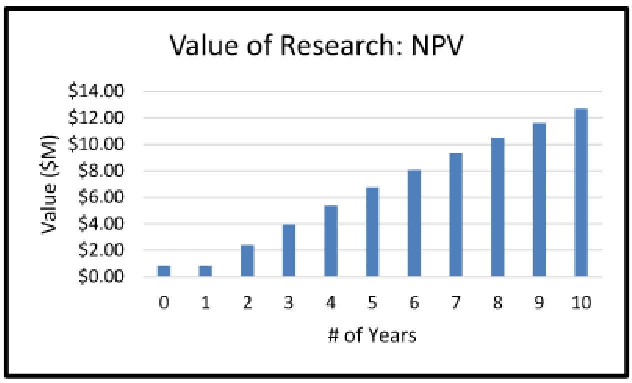

Years	Expected Value	Expected Value	Expected Value	NPV
0	$8,66,000	$8,66,000	$0.87	$0.82
1	$0	$8,66,000	$0.87	$0.82
2	$18,46,000	$27,12,000	$2.71	$2.42
3	$18,46,000	$45,58,000	$4.56	$3.94
4	$18,46,000	$64,04,000	$6.40	$5.38
5	$18,46,000	$82,50,000	$8.25	$6.76
6	$18,46,000	$1,00,96,000	$10.10	$8.07
7	$18,46,000	$1,19,42,000	$11.94	$9.32
8	$18,46,000	$1,37,88,000	$13.79	$10.51
9	$18,46,000	$1,56,34,000	$15.63	$11.65
10	$18,46,000	$1,74,80,000	$17.48	$12.73

Figure N-0-2: Snapshot of Value of Research Spreadsheet

N.3.4. Materials and Pavements

The numerical parametric studies conducted in the present study provided an indication of the optimal location of lean-on braces on the bridge. Based on the findings of both experimental and numerical studies, recommendations are provided for the selection of cross-frame layouts. As these cross-frames will not be placed in each bay along the bridge length and width, there will be significant savings in the amount of steel used.

N.4. Both Qualitative and Economic Values

This section describes fundamental areas such as engineering design improvements that have qualitative and economic value for the state of Texas and TxDOT.

N.4.1. Engineering Design Improvement

The research conducted in this investigation provided vital data in understanding the design and behavior of lean-on braces. The combined experimental and FEA data improved understanding of the fundamental behavior and design requirements for cross-frame layouts. Design examples that utilize this concept are presented for better guidance on using the recommendations provided.

N.5. Value of Research References

Connor, R. J., Dexter, R., & Mahmoud, H. (2005). *Inspection and management of bridges with fracture-critical details*: Transportation Research Board Washington, DC.

TxDOT. (2015). *University handbook 2016*: Texas Department of Transportation, The Research and Technology Implementation Office.

TxDOT. (2023). *TxDOT Open Data Portal.* <https://gis-txdot.opendata.arcgis.com/datasets/83af0d2957ca4c2eb340e4bd04a1046f/explore>.

US Bureau of Labor Statistics. (2023). <https://www.bls.gov/oes/current/oes472061.htm>.